How Well Do We Understand the Land-Ocean-Atmosphere Carbon Cycle?

David Crisp[1], Han Dolman[2], Toste Tanhua[3], Galen A. McKinley[4], Judith Hauck[5], Ana Bastos[6], Stephen Sitch[7], Simon Eggleston[8], Valentin Aich[8]

[1]Jet Propulsion Laboratory, California Institute of Technology, Pasadena, CA, USA.

[2] Royal NIOZ, Texel, Netherlands and Department of Earth Sciences, Vrije Universiteit Amsterdam, Amsterdam, The Netherlands.

[3]GEOMAR Helmholtz Centre for Ocean Research Kiel, Marine Biogeochemistry, Kiel, Germany.

[4]Columbia University and Lamont Doherty Earth Observatory, Palisades, NY, USA.

[5]Alfred-Wegener-Institut, Helmholtz-Zentrum für Polar und Meeresforschung, Bremerhaven, Germany.

[6]Max Planck Institute for Biogeochemistry Department Biogeochemical Integration, Jena, Germany

[7]College of Life and Environmental Sciences, University of Exeter, Exeter, EX4 4RJ, UK.

[8]Global Climate Observing System, World Meteorological Organization, Geneva, Switzerland.

Corresponding author: first and last name (David Crisp davidcri@gmail.com)

Key Points:

- Anthropogenic CO_2 emissions would have produced larger atmospheric increases if ocean and land sinks had not removed over half of this CO_2.
- Uptake by both ocean and land sinks increased in response to rising atmospheric CO_2 levels, maintaining the airborne fraction near 45%.
- Improved measurements and models can help track changes in land and ocean sinks and enhance the scientific basis for carbon management.

Abstract

Fossil fuel combustion, land use change and other human activities have increased the atmospheric carbon dioxide (CO_2) abundance by about 50% since the beginning of the industrial age. The atmospheric CO_2 growth rates would have been much larger if natural sinks in the land biosphere and ocean had not removed over half of this anthropogenic CO_2. As these CO_2 emissions grew, uptake by the ocean increased in response to increases in atmospheric CO_2 partial pressure (pCO_2). On land, gross primary production (GPP) also increased, but the emerging dynamics of other key aspects of the land carbon cycle varied regionally. Over the past three decades, CO_2 uptake by intact tropical humid forests has declined, but these changes are offset by increased uptake across mid- and high-latitudes. While there have been substantial improvements in our ability to study the carbon cycle, measurement and modeling gaps still limit our understanding of the processes driving its evolution. Continued ship-based observations combined with expanded deployments of autonomous platforms are needed to quantify ocean-atmosphere fluxes and interior ocean carbon storage on policy-relevant spatial and temporal scales. There is also an urgent need for more comprehensive measurements of stocks, fluxes and atmospheric CO_2 in humid tropical forests and across the Arctic and boreal regions, which are experiencing rapid change. Here, we review the current state of knowledge of the atmosphere, ocean, and land carbon cycles and their interactions and identify emerging measurement and modeling capabilities and gaps.

Plain Language Summary

Since the beginning of the industrial age in the mid-1700s, fossil fuel combustion, land use change and other human activities have increased the atmospheric carbon dioxide (CO_2) concentration to levels never seen before in human history. The atmospheric CO_2 growth rate would have been much larger if natural sinks in the ocean and on land carbon cycle had not removed over half of the CO_2 emitted by human activities. While the uptake of anthropogenic CO_2 by the ocean has increased with the increasing atmospheric CO_2 partial pressure, the land biosphere response has varied spatially and with time. Over the industrial age, CO_2 uptake by intact forests and other natural parts of the land biosphere has roughly balanced emissions from land use change. Since the 1990s, the tropical land sink has diminished while the high latitude land sink has increased. Here, we review our understanding of the natural carbon cycle and the processes controlling its response to human activities and climate change and identify measurement and knowledge gaps.

1 Introduction

Since the beginning of the industrial age, human activities have increased the atmospheric concentrations of carbon dioxide (CO_2) and other greenhouse gases (GHGs) to levels never before seen in human history. These large increases are driving climate change, because CO_2 is an efficient greenhouse gas with an average atmospheric lifetime measured in centuries. Bottom-up statistical inventories indicate that fossil fuel combustion, industry, agriculture, forestry, and other human activities are now adding more than 11.5 petagrams of carbon (Pg C) to the atmosphere each year (Friedlingstein et al., 2019; 2020; 2021). Direct measurements of CO_2 in the atmosphere and in air bubbles in ice cores (Etheridge et al., 1996) indicate that human activities have increased the globally averaged atmospheric CO_2 dry air mole fraction from less than 277 parts per million (ppm) in 1750 (c.f. Joos and Spahni, 2008) to

more than 412.44 ppm in 2020 (Dlugokencky et al., 2018; Rubino et al., 2019). Over half of this increase has been added since 1985 and over a quarter has been added since 2000.

These increases would be much larger if natural processes operating in the land and ocean had not removed over half of these anthropogenic CO_2 emissions. Carbon cycle measurements and modeling studies show that these anthropogenic CO_2 emissions are superimposed on an active natural carbon cycle that regulates CO_2 through photosynthesis and respiration on land and in the ocean (Beer et al., 2010), as well as temperature-driven solubility and carbonate chemistry coupled with the ocean circulation (Takahashi et al., 2002; 2009; Sabine et al., 2004; Gruber et al., 2019a). In pre-industrial times, these processes were roughly in balance, with the land biosphere and ocean emitting gross CO_2 fluxes of ~120 and ~90 Pg C yr^{-1} into the atmosphere, respectively, then removing a comparable amount. Today, these natural fluxes have comparable amplitudes, but now, CO_2 "sinks" the land biosphere and ocean also remove about half of the anthropogenic CO_2 emissions, reducing the atmospheric CO_2 growth rate and mitigating climate change (Canadell et al., 2007; Raupach et al., 2008; Knorr 2009; Bennedsen et al., 2019, Friedlingstein et al., 2020).

While the fraction of the anthropogenic CO_2 that stays in the atmosphere (the "airborne fraction") has remained remarkably constant, at about 0.45 for the multi-year average for the past ~60 years (e.g. Ballantyne et al., 2012; Raupach et al., 2008; 2014; Bennedsen et al., 2019), it can change substantially from year to year (Francey et al., 1995; Keeling et al., 1995; Bousquet et al., 2000). In some years, the airborne fraction can be as high as 80%, while in others, it can be as low as 30% (Raupach et al., 2008; 2014). Some of the largest changes in this airborne fraction appear to be associated with changes in uptake of CO_2 by the land biosphere (the land sink) in response to large-scale temperature and precipitation anomalies, like those associated with major El Niño events or large volcanic aerosol injections into the stratosphere (Frölicher et al., 2011; 2013). The ocean sink also responds to El Niño events and large volcanic eruptions (Keeling et al., 2005; Eddebbar et al., 2019; McKinley et al., 2004; 2017; 2020), but has a smaller impact on the amplitude of variability in the airborne fraction. The relative roles of these and other processes reviewed here that link the land, ocean and atmospheric carbon cycles with the climate are less well understood, compromising our ability to predict how the atmospheric CO_2 growth rate might change as the carbon cycle responds to climate change (Ballantyne et al., 2012).

Over the past two decades, our understanding of the natural and anthropogenic contributions to the carbon cycle has grown steadily with the deployment of progressively more sophisticated ground-based, oceanic, airborne, and space-based measurement systems. These advances have been accompanied by the development of far more comprehensive diagnostic and prognostic carbon cycle modeling tools. For the ocean, measurements of vertical gradients in pCO_2 across the air-sea interface provide the best available estimates of ocean-atmosphere carbon fluxes on annual time-scales, while high spatial resolution space-based observations of vegetation indices, solar induced chlorophyll fluorescence (SIF) and atmospheric CO_2 constrain land fluxes over the seasonal cycle. On decadal time-scales, the storage of anthropogenic carbon in the interior ocean can be assessed by biogeochemical and tracer observations. On land, in situ carbon-13 ($\delta^{13}C$) measurements and estimates of above-ground biomass derived from remote sensing observations provide similar constraints on these time scales.

Both bottom-up stock and flux estimates and "top-down" atmospheric estimates are providing key insights into the carbon cycle. Bottom-up methods use empirical or process-based models to estimate fluxes, or to upscale in situ measurements of the time change of stocks or of

direct flux observations of the oceans (e.g. Sabine et al., 2004; Doney et al., 2004; Rödenbeck et al., 2014; 2015; Gruber et al., 2019a; Landschützer, et al., 2013; Long et al., 2013; Hauck et al., 2020; Carroll et al., 2020; Gregor et al., 2019; Watson et al., 2020) or land biosphere (Pan et al., 2011; Sitch et al., 2015; Hubau et al., 2020; Piao et al., 2020a; Jung et al., 2020). "Top-down" models use inverse methods to estimate the surface CO_2 fluxes from the land or ocean needed to match the observed atmospheric or ocean CO_2 concentrations, within their uncertainties, in the presence of the prevailing winds and ocean circulation (e.g. Enting et al., 1995; Mikaloff-Fletcher et al., 2006; Jacobson et al., 2007; Khatiwala et al., 2009; Chevallier et al., 2010; 2019; DeVries, 2014; Crowell et al., 2019; Wu et al., 2018; Nasar et al. 2021).

Both bottom-up and top-down methods benefit from remote sensing as well as in situ data. For example, a bottom-up forest stock inventory might use in situ measurements to estimate the above ground biomass from an ensemble of specific plots and then use remote sensing measurements to upscale those measurements to larger areas. Similarly, a top-down approach might combine in situ and remote sensing observations of atmospheric CO_2 along with models of atmospheric transport to estimate regional-scale fluxes.

In practice, top-down and bottom-up methods are often combined. For example, top-down inverse methods for estimating net biospheric exchange (NBE) often use prior biospheric and fossil flux estimates derived from bottom-up methods (i.e. Crowell et al., 2019; Piero et al., 2021). They are also often compared to characterize processes or identify sources of uncertainty (Kondo et al., 2020; Bastos et al. 2020). However, some caution is needed when comparing and combing results from top-down and bottom-up methods because these approaches include different processes and often use different definitions of stocks and fluxes (Ciais et al., 2020a).

As the world embarks on efforts to monitor and control anthropogenic CO_2 emissions, there is growing evidence that the natural carbon cycle is evolving in response to human activities, severe weather, disturbances and climate change. If these changes affect the efficiency of the land or ocean CO_2 sinks, they could impede or confuse efforts to monitor progress toward emission reduction goals. An improved understanding of both the anthropogenic and natural processes that control the emissions and removals of atmospheric CO_2 by the land biosphere and ocean is critical to our ability to monitor and predict the rate of CO_2 increase in the atmosphere and its impact on the climate.

Anthropogenic processes emitting CO_2 into the atmosphere are now routinely tracked in the annual reports by the Global Carbon Project (i.e. Le Quéré et al., 2007; 2009; 2013; 2014; 2015a,b, 2016;2018 a,b; Friedlingstein et al., 2019; 2020; 2021) and in more focused reviews by others (e.g. Andrew, 2019; 2020; Hong et al., 2021). Similarly, carbon-climate interactions on long ("slow domain") and short ("fast domain") timescales, their representation in state-of-the art Earth System Models and their implications for climate change are describe in Hansen et al. (2013a) and routinely reviewed in the IPCC reports. See, for example, Chapter 6 of IPCC AR5 (IPCC, 2014; Ciais et al., 2013) and the soon to be released IPCC AR6 reports (IPCC 2021).

Here, we begin with a brief review of the atmospheric carbon cycle, including the anthropogenic drivers. We then focus on the contemporary processes controlling the fluxes of CO_2 between the ocean and land carbon reservoirs and the atmosphere and their implications for the evolution of the ocean and land carbon sinks. We update earlier works (e.g. Ciais et al., 2014; Ballantyne, et al., 2015) by reviewing the mean state and emerging trends in carbon stocks and fluxes revealed by various approaches, including new observing capabilities and analysis

157 techniques. Finally, we summarize critical measurement and modeling gaps that must be
158 addressed to produce an effective system for monitoring the carbon cycle as it continues to
159 respond to human activities and climate change.

160 **2 A Note on Units**

161 Because the bottom-up and top-down atmospheric, ocean and land carbon communities
162 focus on different aspects of the carbon cycle, they have developed a diverse array of units to
163 quantify stocks and fluxes of carbon and CO_2. For example, the land carbon community typically
164 quantifies the mass of stocks and fluxes of carbon, the atmospheric remote sensing community
165 typically measures and reports the column-averaged CO_2 dry air mole fraction, XCO_2, and the
166 ocean community uses the partial pressure, pCO_2, fugacity, fCO_2, and the air-sea carbon flux.
167 For the atmosphere, it is useful to note that one petagram of carbon (1 Pg C) yields 3.66
168 petagrams of CO_2 and that this is equivalent to a concentration change of ~ 2.124 ppm in the
169 atmospheric CO_2 (c.f. Ballantyne et al., 2012; Friedlingstein et al., 2020). Table 1 summarizes
170 these and other commonly used quantities and units used by the carbon cycle community and
171 describes their relationships.

172

Table 1. Quantities and units commonly used to quantify stocks and fluxes by the atmosphere (white), ocean (blue) and land (yellow) carbon cycle communities.

Quantity	Acronym	Typical units	Description
Carbon dioxide dry air mole fraction	CO_2 or xCO_2	parts per million by volume (ppm)	Number of CO_2 molecules relative to each million (10^6) molecules of dry air. If CO_2 is assumed to be an ideal gas and its dry air mole fraction is increased by 1 ppm at constant temperature, the CO_2 partial pressure will increase by one micro atmosphere (μatm).
Column-averaged carbon dioxide dry air mole fraction	XCO_2	ppm	A vertically-averaged quantity used by the atmospheric remote sensing community derived from the ratio of the CO_2 column abundance and the dry air column abundance. The dry air column abundance is estimated from the measured molecular oxygen (O_2) column abundance (assuming an O_2 dry air mole fraction of 0.20955) or from surface pressure and humidity.
partial pressure of carbon dioxide	pCO_2	μatm	At sea level, $pCO_2 = (P - pH_2O) \times X_{CO2}$, where P is the total atmospheric pressure and pH_2O is the water vapor saturation vapor pressure (see Woolf et al., 2016). 1 μatm = 10^{-6} atmospheres = 0.10325 Pascals.
Carbon dioxide fugacity	fCO_2	μatm	Effective partial pressure of CO_2 that has the same temperature and Gibbs free energy as the real gas. At the surface, $fCO_2 = xCO_2 \times \varphi_{CO2}$, where $\varphi_{CO2} \approx 0.0002/K$ is the fugacity coefficient for CO_2 and K is the temperature in Kelvin.
Net Community Production	NCP	mol C m^{-2} yr^{-1}	The net carbon removed from the atmosphere by the ocean biological pump.
Dissolved Inorganic Carbon	DIC	μmol/kg	Total amount of inorganic carbon in water.
Carbon stock or stock change		petagrams of carbon/year (Pg C yr^{-1})	1 Pg C = 10^{15} g C. 1 Pg C = 10^{12} kg C = 10^9 tons of carbon = 1 Gt C. When oxidized to form CO_2, 1 Pg C = 3.664 Pg CO_2.
Gross Primary Production	GPP	Pg C yr^{-1}	Total flux of carbon fixed through photosynthetic reduction of CO_2 by plants in an ecosystem.
Net Primary Production	NPP	Pg C yr^{-1}	Net flux of organic carbon produced by plants in an ecosystem. NPP- GPP - R_a, where R_a is autotrophic respiration by plants
Net Ecosystem Exchange or Net Ecosystem Production	NEE or NEP	Pg C yr^{-1}	NPP - R_h, where R_h is the carbon loss by heterotrophic (non-plant) respiration. NEE = -NEP but these terms are otherwise generally interchangeable, with NEE used more often to refer to fluxes measured in the atmosphere, while NEP is more often used for fluxes inferred from measurements of carbon stock changes.
Net Biospheric (Biome) Exchange	NBE	Pg C yr^{-1}	Change in mass of carbon stocks after episodic carbon losses due to natural or anthropogenic disturbance.

3 The Atmospheric Carbon Cycle

The atmosphere is the smallest, but most rapidly changing component of the global carbon cycle. It also serves as the primary medium for the exchange of carbon between the land biosphere, oceans and fossil reservoirs. The vast majority of the atmospheric carbon is in the form of CO_2. If we assume a total dry air mass of 5.1352×10^{18} kg (Trenberth and Smith, 2005), a CO_2 dry air mole fraction of 412 ppm, a mean CO_2 molecular weight of 44.01 kg/kmole, and a mean atmospheric molecular weight of 28.97 kg/kmole, the total mass of CO_2 in the atmosphere was ~3.214 Pg (~877 Pg C) in 2020. The next largest contributor to the atmospheric carbon reservoir is methane (CH_4), which is 220 times less abundant. For that reason, the atmospheric section of this carbon cycle review focuses on CO_2.

The largest net sources of atmospheric CO_2 are fossil fuel combustion, land use change and other human activities, which have added 700 ± 75 Pg C to the atmosphere between 1750 and 2019. Of that, 41 ± 11% has remained in the atmosphere (Friedlingstein et al., 2021). Because CO_2 has no significant photochemical sinks in the atmosphere, the remainder has been removed by natural sinks in the land biosphere and oceans. This section reviews our current understanding of the atmospheric carbon cycle, starting with observations, and then summarizing the insights contributed by top-down models and bottom-up inventories.

3.1 Observations of Atmospheric CO_2

Continuous measurements of atmospheric CO_2 were initiated in 1958 by Charles David Keeling of the Scripps Institution of Oceanography, when he established stations at Mauna Loa, Hawaii and the South Pole. Weekly flask samples and continuous measurements are now being returned by a global network that includes the U.S. National Oceanic and Atmospheric Administration (NOAA) Global Monitoring Laboratory (GML) Global Greenhouse Gas Reference Network (GGGRN) and other stations in their Carbon Cycle Greenhouse Gas (CCGG) Cooperative Global Air Sampling Network, the European Integrated Carbon Observation System (ICOS) network and other partners of the World Meteorological Organization Global Atmospheric Watch (WMO GAW) program (Figure 1).

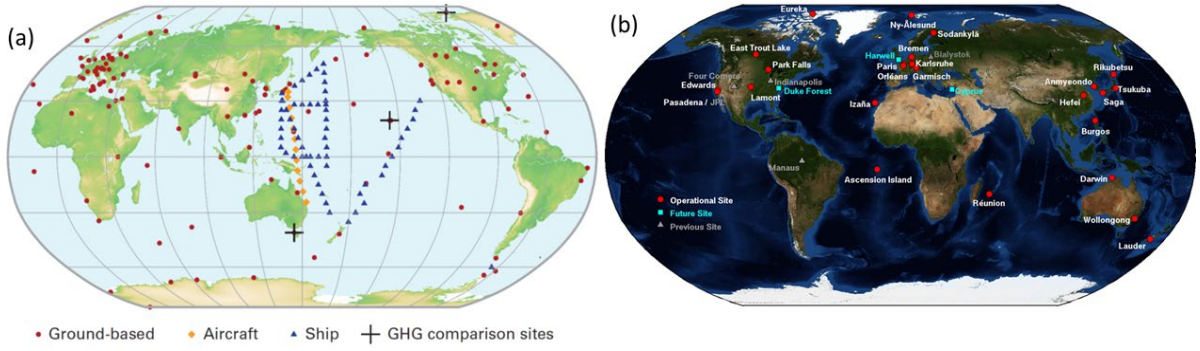

Figure 1: Spatial distribution of stations in the ground-based atmospheric CO_2 monitoring network. The vast majority of the stations are in North America and western Europe. (a) In situ CO_2 measurements are collected routinely at the WMO Global Atmospheric Watch Stations (from WMO Greenhouse Gas Bulletin, 25 Nov. 2019). (b) Solar-looking remote sensing observations of CO_2 are collected at Total Carbon Column Observing Network (TCCON) stations.

These in situ measurements provide the most accurate estimates of the CO_2 and CH_4 concentrations and their trends on global scales. The flask samples are also analyzed to quantify non-carbon greenhouse gases including nitrous oxide (N_2O), halocarbons, sulfur hexafluoride (SF_6), molecular hydrogen (H_2) and carbon isotopes including carbon-13 (^{13}C) and carbon-14 (^{14}C), which help to distinguish fossil fuel from biogenic contributions to the observed CO_2 trends.

More recently, these ground-based in situ networks have been joined by expanding networks of airborne in situ systems and ground-based remote sensing networks. NOAA routinely collects airborne profiles of CO_2 and other GHGs from 17 sites across North America using fixed-wing aircraft (see https://gml.noaa.gov/dv/data/). Vertical profiles of CO_2, CH_4 and other trace gases are also being returned by the balloon-borne AirCore systems (Karion et al., 2010; Baier et al., 2020), which are being deployed from an increasing number of sites. These research observations are now being augmented by GHG sensors deployed in the cargo holds of commercial aircraft as part of Japan's Comprehensive Observation Network for TRace gases by AIrLiner (CONTRAIL; Umezawa et al., 2018; Müller et al., 2021; data available at https://www.cger.nies.go.jp/contrail/protocol.html) program and Europe's In-service Aircraft for Global Observations (IAGOS; Clark et al., 2021; data available at https://www.iagos.org/iagos-data/) program. So far, GHG systems have been deployed on a small number of commercial aircraft, but that number is expected to grow as the size and operational complexity of the sensor systems is reduced.

The atmospheric CO_2 content can also be monitored remotely by measuring the amount of sunlight that it absorbs as it traverses the atmosphere. The Total Carbon Column Observing Network (TCCON) exploits this approach from 27 stations in 14 countries spanning latitudes between Eureka, Canada (80.05°N) and Lauder, New Zealand (45.038°S; Figure 1b). Each station collects high-resolution spectra that analyzed to yield estimates of the column-averaged dry air mole fractions of CO_2, CH_4, and other trace gases. These estimates are related to the WMO standard through comparisons with in situ measurements collected by over the stations by fixed-wing aircraft and AirCore instruments (Wunch et al., 2011).

One of the most important assets of the ground-based and airborne CO_2 measurement time series is their length, which now extends over 70 years at Mauna Loa and 40 years for the globe (Figure 2). These measurements show that the global atmospheric CO_2 dry air mole fraction has increased by almost 200 ppm, from less than 340 ppm in 1989 to more than to 412 ppm in 2020. Over this period, the atmospheric growth rate increased from less than 1 ppm yr^{-1} in the 1960s to more than 2.5 ppm yr^{-1} during the 2010s, driven primarily by steadily increasing fossil fuel emissions (c.f. IPCC, 2014; Friedlingstein et al., 2021). In addition to this long-term trend, the growth rate also varies by up to 2 ppm from year to year. Because these variations occur in the context of much more uniformly increasing anthropogenic emissions, they are attributed to interannual changes in the anthropogenic CO_2 airborne fraction and thus the efficiency of the land and ocean CO_2 sinks (Keeling et al., 1989; 1995; Francey et al., 1995).

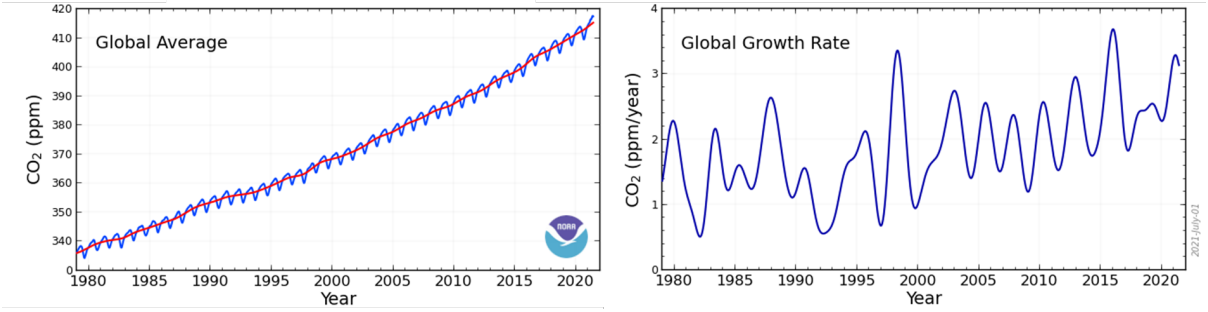

Figure 2: (a) Global averaged, monthly mean CO_2 dry air mole fraction from 1979 and 2021 (blue line) and long-term trend (red line) derived from the NOAA Carbon Cycle cooperative air sampling network. (b) Global, annual growth rate in atmospheric CO_2. (Adapted from a plot created by NOAA GML, https://gml.noaa.gov/ccgg/figures/).

During the first 30 years of this atmospheric CO_2 record, while there were still fewer than 10 stations regularly reporting data, innovative methods were already beginning to yield additional insights into the behavior of the land and ocean sinks. For example, Keeling et al. (1973; 1989; 1995) combined measurements of the atmospheric CO_2 growth rates from Mauna Loa and South Pole with $^{13}C/^{12}C$ ratios ($\delta^{13}C$) to assess the relative contributions to this variability from the land biosphere and ocean sinks. They found that the CO_2 growth rate anomalies were well correlated with atmospheric temperature increases during the warm phase of El Niño and decreases following the Pinatubo eruption. Their isotopic analysis suggested that El Niño typically enhanced the efficiency of the ocean sink and decreased the uptake by the land sink. These early conclusions have been reinforced by more recent measurements and modeling studies (c.f. Bousquet et al., 2000; Canadell et al., 2007; Raupach et al., 2008; Bennedsen et al., 2019).

In addition to the global-scale perspectives, the ground-based record has provided new insights into regional-scale phenomena. For example, they not only provided the first evidence for the now well-known atmospheric CO_2 seasonal cycle (Keeling, 1960), they also provided the first evidence for long-term changes in the CO_2 seasonal cycle amplitude (SCA) across the northern hemisphere (Bacastow et al., 1985; Keeling et al., 1996). These results have also been reinforced by more recent experiments that exploit an expanded ground-based network and longer CO_2 data record (Graven et al., 2013; Byrne et al., 2018; 2020a; Liu et al., 2020a).

Recent advances in space-based remote sensing technologies are now providing new opportunities to dramatically improve the spatial and temporal coverage and resolution of atmospheric CO_2 observations. These space-based sensors collect high-resolution spectra of reflected sunlight within molecular oxygen (O_2) and CO_2 bands that can be analyzed to yield precise, spatially resolved estimates of XCO_2. The first space-based sensor to use this approach was the German-Dutch-Belgian SCanning Imaging Absorption spectroMeter for Atmospheric CartograpHY (SCIAMACHY) onboard the European Space Agency (ESA) Environmental Satellite (ENVISAT), which operated from 2002 to 2012. ENVISAT/SCIAMACHY was followed by Japan's Greenhouse gases Observing SATellite, GOSAT in 2009 (Kuze et al., 2009; 2016; Yoshida et al., 2011;), and then by NASA's Orbiting Carbon Observatory-2 (OCO-2) in 2014 (Crisp et al., 2004; 2008, Eldering et al., 2017). OCO-2 returns about three million XCO_2 estimates over the sunlit hemisphere each month (Figure 3) with single sounding random errors

of ~0.5 ppm and accuracies of ~1 ppm (Wunch et al., 2017; O'Dell et al., 2018; Müller et al., 2021). GOSAT and OCO-2 have recently been joined by their sister missions, GOSAT-2 (2018) and OCO-3 (2019), providing additional coverage and resolution.

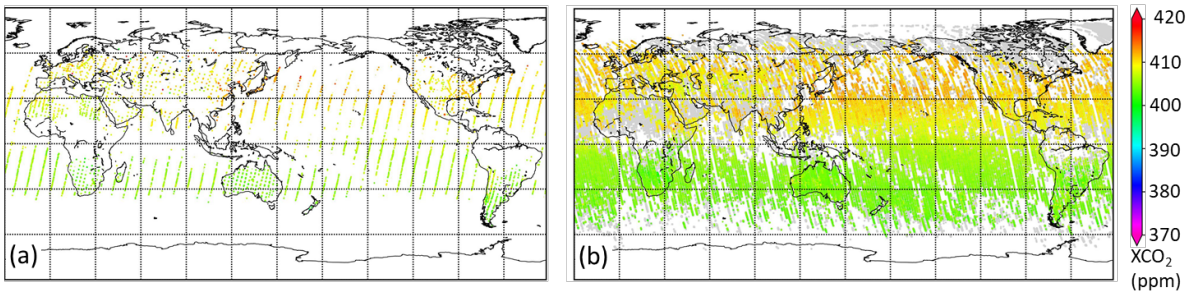

Figure 3. Monthly maps of XCO_2 estimates derived from (a) GOSAT and (b) OCO-2 measurements for April 2018. OCO-2 collects ~100 times as many samples each day as GOSAT, providing much greater data density. For both satellite products, the coverage at high latitudes varies with the availability of sunlight. Persistent optically-thick clouds and airborne dust (Sahara) limit the coverage (Images from the World Data Center for Greenhouse Gases, https://gaw.kishou.go.jp/satellite/file/0149-9011-1001-08-08-9999).

These data are now providing a record of the atmospheric CO_2 distribution with unprecedented detail, revealing trends in atmospheric CO_2 concentrations that are providing new insights into atmospheric sources and sinks. For example, each month, XCO_2 estimates derived from OCO-2 observations using the Atmospheric CO_2 Observations from Space (ACOS) algorithm (O'Dell et al., 2018) provide a global maps of CO_2, reflecting the net effects of emissions, removals, and atmospheric transport. These maps provide snapshots of most robust features of the atmospheric carbon cycle. For example, during the early northern hemisphere (NH) spring, they reveal the relatively large (> 10 ppm) north-south gradient in XCO_2, driven by the CO_2 buildup across the NH during the winter, when photosynthetic uptake by the land biosphere is suppressed. The gap-filed maps also indicate enhanced values east Asia that might be associated with intense fossil fuel combustion.

While CO_2 time series and XCO_2 maps provide some direct insight into the sources and sinks of atmospheric CO_2, methods that account for atmospheric transport are needed to quantify CO_2 fluxes on sub-regional to continental scales. Atmospheric inverse systems address this need. Inverse systems designed to constrain fluxes on these scales typically incorporate a global chemical transport model that assimilates estimates of the atmospheric CO_2 dry air mole fraction with an optimization algorithm that derives estimates of the net surface CO_2 fluxes needed to match the observed CO_2 distribution to within its uncertainties in the presence of the imposed wind field (Enting et al., 1995; Bousquet et al., 2000; Enting 2002, Peters et al., 2005; Baker et al., 2006a). For studies of anthropogenic emissions from point sources or large urban areas typically employ simpler emission plume mass balance models (Nassar et al., 2017; 2021; Varon et al., 2018; Reuter et al., 2019) although some use more sophisticated inverse models with Eulerian (Ye et al., 2020; Lei et al., 2021) or Lagangian transport schemes (Wu et al., 2018). Both types of systems are summarized here.

3.2 Constraining CO_2 fluxes with Regional-scale Atmospheric Inverse Models

Most inverse modeling systems use a form of Bayesian inference that adjusts surface fluxes to minimize a cost function, a mathematical expression that describes the mismatch between the observations and the simulated observations based on prior estimates of surface fluxes, accounting for their respective uncertainties (i.e. Enting, 2002). Commonly-used inverse methods include variational data assimilation (3-D and 4-D VAR), ensemble Kalman filter, and the Markov Chain Monte Carlo methods. These systems are typically initialized with "prior" CO_2 concentration and flux distributions derived from bottom-up inventories, climatologies and biogeochemical models. Most inverse modeling systems use precomputed (off-line) atmospheric winds fields from a meteorological reanalysis in a global, 3-dimensional chemical tracer transport models, such as the Goddard Earth Observing System (GEOS) Chemistry (GEOS-Chem), Tracer Model 5 (TM5) (c.f. Crowell et al., 2019; Peiro et al., 2021).

3.2.1 Constraining Regional-scale CO_2 Sources and Sinks with Atmospheric Inverse Systems

Historically, top-down estimates of CO_2 fluxes from atmospheric inverse systems have relied on *in situ* measurements collected by the surface network (Figure 1). To exploit this sparse network, CO_2 fluxes were derived for a small number of pre-defined continental and oceanic regions and anthropogenic emissions were prescribed from bottom-up inventories to diagnose the behavior of the ocean and land carbon cycles. For example, Tans et al. (1990) found that the observed pole-to-pole gradient in atmospheric CO_2 indicated the presence of a large land sink in the northern extratropics, a result that was confirmed by other studies (c.f. Ciais et al., 1995). Others used inverse models to study the variability of the airborne fraction and concluded that terrestrial carbon fluxes were roughly twice as variable as ocean fluxes during the 1980s and 1990s, and that tropical land ecosystems contributed the most to this variability (Bousquet et al., 2000; Rödenbeck et al., 2003; Peylin et al., 2005). However, there was significant disagreement in the relative contributions by the different ocean basins or the land sinks in North America and Asia (c.f. Fan et al., 1998; King et al., 2015). These differences were ascribed primarily to limitations in the observing network the transport models adopted and other differences in the inversion methods.

To make progress the latter two areas, large multi-model intercomparison projects, such as the Atmospheric Carbon Cycle Inversion Intercomparison (TransCom 3; Gurney et al., 2002; 2003) and REgional Carbon Cycle Assessment and Processes (RECCAP) projects (Canadell et al., 2011; Peylin et al., 2013) were launched. Early results from these projects confirmed that model transport uncertainties were as large a source of error as the sampling uncertainties introduced by the sparse CO_2 measurement network (Gurney et al., 2002; 2003) and that transport errors had their largest impacts on northern latitudes (Baker et al., 2006b). More recent multi-model intercomparison experiments constrained by in situ observations, alone, show significant reductions in the spread of the model estimates when compared to independent observations (Gaubert et al., 2019; Ciais et al., 2020a). However, these inverse model experiments still do not have the spatial resolution needed to separately quantify natural and anthropogenic emissions on regional scales or to constrain the relative contributions of the global ocean and land sinks to better than ~1 Pg C yr^{-1} (Jacobson et al., 2007; Chevallier et al., 2010; Sarmiento et al., 2010; Tohjima et al., 2019; Kondo et al., 2020; Friedlingstein et al., 2021).

With their improved spatial resolution and temporal coverage, atmospheric XCO_2 estimates derived from space-based observations are now providing new opportunities to study CO_2 emissions and uptake at policy-relevant spatial and temporal scales (c.f. Zhang et al., 2021;

Chevallier, 2021). CO_2 estimates retrieved from GOSAT and OCO-2 measurements clearly show persistent positive anomalies associated with anthropogenic emissions over East Asia, Western Europe and eastern North America (Hakkarainen et al., 2016; 2019; Wang et al., 2018). They also show persistent positive anomalies over northern tropical Africa and northern tropical South America.

When these space-based XCO_2 estimates are analyzed with flux inversion models (e.g. Maksyutov et al., 2013; Chevallier et al., 2019; Crowell, et al., 2019; Peiro et al., 2021), they produce annual-averaged fluxes at sub-regional scales that reinforce and sometimes conflict with those derived from bottom-up methods or inverse modeling methods constrained by in situ CO_2 measurements, alone. For example, there is generally good agreement between the NBE estimates for northern hemisphere extratropical land derived using inverse methods constrained in situ and OCO-2 v9 XCO_2 estimates (Peiro et al., 2021; Zhang et al., 2021). However, both in situ and space-based inverse modeling results indicate a substantially larger summertime seasonal drawdown than the prior, which was constrained by bottom-up results from dynamic global vegetation models (DGVMs). Over tropical land, NBE estimates from ensembles of inverse models constrained by space-based measurements are both more positive and have a smaller spread across then ensemble than those constrained only by in situ measurements from the sparse tropical network or ensembles of DGVMs (Palmer et al., 2019; Crowell, et al., 2019; Peiro et al., 2021). These differences are explored in greater detail in Section 5.

Over the ocean, results from atmospheric inversions constrained by in situ and space-based observations are less conclusive. For example, Chevallier et al. (2019) find that inversions constrained by ACOS/GOSAT XCO_2 estimates reduce the ocean sink by ~0.5 Pg C yr^{-1} in 2015, relative to a prior constrained by ocean pCO_2 estimates (Landschützer et al., 2017), a result that is consistent with the onset of the strong 2015-2016 El Niño. However, when ACOS/OCO-2 version 9 (v9) XCO_2 ocean glint estimates are used to constrain inverse models, a known ~1 ppm negative bias in this product, produces an unrealistically large (3.75 Pg C yr^{-1}) ocean sink during that period (Peiro et al., 2021), while methods constrained by ocean pCO_2 indicate an ocean sink between 2 and 3 Pg C yr^{-1} during the 2010s' (Friedlingstein et al., 2019; 2020; 2021). Because of this, the OCO-2 v9 ocean glint observations have been excluded from most inverse model studies. This ocean glint bias was reduced by over 90% in the v10 ACOS/OCO-2 XCO_2 product (Müller et al., 2021), but there is still little evidence that space-based XCO_2 estimates can provide useful constraints on the ocean sink.

Atmospheric inverse models are also being used to constrain anthropogenic CO_2 emissions and removals (Chevallier, 2021; Deng et al., 2021; Hwang et al., 2021; Petrescu et al., 2021). On regional scales, estimates of CO_2 emissions and removals derived from atmospheric measurements of XCO_2 are not as source specific as the traditional bottom-up statistical methods used to compile national inventories, which infer CO_2 emissions from fuel use (i.e. Andrew 2020), land use change (i.e. Houghton and Nassikas, 2017) and other human activities. However, they complement those methods by providing an integral constraint on the total amount of CO_2 added to or removed from the atmosphere by all natural and anthropogenic processes. They can also be used to identify and track rapidly-evolving emission hotspots that are often missed in the bottom-up statistical inventories. As these tools are integrated into a more comprehensive carbon management system, they could also help carbon managers to assess the effectiveness of their carbon management strategies, and help to identify emerging emission reduction opportunities.

The current ground-based, airborne and space-based CO_2 measurement and modeling capabilities do not yet provide the resolution and coverage needed to estimate net emissions for all countries. In addition, ongoing concerns about the accuracy of the space-based estimates also compromise the reliability of these top-down products as an independent Monitoring and Verification System (MVS) for evaluating national inventory reports (Janssens-Maenhout et al., 2020). The current atmospheric CO_2 measurements and inverse modeling systems are not adequate to clearly distinguish the contributions of fossil fuel sources from land and ocean sources and sinks of CO_2 on regional scales (Ciais et al., 2020b; Chevallier, 2021).

However, atmospheric inverse systems are improving rapidly. Existing systems clearly illustrate many of the strengths and weaknesses of top-down methods for inventory development and assessment. To demonstrate these capabilities, pilot, national-scale flux inversion efforts focus on the largest countries. Most of these studies prescribe fossil fuel CO_2 emissions from a bottom-up emissions inventory and hold these as fixed, and then optimize the terrestrial and ocean carbon fluxes to match the spatial and temporal fluctuations in the observations within their uncertainties (c.f. Chevallier, 2021; Deng et al., 2021). Ongoing efforts to expand the ground-based and space-based atmospheric measurement and inverse modeling capabilities are expected to mitigate this limitation to some extent through the use of proxies, such as nitrogen dioxide (NO_2), carbon monoxide (CO), and ^{14}C to distinguish emissions fossil fuel emissions from biomass burning (c.f. Heymann et al., 2017; Reuter et al., 2019; Hakkarainen et al., 2021). Others are combining CO_2 observations with observations of carbonyl sulfide, OCS (Remaud et al., 2021) or SIF (Liu et al., 2017; Palmer et al. 2019; Yin et al., 2020) to discriminate the relative roles relative roles of photosynthesis and respiration.

3.2.2 Constraining Atmospheric CO_2 emissions from Local Sources

On smaller scales, space-based XCO_2 estimates are being combined with ground-based and airborne measurements to quantify CO_2 emissions from large urban areas (Hedelius et al., 2018; Wu et al., 2018; Wu et al., 2020) and individual power plants (Nassar et al., 2017; 2021; Reuter et al., 2019; Hakkarainen et al., 2021). Space-based sensors do not yet have the coverage needed to track all local sources, but they do provide opportunities to assess the precision that could be delivered by future space-based instruments. For example, Nassar et al. (2017; 2021) has used OCO-2 XCO_2 estimates to quantify emissions from an individual coal-fired power plants (Figure 4). They combine these estimates with wind speed and direction from ERA-5 (Hersbach et al., 2020) and MERRA-2 (Molod et al., 2015) in a simple Gaussian plume model to estimate the fluxes. They find emission rates of near 98 kilotons per day (kT day^{-1}), which compare well with the reported value on that day of 103 kT/day. OCO-2 XCO_2 observations are also being combined with NO_2 observations from the Copernicus Sentinel 5 Precursor TROPOMI instrument to track and quantify CO_2 emission plumes tens of km downwind of large powerplants (Reuter et al., 2019; Hakkarainen et al., 2021).

Other studies have focused on top-down estimates of emissions from large urban areas, which are responsible for ~70% of all anthropogenic CO_2 emissions. For example, Hedelius et al. (2018) estimate the net CO_2, CH_4, and CO flux from the Los Angeles South Coast Air Basin (So-CAB) using an inversion system that couples TCCON and OCO-2 observations with the Hybrid Single Particle Lagrangian Integrated Trajectory (HYSPLIT) model and the Open-source Data Inventory for Anthropogenic CO_2 (ODIAC). TCCON XCO_2 measurements indicate that the net CO_2 flux from the So-CAB is 104 ± 26 megaton of CO_2 per year ($MtCO_2$ yr^{-1}) for the study period of July 2013–August 2016. A slightly higher estimate of 120 ± 30 $MtCO_2$ yr^{-1} is obtained

using OCO-2 data. These CO_2 emission estimates are slightly lower than those from previous work. In another study, Wu et al. (2020) analyzed OCO-2 XCO_2 data with an advanced version of the Stochastic Time-Inverted Lagrangian Transport model, XSTILT, to quantify per capita CO_2 emissions from 20 major urban areas. In general, they find that cities with greater population density have lower per capita emissions, which is consistent with earlier bottom-up estimates. However, they find that cities with heavy power industries or greater affluence stand out with higher per capita emissions. These studies suggest that that space-based measurements could eventually play a significant role in emissions monitoring efforts.

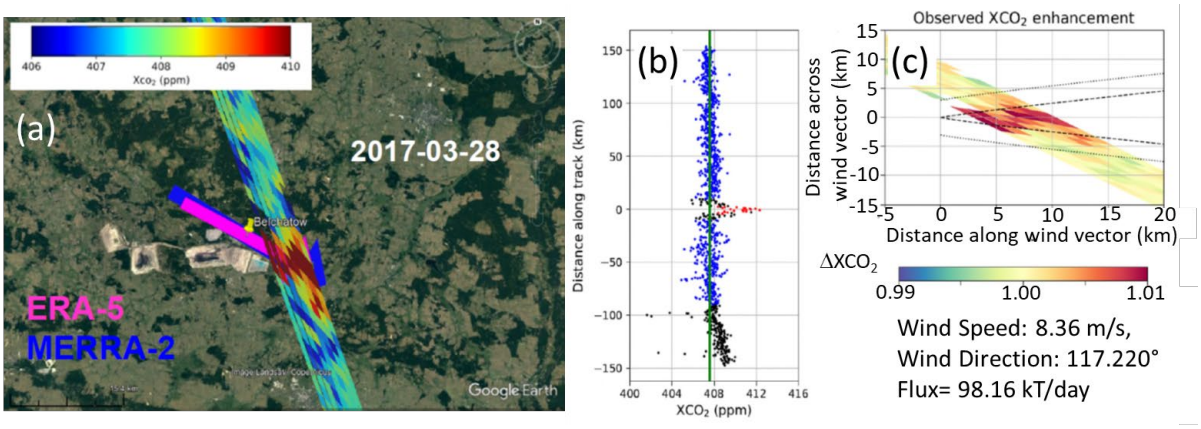

Figure 4. (a) OCO-2 flight track over the over the Bełchatów power station (Poland) on 28 March 2017, showing enhanced XCO_2 (red) downwind of the plume. (b) XCO_2 values along ground track, showing a ~4 ppm enhancement downwind. (c) Gaussian plume model used to estimate the fluxes (adapted from Nassar et al., 2021).

The principal challenge of the space-based measurements is the need for unprecedented levels of precision and accuracy. While intense local sources, such as large coal-fired power plants or large urban areas can increase the near-surface CO_2 concentrations by more than 10%, these variations decay rapidly with altitude, such that they rarely yield XCO_2 variations larger than 1-2 ppm (0.25 to 0.5%) on the spatial scale of a satellite footprint (1 to 100 km^2). Natural sinks of CO_2, such as forests or ocean basins, are characterized by weak, spatially extensive, local fluxes and thus produce even smaller changes in XCO_2, which place much greater demands on measurement precision and accuracy.

To ensure that that these space-based XCO_2 estimates meet these demanding requirements, they are routinely validated through comparisons with co-incident, ground-based remote sensing estimates of XCO_2 derived from TCCON observations, which provide a transfer standard to the WMO in situ standard (Wunch et al., 2011; 2017). Using this approach, the current state of the art for space-based XCO_2 estimates is single-sounding random errors and biases between 0.5 and 1 ppm (Hedelius et al., 2017; O'Dell et al., 2018; Kiel et al., 2019; Müller et al., 2021). This is adequate to track regional scale changes in surface sources and sinks as small as those produced by the COVID-19 lockdowns (Weir et al., 2021), but not yet adequate to constrain relative roles of the ocean and land biospheric sinks to much better than 1 Pg C yr^{-1}.

These new measurement capabilities are also driving the development of atmospheric inverse systems, spawning a new series of multi-model intercomparison experiments that use only ground-based and airborne in situ observations, space-based measurements, or both

(Houwelling et al., 2015; Chevallier et al., 2019; Crowell et al., 2019; Kondo et al., 2020; Ciais et al., 2020a,b; Peiro et al., 2021). These experiments are providing new insights into the relative roles of CO_2 measurement accuracy, atmospheric transport (Schuh et al., 2019; Gaubert et al., 2019; Torres et al., 2019) and other aspects of the model setup (Peiro et al., 2021). These efforts are expected to improve both the spatial resolution and accuracy of these methods and to help reconcile their results with bottom-up methods (Kondo et al., 2020; Ciais et al., 2020a).

3.3 Bottom-up Estimates of Anthropogenic Contributions to the Atmospheric Carbon Cycle

CO_2 emissions from fossil fuel combustion in the energy sector constitute the largest direct anthropogenic contribution to the global carbon cycle (Andrew, 2020; Friedlingstein et al., 2021). Emissions of CO_2 and other GHGs from land use and land use change (LUC) on managed lands are the second largest contribution, accounting for almost one quarter of all anthropogenic GHG emissions (Houghton, 2003; Smith et al., 2014; Houghton and Nassikas, 2017). These emissions originate primarily from deforestation and forest degradation, but also include contributions from agricultural land, livestock, forest management, and secondary forest regrowth. This section summarizes the approaches used to track the emissions and removals of CO_2 by these and other human activities and quantifies their current values and uncertainties.

3.3.1 Anthropogenic CO_2 emissions inventories for regulation and commerce

Atmospheric GHG emissions from fossil fuel use (Andrew, 2020) and cement production (Andrew, 2019) are currently being tracked by the regulatory, commercial and scientific communities. National regulatory organizations such as the U.S. Environmental Protection Agency (EPA), Japan's Ministry of the Environment (MOE) and the European Union's European Environment Agency (EEA) compile statistics for regulating and reporting national emissions to other government agencies or organizations such as the United Nations Framework Convention on Climate Change (UNFCCC). These inventories are compiled using best practices recommended in the Intergovernmental Panel on Climate Change (IPCC 2006; 2019) Guidelines for National Greenhouse Gas Inventories, which require reports of annual emissions by sources and removals by sinks in specific sectors and categories. For example, fossil fuel combustion is tracked in in the energy sector while those from managed lands are tracked in the agriculture, forestry and other land use (AFOLU) sector. Net emissions and removals in each category of each sector are approximated either by multiplying the measured *activity data* (i.e. number of liters of oil burned) by an assumed *emission factor* (number of kilograms CO_2 emitted per liter of oil) or by sampling carbon stock changes directly, and summing the results to yield totals.

Additional information about GHG emissions associated with the extraction, transport and use of fossil fuels is compiled by several organizations. For example, the International Energy Agency (IEA) originally compiled fossil fuel statistics to avoid disruptions in the world's oil supplies, but now provide annual reports on a range of technologies to support sustainable energy development (IEA 2020). Commercial organizations, such as British Petroleum, produce inventories to track trends in energy markets (BP 2020). Those from national organizations, such as the U.S. Energy Information Administration (EIA) serve a similar purpose, tracking short-term and long-term trends in supply and demand globally to support the energy industry.

Similarly, to track emissions from LUC, international organizations such as the United Nations Food and Agriculture Organization (FAO) collect and disseminate global information on AFOLU. Several methods are used to track fluxes from LUC. For example, statistical data on land cover area collected by FAO are used in so-called bookkeeping models that prescribe

carbon changes in biomass and soil pools over time and their resulting fluxes to the atmosphere (Hansis et al., 2015, Houghton and Nassikas, 2017). For tracking historical LUC, a map of historical land use is required such as LUH2-GCB2020 (Hurtt et al., 2020; see also Friedlingstein et al., 2020; Chini et al., 2021). Using this information, it is also possible to estimate fluxes from land-use change using the new generation of dynamic global vegetation models (DGVMs). Another approach uses satellite remote sensing data to determine the amount of land cover change (LCC) and to associate emission losses with LCC by applying emission factors or detailed biogeochemical models, e.g. emissions from fires associated with deforestation and forest degradation (van der Werf et al., 2017). Finally, at the national level, LCC emissions are compiled and delivered to the UNFCCC by country level organizations such as the U.S. EPA, Japan's MOE and the European Union's EEA. These LCC estimates often differ from those derived by the carbon cycle community because they include different processes and quantities (Grassi et al., 2018; Ciais et al., 2020a; Chevallier 2021).

3.3.2 Inventories of anthropogenic CO_2 supporting carbon cycle research

Scientific inventories, such as those compiled by the Carbon Dioxide Information Analysis Center (CDIAC; Boden et al., 2017) and the annual reports compiled by the Global Carbon Project (GCP), combine information from all of these sources to support scientific investigations and modeling of the energy and carbon cycles as well as other applications. The science community has also produced high resolution gridded inventories such as the Emissions Database for Global Atmospheric Research, EDGAR (Janssens-Maehout et al., 2019), Open-source Data Inventory for Anthropogenic CO_2, ODIAC (Oda et al., 2018), and Hestia (Gurney et al., 2019). These inventories use other data (population, night lights, etc.) to disaggregate national-scale emissions from fossil fuel combustion, industry, LUC and other processes to support carbon cycle investigations on spatial scales spanning individual urban areas to countries. These gridded inventories also provide more actionable information on anthropogenic CO_2 emissions for policy makers working on urban to sub-national scales.

One limitation of these inventories is that there is typically a year or more lag in their availability. Motivated by reports of large reductions in fossil fuel use during the initial COVID-19 lockdowns in 2020, several groups began investigating the feasibility and utility of near-real-time (NRT) emission inventories based on proxy data. Le Quéré et al. (2020) derived daily, national estimates of emission changes based on a three-level Confinement Index that was based on historical relationships between confinement and activity data from six categories of the energy sector (power, industry, surface transport, public, and residential). They report that daily global CO_2 emissions decreased by 17% by early April 2020, compared to 2019 values. Liu et al. (2020b) created the near-real-time Carbon Monitor (https://carbonmonitor.org/) inventory by combining data from a variety sources including hourly datasets of electrical power use from 31 countries, daily vehicle traffic data from 416 cities, daily global passenger aircraft flights, and other sources. They found emission reductions similar to those reported Le Quéré et al., but with somewhat larger variability. These NRT inventories are not as complete or accurate as the more conventional scientific inventories, but are useful for tracking rapid changes in emissions associated with energy use.

The Global Carbon Project compiles the Global Carbon Budget (GCB) annually (LeQuéré et al., 2009; 2013; 2014; 2015a,b; 2016; 2018a,b; Friedlingstein et al., 2019; 2020; 2021) These papers document global and national budgets of anthropogenic carbon fluxes for five key components: atmosphere, fossil fuel emissions, LUC, uptake by the terrestrial biosphere

("land sink") and uptake by the ocean ("ocean sink"). The net land carbon balance represents the difference between the fluxes from land-use change (i.e. deforestation, degradation, secondary forest regrowth, forestry and crop management) and the natural land carbon sink. Decadal mean emissions from fossil fuel use and cement production increased from 7.7±0.4 Pg C yr^{-1} in 2000-2010 to 9.5 Pg C yr^{-1} for 2011-2020 with a peak of 9.9 ±0.5 Pg C yr^{-1} in 2019. Over this same period, land use change emissions increased from 1.4±0.7 Pg C yr^{-1} to 1.6±0.7 Pg C yr^{-1}.

In 2020, fossil fuel emissions decreased to 9.5±0.5 Pg C yr^{-1} due to lockdowns and other measures adopted in response to the COVID-19 pandemic, but are projected to rebound to values around those from 2019 in 2021 (Friedlingstein et al., 2021). LUC emissions decreased slightly from 1.2±0.7 Pg C yr^{-1} in the decade, 2000-2010, to 1.1±0.7 Pg C yr^{-1} in the decade, 2011-2020. The ocean and land sinks increased during the same time from 2.2 to 2.8±0.4 Pg C yr^{-1} and 2.6 to 3.1 Pg C yr^{-1} respectively (Friedlingstein et al., 2021). The anthropogenic land and ocean sinks are defined as their responses to the direct effects of increasing atmospheric CO_2 and indirect effects associated with climate change.

3.3.3 Tracking Uncertainties in Anthropogenic CO_2 Inventories

In addition to these flux estimates, the GCBs document uncertainties, expressed as one standard deviation around the mean. Figure 5 shows the relative error of these estimates (uncertainty/mean) as they progress through the years for the 2006-2019 budgets. The estimates refer to each individual year for which the budget was prepared. As such, they indicate the progression in understanding of the uncertainties in the budget at that time (as opposed to an *a posteriori* analysis of the uncertainties of all years in a similar manner).

The relatively low, stable uncertainties associated with both the fossil fuel emissions and atmospheric CO_2 concentrations result from two factors (Ballantyne et al., 2012). The first is the precision of the atmospheric in situ CO_2 measurements and efficient mixing of CO_2 throughout the atmosphere, although analytical errors and sampling bias do play a role. Second, while fossil fuel combustion is the primary source of anthropogenic CO_2 emissions, the relative error on this contribution is small (~11%, c.f. Quilcaille et al., 2018) because the fossil fuel industry provides reliable numbers on their sales, which are well correlated with the amount of fossil fuel burned. The largest relative errors are associated with LUC emissions. Compared to the early period, 2000-2010, the relative error for this component has not substantially decreased, nor has the mean value substantially changed.

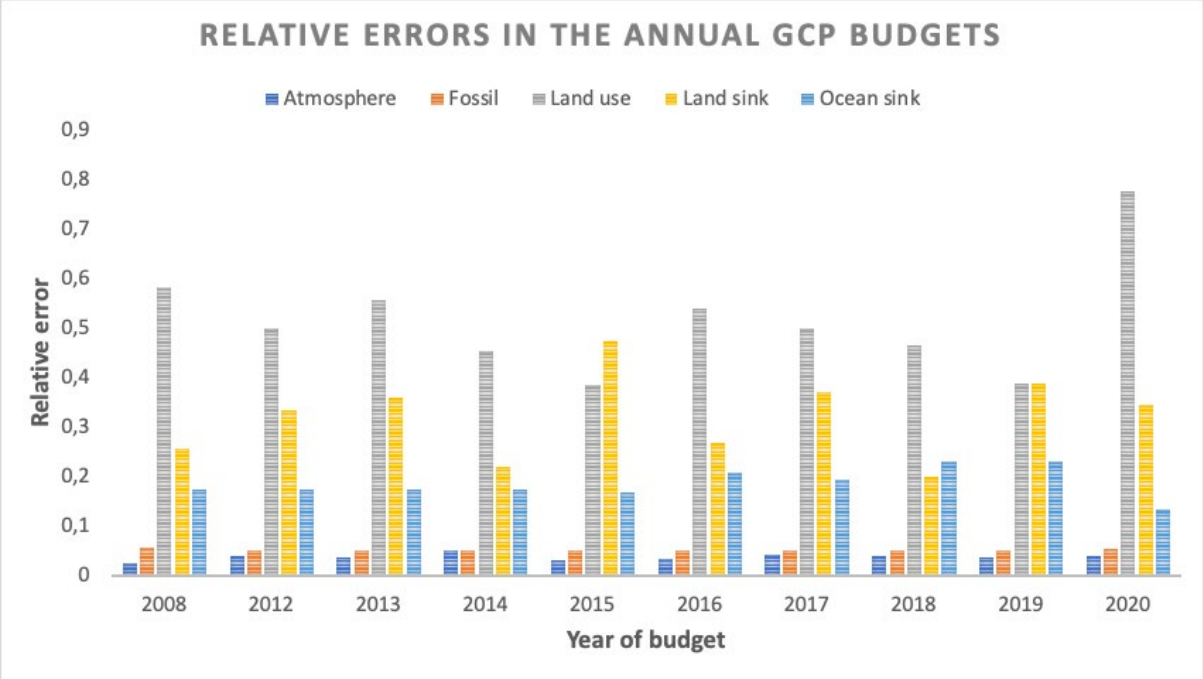

Figure 5. Relative error (1 standard deviation uncertainty / mean) for the Global Carbon Budget estimates since 2000. Numbers are taken for the individual year(s) reported each year from Canadell et al. (2007), LeQuéré et al. (2009) and LeQuéré et al. (2013-2018) and Friedlingstein et al. (2019-2021) and refer to the annual estimates.

In the 2015 GCB (LeQuéré et al., 2016) and before, the land sink was calculated as a residual, as described in Eq. 1:

$$land\ sink = emissions\ (fossil\ fuel\ and\ LUC) - atmospheric\ growth\ rate - ocean\ sink \quad (1)$$

Since 2017 (year 2016), the GCB has estimated LUC directly from bookkeeping models (Hansis et al., 2015; Gasser et al., 2020; Houghton and Nassikas, 2017). Uncertainties in these estimates are derived from the spread of these models and that of an ensemble of DGVMs (Friedlingstein et al., 2021).

At the same time, a normalization of the ocean sink estimate from models to a data-based estimate from the 1990s (Denman et al., 2007) was also discontinued. This normalization had previously been applied to ensure that the land sink estimate from the budget residual had a realistic mean value. This change in methodology led to a smaller mean 1990s ocean sink, and thus slightly increased the estimate of the relative uncertainty from 17% in 2015 to 19% in 2016. The ocean sink uncertainty had also varied between 17 and 19% for the years 2006 to 2015. In Friedlingstein et al., (2021), the ocean sink is derived from models and observation-based products and the uncertainty was re-assessed based on a combination of ensemble standard deviation and propagation of known uncertainties in the calculations.

With the advent of a direct estimate of the land sink from DGVMs, the GCP can now assess the degree to which the overall global carbon budget can be closed, i.e., the difference between the sum of the fluxes and the atmospheric accumulation. A budget imbalance represents a measure of our imperfect understanding of the carbon cycle and uncertainty in related measurements. Over decadal scales, the budget imbalance is near to zero, but with substantial interannual to semi-decadal variability, possibly relating to the response of natural sinks to climate variability. The budget imbalance was estimated at -0.3 Pg C for the decade 2011-2020, or approximately 10% of the magnitude of the land and ocean sinks (Friedlingstein et al., 2019, 2020; 2021). This budget imbalance and its associated uncertainties illustrates the limitations to our understanding of global annual mean fluxes at the interannual time scale.

4 The Ocean Carbon Cycle

The ocean holds a large natural reservoir of carbon that exchanges with the atmosphere on time-scales of decades up to hundreds of thousands of years. Superimposed upon the cycling of this natural reservoir, the increasing atmospheric CO_2 partial pressure is causing the ocean to absorb a significant fraction of anthropogenic carbon emissions. Due to the natural carbon cycle of the ocean, 39,000 Pg C is stored in the ocean, which amounts to ~90% of the carbon contained in the combined land, ocean and atmosphere domains (Bolin 1983; Sundquist 1993; Sabine and Tanhua, 2010). The natural carbon cycle is driven by ocean circulation, seasonal heating and cooling, and biological processes (Figure 7, left).

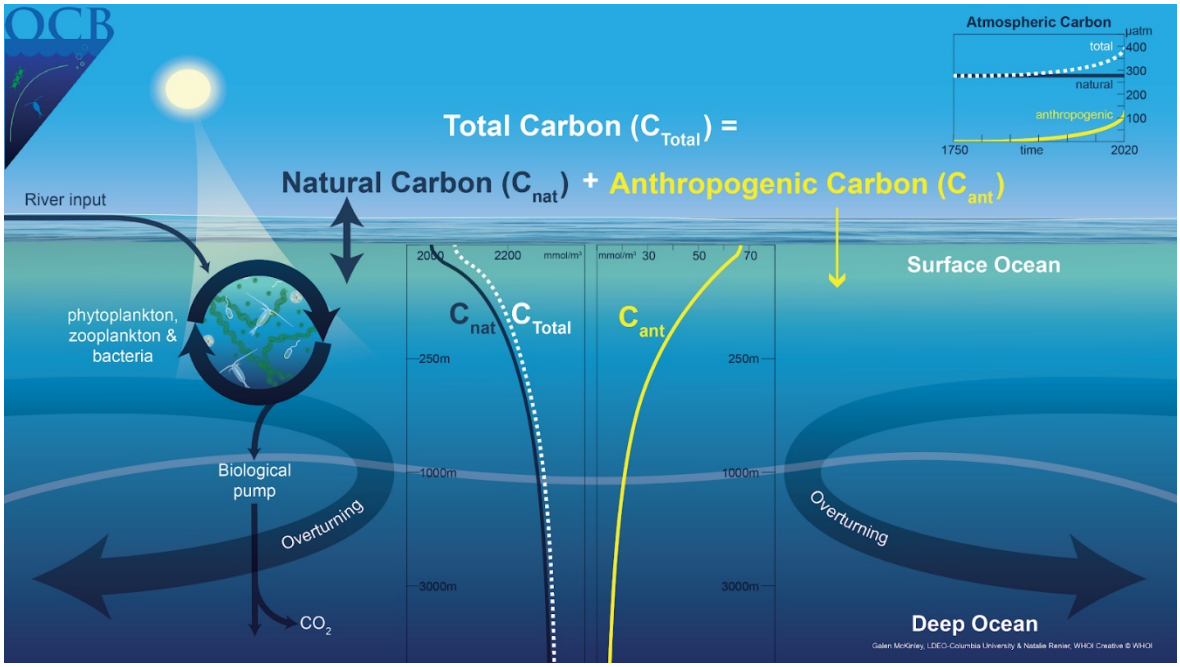

Figure 6. The total carbon cycle in the ocean (C_{Total}) is the sum of the natural carbon cycle (C_{nat}) and the anthropogenic carbon cycle (C_{ant}). The natural carbon cycle is quantitatively dominant, as shown in the observed data (GLODAPv2, Olsen et al., 2016) plotted in the center, and includes contributions from biological activity and the large-scale circulation of the ocean. Overlain is the uptake of additional carbon due to anthropogenic emissions to the atmosphere that occurs in the present ocean as atmospheric pCO_2 continues to rise. The air-sea flux associated with C_{Total} is F_{net} (see text).

The ocean carbon budget can be quantified as the storage of inorganic and organic carbon in the ocean, the fluxes of carbon across the air-sea interface, river input, and a small term for sedimentation. The natural carbon inventory is very large compared to the anthropogenic component and is believed to have been near a long-term steady state in preindustrial times, such that there was zero net flux to the global ocean of natural carbon (F_{nat}), i.e. there was a balance between riverine input, sedimentation rates and air-sea flux. The anthropogenic uptake flux (F_{ant}) is the additional ocean uptake due to the direct effect of increasing atmospheric CO_2 mixing ratio and occurs as a perturbation to the vigorous natural cycle (Figure 6, right), with the column inventory of anthropogenic carbon (C_{ant}) from the latest data-based estimates mapped in Figure 7 (bottom).

The increase in natural carbon (C_{nat}) from surface to depth (Figure 6) is largely due to the biological carbon pump (BCP) (Sarmiento and Gruber, 2006). If the BCP did not operate, the atmospheric CO_2 mixing ratio would be around 200 ppm higher (Maier-Reimer et al., 1996). During the last glacial maximum, changes in the efficiency of the BCP may have played an important role in lowering atmospheric CO_2 (Galbraith and Skinner, 2020; Sigman et al., 2010). Biological feedbacks may accompany anthropogenic climate change (Sabine & Tanhua, 2010, Hauck et al., 2015, Moore et al., 2018), but there is significant spread in model projections (Laufkötter et al., 2015, 2016; Frölicher et al., 2016). To date, observed time-series are too short to provide evidence for long-term biologically-driven trends in the ocean carbon cycle (Henson et al., 2016). Thus, the ocean carbon sink for anthropogenic carbon over the industrial era is currently understood as a physical and chemical process. In Figure 6, the contemporary (or 'net') air-sea CO_2 flux (F_{net}) is the sum of F_{nat} and F_{ant}. C_{Total} is the carbon concentration corresponding to F_{net}. Global maps of pCO_2, the CO_2 flux and the interior ocean inventory of anthropogenic carbon (C_{ant}) are shown in Figure 7.

The ocean surface layer carbon content equilibrates with the atmosphere on time-scales of months. The ocean continually removes C_{ant} from the atmosphere because the ocean circulation transports C_{ant}-laden waters away from the surface layer and into the ocean interior, while the water that returns to the surface tends to have low C_{ant} content. Thus, the ocean circulation is essential to continued CO_2 uptake. At the global scale, the ocean mixes from surface to depth relatively slowly, on timescales of 1000 years. Thus, 75% of all anthropogenic carbon attributable to the industrial age remains in the upper 1000 m (Gruber et al., 2019a). Because carbon is highly soluble and exists as DIC in ocean water, the fundamental limit on the rate of anthropogenic carbon uptake by the ocean is the rate of exchange between surface and the deep ocean across the mixed layer depth and, ultimately, the large scale overturning circulation; these processes determine how fast intermediate and deep waters with C_{ant} uptake capacity are exposed to the surface.

Since the beginning of the industrial era, the ocean has been the primary cumulative C_{ant} sink (Friedlingstein et al., 2019; 2020), although there are large regional differences in the magnitude, and sign of the flux (Figure 7, middle panel). Looking forward, the behavior of the ocean carbon sink is expected to continue playing a critical role in determining how much anthropogenic carbon remains in the atmosphere (Randerson et al., 2015, Zickfeld et al., 2016, Schwinger and Tjiputra, 2018, Ridge and McKinley, 2021).

664 The following sections describe the approaches used to study the ocean carbon sink. A
665 mechanistic understanding of this sink is essential for diagnosing its state and for making reliable
666 future predictions. This requires quantification of air-sea fluxes at higher spatial and temporal
667 resolution than is available from interior data alone. Air-sea fluxes on monthly to decadal
668 timescales are quantified using surface ocean observations and ocean models of varying

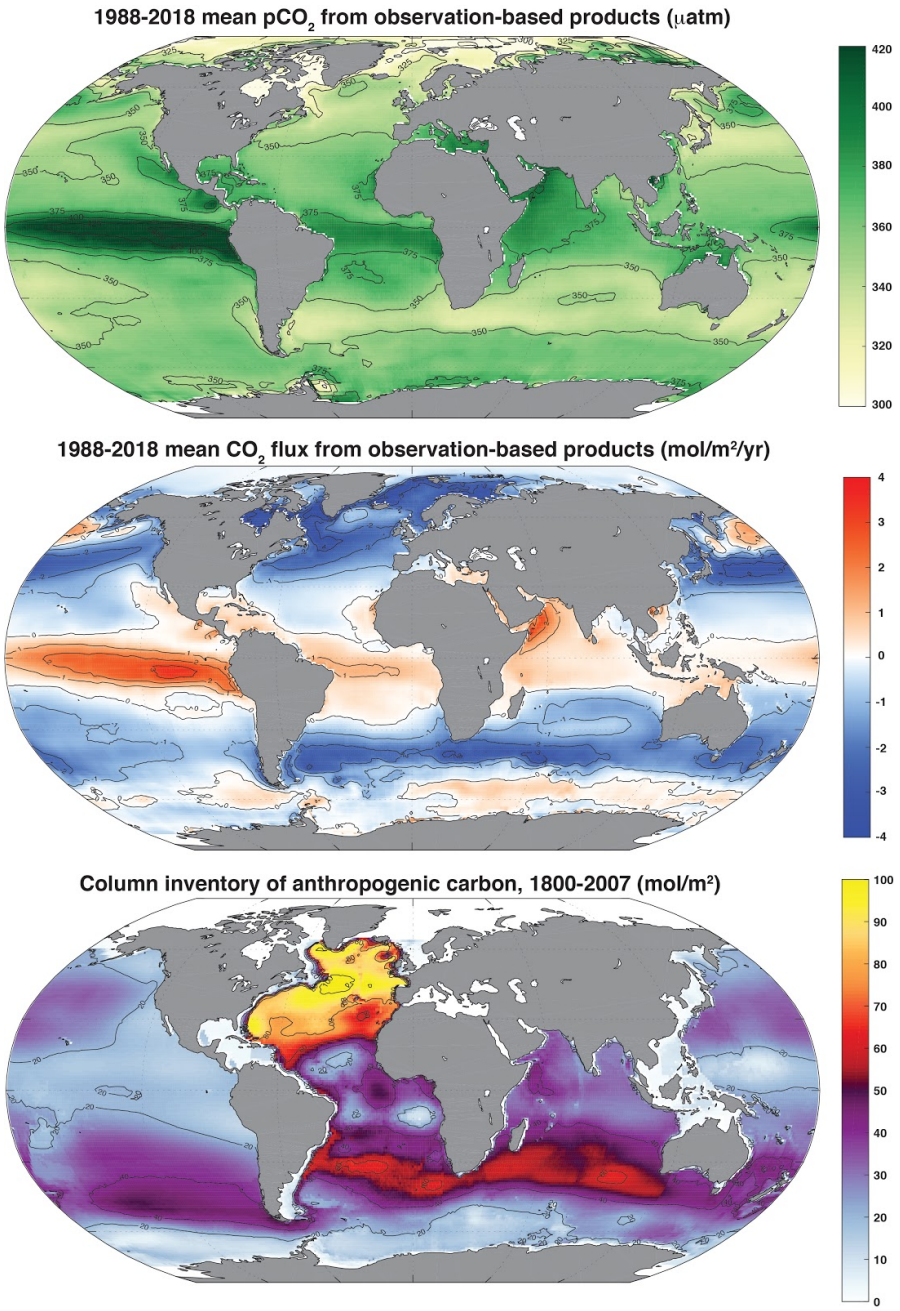

Figure 7. Surface ocean pCO_2 (top); and air-sea CO_2 flux (F_{net}), positive flux to the atmosphere (middle), 1988-2018, mean of 6 observation-based products (Fay et al., 2021); column inventory of anthropogenic carbon (C_{ant}, bottom), 1800-2007 (Sabine et al., 2004, Gruber et al., 2019a).

669 complexity. Agreement between independent estimates for mean fluxes and temporal variability
670 indicates growing confidence in global-scale mechanistic understanding. Yet, uncertainties
671 remain and must be resolved to support better predictions for future ocean carbon sink and to
672 allow for reduced diagnostic uncertainty for the global carbon cycle as it evolves. Substantial
673 advances in observing systems, quantification of land-to-ocean fluxes of carbon, and models of
674 ocean circulation and biogeochemistry are needed to reduce these uncertainties. In addition, as
675 nations implement substantial reductions in carbon emissions, the near-term response of the
676 ocean carbon sink to reduced atmospheric CO_2 growth rates must be accurately diagnosed and
677 mechanistically explained.

678 ### *4.1 Bottom-up Estimates of Anthropogenic Carbon Accumulation in the Ocean from*
679 ### *Interior Observations*

680 Based on a bottom-up accounting method using interior ocean data, Gruber et al. (2019a)
681 find a total ocean C_{ant} accumulation of 152 ± 20 Pg C for the industrial era through 2007. By
682 combining evidence from top-down and bottom-up approaches, Khatiwala et al. (2013) find an
683 inventory of 160 ± 26 Pg C in 2010. Consistent with previous inventories (Sabine et al., 2004),
684 these studies find that the ocean has cumulatively absorbed excess carbon equivalent to 45% of
685 industrial-era fossil fuel emissions until 2010, or 30% of total anthropogenic emissions,
686 including land use change. The column inventory of ocean C_{ant} accumulation from Sabine et al.
687 (2004) and Gruber et al. (2019a) is shown in Figure 7 (bottom).

688 The amount of C_{ant} estimated for 2010 (160 ± 26 Pg C) represents only about ~0.4% of
689 the ocean carbon stock, indicating the significant challenge of directly observing the temporal
690 change in carbon stock over time. Direct measurements are only possible in areas with rapid
691 change in dissolved inorganic carbon (DIC; e.g. Tanhua and Keeling, 2012). Instead, it is more
692 practical to infer ocean storage of C_{ant} against the large natural background, and then to calculate
693 the change in storage over time. A few different methods have been used to estimate the storage
694 of C_{ant}, either based on observations of biogeochemistry variables, or by transient tracers (see
695 Sabine and Tanhua (2010) for a review).

696 On a global scale, different methods converge within the uncertainties, but significant
697 differences persist regionally (e.g. Waugh et al., 2006, Khatiwala et al., 2009). Multivariate
698 techniques (e.g. Friis et al., 2005, Clement and Gruber, 2018) can be used to disentangle
699 variability and calculate decadal-scale trends. A global estimate of the storage of anthropogenic
700 carbon finds an increase of 34 ± 4 Pg C between 1994 and 2007 (Gruber et al., 2019a), indicating
701 a mean F_{ant} uptake of -2.6 ± 0.3 Pg C (negative flux into the ocean) annually over this time
702 frame. This relatively accurate (~12%) estimate provides an important benchmark for the ocean's
703 role in sequestering anthropogenic carbon, and acts as a direct constraint on the net magnitude of
704 the land flux given low uncertainty on fossil fuel emissions and atmospheric carbon
705 accumulation. The magnitude of the uptake implies that the ocean is continuing to take up
706 anthropogenic carbon at a rate proportional to anthropogenic carbon emissions.

707 Critical elements to the success of global estimates of anthropogenic carbon stocks and
708 changes in carbon storage are ship-based hydrographic sampling that collects carbon-relevant
709 interior ocean (Sloyan et al., 2019) and GLODAP data products (Key et al., 2004; Olsen et al.,
710 2020), which collates these interior data into a product after extensive quality control (Tanhua et
711 al., 2010). These data are required to quantify small changes over a large background. This data

product is now being released on an annual basis and the GLODAPv2.2020 version contains data from over 1.2 million water samples collected during 946 cruises (Lauvset et al., 2021).

4.2 Bottom-up Estimates of Ocean-Atmosphere CO_2 Fluxes from Observations of Surface Ocean pCO_2

In order to understand the ocean carbon sink on annual to interannual timescales relevant to climate change policy, more frequent estimates of the sink are required than those produced from decadal timescale interior ocean observations. These data come from observations of pCO_2, and are used to estimate net air-sea CO_2 fluxes (F_{net}). The reported variable is surface ocean fugacity of CO_2 (fCO_2) which equals the partial pressure of CO_2 corrected for the non-ideal behavior of the gas (Pfeil et al., 2013). The fugacity of CO_2 is 0.3-0.4% smaller than the partial pressure of CO_2 (Zeebe and Wolf-Gladrow, 2001). However, the air-sea gradient, ΔpCO_2 or ΔfCO_2, are essentially the same as the correction of the non-ideal gas behavior applies to both the ocean and atmospheric CO_2. For simplicity, we use the terminology pCO_2 to refer to these data for the remainder of this paper. Over the past decade, the number of publicly available observations of pCO_2 has increased rapidly from 6 million in the first release of the Surface Ocean CO_2 Atlas (SOCAT) database (Pfeil et al., 2013, Bakker et al., 2014; 2016; 2020) in 2011 to 28 million in 2020 (www.socat.info). These observations and their automated organization into a consistent database have enabled scientists to create a variety of new observationally-based estimates of the ocean carbon sink that use co-located data from satellite (sea surface temperature, height, and chlorophyll) or from climatologies of in situ data (sea surface salinity and mixed layer depth) to drive upper ocean extrapolation techniques and machine-learning algorithms so as to fill the observational gaps (Rödenbeck et al., 2014; 2015, Landschützer et al., 2013; 2014; 2020; Denvil-Sommer et al., 2019, Gregor et al., 2019).

As the SOCAT database provides pCO_2 data for only ~2% of all months and 1° x 1° locations across the surface ocean from 1982 to present, extrapolation to create monthly full-coverage fields is quite significant. Nonetheless, comparisons of the extrapolated, observationally-based products to independent data indicate relatively low bias and convergence of the independent estimates (Gregor et al., 2019). Root mean square errors (RMSE) range from 10 to 35 µatm. The fact that bias and RMSE comparisons are largely consistent across the variety of approaches suggests that it is data sparsity rather than extrapolation methodology that is now a fundamental limitation on further error reduction (Gregor et al., 2019). Additional tests of the machine-learning based extrapolation approaches using an Earth System Model testbed indicate that the techniques are able to reconstruct from sparse data with low bias and show skill for the amplitude and timing of seasonality across the global ocean. However, higher and lower frequency variations are more poorly represented because of inadequate sampling on these timescales (Gloege et al., 2021, Stamell et al., 2021). Several challenges remain in using these data, including the uneven distribution of data over time, methodological differences in the calculation of air-sea flux from pCO_2 (Fay et al., 2021, Woolf et al., 2019, Zavarsky and Marandino, 2019), and the potential need for adjustments to pCO_2 data to account for near-surface temperature and salinity gradients (Watson et al., 2020).

Despite the significant extrapolation and remaining uncertainties, it is a major advance for ocean carbon cycle science to have spatially-resolved, data-based estimates of air-sea CO_2 fluxes on monthly timescales. This allows for new investigation into the magnitudes and mechanisms of interannual and decadal variability in the ocean carbon sink, and a key point of

comparison to ocean models that were previously the only basis for this analysis. Models are discussed in the next section, and results are compared in the following.

4.3 Bottom-Up Estimates of Ocean-Atmosphere CO_2 Fluxes from Ocean Models

Global ocean biogeochemical hindcast models estimate interior ocean carbon cycling and, from this, air-sea CO_2 fluxes. Models simulate the carbon distribution in the ocean due to the influences of currents, water mass formation and mixing, and biological processes. The bottleneck for ocean carbon uptake in the models, as in the real world, is the carbon transport across the mixed layer depth and its redistribution to greater depths via the overturning circulation. As a result, the models' carbon uptake is sensitive to simulated physics (Doney et al., 2004; Goris et al., 2018; Huber and Zanna, 2017). Models can also provide air-sea flux estimates prior to the 1990s when surface pCO_2 observations were rare.

Models are routinely evaluated against observations or observation-derived estimates that characterize the physical and biogeochemical state of the ocean for the last several decades (Doney et al., 2004; Schourup-Kristensen et al., 2014; Aumont et al., 2015; Schwinger et al., 2016; Stock et al., 2020; Séférian et al., 2020; Fay and McKinley, 2021). For the suite of models used in the GCP, comparison of pCO_2 at locations observed by SOCAT reveals the models' ability to capture variability and trends on annual (RMSE <10 μatm) and decadal timescales (RMSE <10 μatm). However, large model-data mismatches on the seasonal timescale also exist (RMSE of 20–80 μatm; Hauck et al., 2020).

Despite the overall concurrence with pCO_2 observations on annual and decadal timescales, modelled ocean carbon sink estimates fall into two distinct groups. Furthermore, models and data-based estimates have started to diverge from each other since around 2002, particularly in the Southern Ocean (Hauck et al., 2020), reinforcing the need for evaluation of models in addition to that of data-products (section 4.2). As one way forward, Fay and McKinley (2021) evaluate the spatial distribution of modelled mean fluxes against an ensemble of these products adjusted by lateral fluxes from rivers, $F_{nat,riv}$. They find that few models fall within 3 standard deviations of the product spread for each of five large regions that together cover the globe. The regional differences are to a large extent governed by the natural carbon fluxes and this metric therefore identifies models with the balance between physical and biological processes that is most consistent with observations.

Another approach evaluates models using the global anthropogenic carbon accumulation, thus assessing the global balance between atmospheric pCO_2 growth and global surface-to-deep ventilation instead of regional processes. Using simulations mimicking the anthropogenic carbon accumulation ($F_{ant,ss}$), Friedlingstein et al. (2021) compare the simulated ocean interior anthropogenic DIC inventory for 1994-2007 to the estimate of Gruber et al. (2019a). This reveals an underestimation of anthropogenic carbon uptake by the majority of the models on the order of 20% for the ensemble average. However, uncertainties on the interior estimates are also significant, and other interior estimates are lower for 1994-2007 by about 10% (DeVries, 2014). More models might fall within the constraint if both interior estimates were considered. Nonetheless, atmospheric inversions that take advantage of the constraint provided by the atmospheric CO_2 observation network also suggest that some models have too low a sink (Friedlingstein et al., 2021). This conclusion is further supported by a recent estimate of the ocean sink from observed O_2/N_2 (Tohjima et al., 2019) and the models' low 1990s estimate compared to the best estimate from different methodologies (Denman et al., 2007).

These are first efforts to exploit an array of observations to quantitatively assess regional and seasonal air-sea flux patterns in models, going beyond the typical discussion of spatial bias patterns (e.g. Séférian et al., 2020). A larger array of targeted metrics including seasonal cycles, trends and the interior ocean carbon inventory needs to be developed. Model development priorities include efforts to improve the regional and sub-regional distribution of mean fluxes and temporal variability from the seasonal cycle to the multi-decadal trend.

Global ocean biogeochemical models were the sole basis for quantifying the ocean sink in the GCB until 2020 (section 3). For example, for 2019, the GCB finds that the ocean sink accounted for 22% of 2019 anthropogenic CO_2 emissions (Friedlingstein et al., 2020). Models have also shed light on processes behind observed variability such as the weakening of the Southern Ocean carbon sink in response to increased westerlies (LeQuéré et al., 2007), and to explore the role of stationary Rossby waves in subduction of anthropogenic carbon (Langlais et al., 2017). As a component of Earth System Models, ocean models are the single tool for future projections. In the future, the rate of the ocean carbon sink will be largely determined by anthropogenic emissions, but ocean chemistry and physics will also play a significant role. On timescales from decadal to centennial, models project a decreased rate of the ocean carbon sink relative to the atmospheric pCO_2 concentration due to the fact that most of anthropogenic carbon already absorbed is in the near-surface ocean, and reduced buffer capacity (Schwinger et al., 2014, Randerson et al., 2015, Zickfeld et al., 2016, Schwinger and Tjiputra, 2018, Ridge and McKinley 2021).

4.4 Reconciling Air-Sea Flux Estimates from Different Methods

We must accurately quantify the ocean sink and understand its underlying mechanisms to diagnose its ongoing evolution and improve projections of future change. The best measure of our current understanding is the degree to which the above-mentioned independent estimates of the present-day sink's magnitude agree. We discuss the degree of agreement in this section, where a negative flux refers to a flux from atmosphere to ocean, and we discuss mechanistic understanding in the next section.

Surface ocean carbon observations indicate the net air-sea flux of carbon into the ocean (implicitly including riverine outgassing), F_{net} ~ -1.6 Pg C yr^{-1}, while analysis of interior measurements yields estimates of the anthropogenic uptake and storage, F_{ant} ~ -2.6 Pg C yr^{-1}, over the period, 1994 to 2007. Dynamic hindcast models used in the GCB, typically estimate the total of anthropogenic perturbations, that is the sum of anthropogenic uptake (F_{ant}) and anthropogenic climate change induced natural carbon fluxes ($F_{nat, ns}$). Closure terms of significant net magnitude (~1 Pg C yr^{-1}) are required to bridge the gap between F_{net} and F_{ant}.

To reconcile flux estimates from pCO_2-based data products with ocean models and estimates from interior data, an adjustment due to the riverine input of natural carbon that outgasses from the ocean ($F_{nat,riv}$) must be applied (Sarmiento and Sundquist, 1992; Aumont et al., 2001; Lacroix et al., 2020). This adjustment is needed because these fluxes are not included in ocean models, but exist in the real world. Unfortunately, high quality direct estimates of $F_{nat,riv}$ do not exist, so the closure between surface flux estimates of F_{net} and F_{ant} remains a significant uncertainty. Lacking better evidence, values typically used are between 0.45 and 0.78 Pg C yr^{-1} (Jacobson et al., 2007, Resplandy et al., 2018), with large uncertainties. Recent work using stable carbon isotopes suggest an even larger efflux of 1.2 Pg C yr^{-1} to the atmosphere from coastal margin inputs, also considering submarine groundwater discharge (Kwon et al., 2021).

Anthropogenic changes to the riverine input of carbon are an additional closure term not usually considered with no temporally-resolved estimates available and one estimate for 2000-2010 suggesting it to be small (0.1 Pg C yr^{-1}, Regnier et al., 2013; Bauer et al., 2013). No estimates on anthropogenic changes to the outgassing of the riverine carbon in the ocean are yet available.

Le Quéré et al., (2010) and Gruber et al. (2019a) propose that climate change is having an effect on the natural carbon cycle fluxes ($F_{nat,ns}$), although the magnitude of this non-steady state component is still uncertain. The first estimates of $F_{nat,ns}$ came from one model for the period 1981-2007 (Le Quéré et al., 2010) and from a back-of-the-envelope calculation for the period 1994-2007 (Gruber et al., 2019a), suggesting a reduction of F_{ant} by 10 to 15%. Gruber et al. (2019a) estimate $F_{nat,\,ns}$ by assuming that the accumulation of anthropogenic carbon in the ocean follows a linear scaling with the atmospheric load. However, this assumption is known to hold only when the atmospheric growth is strictly exponential, which has not been the case (Raupach et al., 2014, Ridge and McKinley, 2021), and thus the resulting estimate of +0.38 Pg C yr^{-1} is likely an upper-bound. Another approach for estimating $F_{nat,\,ns}$ is to use ocean models that represent the natural carbon cycle, and to make a reasonable assumption that the total carbon cycle response to climate variability is dominated by the natural component. With this assumption, models indicate for 1994-2007, $F_{nat,\,ns}$ = +0.06 to +0.31 Pg C yr^{-1} (DeVries et al., 2019; McKinley et al., 2020) and for the recent decade, 2011-2020, $F_{nat,\,ns}$ = +0.12±0.07 Pg C yr^{-1}, equivalent to a 5% reduction of the ocean sink due to climate change (Friedlingstein et al., 2021). Better quantification of this term is clearly needed as well as a mechanistic understanding of the processes at play. Le Quéré et al. (2010) identified wind and temperature changes to be the dominant drivers behind this response, but the degree to which this is model dependent has not yet been investigated.

Estimates of the magnitude of the ocean sink relative to emissions vary between 23% and 48% in the literature (Friedlingstein et al., 2020; Khatiwala et al., 2013; Sabine et al., 2004). These seemingly contradicting numbers result from differences in the way the ocean sink is compared to different components of the emissions (Table 2). Quantitatively, the most important choice is the denominator used. For studies of the interior ocean cumulative ocean sink, the denominator typically used is the anthropogenic fossil emissions, resulting in an ocean sink of 44% for the industrial era through 2010 (Khatiwala et al., 2013), and 48% for the industrial era through 1994 (Sabine et al., 2004). GCB estimates, however, compare the ocean sink to total anthropogenic CO_2 emissions, which also include emissions to the atmosphere from land-use change. Over the industrial era, GCB estimates that the ocean has absorbed 171 Pg C, while the cumulative fossil fuel emission is 446 Pg C and LUC is 238 Pg C. The ocean has thus absorbed 38% of the cumulative fossil fuel emissions, or 25% of the total anthropogenic emissions. For the period 2010-2019, GCB estimates a smaller percentage for the ocean sink, 23% of total anthropogenic emissions (Friedlingstein et al., 2020). A second difference between the estimates is that the GCB's approach also includes climate perturbation effects ($F_{nat,ns} + F_{ant,ns}$), which reduces the magnitude of the ocean sink. Table 2 further illustrates the role of the chosen time-period in the various estimates with general agreement between GCB and interior ocean estimates when considering the spread in emission numbers used. For estimates stretching back to 1800 or before, the time-series extending to more recent years have a smaller proportion of the ocean sink relative to the fossil-fuel emissions, whereas the ratio relative to total emissions is more stable.

Table 2. Comparison of estimates of the relative magnitude of the ocean sink to emissions, ordered from shortest times-series to longest. GCB numbers are taken from Friedlingstein et al (2021). GCB fossil fuel emissions include the cement carbonation sink. GCB land-use change emissions are taken from annual time-series, plus 30 Pg C yr^{-1} for the period 1750-1850 (Friedlingstein et al., 2021), and half of that number for the period 1800-1850. The same uncertainties are used for GCB estimates recomputed for 1750-2010 and 1800-1994 as for 1750-2020.

Source of Estimate	Time range	Cumulative fossil emissions (Pg C)	Cumulative land-use change emissions (Pg C)	Cumulative ocean sink (Pg C)	Ocean sink relative to fossil emissions	Ocean sink relative to total anthropogenic emissions
GCB (Friedlingstein et al., 2021)	2011-2020	95 ± 5	11 ± 7	28 ± 4	29%	26%
Sabine et al. (2004)	1800-1994	244 ± 20	100-180	118 ± 19	48%	28-34%
GCB	1800-1994	245 ± 25	185 ± 75	114 ± 35	47%	27%
Khatiwala et al. (2013)	1750-2010	~350	180 ± 50	155 ± 30	44%	29%
GCB	1750-2010	363 ± 25	220 ± 75	151 ± 35	42%	26%
GCB	1750-2020	458 ± 25	232 ± 75	179 ± 35	39%	26%

The choice to compare studies of interior ocean accumulation to fossil fuel emissions is motivated by the fact that these numbers are cumulative over the industrial era, and over this time, the land use source and land sink have been in approximate balance. Thus, this approach circumvents the large uncertainties associated with separate estimates of land-use change emissions and the land sink. The GCB's approach, on the other hand, acknowledges that fossil fuel and land-use change emissions add to the total atmospheric CO_2 mixing ratio, and that ocean and land carbon sinks respond to this increasing total. This is reinforced by the more stable ratio of the ocean carbon sink relative to total CO_2 emissions rather than the contribution from fossil fuel emissions, alone (Table 2).

4.5 Recent Evidence for Decadal Variability of the Ocean Carbon Sink

In the mid-2000s, studies using ocean hindcast models suggested a slowing of the ocean carbon sink from the mid-1990s and attributed this change to processes in the Southern Ocean (Lovenduski et al., 2007; 2008; Le Quéré et al., 2007). In the following decade, the release of both the LDEO pCO_2 database (Takahashi et al., 2009) and the development of the international SOCAT database (Pfeil et al., 2013; Bakker et al., 2014; 2016; 2020) allowed for new analyses

of trends in air-sea CO_2 fluxes directly from observations (Le Quéré et al., 2009; McKinley et al., 2011; Fay and McKinley, 2013; Xue et al., 2018). Additionally, a variety of extrapolations of these data to global monthly coverage were developed (Rödenbeck et al., 2015), and a recovery of the ocean carbon sink following the low near the year 2000 was noted (Fay and McKinley, 2013; Landschützer et al., 2015; DeVries et al., 2017; Gruber et al., 2019b).

The Southern Ocean was generally identified as a significant regional driver of these mid-1990s to mid-2000s trends. A number of studies agreed that the stagnation of the Southern Ocean carbon sink in the 90s was related to a trend towards a more positive Southern Annular Mode (SAM) index associated with stronger westerly winds leading to more upwelling of natural carbon and hence dampened net air-to sea CO_2 flux (Le Quéré et al., 2007; Lovenduski et al., 2007; Lenton and Matear, 2007; Hauck et al., 2013).

Increasing nutrient concentrations in surface waters of all sectors of the Southern Ocean support a strengthened upwelling during the late 1990s (Iida et al., 2013; Ayers and Strutton, 2013; Hoppema et al., 2015; Pardo et al., 2017; Panassa et al., 2018). However, the same driving mechanisms cannot explain the reinvigoration of the sink in the 2000s, as the trends towards a more positive SAM and stronger winds in the 2000s continued. Asymmetric changes in atmospheric circulation (Landschützer et al., 2015), a weaker upper ocean overturning circulation (DeVries et al., 2017) and regional wind variability (Keppler and Landschützer, 2019) were proposed as possible explanations, but no consensus was reached on the driving mechanisms of the reinvigoration. Several studies concluded that ocean models were substantially underestimating the magnitude of decadal variability in the ocean carbon sink (De Vries et al., 2019; Gruber et al., 2019b).

In the last few years, more observation-based estimates have become available (Denvil-Sommer et al., 2019, Gregor et al., 2019), and now the size of the ensemble of observation-based estimates and of hindcast models is more comparable. With similar size ensembles for both observation-based and hindcast models, estimates of decadal variability are more similar in magnitude and phase, and not as large as the initial observation-based products had suggested (McKinley et al., 2020; Hauck et al., 2020). Both the ensemble of hindcast models and observation-based products indicate a larger ocean carbon sink in the early 1990s, then a slowing of the sink through about 2000, and then a strong and steady recovery through 2018 (Figure 8). In both the products and models, flux variability is largely homogenous across the globe outside the equatorial Pacific (McKinley et al., 2020).

By representing the surface ocean as a single abiotic box that exchanges water with the deep ocean at a constant rate, McKinley et al. (2020) are able to reproduce the variability of the ocean carbon sink with two external forcings (Figure 8). The two external forcings are the observed atmospheric pCO_2 and the forced change in upper ocean temperature due to the eruptions of large volcanoes (El Chichon, 1982; Mt Pinatubo, 1991). This result emerges because the globally-averaged air to sea pCO_2 gradient - the fundamental driver of the flux - is only 6-10 µatm, and thus anomalies in the atmospheric growth rate of a few µatm over several years can rapidly modify the global air-sea gradient. Large volcanic eruptions, such as Mt Pinatubo in 1991, cause a rapid surface ocean cooling, which increases solubility and creates an uptake pulse (Church et al., 2005; Eddebbar et al., 2019). Then, as the ocean warms from this rapid cooling, solubility is lowered, and there is excess DIC in the upper ocean relative to what would have occurred without the eruption. These two effects contribute to a reduced growth rate of the sink for 5-7 years beyond the eruption (Figure 8).

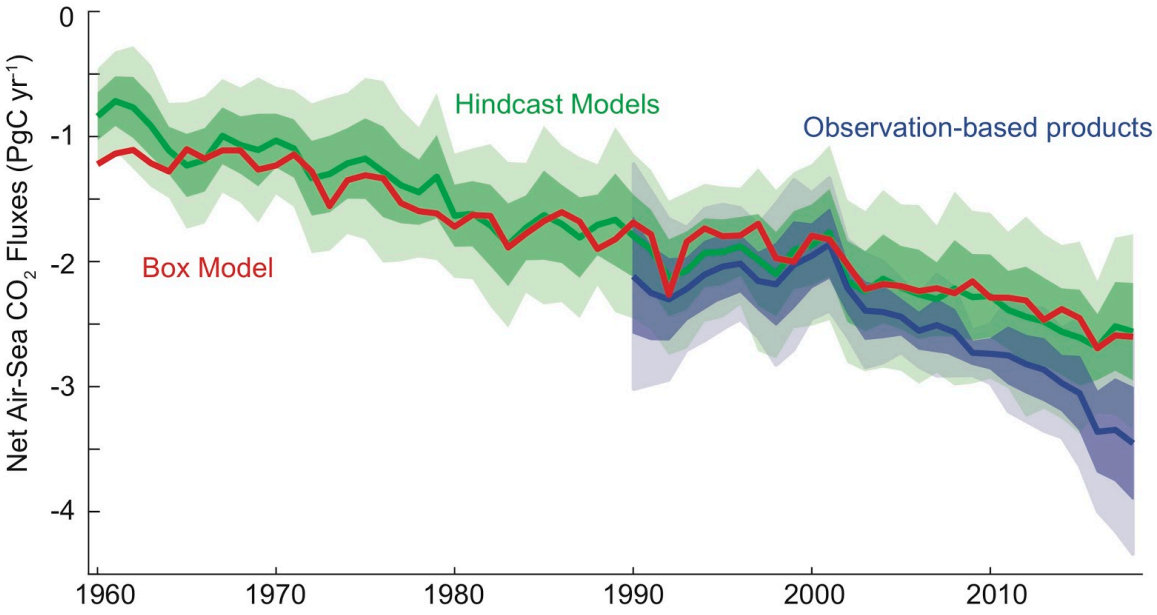

Figure 8. Air-sea CO_2 flux of carbon (F_{ant} + $F_{nat,ns}$) from observationally-based products (blue), hindcast models (green) and upper ocean diagnostic box model (red); negative flux into the ocean. Global ensemble means (bold), with 1 sigma and 2 sigma of individual members (shading). Hindcast ocean models from Global Carbon Budget 2020 (Friedlingstein et al., 2020). Observationally-based product pCO_2 fields have missing ocean areas filled with a full-coverage climatology (Landschützer et al., 2020) and air-sea flux calculated as average of 3 wind reanalyses (CCMP, ERA5, JRA55) with a quadratic parameterization (Wanninkhof 2014, Fay et al., 2021); to this F_{net} estimate, $F_{nat,riv}$ = 0.62 Pg C yr^{-1} (Jacobson et al., 2007, Resplandy et al., 2018) is added. The upper ocean diagnostic box model (McKinley et al., 2020) is forced with observed atmospheric pCO_2 and surface ocean temperature changes forced by the eruptions of three large volcanoes of this period (Agung 1963, El Chichon 1982, and Mt. Pinatubo 1991; Eddebbar et al., 2019).

This model of McKinley et al. (2020) is simple, considering a global surface ocean of 200 m depth that is uniformly impacted by atmospheric pCO_2 and upper ocean heat content anomalies forced by large volcanos. Yet, it can reproduce the ocean carbon uptake that occurs in the ensemble mean of much more complex models and observation-based products. What does this mean? It can be interpreted simply as Henry's Law operating at the global scale, wherein the partial pressure in the water is moving toward equilibration with the partial pressure in the air. Since the atmospheric pCO_2 continues to increase, the ocean continues to adjust toward equilibrium. McKinley et al. (2020) demonstrate that the ocean carbon sink temporal variability today is likely dominated by the external forcing from slight variations in the atmospheric pCO_2 growth rate. This perspective is consistent with recent analysis that shows heat uptake and interior redistribution in the ocean is far more sensitive to the details of the ocean circulation than is the pattern and magnitude of carbon uptake and storage (Bronselaer and Zanna, 2020). Ultimately, the mechanisms driving interannual to decadal timescale variability remains a topic of debate, and the focus of a significant research effort by the ocean carbon cycle community.

965 Observation-based products and hindcast models differ in the strength of sink increase
966 since around 2002 (Figure 8). The growth rate of the ocean sink since 2010 is uncertain by a
967 factor of three. Observation-based products indicate that the sink has increased by 0.9 Pg C yr^{-1}
968 between 2010 and 2020 whereas models only simulate an increase of 0.3 Pg C yr^{-1}
969 (Friedlingstein et al. 2021). This discrepancy is unresolved despite its importance for the near-
970 term predictions of the remaining carbon budget and climate targets. Observation-based products
971 may overestimate decadal variability of the ocean sink, consistent with too large a trend for these
972 years (Gloege et al., 2021). Watson et al (2020) evidenced that the uncertainty of the sink
973 estimate is generally a factor two higher at both ends of the time-series, independent of temporal
974 and spatial data coverage, making the trend over the final one to two decades more uncertain.

975 Some models, however, underestimate the accumulation of anthropogenic carbon in the
976 ocean interior for 1994-2007 (section 4.3; Friedlingstein et al., 2021), although the rate used as
977 the basis for comparison (Gruber et al., 2019a) is on the high end of existing estimates (DeVries,
978 2014). If one assumes a steady state rate of anthropogenic carbon accumulation, an
979 underestimated mean uptake rate for 1994-2007 would also imply an underestimated mean rate
980 for 2002 to present. One possible explanation for this is that too little carbon is transported out of
981 the mixed layer, which leads to a too strong increase in the buffer factor and hence to a reduction
982 of ocean carbon uptake. Analysis of CMIP5 models in the Atlantic reveals that models that better
983 represent current interior carbon storage have larger present-day and future carbon uptake (Goris
984 et al., 2018). Biases in simulated ocean ventilation were identified as one process that affects
985 ocean heat uptake (Bonselaer and Zanna, 2020) and to be the dominant cause of underestimated
986 historical trends in modeled ocean oxygen decrease (Buchanan and Tagliabue, 2021). If ocean
987 ventilation is too slow, models should underestimate the rate of the ocean carbon sink, and
988 potentially also the sink's rate of change. At the same time, it is also possible that variability in
989 the ocean ventilation (DeVries et al., 2017) somewhat decouples the 1994-2007 rate of
990 anthropogenic accumulation and ocean sink trends since 2002.

991 ### *4.6 Advancing Understanding of the Current and Future Ocean Carbon Sink*

992 To quantify the global carbon cycle, the constraint provided by the relatively low-
993 uncertainty estimates for decadal anthropogenic carbon accumulation must be maintained. To
994 better quantify fluxes on monthly to decadal timescales, increased observations of surface pCO_2
995 and higher fidelity models are needed. In order to be prepared to support climate management
996 efforts in the near-term, the likely behavior of the ocean sink under emissions mitigation must
997 receive increased attention.

998 Observations of ocean interior carbon require measurements with high accuracy and
999 precision due to the small perturbations on a large background signal. For example, in 2010, the
1000 C_{ant} content was ~160 Pg C out of a total inorganic carbon content of ~39,000 Pg C. For the
1001 surface ocean flux estimates, the high spatiotemporal variability in pCO_2 and a low average
1002 deviation from air-sea equilibrium concentration needed to drive the observed net flux, i.e. a net
1003 flux of ~2.5 Pg C yr^{-1} over a gross flux of ~90 Pg C yr^{-1}, indicates that accuracy and data
1004 coverage are possibly the most important components of the observing system. There is a
1005 seasonal bias in the observing system, with fewer observations being made in winter at high
1006 latitudes. This is particularly important for observations of surface fluxes, which tend to be high
1007 in winter, but less so for the interior ocean observations where seasonality tends to be low below
1008 the winter mixed layer.

4.6.1 Expanding Autonomous Observations

Although ship-based observations remain a central resource for the carbon observing system, these are expensive and tend to be seasonally biased. Driven by these demands, there is a continuous development of sensors for inorganic carbon system measurements with at least some of these attributes; increased precision and accuracy, lower power consumption and lower instrument drift (Johnson et al., 2016; Sabine et al., 2020; Seelmann et al., 2019; Sutton et al., 2014). Similarly, there is a continuous development of autonomous platforms capable of carrying sensors for ocean carbon. These include moorings (Sutton et al., 2014), profiling floats (e.g. BGC Argo, Claustre et al., 2020), underwater gliders (Rudnick, 2016, Sutton et al., 2021), and autonomous surface vehicles powered by wind or waves (Sabine et al., 2020). These developments are rapidly changing the capability to monitor ocean carbon with higher spatial and temporal resolution. For instance, observations from Biogeochemical (BGC) Argos floats enable the calculation of surface pCO_2 (from pH and alkalinity estimates) with reasonable accuracy and precision, ~11 µatm (Takeshita et al., 2018; Williams et al., 2017). Although not as good as the 2 µatm target for the ship-based observations, this system has shown potential to fill spatiotemporal gaps in the observations, with important implications for the carbon flux estimates. For example, Bushinsky et al. (2019) report on significantly lower uptake of carbon in the Southern Ocean by including winter time pCO_2 from BGC-Argo floats using a neural network interpolation. Uncrewed Surface Vehicles (USVs) directly measure pCO_2 with an uncertainty of 2 µatm, which is comparable to ship-based observations The strong winter outgassing observed by floats in 2015-2016 was not detected by USVs in 2019, illustrating how these novel techniques can progress research on interannual variability (Sutton et al., 2021).

4.6.2 Improving Constraints on Carbonate Chemistry

Although individual components of the ocean carbon observing system have high technical readiness levels, the new capabilities have not yet been integrated with existing, well-tested technologies to provide an observing system that can quantify ocean carbon uptake to within 10%. One critical need is an improved understanding of the ocean inorganic carbonate system. There are four measurable inorganic carbon variables in the ocean - total alkalinity (TA), total dissolved inorganic carbon (DIC), pH and fCO_2. By measuring two out of those, the complete inorganic carbon system can, in theory, be calculated. Small errors in the dissociation constants, the boron-salinity ratio, and small contribution to the total alkalinity from unknown bases, can cause significant discrepancies in directly measured and calculated carbon variables (Fong and Dickson, 2019, Takeshita et al., 2020). A recent study by Álvarez et al. (2020) shows that inconsistencies between calculated and measured pH has decreased during the last decade, and they conclude that improved standard operating procedures for measurements and calculation of pH are urgently needed. An improved understanding of these issues is essential to fully utilize data from, for instance, BGC Argo floats equipped with pH sensors.

4.6.3 Ensuring Quality Control and Timely Data Delivery

As noted above, the anthropogenic perturbation in the global ocean is more than an order of magnitude smaller than the background natural state. Thus, to track the changing anthropogenic carbon uptake by the ocean, very high standards for accuracy and precision of carbon system data must be maintained. New autonomous technologies offer great promise for expanding the observing system, but cannot be incorporated into the observing system if this substantially increases overall uncertainties. For the foreseeable future, ship-based measurements will continue to be required to calibrate and validate autonomous observations. Cross-over

evaluations should occur both with deployment and post-deployment (Fay et al., 2018). At the same time, ocean carbon data must be ingested into public databases or products (e.g. SOCAT, GLODAP) in a timely manner that supports annual diagnoses of the ocean carbon sink. It is essential that these data be carefully quality controlled. As the timescales at which the user community requires these diagnoses become shorter, these data will need to be available more quickly. One key component of this integration into scientific products is certified reference materials (CRMs). CRMs are critical because they allow for consistent observations across independent laboratories, which is essential for the development of high-quality global datasets. Currently, a single laboratory is the source for these materials and a plan for a long-term future source remains unclear (Catherman, 2021).

Similarly, better observational constraints on ocean carbon perturbation can be gained from stable carbon isotope observations. The ocean inorganic carbon pool is lightening due to the uptake of CO_2 originating from the burning of ^{13}C-depleted fossil fuel carbon, a phenomenon also known as oceanic ^{13}C Suess effect. By observing this temporal development, estimates of the anthropogenic carbon fraction of DIC are possible. Recent improvements in observations are making this approach attractive (e.g. Becker et al., 2012, Cheng et al., 2019, Cheng et al., 2021).

4.6.4 Quantifying Closure Terms to Link Estimates of Surface Flux and Interior C_{ant} Accumulation

In order to reduce uncertainties in the global and regional ocean carbon cycle, we need to understand how interior-based estimates of F_{ant} and surface flux estimates of F_{net} are quantitatively linked. An important barrier to this is the significant magnitude and high uncertainty in current estimates for natural fluxes of carbon in rivers ($F_{nat,riv}$) and interannual variability in the natural carbon cycle ($F_{nat,\,ns}$). More observations of these two quantities are needed to improve our understanding and reduce the uncertainties.

4.6.5 Constraining Mechanisms of Surface Flux Variability

Recent work has identified the important role of external forcing from atmospheric pCO_2 and volcanoes in driving ensemble-mean estimates of recent variability of the ocean carbon sink, but individual models and individual observation-based products deviate from the mean of the ensembles (Hauck et al., 2020, McKinley et al., 2020). These deviations are due to different methods for simulating the ocean circulation and biology in each individual ensemble member. We do not yet understand which of these individual estimates best represent the real ocean. To understand the actual total variability of the real ocean carbon sink (total = forced + internal), we need to select the observation-based products and models of highest fidelity. More stringent application of observational constraints (Fay and McKinley, 2021; Friedlingstein et al., 2021) would facilitate weighting of the models for global budgeting, focused analysis of the mechanisms driving variability in the highest-fidelity models and guidance for improving others.

Another approach for combining observations and models is through data-assimilation that constrains the model ocean state and fluxes using observations, and closes data gaps by model dynamics rather than extrapolation. While assimilation applications so far have not provided annually updated global ocean sink estimates with full spatial and temporal resolution (e.g., Mikaloff Fletcher et al., 2006; DeVries, 2014; Verdy and Mazloff, 2017; DeVries et al., 2019), the first spatially and temporally resolved global data-assimilated models are starting to become available (Carroll et al., 2020).

4.6.6 Tracking the Magnitude of Trends in the Ocean Carbon Sink Since 2002

The current divergence of ocean sink trends in observation-based products and models has implications for closure of the global carbon budget and remaining allowable emissions and the feasibility of internationally agreed climate targets. These trends may be methodological or may illustrate a fundamental knowledge gap in how the ocean sink responds to rising atmospheric CO_2 levels and the natural and anthropogenic physical changes occurring in the ocean. There are indications that observation-based products may overestimate decadal timescale trends (Gloege et al., 2021) and also that models may underestimate this trend (Goris et al., 2018) due to biases in ocean ventilation (Bronselaer and Zanna, 2020, Buchanan and Tagliabue, 2021). Understanding this deviation, and fixing potential methodological issues in both approaches is necessary to more accurately track the evolution of the ocean carbon sink.

4.6.7 Quantifying the Impact of Interactions Between the Natural Carbon Cycle and Climate

Climate change induced modifications of the ocean, such as ocean acidification, warming and ecosystem composition could significantly influence the transport of particulate and dissolved organic carbon from the surface to the interior ocean, i.e. the "biological pump". The efficiency of this transport is a key factor regulating the atmospheric CO_2 mixing ratio and is thought to play a role in regulating glacial / deglacial atmospheric CO_2 (e.g. Galbraith and Skinner, 2020). For instance, Marsay et al. (2015) suggest that a warmer ocean might lead to reduced sequestration of CO_2 by the biological pump. Complex interactions in the marine ecosystem will affect carbon export in a changing climate in ways that are difficult to predict and currently inadequately quantified (Laufkötter et al., 2015, 2016, Frölicher et al., 2016). In a recent work Claustre et al. (2021) provide a research framework to improve the understanding of the oceans' biological carbon pump.

4.6.8 Tracking the Future Ocean Sink Under Scenarios of Emission Mitigation

On centennial timescales under high emissions scenarios, slowing of the overturning circulation and reduced buffer capacity will significantly reduce the rate of ocean carbon uptake (Randerson et al., 2015, Ridge and McKinley, 2020; 2021). But how will the ocean sink evolve under the increasingly more likely scenario of substantial emissions mitigation (Hausfather and Peters, 2020)? Given that the long-term growth and interannual variability of the ocean sink observed to date is driven by the exponential growth of atmospheric pCO_2 (Joos et al., 1996, Raupach et al., 2014, McKinley et al., 2020, Ridge and McKinley, 2021), the ocean sink is expected to slow in response to reduced growth rates of atmospheric pCO_2. In effect, the anthropogenic carbon trapped in the near-surface ocean will begin to equilibrate with the atmosphere and the sink will be significantly reduced in response to the mitigation of emissions. This will occur simply due a change in the growth of atmospheric pCO_2 - no change in the ocean circulation or buffer capacity is required (Ridge and McKinley, 2021). Slowing of the ocean sink will further offset the effect of reduced emissions. This will reduce the apparent effectiveness of mitigation actions in limiting climate warming (Jones et al., 2016). Despite a slowed rate of the sink, the largest share of cumulative emissions will be taken up by the ocean and land sink if a low emissions trajectory is followed (IPCC, 2021).

Though a series of idealized studies have established the general fact that the ocean sink will be reduced with mitigation (Joos et al., 1996, Raupach et al., 2014, Zickfeld et al., 2016, Schwinger and Tjiputra, 2018, MacDougall et al., 2020, Ridge and McKinley, 2021), the spatially and temporally resolved response of the ocean sink to emission mitigation has received

1142 little attention. Thus, we do not know how rapidly the ocean sink will slow, nor where surface
1143 flux changes will be most substantial. We do not know what will be required from our
1144 monitoring systems to detect these changes.

1145 Current uncertainties in ocean models suggest that, despite the fact that the current
1146 ensemble of models largely agrees as to the recent evolution of the sink (Figure 8), there may be
1147 substantial divergence in feedback strength and ocean sink response to emission mitigation.
1148 Since the majority of the anthropogenic carbon is held in the ocean's thermocline (Gruber et al.,
1149 2019a), the circulation here is critical to the ocean sink's near-term response to mitigation
1150 (Iudicone et al., 2016; Rodgers et al., 2020; Ridge and McKinley, 2020). There is substantial
1151 spread in the regional distribution of ocean carbon uptake in current models (McKinley et al.,
1152 2016, Hauck et al., 2020; Fay and McKinley 2021), and major differences in representations of
1153 seasonality (Mongwe et al., 2018), which illustrates knowledge gaps with respect to physical and
1154 biological processes and their representations in models. In addition, circulation in these critical
1155 upper-ocean regions is not consistently represented in state-of-the-art models (Bronselaer and
1156 Zanna, 2020). Uncertainties in the response of the ocean sink to emissions mitigation strategies
1157 need to be assessed, and then they need to be reduced by model development efforts and verified
1158 by observations, so that robust projections can be made. Especially in these first decades of
1159 climate management via emission mitigation, there will be great public interest in how emission
1160 cuts are changing atmospheric CO_2. Scientists need to be prepared to explain ocean carbon sink
1161 changes as they occur.

1162 **5 The Terrestrial Carbon Cycle**

1163 The terrestrial carbon cycle is characterized by large, spatially heterogeneous fluxes from
1164 anthropogenic activity and natural processes dominated by biospheric activity at daily, seasonal
1165 through interannual and multidecadal time-scales. Its primary stocks and fluxes are illustrated in
1166 Figure 9 and summarized in Table 3. The largest carbon stocks are held in aboveground biomass
1167 and soils in tropical and high latitude forests, respectively, with total stocks in vegetation and
1168 soils of 450-650 Pg C and 1500-2400 Pg C, respectively (Ciais et al., 2013; Scharlemann et al.,
1169 2014). As noted in Section 3, excluding fossil fuel combustion and other industrial activities
1170 (Section 3), the largest components of the net land-atmosphere CO_2 fluxes are from land-use
1171 change and management and a sink in the terrestrial biosphere (Friedlingstein et al., 2021).

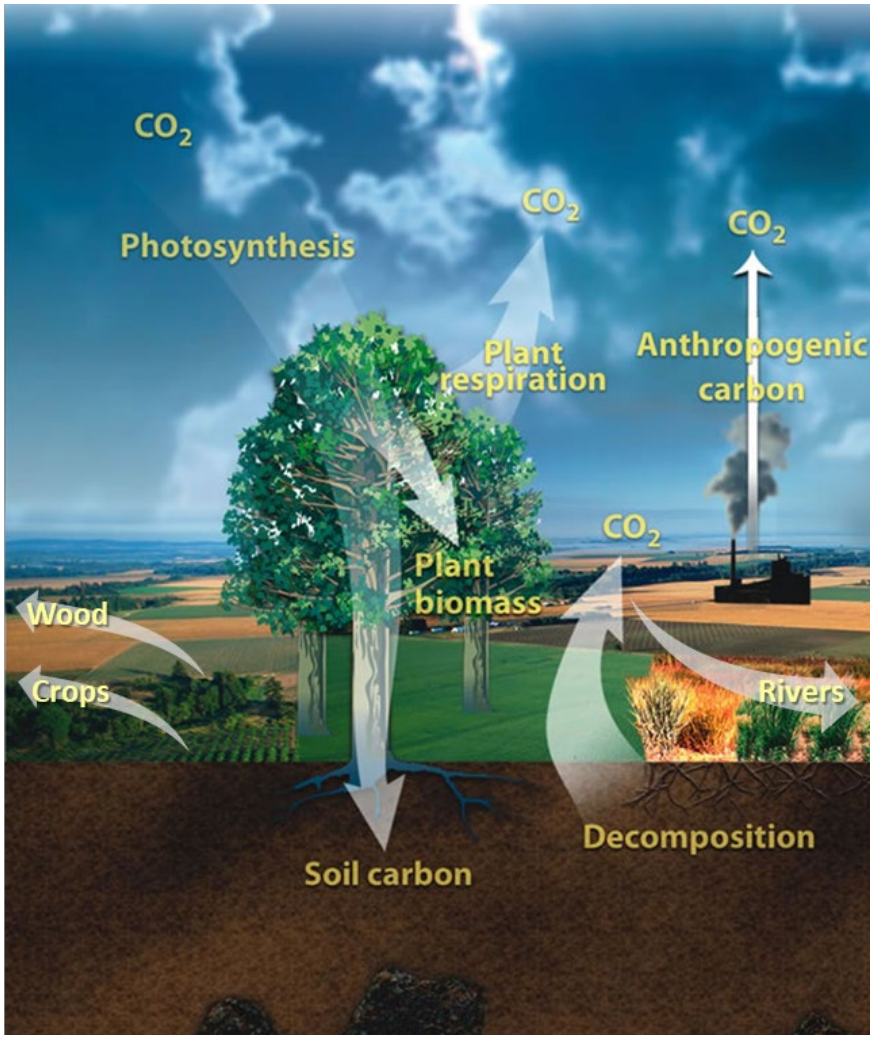

Figure 9. The land carbon cycle, showing the primary fluxes and reservoirs. The amplitudes of the primary land-atmosphere fluxes (white arrows), are listed in Table 3. "Lateral" land carbon fluxes such as land-to-ocean transfer of carbon by rivers and the import/export of harvested wood and agricultural products are also shown. (Adapted from U.S. Department of Energy Genomic Science program - https://genomicscience.energy.gov).

5.1 Processes Controlling Net Ecosystem Production

The net land carbon balance is determined primarily by the balance of CO_2 uptake through photosynthesis (GPP) and release by autotrophic respiration (R_a), litter and soil organic matter decomposition (soil heterotrophic respiration, *SHR*). It also includes smaller contributions such as source/sink dynamics from fires and other disturbances (F_{dist}), emissions from crop product consumption and grazing (F_{crop}, $F_{grazing}$), wood product decay (F_{wood}), outgassing from water bodies and lateral exports such as DIC/DOC ($F_{nat,riv}$) and trade of crop and wood products (F_{trade}). These quantities are related to Net Ecosystem Product (NEP) in Eqs. 2-4.

$$NEP = GPP - R_a - SHR - F_{dist} - F_{crop} - F_{grazing} - F_{wood} - F_{nat,riv} - F_{trade} - F_{others}\,, \qquad (2)$$

$$NPP = GPP - R_a\,, \quad (3)$$

$$TER = Ra + SHR\,. \quad (4)$$

Additional fluxes of carbon in the form of carbon monoxide (CO), methane (CH_4) or biogenic volatile compounds are included in F_{others}. These terms much smaller than those included here, and not considered further.

Table 3. Contemporary Land Carbon Fluxes (Note: numbers without uncertainties are assumed to have uncertainties comparable to their stated values.).

Quantity	Flux (P C yr^{-1})	Reference
Gross Primary Production (GPP)	123 ± 8	1
Net Primary Production (NPP)	~50 (44 to 57)	2
Autotrophic Respiration (R_a)	~64 ± 12	3
Soil Heterotrophic Respiration (SHR)	39 (33 to 46)	2
Outgassing by Rivers, Lakes and Estuaries	0.8 to 2.3	2
Fires	1.6	2
Consumption of Harvested Crops	1.5	2
Land Use Change (LUC)	1.1	2
Grazing	1.0	2
Biogenic Reduced Carbon	0.8	2
Decay and Burning of Wood Products	0.7	2

[1]*Beer et al. (2010);* [2]*Ciais et al. (2020c);* [3]*Ito (2020*)

Land carbon stocks and fluxes, and thus the natural land sink, are affected by increases in atmospheric CO_2 as well as changes in nitrogen deposition, land use change (LUC) and the response of ecosystems to climate variability since the beginning of the industrial age. Elevated atmospheric CO_2 mixing ratios directly stimulate plant productivity through CO_2 fertilization and to enhance plant water use efficiency in arid regions (Schimel et al., 2015; Gonsamo et al., 2021). These factors, combined with its contributions to warming at high latitudes, contribute to longer growing seasons. The magnitude of these effects is debated (Walker et al., 2021), underscoring remaining uncertainties in empirical understanding and modelling (Medlyn et al., 2015).

The current paradigm for nutrient control on productivity is for the high-latitude ecosystems to be potentially nitrogen limited. This reflects the young age of soils post glaciation, since nitrogen sourced through biological nitrogen fixation from the atmosphere and cold environments limit nutrient mineralization. In contrast, the tropics are more likely to be phosphorus limited as they typically have older and often highly weathered soils (phosphorus being sourced from bedrock). In terms of climate constraints on primary productivity, tropical systems are often characterized by distinct wet and dry seasons, and are water and/or radiation limited, the latter due to clouds (over moist tropical forests), whereas mid- and high-latitudes are

typically temperature and light limited, except semi-arid and drylands, which are typically water limited (Nemani et al., 2003).

The net carbon balance can be determined by bottom-up methods, such as biomass inventories and processed based models (e.g. DGVMs). Two biomass-based, bottom-up approaches are considered in this review: 1) stock change (difference between carbon stocks over a period of time) 2) gain/loss method (sum of removal -carbon uptake through growth- and emissions - losses through disturbance/harvest). The net carbon balance can also be inferred from top-down methods that infer net land-atmosphere CO_2 fluxes by analyzing spatially-and temporally-resolved measurements of CO_2 concentrations using atmospheric inverse models. Top-down atmospheric inversions provide spatially-explicit and temporally continuous estimates of the surface (land and ocean) fluxes that are consistent with CO_2 concentration measurements and ensure mass-balance, but require the choice of an atmospheric transport model, assumptions about uncertainties and depend on the priors used when the observational network is too sparse (Kaminski and Heimann, 2001). The extent to which the top-down and bottom-up estimates of the net carbon balance agree provides a measure of our understanding of the carbon cycle. Results from both approaches are summarized in the following sections. Here, we focus on contemporary fluxes, covering the past three decades (1990 – 2020), broadly aligning with the availability of global satellite remote-sensing data, although exact time periods will differ among individual studies reported.

5.2 Bottom-up Inventories of Net Ecosystem Exchange

CO_2 emissions or uptake by natural ecosystems, including those associated with deforestation, reforestation, disturbance, or land management are usually expressed in terms of the Net Ecosystem Exchange, NEE = - NEP. Bottom-up methods estimate NEE based on information about (i) the area affected by a given process, (ii) the corresponding carbon stock per unit area (and its trends) and (iii) the fraction of carbon exchanged with the atmosphere due to the observed change (e.g. Hubau et al., 2020). In practice, all three of these properties are challenging to quantify accurately (e.g., Saatchi et al., 2011; Ramankutty et al., 2007; Pearson et al., 2017, Xu et al., 2021), but all have benefited from new in situ and remote sensing measurement techniques and more advanced bottom-up modeling techniques.

The areal extent of land cover change (LCC) associated with human activities and natural processes are typically tracked using the bookkeeping methods and remote sensing observations summarized in Section 3.1. Recent advances in the remote sensing methods are summarized in Section 5.4. Estimates of the carbon stock per unit area are derived from estimates of above ground and below ground biomass. Until recently, estimates of both quantities relied primarily on in situ measurements collected from a limited number of dedicated research plots at regular intervals (e.g. Pan et al., 2011). Soil carbon inventories still rely exclusively on in situ measurements, which are often characterized by limited spatial coverage and infrequent (decadal) repeat intervals (Scharlemann et al., 2014; Ciais et al., 2014). However, recent advances in microwave and lidar remote sensing technologies have provided dramatic improvements in above ground biomass measurements (see Section 5.4.2).

Alternately, NEE can also be estimated from direct measurement of CO_2 fluxes between the surface and the atmosphere using networks of eddy covariance flux towers, such as those deployed by FLUXNET (Baldocchi et al., 2001). The global network of eddy covariance sites has grown substantially over the past 25 years, with some records spanning that full period.

These data provide unique constraints on the CO_2 fluxes from a broad range of vegetation types, climate regions and disturbance types. Eddy flux data have been combined with other

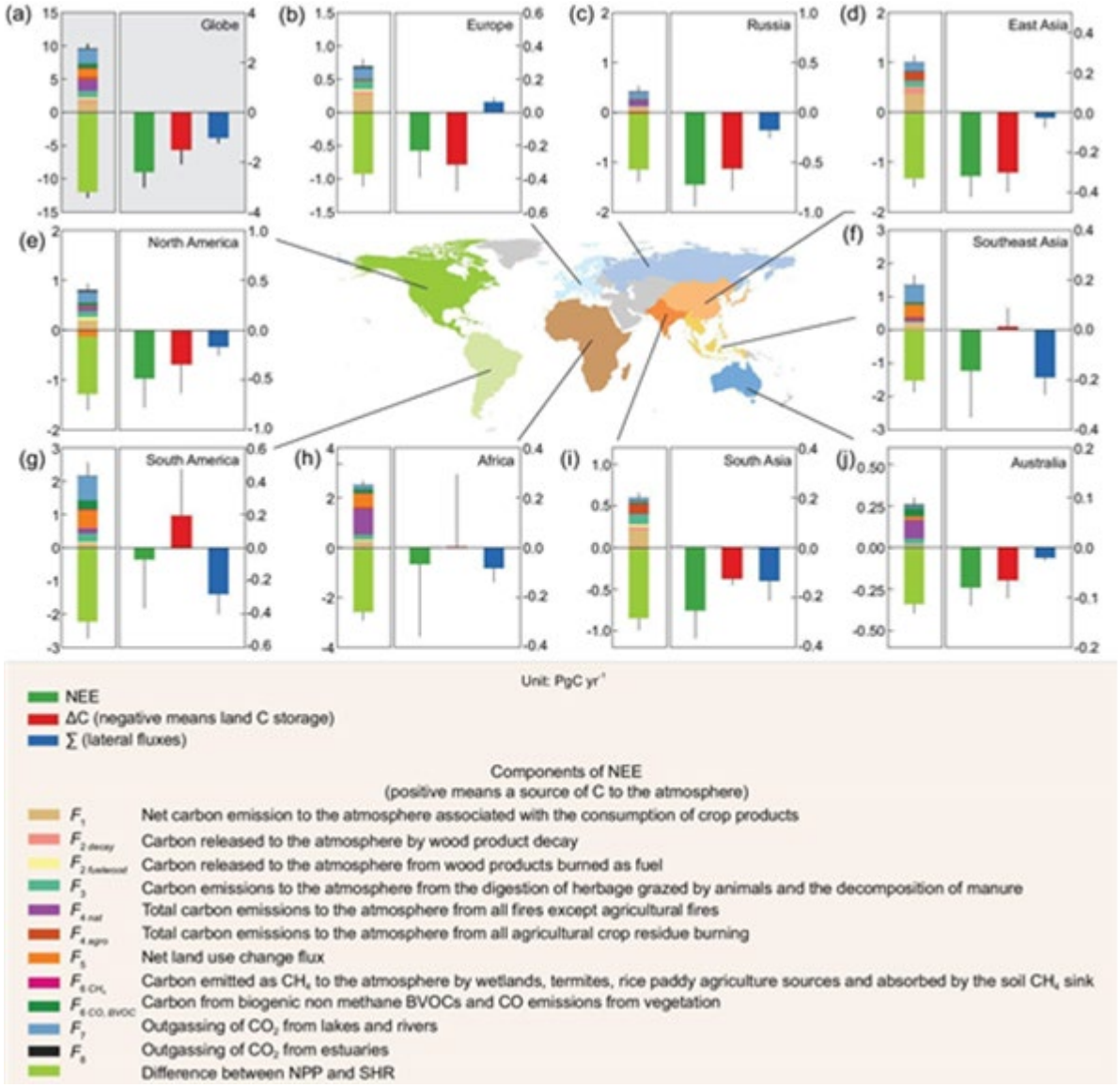

Figure 10. Contributions to NEE at continental scales from bottom-up inventories, compiled by RECCAP2. All major flux components are shown in the left sub-panel of each plot. The right sub-panels summarize NEE (green bars), the carbon-storage change, ΔC (red bars) and the combined lateral fluxes from trade and riverine-carbon export to the ocean, $F_{trade} + F_{nat,riv}$ (blue bars) for different regions of the globe for the 2000s. After Ciais et al. (2020c).

climatological data to provide insights into the processes acting across these domains and their changes over time. Over the past two decades, the eddy flux network has expanded to span the globe, but still has large gaps, particularly in the tropics and at high latitudes, and each flux tower characterizes the fluxes within a limited spatial footprint. Because of this, efforts to upscale results from local to regional or global scales are often associated with large uncertainties in the magnitude of the land CO_2 sink and especially its interannual variability (Baldocchi, 2003; Jung et al., 2009; Beer et al., 2010; Xiao et al., 2012; Keenan and Williams, 2018; Jung et al., 2020).

Figure 10 shows the net carbon balance expressed as NEE across continents, drawn from a comparison of bottom- up methods employed in the REgional Carbon Cycle Assessment and Processes-2 (RECCAP2) project (Ciais et al., 2020a). Here, NEE is defined by subtracting lateral carbon fluxes ($F_{nat,riv}$, F_{trade}) from the total net land carbon stock change, ΔC. In Europe, Russia and East Asia, the lateral fluxes tend to be small, and NEE almost equals the change in carbon stocks as observed from inventories. Overall, Ciais et al. (2020a) find a global sink of -2.6±0.6 Pg C yr^{-1}, which is comparable to the independent estimate obtained by the DGVMs used in the GCB (Friedlingstein et al., 2021) of -2.4 ±0.7 Pg C yr^{-1}. The results from bottom-up estimates in Ciais et al. (2020a) are also roughly consistent with results from an ensemble of atmospheric inversions (Peylin et al., 2013), which estimate a global net land sink of -1.32± 0.39 Pg C yr^{-1}, with a sink of -2.18±0.53 Pg C yr^{-1} in the northern hemisphere but a highly uncertain source of 0.91±0.93 Pg C yr^{-1} in the tropics (estimated as a sink by Ciais et al., 2020a).

5.3 Bottom-up Estimates of Gross CO_2 fluxes from land ecosystems – GPP and R_a

To understand variability and trends in NEE, the component fluxes (Eq. 2) must be quantified. Gross primary productivity (GPP) reflects the total uptake of carbon through photosynthesis and is an essential variable to understand the carbon cycle. Up to 40% of the carbon in the atmosphere passes through leaf stomata annually, and approximately 16% (120 Pg C yr^{-1}) is assimilated in vegetation (GPP) (Ciais et al., 1997). Some of this carbon is used for plant functioning and growth, and the remainder being released back to the atmosphere through respiration. GPP minus autotrophic respiration (Ra) equals Net Primary Production (NPP) and this is further reduced by soil heterotrophic respiration and disturbances.

Table 4. Comparisons of Published Contemporary (1990-2020) Gross Primary Productivity Estimates.

Estimate (Pg C yr^{-1})	Method	Reference
140	MODIS, SIF, Fluxnet	Joiner et al., 2018
150-175	isotopes	Welp et al., 2011
123±8	Fluxnet +RS	Beer et al., 2010
108-130	FLUXNET, RS, other	Jung et al., 2020
83-172	TRENDY models	Jung et al., 2020
167 ±5	SIF, model assimilation	Norton et al., 2019
166 ±10	SIF	MacBean et al., 2018
120 ±30	Isotopes	Liang et al., 2017
131–163	NIRv	Badgley et al., 2019

An analysis of direct flux observation made by a network of eddy covariance towers yielded estimates of the global GPP near 123 Pg C yr^{-1} (Beer et al., 2010). Roughly one third of this (40.8 Pg C yr^{-1}) is produced in the tropical forests, and one quarter (31.3 Pg C yr^{-1}) in the tropical savannas, making the tropics by far the largest contributor to global GPP. Temperate and

boreal forests are estimated to have a GPP of only 9.9 Pg C yr^{-1} and 8.3 Pg C yr^{-1}, respectively. When integrated over the globe, croplands contributes an estimated 14.8 Pg C yr^{-1} to GPP.

An alternate analysis using oxygen isotopes (Welp et al., 2011), suggests that this value of Global GPP may be too low and would be closer to 150 -175 Pg C yr^{-1}. However, Anav et al. (2015) argue that Welp et al. used a limited number of observations and a simple model that included gross photosynthesis, but neglected photorespiration by land plants. They note that plants immediately respire away 20-40% of the carbon fixed by photosynthesis. When photorespiration is included, they note that these GPP values are more in line with those obtained from other methods. Table 4 presents a comparison of several GPP estimates. Noteworthy features include the large range, and the fact that the more recent estimates using SIF suggest a rather higher global total than the earlier estimates (see also Campbell et al., 2017).

Global autotrophic respiration, R_a, is estimated at 64 ±12 Pg C yr^{-1} (Ito, 2020). This is the term that is also called maintenance respiration and consists mainly of dark respiration. Precise determination of R_a is difficult as it also involves a substantial below ground component, and is expected to vary with biome and climate. Estimates of NPP (GPP – R_a), are generally assumed to be of the order of 50% of GPP (i.e. Ito, 2020), but Ciais et al. (2020c) suggest that decomposition of organic matter or soil (heterotrophic) respiration (SHR) produces 39 Pg C yr^{-1} within an interquartile range of 33-46 Pg C yr^{-1}. This estimate is lower than conventionally assumed but agrees with recent large-scale estimates based on site soil respiration measurements (e.g. Jian et al., 2021). An additional flux to the atmosphere of 8.3 ± 9 Pg C yr^{-1} is due to a series of processes listed in Table 3. The remainder of GPP-Ra-SHR and these additional losses constitutes how much carbon is currently taken up by the land, and yields a value of the Net Ecosystem Exchange (NEE) of -2.2 ± 0.6 Pg C yr^{-1}.

More recent methods that combine flux tower data with remote sensing data in machine learning algorithms to produce upscaled fluxes (see Jung et al., 2020) yield global GPP estimates that agree well with those obtained from other methods, while providing insights into the processes controlling the carbon cycle of the land biosphere and their changes over time, particularly in the temperate Northern latitudes. Using radar derived estimates of biomass and soil carbon data from the harmonized world soil database and other sources combined with flux estimates of the global product of Beer et al. (2010), Carvalhais et al. (2014) calculated residence times of carbon. They found that the sensitivity of the residence time to soil moisture and temperature did not agree with the sensitivity of a set of DGVMs, while the overall pattern of increasing residence time at higher latitudes was reproduced. The following sections summarize recent results from bottom-up inventories that combine plot-based in situ measurements and remote sensing observations to constrain carbon uptake and emissions from the land biosphere.

5.4 Advances in Remote Sensing of Primary Productivity and Biomass

Since the launch of LandSat 1 in 1972, carbon cycle scientists have used a variety of optical and near infrared remote sensing observations to characterize plant productivity. One of the earliest indicators was the Normalized Difference Vegetation Index (NDVI), which is defined as the difference between the observed radiances within near-infrared (NIR) and red channels divided by their sum. NDVI and other vegetation indices such as Leaf Area Index (LAI; Zhu et al. 2013) or fraction of Absorbed Photosynthetically Active Radiation (fAPAR; Myneni et al., 2015) have been used as proxies for vegetation activity and photosynthesis. Such indices have also been used as proxies for fAPAR in semi-empirical light-use efficiency models, and

combined with estimates of photosynthetically active radiation (PAR) (Zhao and Running, 2010; Smith et al., 2015) or more complex radiative transfer models (Jiang and Ryu, 2016) to estimate GPP. More recently, NDVI has been joined by other optical and near infrared indicators such as the Near Infrared Reflectance of Vegetation, NIRv, and SIF. Recent results derived from these indicators are summarized in this section.

5.4.1 Remote Sensing proxies for Photosynthesis and GPP

SIF provides a closer proxy for photosynthesis than NDVI. As plants absorb sunlight to perform photosynthesis, a fraction of that light (< 2%) is re-emitted at longer NIR wavelengths (fluorescence), which can be detected in the cores of strong solar Fraunhofer lines or in the molecular oxygen (O_2) A- and B-bands by high resolution space-based spectrometers (Meroni et al., 2009; Frankenberg et al., 2014; Guan et al., 2016; Sun et al., 2018).

SIF is a rapidly-responding indicator that shows strong linear relationships with GPP at site-scale and thus has been adopted as a functional proxy for photosynthesis and GPP. The availability of global SIF datasets from space-based sensors, such as GOME-2, GOSAT, OCO-2 and TROPOMI (Figure 11) have substantially expanded the use of this product in studies of the terrestrial carbon cycle. SIF-based estimates of global GPP are beginning to converge, but still differ, ranging from 166 ± 10 Pg C yr^{-1} (Table 3). While SIF provides robust estimates of spatial distribution and seasonality of GPP, the strong relationship between SIF and GPP is largely explained by their common dependence on APAR (Mohammed et al., 2019), so that SIF might not be a good proxy for photosynthesis when down regulation occurs under stress conditions (Wohlfahrt et al., 2018; Marrs et al., 2020). SIF is now being combined with other vegetation indices and climate properties in diagnostic process models (c.f. Bacour et al. 2019; Bloom et al. 2020) to provide additional insight into NBE and GPP on regional-scales.

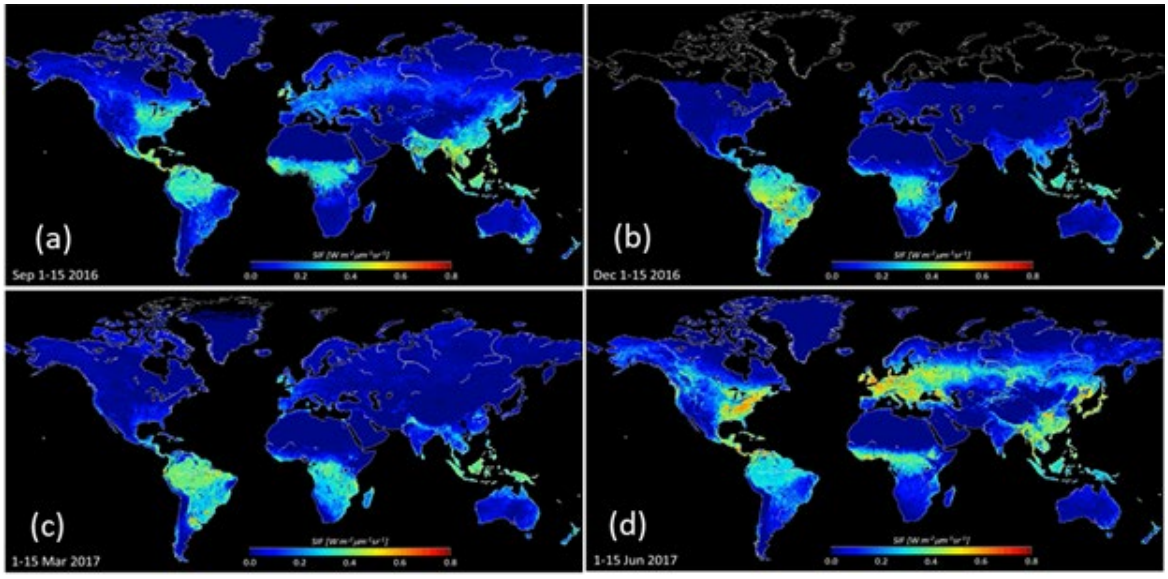

Figure 11. OCO-2 observations of SIF for (a) 1-15 September 2016; (b) 1-15 December 2016; (c) 1-15 March 2017, and 1-15 June 2017. Blue indicates low SIF and therefore low photosynthetic activity. The warmer colors indicate higher SIF and higher photosynthetic activity (Ying Sun, Personal communication,2018).

Recently, the NIRv (the product of NIR reflectance by NDVI) has been proposed as an alternative method to estimate GPP that overcomes some of the challenges of other indices and that shows high correlation with SIF. Using NIRv, Badgley et al. (2017) estimate global GPP to be 131-163Pg C yr^{-1}, in line with upper estimates of other studies and in line with isotope-based estimates by Welp et al. (2011) and Liang et al. (2017) (Table 4).

5.4.2 Advances in Measurements of Above Ground Biomass

Vegetation optical depth (VOD) retrievals from satellite-based passive microwave instruments are sensitive to vegetation cover and water content (c.f. Liu et al., 2015). Passive microwave measurements have the advantage of not being affected by cloud cover, a common problem with other remote-sensing datasets. High frequency microwave measurements have been used to analyze seasonality and trends in vegetation (Barichivich et al., 2013) and to derive estimates above-ground biomass (AGB) based on empirical relationships between AGB and VOD (e.g. Liu et al., 2011; 2015).

Merging VOD data from multiple space-based microwave sensors, Liu et al. (2015) produced a global survey of AGB based on two decades of observations for both forests and non-forest biomes. They estimate a global average AGB of ~362 Pg C (310 – 422 Pg C) between 1998-2002, of which, 65% was in forests and 17% was in savannahs. Spawn et al. (2020) used satellite products of biomass with land cover with machine learning techniques to produce estimates of global AGB, and link this to below ground carbon density information. These estimates yield a total living terrestrial biomass of 409 Pg C, composed of an AGB of 287 Pg C and a below ground biomass carbon density of 122 Pg C (Figure 12).

Since 2010, the European Space Agency's Soil Moisture and Ocean Salinity (SMOS) measurements of lower frequency L-band microwave radiation at multiple angles can be used to simultaneously obtain information about soil-moisture and vegetation structure, which are not fully attenuated at high biomass (Konings et al., 2017). Changes in peak VOD between years can be used to infer biomass changes, albeit at coarse (~25 km) spatial resolution (Brandt et al., 2018, Qin et al., 2021). VOD has also been used to derive GPP fluxes (Teubner et al., 2018).

The increasing availability of above-ground biomass estimates derived from light detection and ranging (Lidar) and radio detection and ranging (radar) sensors on airborne and space-based platforms are now providing improved spatial coverage and temporal sampling frequency (Xu et al., 2021). The availability of high-resolution space-based remote sensing observations from sensors such as LandSat Operational Land Imager (OLI), Moderate Resolution Spectroradiometer (MODIS) and Sentinel-2 Multi-Spectral Instrument (MSI) have facilitated improved estimates of the land cover changes (Lamarche et al., 2017) and of burned areas (Chuvieco et al., 2016), and detection of changes in biomass to forest losses and gains (Hansen et al., 2013b). When combined with AGB estimates from VOD, these allow quantifying and attributing changes in biomass to human vs. natural sources (Harris et al., 2016; 2021), as discussed in Sections 5.7 and 5.8.

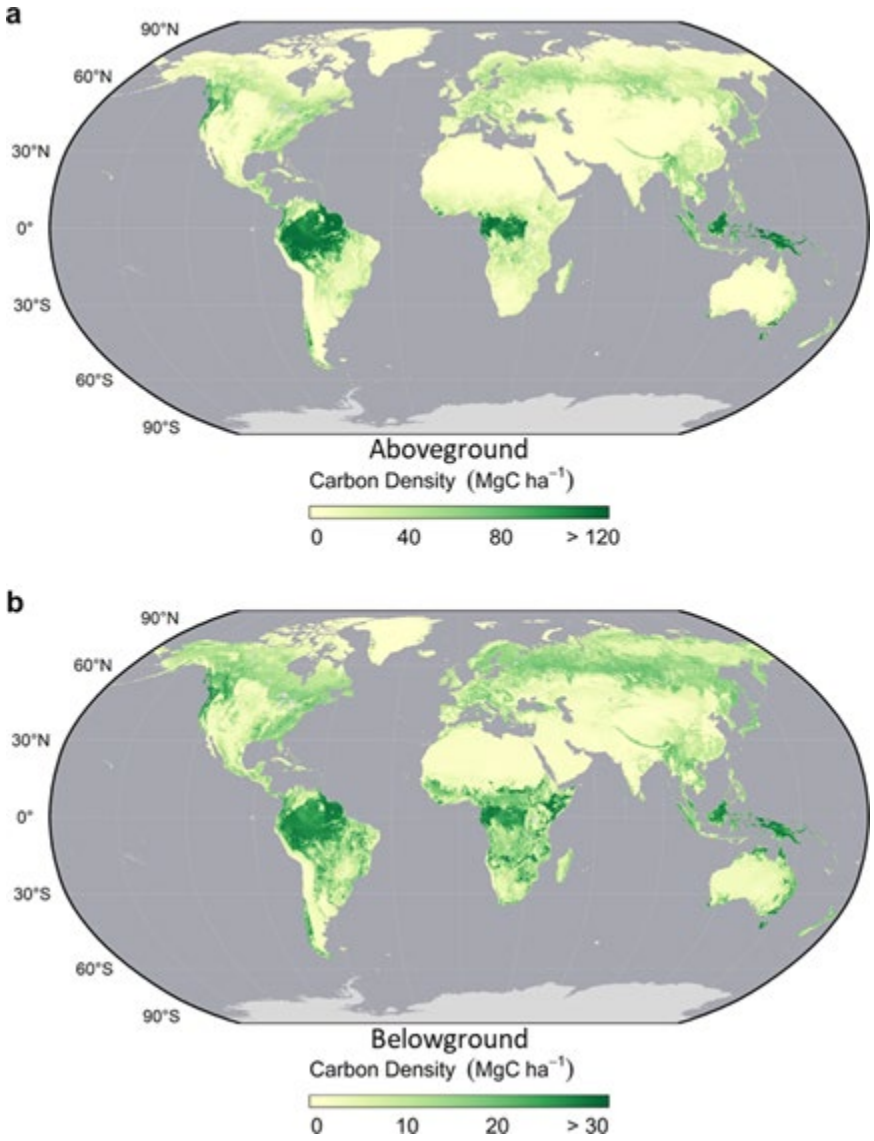

Figure 12. Maps of above and belowground living biomass carbon densities. (a) Aboveground biomass carbon density (AGBC) and (b) belowground biomass carbon density (BGBC). Maps have been aggregated at 5 km spatial resolution (Spawn et al., 2020).

5.5 Progress in Modelling Forest Land Use Change

For several decades, estimates of emissions from land-use change by the research community were based primarily on a book-keeping model using a stock-change approach (Houghton and Nassikas 2017). This approach combines information on forest area and deforestation rates from the FAO Forest Resource Assessment (FRA) and other sources. Carbon fluxes are based on country-level surveys of vegetation and soil carbon density for different forest ecosystems and response curves for temporal carbon dynamics following disturbance and recovery, e.g. legacy fluxes and regrowth. More recently, satellite-based biomass data are being used in book-keeping approaches (e.g. Rosan et al., 2021) to more accurately reflect spatial variation in carbon stocks, and implicitly include the influence of environmental factors.

Process-based models offer an alternate, complementary approach to estimate land-use emissions. The first generation of DGVMs have been extensively used in the land carbon-cycle research (Sitch et al., 2015). They typically build upon a detailed representation of leaf photosynthesis coupled to a water balance scheme and simulate gross fluxes, GPP, R_a, NPP, and carbon stocks in vegetation and soils. A new generation of DGVMs include more biological processes. These include nutrient cycling (N and now P), and more comprehensive representations of vegetation demography (Smith et al., 2001; Argles et al., 2020) with explicit representation of mortality, plant succession and temporal development of age/size classes, and explicit disturbance (e.g. fire-enabled DGVMs, Rabin et al., 2017). This enables comprehensive assessments of the impact of land management on the carbon cycle (e.g. forest growth and harvest), and separates effects of environmental and human drivers on the land carbon sink (Houghton et al., 2012). McGuire et al. (2001) pioneered the use of DGVMs in factorial experiment design to enable attribution of the land C sink to processes, CO_2, Climate and Land Use and Land Cover Change (LULCC) over the 20th century.

A similar protocol is adopted for the DGVMs in the annual GCB assessment (Friedlingstein et al., 2021). The DGVM land-use flux is calculated as the difference between two simulations (1700 to present-day): the first (S2) with varying observed historical CO_2 and climate but fixed pre-industrial LU and a second (S3) with all three varying (CO_2, climate and LUC). However, the natural vegetation in S2 is affected by temporal changes in environmental factors (e.g. CO_2 fertilization) - not included in static carbon density maps employed by book-keeping models. One would expect an additional carbon sink in forests relative to faster-turnover cultivated systems, which would be lost with deforestation; this foregone sink is referred to as the Loss of Additional Sink Capacity (Gitz and Ciais, 2003, Sitch et al., 2005; Gasser et al., 2020; Pongratz et al., 2014). Obermeier et al. (2021) has attempted to reconcile these methodological differences between the DGVM approach employed in GCB and book-keeping models.

More recent DGVMs updates capture more land-use change related processes, e.g. shifting cultivation (gross land-cover transitions), grazing/crop harvest and cropland management and wood harvest. Results including these newly incorporated processes suggest a substantial underestimation in land-use emissions in earlier DGVMs, with implications for the magnitude of the natural land sink, given the net land sink is constrained (Arneth et al., 2017). Recent attempts attempt to reconcile DGVMs estimates with country reporting of anthropogenic forest CO_2 sinks, by addressing conceptual differences in definitions of anthropogenic land fluxes between DGVMs (used in IPCC) and national GHG Inventories (Grassi et al., 2018).

5.6 Net Ecosystem Exchange from Atmospheric Measurements and Inverse Models

As noted in Section 3, top-down atmospheric inverse models have been used to study the land carbon cycle for more than 40 years. Early in this period, when there were only a few dozen ground-based stations, these flux inversions focused on continental to regional scales, with uncertainty increasing for smaller scales (Kaminski and Heimann, 2001; Chevallier et al., 2010). As the ground-based and airborne in situ network has expanded, its data have been used support flux estimates at regional scales for well-sampled regions, such as Europe (Monteil et al., 2020; Petrescu et al., 2021).

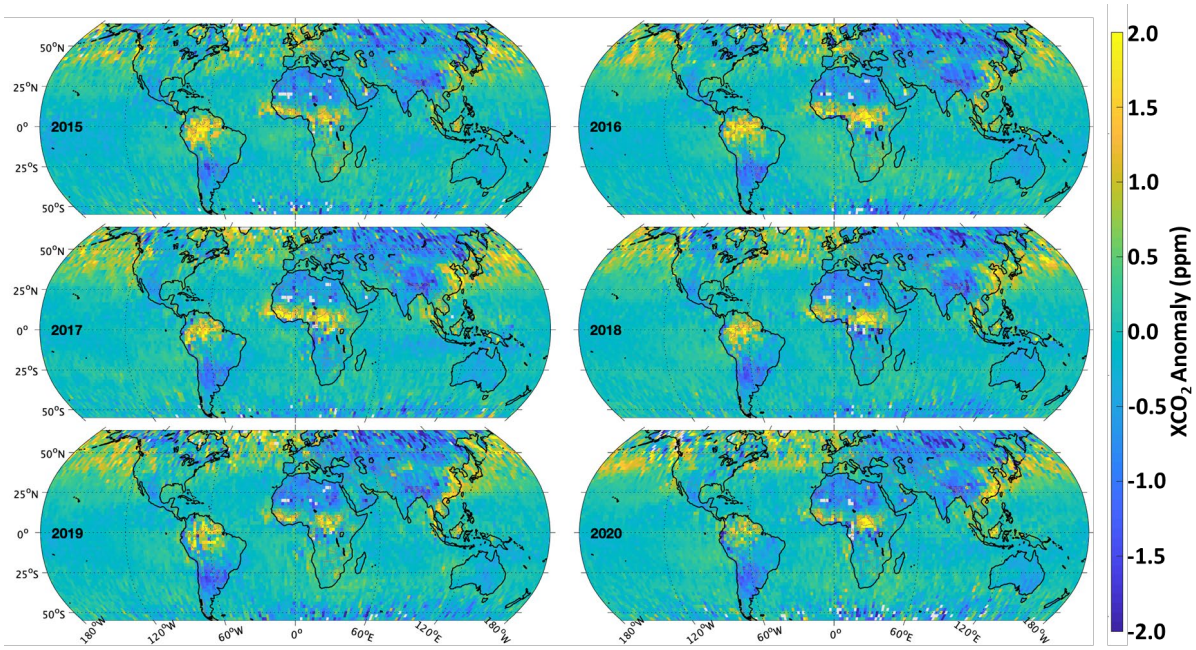

Figure 13. Maps of annually-averaged XCO_2 anomalies derived from OCO-2 XCO_2 estimates from 2015 - 2020. Positive anomalies (yellow) indicate regions have XCO_2 values that are persistently higher than their surroundings while negative anomalies (blue) indicate regions where XCO_2 is lower than in the surrounding areas. (Updated from Hakkarainen et al., 2019 with the OCO-2 v10 product).

Space-based remote sensing estimates of XCO_2 have dramatically improved the spatial and temporal resolution and coverage of the atmospheric CO_2 field, enabling studies at much finer spatial and temporal scales. For example, Hakkarainen et al. (2016; 2019) processed OCO-2 XCO_2 observations to filter out the annual growth rate and seasonal cycle to yield maps of temporally-persistent spatial anomalies (Figure 13). Here, positive XCO_2 anomalies are associated with persistent sources while negative XCO_2 anomalies are interpreted as persistent sinks. When averaged over the annual cycle, tropical land regions, including the Amazon, north equatorial Africa, and equatorial Asia have positive XCO_2 anomalies while, mid- and high-latitude land regions of Asia, North and South America have negative XCO_2. The positive anomalies in east Asia and western Europe include contributions from intense fossil fuel combustion, biomass burning or other human activities. The positive anomalies over the north Pacific and Atlantic Oceans are just downwind of persistent CO_2 sources in east Asia and North America, respectively, indicating the effects of transport rather than local sources.

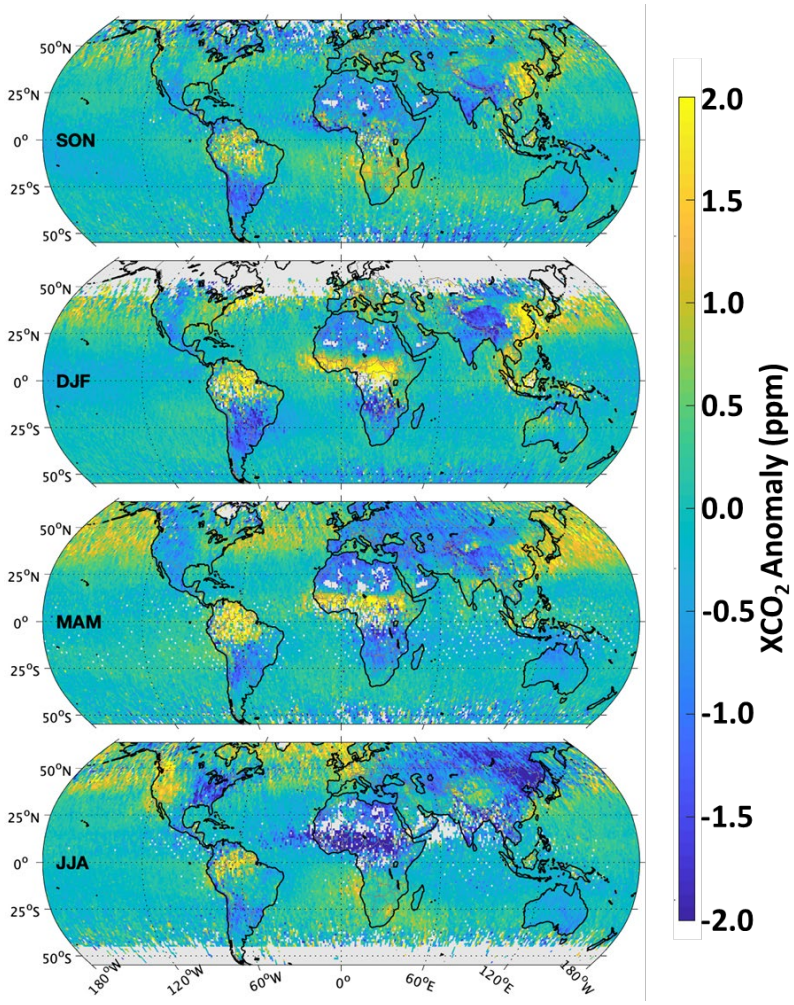

Figure 14. Maps of seasonally-averaged XCO_2 anomalies derived from OCO-2 XCO_2 estimates from 2015 – 2020, including September-October-November (SON), December-January-February (DJF), March-April-May (MAM) and June-July August (JJA). (Updated from Hakkarainen et al., 2019 with the OCO-2 v10 product).

Seasonally averaged maps (Figure 14) show that the XCO_2 anomalies over north equatorial Africa transition from negative values during June-August to positive values from December-May. In contrast, the Amazon appears to exhibit mostly positive XCO_2 anomalies throughout the year during this period. Strong negative XCO_2 anomalies over mid- and high latitudes in the northern hemisphere in JJA are associated with strong uptake by the land biosphere. These negative anomalies even extend across heavily-industrialized east Asia during this season, as biospheric uptake temporarily balances anthropogenic emissions. The variations across North America are also noteworthy, with the western regions showing positive anomalies during JJA, while the mid-west and eastern United States shows strong negative anomalies. While none of these features are especially surprising, this is the first time that we have been able to quantify the atmospheric CO_2 distribution on sub-regional scales over the entire globe on seasonal to annual time scales.

These space-based XCO_2 estimates are being combined with ground-based and airborne in situ CO_2 measurements and analyzed with atmospheric inverse modeling systems to quantify sub-regional to continental changes in the land biosphere. Early efforts exploited the global coverage provided by GOSAT to constrain regional-scale CO_2 flux estimates. These investigations demonstrated the value of the improved coverage provided by the GOSAT data for reducing flux uncertainties, particularly in the tropics, where there are few in situ observations (c.f. Maksyutov et al., 2013; Deng et al., 2016; Byrne et al., 2020b). However, other inverse modeling revealed large differences between top-down and bottom-up flux estimates in some regions, revealing limitations of this approach (c.f. Kondo et al., 2015; Reuter et al., 2014). For example, an unrealistically large sink in Europe (Reuter et al., 2014; Kaminski et al., 2017) has been ascribed to biases in the seasonal coverage (Houweling et al., 2015) and/or in the XCO_2 estimates themselves (Scholze et al., 2019).

As the accuracy, resolution and coverage of the atmospheric CO_2 measurements and inverse modeling systems have improved, the spread between the global land flux estimates from these top-down methods has decreased from > 3 Pg C yr^{-1} to ~1 Pg C yr^{-1} (i.e. Kondo et al., 2020). Significant improvements have been achieved on regional scales as well (Zhang et al., 2021). An ensemble of six inverse models constrained by in situ data used in the 2020 GCB (Friedlingstein et al., 2021) indicates that the Northern extratropics (>30°N) were indeed the main contributor to the global NEE land sink between 2010 and 2019, with a amplitude of -2.9±0.6 Pg C yr^{-1}. This is slightly stronger than the northern extra-tropical land sink derived from DGVMs, -2.3±0.6 Pg C yr^{-1}. On shorter time scales, an ensemble of nine inverse models constrained by OCO-2 v9 data (Peiro et al., 2021) indicates that the northern extratropical land sink increased from -2.5 to -3±0.25 Pg C yr^{-1} between 2015-2016 and then decreased to -2±0.25 Pg C yr^{-1} in 2017 and to -1.75±0.25 Pg C yr^{-1} in 2018. When this ensemble is constrained by in situ data, the results from 2015-2016 are the same, but the sink increases to -2.75 Pg C yr^{-1} in 2017 and returns to -2.5±.25 in 2018. The source of the CO_2 data used to constrain the inverse models explains some of the remaining differences between the top-down and bottom-up results.

Meanwhile, recent inverse modeling intercomparisons indicate that tropical land is not a significant net sink for atmospheric CO_2 (Gaubert et al., 2019; Palmer et al., 2019; Crowell et al., 2019; Friedlingstein et al., 2021; Peiro et al., 2021). Gaubert et al. (2019) find near neutral tropical uptake for 2009-2011, but note that given reported emissions from deforestation, this result indicates substantial uptake by intact tropical forests. Friedlingstein et al. (2020) also use an inverse model ensemble constrained by in situ data and find that tropical land was roughly in total carbon balance between 2010 and 2019.

Inverse model ensembles constrained by space-based XCO_2 estimates indicate that the tropics are now a net source of CO_2 as the XCO_2 anomaly maps (Figures 13, 14) suggest. For example, Peiro et al. (2021) find that tropical land was strong source (1.0 to 2.0 Pg C yr^{-1}) during the 2015-2016 El Niño, supporting earlier results by Crowell et al (2019) and Palmer et al. (2019), but then returned to near neutral conditions (-0.5 to 0.5 Pg C yr^{-1}) in 2017 and 2018. These results support other recent studies that attribute these net emissions to deforestation, forest degradation, drought and other factors (i.e. Aragão et al., 2018; Wigeron et al., 2020; Qin et al., 2021, Gatti et al., 2014; 2021). However, given the sparseness of the tropical in situ CO_2 network and the shortness of the satellite XCO_2 data records, it is too soon to determine whether this represents a slow recovery from the intense 2015-2016 El Niño, or if tropical land has permanently transitioned from a net sink to a net source of CO_2.

A key set of quantities that explain some of the bias between the top-down and bottom-up estimates are the lateral fluxes of carbon, which are implicitly included in net land-atmosphere fluxes by inversions, but not in those estimated by DGVMs (Ciais et al., 2020a). When adjusted for lateral fluxes, the top-down and bottom-up estimates show good agreement on the long-term average land sink, but still show disagreements in the regional partitioning and inter-annual variability of the land sink (Bastos et al., 2020). Several processes contribute to the challenges in constraining the land-sink: large uncertainty in the regional partitioning of fluxes between individual inversions, the representation of land-use change and management in DGVMs, and the ability of DGVMs to simulate responses to disturbances and extreme events such as droughts or fires (Friedlingstein et al., 2020; Bastos et al., 2020).

However, flux inversions provide an integrated estimate of the net surface fluxes, including contributions from fossil fuel burning, land-use change and management, disturbances, CO_2 outgassing, etc. This makes attribution of inverse model-based fluxes to specific sectors (e.g. separating between natural and anthropogenic fluxes or fossil fuel and LUC contributions) challenging, especially given the high uncertainty associated with some of these terms. One approach for addressing this limitation combines geostatistical inverse models with MERRA-2 estimates of air and soil temperature, precipitation, soil moisture, humidity, PAR and other variables to identify the processes driving interannual variability (IAV) in the observed CO_2 fluxes (Chen et al., 2021 a, b). Their results from OCO-2 observations indicate that the tropical grassland biome, including grasslands, savanna, and agricultural lands, contribute as much to IAV as the tropical forests and that temperature and precipitation produce comparable contributions to IAV. This supports the conclusion of Ahlström et al. (2015), but Chen et al. (2021b) note that that these results contradict those from most the DGVMs included in the TRENDY project (Sitch et al., 2015; Friedlingstein, et al., 2019; 2020; Piao et al., 2020b).

5.7 Long-term Trends in the Land Sink

Multiple lines of evidence support an increasing sink in the terrestrial biosphere. Innovative studies using atmospheric CO_2 and $\delta^{13}C$ measurements, Keeling et al. (1989) pointed out an increase in the retention of CO_2 emitted from fossil fuel combustion, which they attributed to an increasing sink in the terrestrial biosphere. These results have been supported by subsequent updates (Keeling et al., 2001) and additional studies using different approaches (McGuire et al., 2001; Khatiwala et al., 2009; Ballantyne et al., 2012; Le Quéré et al., 2009; 2013; 2018a,b; Friedlingstein et al., 2019; 2020; 2021). While the existence of an increasing global land sink is undisputed (Friedlingstein et al., 2020, Ciais et al., 2020a, Fernández-Martínez et al., 2019), the location and drivers of the inferred increase in the past decades remain a matter of debate (Casperson et al., 2000; McGuire et al., 2001, Pacala et al., 2001; Nabuurs et al., 2013; Piao et al., 2009). These include the fertilization effects of elevated CO_2 (McGuire et al., 2001), increased nitrogen deposition in northern latitudes (Fernández-Martínez et al., 2019), agricultural intensification (Zeng et al., 2014), lengthening of the growing seasons in the northern hemisphere and/or vegetation expansion (Forkel et al., 2019) and forest expansion (Casperson et al., 2000) and management (Nabuurs et al., 2013; Erb et al., 2018). Disentangling the compound effects of CO_2 fertilization, i.e. the increased rate of photosynthesis resulting from increased levels of CO_2 in the atmosphere, and increased temperature and drought, is, however, challenging. Here, we discuss the observational evidence for some of these effects.

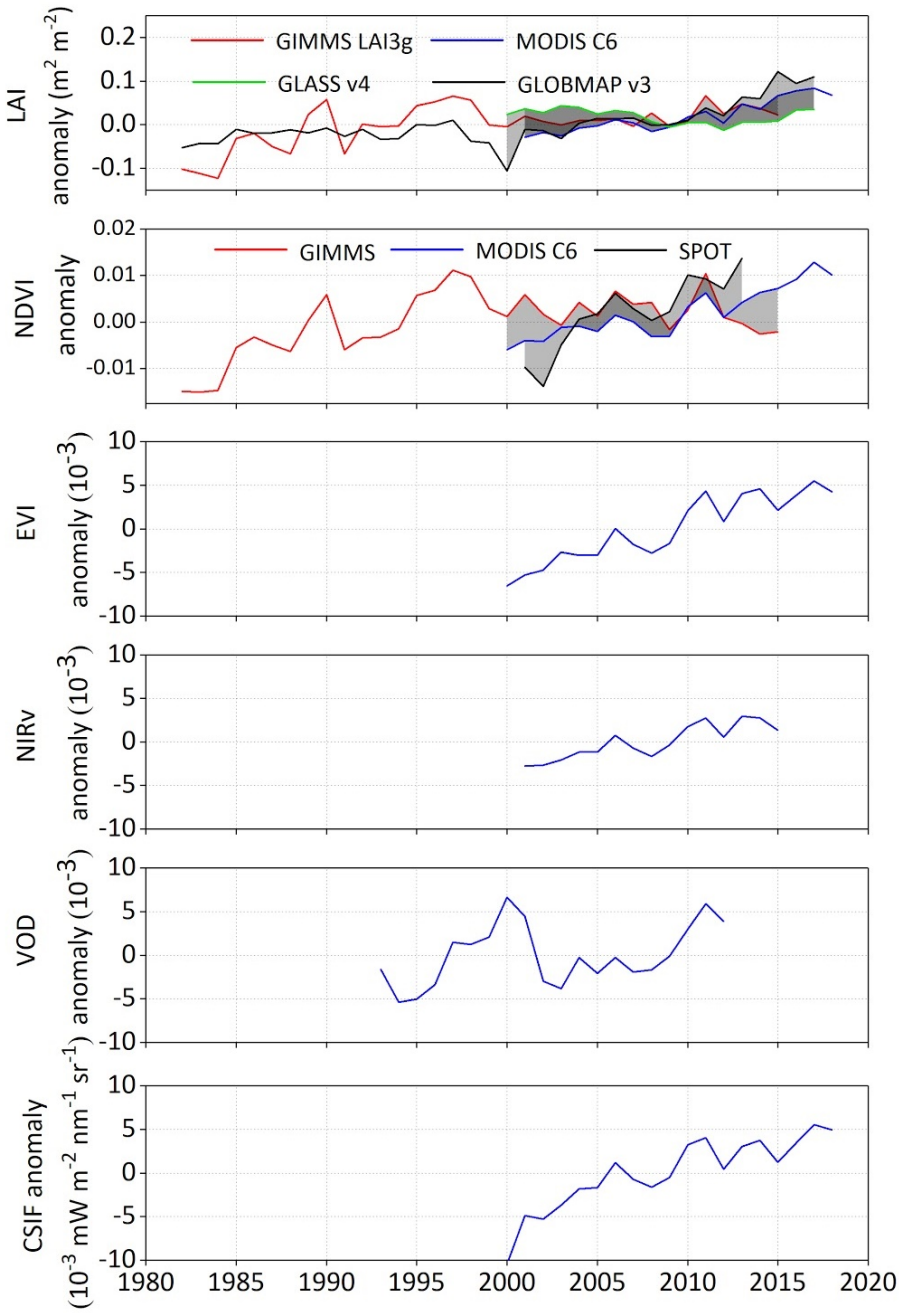

Figure 15. Changes in satellite- derived global vegetation indices, including anomalies in the normalized difference vegetation index (NDVI), Enhanced Vegetation Index (EVI), near-infrared reflectance of vegetation (NIRv), vegetation optical depth (VOD) and contiguous solar- induced fluorescence (CSIF) (Data: Piao et al., 2020b.)

The global AGB dataset compiled from microwave VOD measurements by Liu et al. (2015) indicate no statistically significant global trend in AGB (-0.07 Pg C yr^{-1}) from 1993-2012. However, they do show large losses over tropical forests (-0.26 Pg C yr^{-1}) that were offset by net gains (0.13 Pg C yr^{-1}) over temperate and boreal forests. More recently, Xu et al. (2021) used forest inventory plots, airborne laser scanning (ALS) data and satellite lidar inventories of

forest height to estimate global AGB and adopted allometric relationships to derive below ground carbon stocks. They conclude that globally, woody carbon stocks are increasing at 0.23 ± 0.09 Pg C yr^{-1}. Regions with carbon gains are located in western conifer and boreal forests of North America, tropical forests in Africa, subtropical forests in eastern China, and the boreal forests of eastern Siberia. Tropical forest and subtropical dry forest and savannah lands gained carbon at a rate of 0.09 ±0.04 Pg C yr^{-1}. Temperate and boreal forests had accumulation at rates of 0.10 ±0.03 and 0.04±0.02 Pg C yr^{-1}.

Satellite observations collected since the 1980s indicate a significant global increase in the area covered by green vegetation, or "greening" (IPCC, 2014; Zhu et al., 2016; Piao et al., 2020b; Cortez et al., 2021). Zhu et al., (2016) used long-term satellite observations of LAI to study this greening trend from 1982-2009. They report a persistent, widespread greening over 25-50% of the global vegetated area. In a more recent study, Piao et al. (2020b) use a combination of vegetation indices (NDVI, LAI, EVI, and NIRv) to quantify global greening between the early 1980s and 2018. They conclude that globally, ~34% of vegetated land shows signs of greening over this period (Figure 15). They also note significant greening over China and India, which they attribute primarily to afforestation and agricultural intensification.

Both studies also note that a small fraction (3 – 4%) of vegetated land experienced browning (less greening) between 1982 and 2014. Piao et al. (2020b) note that there is considerable debate about the relative roles of greenness and brownness over the Amazon due to saturation effects in dense vegetation and contamination by clouds and aerosols. However, they conclude that about 5% of the area has experienced browning, which they attribute to drought, heat stress and human activities, but concede that the relative roles of these processes are not well resolved by these data. In the Arctic, browning is seen over ~3% of the land area, with North American boreal forests exhibiting browning areas nearly 20 times larger than the Eurasian boreal forests (Piao et al., 2020b).

At mid- and high-latitudes, bottom-up and top-down models constrained by space-based remote sensing measurements largely reinforce the in situ results, showing a long term increase in the CO_2 seasonal cycle amplitude (SCA) and indicate that mid-latitude and boreal forests are strong net sinks of CO_2 (Keeling et al., 1996; Graven et al., 2013; Jeong et al., 2018; Byrne et al., 2018; 2020a; Piao et al., 2020b; Liu et al., 2020a). It is important to note that estimates derived using the stock change approach still differ by as much as a factor of two or three in the rates quoted above (Xu et al., 2021, see their Table 2). With increasing data availability, new satellites (e.g. BIOMASS expected to launch in 2023, and the GEDI instrument on board of the ISS) are expected to reduce uncertainties and increase consistency in the global estimates.

Based on the results presented above, two things can be stated with relative certainty: (1) in the tropics, LUC approximately balances the land sink (Grace et al., 2014, Gatti et al., 2021) and (2) in the northern extratropics, a sink exists that is still growing. The mechanisms driving these long term trends are explored in the following two sub-sections.

5.7.1 Mechanisms Driving Long-Term Trends in the Tropical Land Sink

Long-term changes in the land sink are typically attributed to CO_2 fertilization, secular trends in nutrient and water availability, temperature changes, disturbance or other factors, but the relative roles of these processes are often challenging to diagnose because they often work in concert (c.f. Bastos et al., 2019: Piao et al., 2020a; Hubau et al., 2020; Liu et al., 2020a; Gampe et al., 2021). All of these factors have been considered in studies of long term trends in the

tropical forest sink. For example, Hubau et al. (2020) assess the carbon sink in intact African and Amazon forests (Figure 16) and conclude that while the African sink strength showed no trend (0.66 Mg C ha^{-1} yr^{-1}), the Amazon forest sink slowed down –0.034 Mg C ha^{-1} yr^{-2} between 1983 and 2010, citing Brienen et al. (2015). The results presented in Figure 16 show that this trend has persisted. Hubau et al. (2020) attribute the downward trend in sink strength by intact forests primarily due to higher temperature and droughts, leading to increased tree mortality. DGVMs simulate strong CO_2-induced sinks in moist tropical forests, counterbalanced by a negative effect of climate change and variability. An improved representation of mortality processes is needed in DGVMs, particularly those relating to drought response.

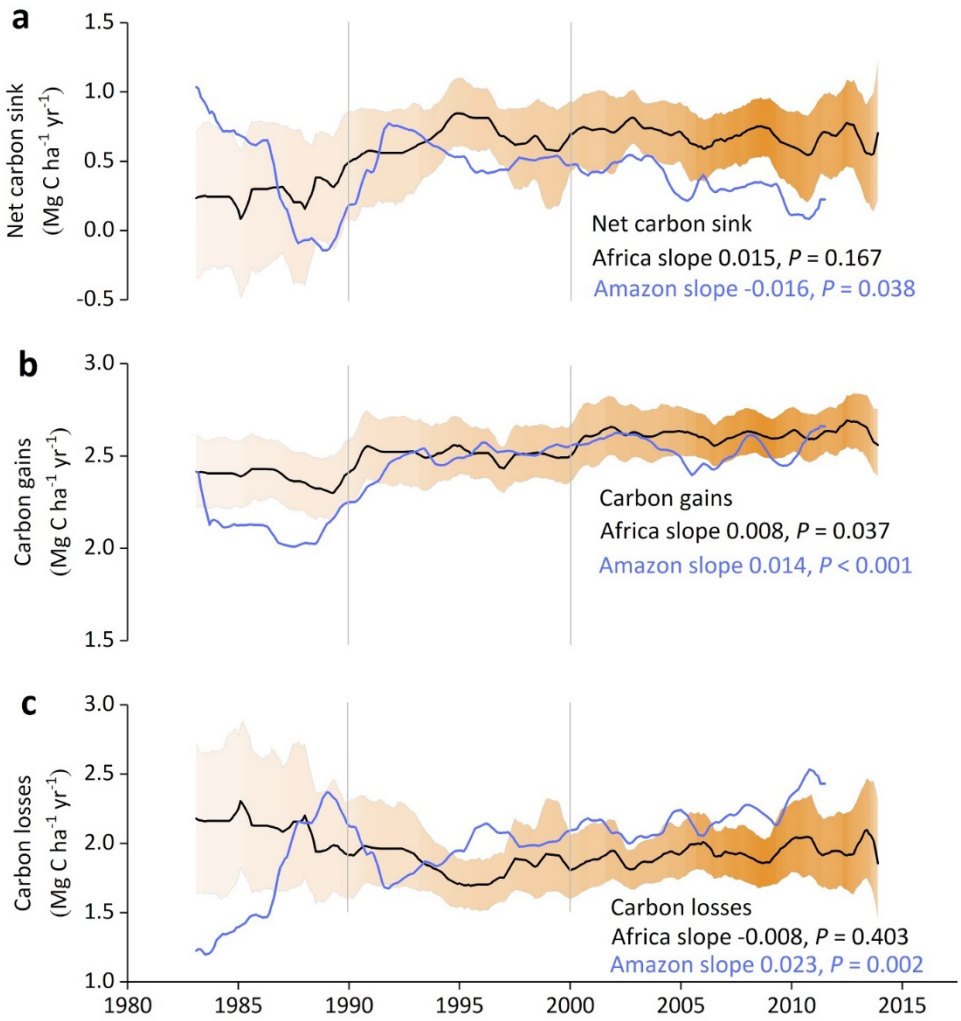

Figure 16. Time series of carbon dynamics from structurally-intact old-growth tropical forests in Africa and Amazonia from 1985 through 2015 (Data: Hubau et al., 2020). Note, the net carbon sink in Panel, a, refers to the net of two processes, carbon gains (productivity) and carbon losses (mortality), over intact tropical forests only. To attain a, net carbon sink estimate for the whole-region, e.g. to compare with atmospheric measurements and inversions (e.g. Gatti et al., 2021), in addition to the intact forest sink, fluxes associated with disturbance (deforestation, degradation through fire and selective logging), secondary forest regrowth and land-use fluxes (fluxes over crop and pasture), must be considered.

Other studies have focused on the differing impacts of increasing temperature on photosynthesis and heterotrophic respiration in the tropics. For example, Doughty and Goulden (2008) show that on short time scales, the efficiency of photosynthesis decreases beyond a critical temperature, while that of heterotrophic respiration continues to increase. Mau et al. (2018) suggest that many species of tropical trees may be especially sensitive to these effects. Possible evidence for this behavior was recently obtained by Duffy et al. (2021) using FLUXNET data, albeit with the caveat that CO_2 effects on GPP were not considered in their temporal extrapolation. Meanwhile, process-based models provide conflicting insights into the role of plant physiological processes including plant thermal responses and acclimation (McGuire et al., 2001; Friedlingstein et al., 2006; Booth et al., 2012, Mercado et al., 2018). There is also little consensus on how these changes will progress on longer time scales, when heterotrophic carbon limitation on microbial decomposition may also start playing a role (Soong et al., 2019).

5.7.2 Mechanisms Driving Long-term Trends in the Extratropical Land Sink

In the extratropics, studies have focused on identifying the mechanisms responsible for the changes in greening, seasonal cycle amplitude (SCA) and net CO_2 uptake across the high-latitude northern forests since at least the 1960s. Unlike the tropics, where heat-related increases in respiration and water stress are key growth limiters, here, the forests have adequate water, but their growth is thought to be limited primary by low light levels, low summer temperatures and short growing seasons (Song et al., 2018). Therefore, vegetation cover and phenology changes in response to warming trends and the effects elevated CO_2 have been identified as the likely drivers of increase in SCA (Graven et al., 2013; Forkel et al., 2019; Piao et al., 2017). At mid-latitudes, Zhu et al. (2016) and Piao et al. (2020b) analyzed their greenness time series with ensembles of DGVMs to identify the primary drivers of the observed increases. Both studies conclude that CO_2 fertilization is the primary driver of global greening since the 1980s However, they concede that other processes dominate on regional scales. For example, Piao et al. (2020b) attribute the enhanced greening over China and India primarily to afforestation and agricultural intensification.

To explain the mechanisms behind the enhanced SCA at higher northern latitudes, Keenan and Riley (2018) used observations of fAPAR collected between 1982 and 2012 to characterize the relationship between maximum annual foliage cover and summer warmth index. They attribute these changes to the recent warming (reduced spatial extent of temperature limitation) rather than CO_2 fertilization. In another observation-based study, Liu et al. (2020a) analyzed data from a variety of sources to determine the extent to which temperature changes alone could account for the long-term trends in SCA and CO_2 uptake of high latitude northern forests. They analyze space-based observations of SIF and XCO_2 from OCO-2 to estimate monthly mean GPP and NEE, respectively, at 4°×5° resolution for 2015-2017 and derive ecosystem respiration, TER as the difference between NEE and GPP. They fit simple exponential functions to the observed temperature dependence of GPP/PAR and TER and then hindcast spatially-resolved, monthly mean estimates of these variables to produce a time series spanning 1960 to 2014. They find that growing season mean temperature (GSMT) is the dominant driver of fPAR and GPP, explaining 70% of the observed spatial and temporal variability at latitudes between 50N and 75N over this time period, accounting for a 60% to 70% of the observed ~20% growth in SCA.

While these results support the conclusions of Keenan and Riley (2018), they appear to contradict the studies by Zhu et al. (2016) and Piao et al. (2020b), which analyzed greenness time series with ensembles of DGVMs to identify the primary drivers of the observed greening trends. Both studies conclude that CO_2 fertilization is the primary driver of global greening since the 1980s. Other studies based on atmospheric data and biogeochemical models have also pointed out a key role of CO_2 fertilization in SCA trends (Forkel et al., 2019; Thomas et al., 2016 Bastos et al., 2019; Piao et al., 2017).

An noteworthy difference between the observation-based studies and the model-based studies is the relationship between SCA and temperature adopted at high northern latitudes. While Keenan and Riley (2018) and Liu et al. (2020a) found that that fPAR, NEE, and SCA are positively correlated with temperature at 50N-75N, model-based studies (e.g. Bastos et al., 2019) find a negative relationship between SCA and temperature during the growing season at latitudes > 40N, which they attribute to moisture deficits and fires. This would be consistent with browning trends at high latitudes, attributed to disturbances such as fires, harvesting and insect defoliation (Beck and Goetz, 2011, Cortés et al., 2021). Regional differences across the arctic and boreal regions might also play a role. For example, North American boreal forests exhibit browning areas nearly 20 times larger than the Eurasian boreal forests (Harris et al., 2016; Piao et al., 2020b). Large-scale fire disturbances and insect infestation such as those from the bark beetle (Hlásny et al., 2021) have also been seen in browning areas in temperate regions in the past decade. Peñuelas et al. (2017) identified recent signs of slow-down of SCA increase at Barrow, pointing to a limitation of the positive effect of temperature in stimulating northern hemisphere CO_2 uptake, possibly due to increasingly negative impacts of weather extremes and disturbances. This lack of consensus on the relative roles of temperature, CO_2 fertilization and disturbance at high latitudes must be resolved, given their implications for the future evolution of this rapidly changing part of the land carbon cycle.

5.8 Patterns and Drivers of Interannual Variability in the Land Sink

In spite of the steady increase in fossil fuel CO_2 emissions over recent decades, the annual growth rate in atmospheric CO_2 varies markedly from year to year (Ballantyne et al., 2012; Piao et al., 2020a). The global growth rate of atmospheric CO_2 positively correlates with temperature. This relationship has been used to diagnose and constrain the future climate-carbon cycle feedback (Cox et al., 2013). The strong positive correlation between atmospheric growth rate and tropical temperature has been a conundrum, since the dynamics in tropical ecosystems are thought to be primarily driven by variations in moisture, i.e. dry season length and severity. Indeed, Jung et al. (2017) argue that at the local scale, the tropical carbon cycle is driven by moisture but at larger spatially scales the moisture signal is lost due to compensatory water effects (essentially there is greater spatial variability in moisture and thus regional signals counterbalance) leaving the temperature signal, which is more spatially coherent at the larger spatial scales.

Humphrey et al. (2018) challenged this conclusion showing a strong relationship between atmospheric CO_2 growth rate and observed changes in terrestrial water storage. Disentangling the land response to variation in temperature and water is complicated, for a variety of reasons. For example, soil-moisture-atmosphere feedbacks modify temperature and humidity, which impact vapor pressure deficit (VPD), which drive plant stomata opening and closure. Yuan et al. (2019) found that an increase in VPD reduces global vegetation growth, while Liu et al. (2020a)

suggest that soil moisture dominates dryness-related stress on global productivity, using SIF as a proxy. Finally, Humphrey et al. (2021) clarified the picture, showing how global NEE variability is driven by temperature and VPD effects controlled by soil moisture.

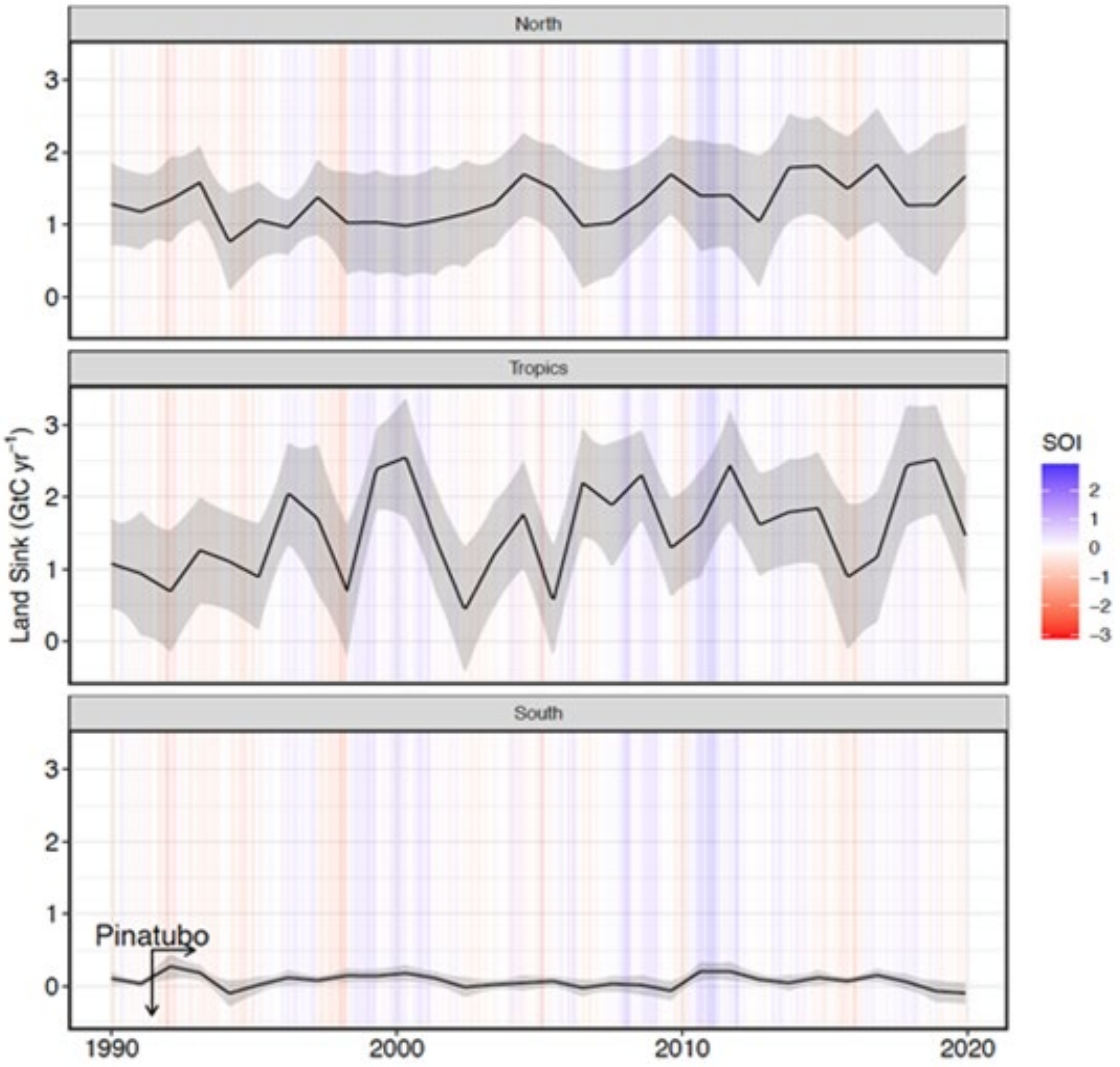

Figure 17. The multi-model mean land sink as derived from 14 TRENDY DGVMs for three regions and Southern Oscillation Index (SOI) between 1990 and 2020. The grey band represents 1 standard deviation. The Mount Pinatubo eruption in June 1991 in the Philippines is indicated with a vertical arrow with a horizontal arrow showing the duration of its effect on regional and global climate.

5.8.1 The Role of Climate Variability in the Interannual Variations of the Land Sink

Large interannual variations in global NEE are attributed to modes of climate variability, e.g., the impacts of the El Niño Southern Oscillation (ENSO) in tropical and southern regions (Figure 17). Two other modes of coupled ocean-atmosphere variability in addition to ENSO influence land-atmosphere CO_2 fluxes over the globe. The Pacific Decadal Oscillation (PDO) impacts tropical regions and extratropical North and South American regions. The Atlantic

Multidecadal Oscillation (AMO), influences CO_2 fluxes in Eurasia, northern North-America, and is an important influence in the Sahel and sub-tropical south American regions (Bastos et al., 2017; Zhu et al., 2017). These three modes of climate variability are thought to explain inter-annual variability (IAV) in CO_2 fluxes over more than 50% of the land surface (Zhu et al., 2017). Other processes, such as global cooling following large volcanic eruptions also contribute to IAV (i.e. Lucht et al., 2002; Angert et al., 2004).

In the Northern extratropics, regional modes of atmospheric variability also play a role in IAV in CO_2 fluxes. Dannenberg et al. (2018) showed that two leading modes of north Pacific variability controlled the onset of growing seasons over large regions in North America: the West-Pacific and the Pacific-North American patterns. In the Southern Hemisphere, in addition to ENSO, two other modes influence land carbon uptake: the Indian Ocean Dipole (IOD: Marchant et al., 2006) and the Southern Annular Mode (Marshall, 2003). Positive phases of IOD have been associated with reduced GPP and increased bushfires in Australia, and increased productivity in South Africa (Cai et al., 2009, Wang et al., 2021). Cleverly et al. (2016) have shown that periods when synchrony between ENSO, the IOD and the Southern Annular Mode occur, they were associated with carbon cycle extremes in Australia.

Extreme weather and climate conditions and associated disturbances are important contributors to the regional land carbon cycle (Reichstein et al., 2013; Zscheischler et al., 2014). While a few extremes have been found to explain 78% of IAV in GPP, they only accounted for 8-22% of IAV in NEE (Zscheischler et al., 2014). In their study, Zscheischler et al. (2014) indicate drought is the most common driver of negative extremes in GPP (>50% of the events), followed by fires (20-30% of events). There is also evidence for an increasing impact of warm droughts on northern ecosystem productivity in recent decades (Gampe et al., 2021).

Drought is a primary driver of reductions in photosynthesis and enhanced tree mortality through hydraulic failure (Rowland et al., 2015). Major droughts in recent years have been associated to strong reductions in regional GPP and net carbon uptake (Ma et al., 2016; Wolf et al., 2016; Peters et al., 2020), in some cases even turning ecosystems from sinks to sources of CO_2 (Ciais et al., 2005; van der Laan-Luijkx et al., 2015). In addition to direct impacts, droughts further contribute to subsequent disturbances, e.g. by increasing fire risk or insect outbreaks, and can lead to lagged tree mortality and consequent carbon losses (Anderegg et al., 2015).

Globally, fires constitute a major flux of carbon to the atmosphere (1.3-3.0 Pg C yr^{-1}, van der Werf et al., 2017), which is followed by regrowth sinks in the subsequent years. Even though fires can have both natural and human (e.g. deforestation, degradation and management) drivers, hot and dry conditions increase fire risk through increased fuel flammability. Therefore, all else being equal (i.e. human drivers), hot and dry periods, such as El Niño years, are associated with higher burnt area and CO_2 emissions, e.g. the massive burning associated in part with the 1997 El Niño over equatorial Asia. An increase in "mega- or extreme-" wildfires and associated large carbon emissions are anticipated with continued warming (Bowman et al., 2017; 2021; van der Velde et al., 2021).

5.8.2 ENSO as a Dominant Driver to Interannual Variability

El Niño is a climate mode associated with coupled atmosphere-ocean dynamics, originating in the tropical Pacific basin, with a frequency of between 2 and 7 years (McPhaden et al., 2006, p.200). At the onset of El Niño (ENSO "warm-phase"), the trade-winds weaken, reducing the upwelling along the western coast of South America, allowing the pool of warm

surface water and associated convection and rainfall to move eastwards towards the central Pacific. South East Asia and eastern Australia experience a large reduction in precipitation and increased warming, and teleconnections lead to reductions in precipitation over Amazonia and east Africa (Diaz et al., 2001). Because ENSO usually peaks during the wet seasons over tropical continents, this reduced rainfall leads to longer and more severe dry seasons, decreasing photosynthesis and reducing plant carbon uptake by tropical forests.

In contrast, La Niña (ENSO "cold phase") is associated with stronger than usual trade winds and wetter, cooler conditions that promote enhanced land carbon uptake over Equatorial Asia and Amazonia. The TRENDs in land carbon cYcle (TRENDY; Sitch et al., 2015) results for the tropical latitude band (30^{o}N-30^{o}S) in Figure 10 illustrate the impact of El Niño and La Niña on the land carbon uptake. Because tropical forests usually account for ~50% of the global NPP by terrestrial ecosystems, these impacts are reflected in the global growth rate of atmospheric CO_2. However, there is some evidence for an asymmetry in land response to ENSO (Cadule et al., 2010), whereby rainforests are less responsive to increased precipitation during La Niña than water deficit during El Niño. In addition to the asymmetry between El Niño and La Niña events, two types of ENSO can be distinguished: the "East Pacific", described above, and the "central Pacific" type, where the warm SST pool is shifted to the central Pacific region (Kao and Yu, 2009). Central Pacific El Niño events have been associated with even stronger responses by the land carbon cycle (Dannenberg et al., 2021).

ENSO is also the dominant mode of interannual variability in air-sea CO_2 fluxes (Feely et al., 1999; McKinley et al., 2004; 2017; Chatterjee et al., 2017). With the El Niño phase, upwelling of high-DIC waters in the eastern equatorial Pacific is reduced, lowering surface ocean pCO_2. At the same time, reduced wind speeds slow gas exchange. The net effect is to substantially reduce eastern equatorial Pacific CO_2 outgassing. In the La Niña phase, upwelling is enhanced and outgassing is increased. The magnitude of these variations is up to +-0.5 Pg C yr^{-1}, and the type of ENSO event is a significant modulator of the flux (Liao et al., 2020). The effect on atmospheric CO_2 concentration from the ocean from ENSO is thus the opposite from that from land, with a greater ocean sink during El Niño and a lesser ocean sink during La Niña.

In addition to the tropical regions, ENSO is known to influence IAV in land CO_2 fluxes in some extratropical regions, especially semi-arid regions in the Southern Hemisphere such as Australia, South Africa and parts of Southern South America (Poulter et al., 2014; Bastos et al., 2013). Indeed, tropical drylands are now thought to contribute about equally or more to IAV in the global carbon cycle as humid tropical biomes (Ahlström et al., 2015; Piao et al., 2020a). These ecosystems are characterized with lower biomass and productivity than forests. Nevertheless, their vast spatial area allows them to be important to the global carbon cycle. Extra-tropical ecosystems are estimated to contribute up to 30% to global land sink IAV (Piao et al., 2020a).

While it is difficult to show the impact of climate extremes such as a strong El Niño using in situ inventory data alone, bottom-up inventories of AGB stocks compiled from microwave remote sensing observations provide a temporally denser record of such impacts. For example, contrary to the conclusions of Hubau et al. (2020), who found negligible change in the African forest, Wigneron et al. (2020) show that there was a strong "legacy effect" after the 2015-2016 El Niño event in both African and Amazonian forests, extending the duration of the response in both regions (0.9 and 0.5 Pg C loss in 2014-2017 respectively). For the overall tropics, Fan et al. (2019) use Vegetation Optical Depth (VOD) data from microwave sensors to

show how changes in the AGB biomass of the forests of Tropical Africa and Tropical Asia contributed strongly to the IAV in CO_2 growth rates, but concluded that AGB in semi-arid biomes dominated the IAV in these growth rates.

5.8.3 The Best Observed ENSO Ever - the 2015-2016 El Niño

The record-setting 2015-2016 El Niño was the first large ENSO event for which atmospheric CO_2 and SIF estimates were available at high spatial and temporal resolution from space based platforms. This data-rich perspective provided a more comprehensive description of the impacts of climate perturbations on the exchange of carbon between land and ocean reservoirs and the atmosphere on regional scales. Chatterjee et al. (2017) compared XCO_2 estimates derived from Orbiting Carbon Observatory-2 (OCO-2) observations over the central and eastern tropical Pacific basin to an XCO_2 climatology of this region based on observations from the Greenhouse gases Observing SATellite (GOSAT). Between March and July 2015, these comparisons reveal a 0.5 ppm decrease in XCO_2 that is attributed to reductions in outgassing in the tropical Pacific Ocean (Chatterjee et al., 2017). By September of 2015, these reduced XCO_2 values were replaced by 0.5 to 2 ppm increases in XCO_2 that were attributed to reduced uptake and increased emissions of CO_2 by tropical forests in South America, Africa and tropical Asia (Liu et al., 2017; Heymann et al., 2017; Palmer et al., 2019; Crowell et al., 2019; Figure 18).

Observations of SIF provided similar insights. Koren et al. (2018) find that SIF was strongly suppressed in late 2015 over tropical areas with anomalously high temperatures and reduced soil moisture. Their observations show that SIF fell below its climatological range starting from the end of the 2015 dry season (October), but returned to normal levels by February 2016 when atmospheric conditions returned to normal. Importantly, the impacts of the El Niño were not uniform across the Amazon basin.

Additional insight into the tropical land carbon cycle's response to the 2015-2016 El Niño was gained by comparing coincident observations of XCO_2 anomalies and SIF (Liu et al., 2017). Specifically, the largest positive CO_2 anomalies derived from the space-based XCO_2 estimates are seen in regions where SIF observations indicate the highest photosynthetic activity (Figure 11). This suggests that in spite of significant growth, tropical forests are now emitting more CO_2 than they absorb, when integrated over the annual cycle. This may be due to human activities, such as deforestation and forest degradation or climate related factors such as temperature-dependent respiration increases, drought stress, fires, and other processes.

Liu et al. (2017) find that the pan-tropical biosphere released an additional 2.5 ± 0.34 Pg C into the atmosphere, or about 78% of the global total emissions of CO_2 from the land biosphere during the 2015-2016 El Niño compared with the 2011 La Niña year. These values are substantially larger than those inferred from ensembles of bottom-up land surface models or inverse models constrained the sparse in situ network alone (Bastos et al., 2018; Crowell et al., 2019). Liu et al. find that emissions originated throughout the tropics with 0.91 ± 0.24, 0.85 ± 0.21, and 0.60 ± 0.31 Pg C from tropical South America, tropical Africa, and tropical Asia, respectively.. Although the enhanced emissions from these three regions were comparable, *different* processes appeared to dominate in each region. Fire emissions dominated over tropical Asia. Both increased respiration and fires associated with historically high temperatures dominated over tropical Africa. Increased atmospheric CO_2 mixing ratios over the Amazon in 2015-2016 were attributed to GPP reductions associated with drought. These results support the hypothesis that El Niño related increases in CO_2 growth rates are primarily due to tropical land carbon fluxes, but they show that specific mechanisms can differ from continent to continent.

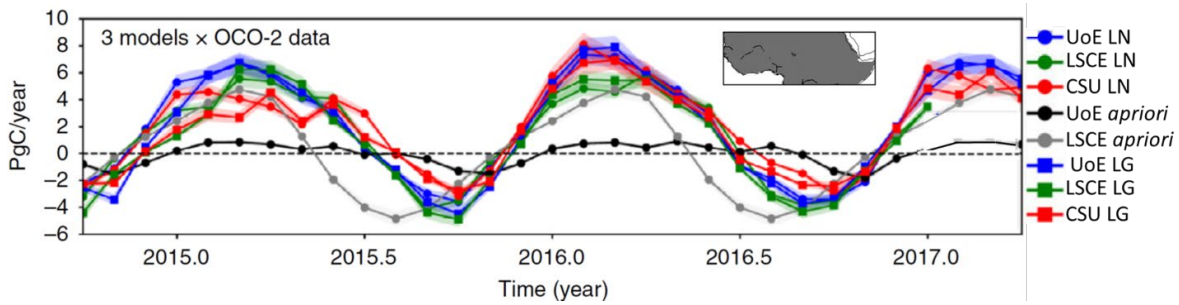

Figure 18. CO_2 fluxes from tropical northern Africa inferred from the University of Edinburgh (UoE), LSCE and Colorado State University (CSU) models constrained by in situ CO_2 measurements as well as XCO_2 data from GOSAT and OCO-2. Positive fluxes indicate CO_2 emissions from the land surface to the atmosphere. LN and LG denote OCO-2 XCO_2 measurements taken using nadir and glint observing modes, respectively. The geographical region is shown in the inset. Fluxes inferred from OCO-2 data have larger amplitudes and a larger seasonal cycle than those from in situ data. An extended mission will provide new opportunities to validate these results and track their changes (Adapted from Palmer et al., 2019).

Palmer et al. (2019) and Crowell et al. (2019) use ensembles of models to analyze in situ CO_2 measurements along with XCO_2 and SIF observations from GOSAT and OCO-2 (Figure 18). Like Liu et al., in 2015–2016, they find that the largest CO_2 emissions were over western Ethiopia and western tropical Africa, where there are large soil organic carbon stores and substantial LUC. While the amplitude of the XCO_2 anomalies that produced these sources may have been overestimated in the early OCO-2 XCO_2 products used in this investigation (version 7), they clearly reveal an important source of emissions from the tropical carbon budget that is largely missing from in carbon flux inverse models constrained by *in situ* measurements alone.

It is interesting to compare the terrestrial carbon cycle's response to the two largest recent El Niño events in 1997 and 2015/16. Large fire emissions in equatorial Asia were responsible for ~1 Pg C yr^{-1} emissions in 1997 (i.e. Page et al., 2002), yet far smaller fire emissions were estimated in 2015/16. This is largely due to the timing of the El Niño in relation to the dry season (i.e. in 2015/16 the El Niño was about 1 month later). The 2015-2016 El Niño is associated with reductions in GPP in Amazonia and a lagged increase in respiration (Braswell et al., 1997). This is likely related to the lagged mortality associated with forest degradation, and thus respiration from the larger necromass pool. More generally, forest degradation is becoming a larger carbon source than deforestation, with highest ground-level forest fires associated with drought years.

As the 2015-2016 El Niño transitioned to a weak La Niña in 2017 and then to more neutral conditions in 2018, OCO-2 XCO_2 estimates indicate that tropical forests, once thought to be significant net sinks of CO_2 (Pan et al., 2011; Sellers et al., 2018) may now be net sources (Palmer et al., 2019; Crowell et al., 2019; Peiro et al., 2021). The atmospheric inversions support the inferences from XCO_2 anomaly maps (Hakkarainen et al., 2016; 2019; Figures 13, 14) which show positive XCO_2 anomalies over tropical forests with amplitudes of 1-2 ppm above the background since 2015. For the Amazon, both the spatial extent of the positive anomaly and the amplitude of the inferred source were greater during the 2015–2016 El Niño (~0.5 Pg C yr^{-1}) than in later years (0.1-0.2 P C yr^{-1}), but both indicate that this region has been a net source from season to season and from year to year throughout the OCO-2 mission. These conclusions are

consistent with results inferred from in situ CO_2 profiles described by Gatti et al. (2021), which indicate that the Amazon has been a source of CO_2, rather than a sink since 2010.

Positive XCO_2 anomalies over topical Africa and Southeast Asia are seen on annual time scales (Figures 13). However, tropical African fluxes are negative during June-July-August (Figure 18), indicating that this region becomes a weak sink during that season (Palmer et al., 2019). These conclusions are supported by some satellite-based aboveground biomass studies (Baccini et al., 2017; Wigneron et al., 2020), but are inconsistent with plot-based studies (Pan et al., 2011; Hubau et al., 2020), which conclude that tropical forests are absorbing less CO_2, but are still a net sink of carbon.

5.9 Observations Needed to Advance Understanding of Trends in the Land Carbon Sink

The overall picture that emerges from recent observations of AGB stocks is that the classical sinks in the tropical humid forests are slowly losing strength, with these changes amplified by deforestation. In extra-tropical areas, greening has taken place due to afforestation, increased agriculture and longer growing seasons. In some parts of the Arctic and boreal regions, browning, i.e. a loss of vegetation activity, is increasing. These trends provide the fragile background for a still slowly increasing land uptake. The underlying causes for these increases are complex and consist of interacting processes of CO_2 fertilization, nutrient and water availability compounded by variability and secular changes in climate. On top of this, the impact of human activities including deforestation, afforestation and intensifying agriculture are additional complications.

This myriad of interacting processes complicates predictions of the future trajectory of the terrestrial sink in a warming climate. Until now, the sink has grown in harmony with increased fossil fuel emissions with the result that the airborne fraction has remained remarkably constant over the past 60 years or so. Theoretical and empirical evidence, such as that summarized in this paper, suggests that the sink may stop growing at some point in the future as water and nutrient shortages will start to impede increased growth.

5.9.1 Linking Stocks and Fluxes with Bottom-up Measurements and DGVMs

One factor that has impeded progress in the analysis of trends inferred from AGB stocks is they are not well represented in the current generation of DGVMs. For example, Sitch et al. (2015) use an ensemble of nine DGVMs to study global and regional processes and trends in the land sink for a period extending from 1990 - 2009. They conclude that for this period, the global land sink is increasing, led by CO_2 fertilization of plant production, with the largest increases seen in the natural ecosystems of the tropics. They find no significant trend in northern land regions. More recent studies with updated versions of DGVMs now estimate increasing trends in the Northern Hemisphere land sink, although with large spread across models (Ciais et al., 2019; Fernández-Martinez et al., 2019) and regional mismatches with observation-based estimated (Bastos et al., 2020).

Fortunately, advances in bottom-up observation capabilities and modeling tools are coming on line to facilitate more comprehensive and responsive monitoring and analysis of the land carbon cycle. Ground-based estimates of stocks and fluxes will continue to provide the most accurate and site-specific information. However, remote sensing observations from airborne and space-based active and passive sensors and modeling tools will play an increasingly important role for upscaling these results to yield useful constraints on regional to global scales. While new

space-based datasets provide an increasingly diverse set of measurements to monitor the land-surface with high spatial and temporal resolution, long-term in situ datasets still provide crucial information to properly constrain patterns and drivers of long-term trends and inter-annual to decadal variability.

5.9.2 Space-based Estimates of Fluxes and Stocks

Xiao et al. (2019) review the evolution of remote sensing observations of terrestrial carbon stocks over the past 50 years, spanning the electromagnetic spectrum from the visible, infrared, and microwave. They then review the methods being used to analyze the observations to yield quantitative estimates of carbon stocks and fluxes, including vegetation indices, SIF, light use efficiency models, DGVMs, as well as data driven (including machine learning) techniques. Xiao et al. discuss the use of these data and analysis techniques to quantify the impacts of disturbances and to quantify uncertainties in carbon stock estimates, noting advances achieved by integrating in situ and remote sensing observations into progressively more advanced, process-based carbon cycle models. Looking forward, they predict substantial improvements in our ability to track AGB stocks through the use of merged datasets, such as the NASA Harmonized LandSat and Sentinel 2 (HLS) products, ultra-high resolution imaging products from QuickBird, IKONOS, and UAVs, lidar measurements from GEDI, future active microwave products from NASA's NISAR (Rosen et al., 2016), TanDEM-L and BIOMASS missions (Quegan et al., 2019).

While in situ and space-based measurements of AGB play a critical role in efforts to monitor trends in managed and natural forests, they do not have the sensitivity needed for monitoring the rapid turnover of carbon stocks in croplands and grasslands, where the biomass changes are spatially extensive, but below the detection limits of these measurements. Until recently, high resolution imaging observations and moderate resolution estimates of vegetation indices provided the primary tools for scaling up plot-based observations to national and continental scales. Recently, these capabilities have been augmented by space-based observations of SIF. SIF relates the emission of excess radiative energy from the photosynthesis process of leaves at two wavelengths 685 nm and 740 nm to photosynthesis, or GPP. Estimates of SIF from GOME, GOME2, GOSAT, OCO-2 and TROPOMI are increasingly being used to monitor crop and grassland productivity and crop yield prediction (Guan et al., 2017; He et al., 2020; Peng et al., 2020; Parazoo et al., 2020; Qiu et al., 2020; Yin et al., 2020). Future SIF observations from the ESA FLuorescence EXplorer (FLEX), Japan's GOSAT-GW, NASA's GeoCarb, and the Copernicus CO2M missions promise substantial improvements in resolution.

Space-based observations of XCO_2 and SIF are being combined with observations of vegetation indices (LAI, NDVI, NIRv), VOD and other environmental properties to provide new insights into the high latitude terrestrial carbon cycle. Unlike for the tropics, top-down estimates of CO_2 fluxes derived from space-based observations of XCO_2 anomalies over northern temperate and boreal forests tend to reinforce the conclusions from other observations and modeling studies. During the northern hemisphere summer (JJA in Figure 13), negative XCO_2 anomalies prevail across most of this region. Annual average flux inversion experiments show moderately strong GPP and negative NBE (Figure 19). These XCO_2 and SIF measurements therefore indicate that northern forests have continued to act as significant net CO_2 sinks as the CO_2 seasonal cycle amplitude has grown in response to warming (Liu et al., 2020a).

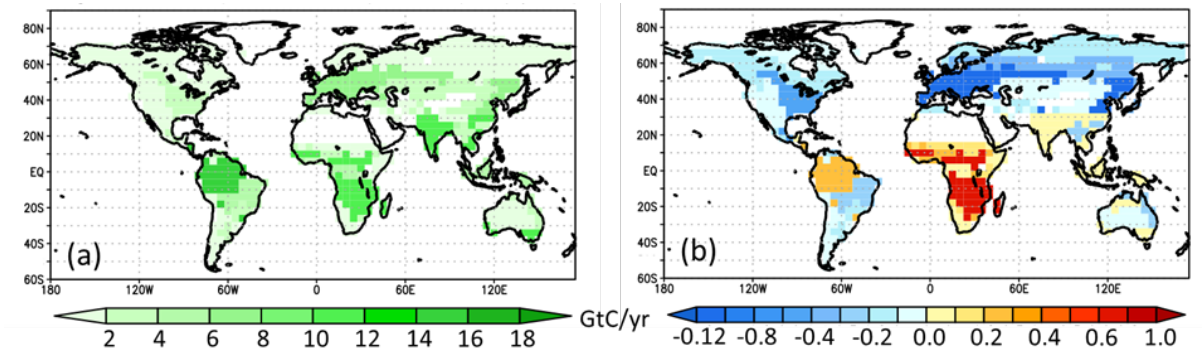

Figure 19. (a) GPP from OCO-2 SIF and (B) Net Biospheric Exchange (NBE) from XCO_2 and SIF, both expressed in gigatons of carbon per year (Pg C yr^{-1}) for 2015-2018. Negative NBE indicates sinks while positive values indicate sources. NBE is typically < 5% of the GPP, but is positive in the tropics where we see the highest GPP, in sharp contrast to existing models (Junjie Liu, Personal communication, 2019).

Observations of XCO_2 and SIF also provide unique opportunities to study the relationships between the land and atmospheric carbon cycles and the hydrological cycle. Yin et al. (2020) combine SIF with atmospheric CO_2 observations to quantify the effects of large-scale flooding on cropland carbon sequestration. Widespread flooding during spring and early summer of 2019 delayed crop planting across the U.S. Midwest. As a result, satellite observations of SIF from OCO-2 and the TROPOspheric Monitoring Instrument (TROPOMI) reveal a delay of 16 days in the seasonal increase of photosynthetic activity relative to 2018, along with a 15% lower peak photosynthesis. Yin et al. find that the 2019 anomaly produced an estimated GPP reduction of -0.21 Pg C in June and July that was partially compensated in August and September with a +0.14 Pg C increase. The growing season integral corresponds to a 4% reduction in cropland GPP for the Midwest, but a 3% increase for areas where cropland occupies less than 10% of the land. Using an atmospheric transport model, they show that a decline of ~0.1 Pg C in the net carbon uptake in June and July is consistent with observed ~10 ppm CO_2 enhancements in the midday boundary layer from the Atmospheric Carbon and Transport - America (ACT-America) aircraft and the ~1 ppm increases in XCO_2 seen by OCO-2.

In another study, Gonsamo et al. (2019) combined OCO-2 SIF observations with soil moisture (SM) observations from NASA's Soil Moisture Active Passive (SMAP) mission to study the impact of environmental limiting factors on terrestrial ecosystem productivity of drylands and croplands. For drylands (dry sub-humid, semi-arid, and arid zones) and the majority of croplands, soil water content is typically low and topsoil moisture is critical for plant growth. As expected, SMAP SM retrievals show positive daily relationships with OCO-2 SIF for drylands and croplands of the tropics and Australia, where SM is limiting plant growth and concurrent data records are sufficient to make statistical inferences. Negative relationships between SIF and SM were observed in forested areas of mid-latitude dry sub humid zones with high average annual SM. In these regions, SIF showed a positive relationship with air temperature. They find strong evidence that the OCO-2 SIF is accurately capturing monthly SMAP SM dynamics, particularly for regions with distinct seasonality of rainfall such as Sub-Saharan North Africa, Indian subcontinent, and southern Africa.

Other advances in remote-sensing capabilities are expected to accelerate progress in monitoring, verification and understanding of temporal changes in biomass and productivity. Until very recently, the remote-sensing community has pioneered static biomass maps, based on a composite of products and field-truthing, or inferred biomass change from products like VOD. Now, with new missions and sensors, e.g. GEDI/BIOMASS, the community is at the cusp of direct monitoring biomass change at scale for the first time. This information in combination with monitoring of productivity directly and land cover change, will revolutionize research on the land carbon cycle.

To fully exploit these new measurements to describe long term trends in the terrestrial carbon cycle, the in situ and remote sensing measurements must be reconciled so that their climate data records can be combined to increase their spatial and temporal resolution and coverage. The protocol for cross-validating aboveground biomass products described by Duncanson et al. (2019) and the effort by the Forest Observation Initiative to develop a global in situ forest biomass databases for validating remote sensing observations (Schepaschenko et al., 2018) are positive steps in this direction.

While the current generation of DGVMs and other terrestrial biosphere models are evolving rapidly and providing important insights into the processes driving the land carbon cycle, these modeling tools are still yielding widely diverging results the uptake of CO_2 by the land biosphere and its trends (i.e. Fisher et al., 2014; Sitch et al., 2015; Keenan and Williams, 2018; Parazoo et al., 2020). These limitations have raised concerns about their use in CO_2 emission inventory development activities (Grassi et al., 2018; Petrescu et al., 2020). Pioneering model intercomparison efforts such as the Carbon-Land Model Intercomparison Project (C-Lamp; Randerson et al., 2009) are being followed up by the International Land Model Benchmarking (ILAMB) project (see https://www.ilamb.org/) to address these concerns and accelerate the development of these critical tools.

6 Discussion

When integrated over the industrial age, the land sink associated with intact forests and other natural parts of the terrestrial biosphere has roughly balanced sources associated with LUC while the ocean has been a cumulative net sink of anthropogenic carbon emissions (Friedlingstein et al., 2021). Since 1958, when continuous atmospheric CO_2 measurements have been available, CO_2 emissions from fossil fuel combustion have increased by about a factor of four, from less than 2.5 Pg C yr^{-1} to almost 10 Pg C yr^{-1} in 2019. During this period, the land sink grew as well, absorbing a near constant fraction of the anthropogenic emissions (~30%). Together, sinks in ocean and on land have absorbed enough anthropogenic CO_2 to limit the fraction that has remained in the atmosphere to a remarkably constant value around 45% (Raupach et al., 2014). This implies that, to first order, the uptake by the ocean and land sinks has increased proportionally with the emissions (Friedlingstein et al., 2021).

There has been debate as to whether increases in the airborne fraction since 1958, i.e. declines in sink efficiency, are already observable (Canadell et al., 2007; Knorr 2009; Gloor et al., 2010; Raupach et al., 2014). Even if an increasing airborne fraction is not yet detectable, process-level understanding and regional trends indicate that the airborne fraction should increase as climate change progresses (Raupach et al., 2014; Canadell et al., 2021). While the exact timing and magnitude of changes in the land and ocean sinks remains unclear, the likelihood is high that substantial climate-carbon feedbacks will occur during this century. Any

upward change in the airborne fraction, or reduction in sink capacity, will decrease the allowable fossil carbon that can still be burned without violating the temperature targets specified in the Paris Agreement.

For the ocean, despite remaining uncertainties and missing closure terms, distinct methodologies for quantifying the ocean uptake of anthropogenic CO_2 agree that the sink has increased over the industrial era, including in recent decades. Since the uptake of atmospheric CO_2 on annual to decadal time scales is primarily controlled by the pCO_2 gradient at its surface, the carbon sink is expected to grow as long as near-exponential growth of atmospheric pCO_2 continues. However, if anthropogenic emissions are reduced, atmospheric pCO_2 will grow more slowly, and thus there will be a reduced ocean carbon sink even if the ocean circulation and chemical buffer capacity do not change (Ridge and McKinley, 2021). To understand these likely changes, it is essential that ocean carbon studies start to focus more attention on the near-term response to emission mitigation scenarios (Hausfather and Peters, 2020). If emissions are not mitigated, current climate models suggest that by the middle to late 21st century, a slowing ocean overturning rate and reduced chemical capacity in the ocean will reduce the rate of growth in the global ocean sink (Randerson et al., 2015).

To develop an integrated ocean carbon observing system that can track the evolution of the ocean sink on the annual to interannual timescales most relevant to climate change policy, we need to sustain existing and continue to develop improved observation systems for the surface and interior ocean. Ocean carbon instruments deployed on autonomous platforms are revolutionizing ocean carbon measurement spatial and temporal resolution and coverage, but reduced uncertainties in the carbonate constants are needed to fully exploit these data. High-quality shipboard observations will continue to be required. We also need improved ocean hindcast models and better understanding of uncertainties in observation-based data products derived through statistical extrapolation of sparse surface ocean pCO_2 data in order to track the real-time evolution of the ocean carbon sink and its decadal trend reliably.

For the land carbon cycle, the current state, trends and near-future evolution is less clear. Classical sinks in the tropical humid forest sinks are slowly losing their strength and these changes are amplified by the losses associated with deforestation, forest degradation and extreme climate events. In the extratropics, multiple data sources support the existence of an increasing terrestrial sink, driven by CO_2 fertilization, afforestation, agricultural intensification and other factors. Across the Arctic and boreal regions, which are experiencing roughly twice the average rate or global warming, most regions have seen significant increases in GPP, NEE and SCA since the 1960s due to higher growing season temperatures and other factors. However, a small fraction of this region is seeing reduced NEE that are attributed to increases in fire disturbances, drought stress, and insect infestation. Both improved observations and models are needed to track these changes as the carbon cycle continues to respond to human activities and climate change.

Space-based remote sensing observations are helping to revolutionize our ability to monitor the response of the global carbon cycle to anthropogenic forcing and a changing climate. In the ocean, sea surface temperature and chlorophyll are critical to process-based and machine learning extrapolations of sparse pCO_2 data to global coverage. From a bottom-up perspective, microwave and lidar measurements are providing higher spatial and temporal resolution estimates of AGB stocks. SIF measurements are providing a more responsive estimate of light use efficiency and CO_2 uptake by plants. From a top-down perspective, space-based remote

sensing estimates of XCO_2 are complementing ground-based and aircraft in situ measurements with much greater spatial and temporal resolution and coverage.

These space-based measurements sometimes reinforce, amplify or contradict conclusions about the land carbon cycle inferred from ground-based in situ measurements, painting a somewhat controversial picture of the evolution of the land carbon cycle. For example, in the tropics, both space-based microwave estimates of AGB (Wigneron et al., 2020) and top-down atmospheric inverse models constrained by space-based estimates of XCO_2 (Liu et al., 2017; 2020; Palmer et al., 2019; Crowell et al., 2019; Gatti et al., 2021) indicate that the humid tropical forests did not fully recover from the 2015-2016 El Niño, and have transitioned from net sinks to net sources of CO_2. More generally, the space-based measurements are also providing more information about rapid changes in the land carbon cycle associated with severe weather, such as droughts (Gonsamo et al., 2019; Castro et al., 2020) and floods (Yin et al., 2020). They are also beginning to provide estimates of CO_2 emissions from fossil fuel combustion and other human activities (Hakkarainen et al., 2016; 2019; Wang et al., 2018; Hedelius et al., 2018; Wu et al., 2018; 2020; Reuter et al., 2019).

In spite of these advances, the reliability of the space-based remote sensing results are still a subject of substantial debate within the land carbon cycle community. This is especially true for the tropics, where CO_2 fluxes derived from the space-based XCO_2 estimates differ in both sign and magnitude from the results of earlier flux inversion experiments constrained by bottom-up stock or flux estimates or ground-based in situ measurements of atmospheric CO_2. This apparent inconsistency suggests one of three possibilities. First, the space-based XCO_2 estimates might still include biases that compromise the accuracy of the top-down flux estimates. Recent efforts to validate the space-based XCO_2 estimates using measurements from TCCON and other standards (Wunch et al., 2017) indicate biases with amplitudes less than one third as large as the observed tropical XCO_2 anomalies. However, there are few TCCON stations or other validation capabilities in the tropics. Second, fluxes constrained by surface in situ measurements, alone, may tell an incomplete story of the land carbon cycle in sparsely sampled regions. The spatial resolution and coverage provided by surface in situ measurements of carbon stocks, fluxes, or atmospheric CO_2 are still very limited, especially in the tropics and boreal regions, where the largest flux differences are seen. Both top-down and bottom-up methods may yield unreliable results where there are few measurements. Third, flux estimates based on the much denser space-based XCO_2 measurements may be tracking changes in the natural carbon cycle on time and space scales too short to be resolved by the in situ measurements of stocks or CO_2 concentrations. A tropical land carbon monitoring system with even greater spatial and temporal coverage is needed to track these changes as the these areas continue to respond to human activity and climate change.

While these space-based observations and top-down inverse models are providing new insights into this system, they have also revealed measurement gaps and modeling limitations that must be addressed to develop a true global carbon monitoring system that can track changes in both natural and anthropogenic sources and sinks of CO_2 on policy relevant time and space scales. For example, space-based remote sensing observations of atmospheric CO_2 and land and ocean surface properties can expand the coverage and resolution of surface-based in situ measurements. However, passive remote sensing observations are largely precluded in persistently cloudy regions such as tropical rain forests, or mid- and high-latitude forests during the fall, winter and spring. These regions are often centers of action in the carbon cycle, but are

also among the most challenging to observe systematically with surface-based in situ measurement systems. Similarly, remote sensing observations provide little insight into the carbon budget of the interior ocean, but here networks of autonomous in situ sensors have great potential to greatly expand opportunities for gathering critical ocean carbon data. Like remote sensing observations, their data typically has larger uncertainties and biases than conventional shipboard in situ measurements. Thus, a robust ocean carbon observing system will require continued shipboard observations for calibration and validation.

These perspectives reinforce the continuing need to maintain and expand the ground-based, ship-based and airborne CO_2 measurement networks. These networks fill three critical needs. First, as noted above, in situ measurements are needed to complement the coverage provided by remote sensing observations in persistently cloudy regions. In addition, because the air-sea flux of CO_2 is determined mainly by the pCO_2 gradient between the ocean surface layer and the atmospheric surface boundary layer, in situ vertical profiles of near-surface atmospheric CO_2 concentrations are critical for validating flux estimates over the ocean. Second, because surface and airborne in situ and surface remote sensing observations are more accurate than space-based remote sensing measurements, these data are critical for validating the space-based remote sensing measurements. Finally, while atmospheric CO_2 and CH_4 can now be measured from space with the accuracies needed to quantify surface fluxes, other critical greenhouse gases (N_2O, CFCs, HCFCs, SF_6 etc.) can only be measured to adequate accuracy with ground-based and airborne sensors. Other species that are useful for distinguishing fossil fuel from biospheric CO_2 emissions, such as carbon-14 (^{14}C) can also only be measured in situ (Miller et al., 2012; 2020).

To address these needs, national agencies such as the U.S. National Oceanic and Atmospheric Administration (NOAA), Japan's National Institute for Environmental Studies (NIES) and European organizations, including the European Space Agency (ESA), Copernicus, Integrated Carbon Observation System (ICOS) and IAGOS, are working with WMO Global Atmospheric Watch (GAW) and the Global Climate Observing System and the Global Ocean Observing System (GCOS, GOOS) to coordinate and expand the deployment of ground-based, ocean and airborne in situ sensors. While the number of ground-based and airborne CO_2 monitoring stations has grown slowly over the past decade, new measurement capabilities are coming on line that promise substantial increases in coverage. The up-looking remote sensing measurements being collected by the TCCON spectrometers are being complemented by measurements from smaller, less costly, and more portable Bruker EM27/SUN systems. These spectrometers are now being deployed as networks in urban settings (Hedelius et al., 2018) and in remote locations (Frey et al., 2019). In situ vertical profiles of CO_2, CH_4 and other gases are now being collected at altitudes as high as 25 km by AirCore instruments deployed on low-cost weather balloons (Karion et al., 2010; Baier et al., 2020). Additional in situ profiles and upper tropospheric measurements are now being made by commercial aircraft in Japan's Comprehensive Observation Network for Trace gases by Airliner (CONTRAIL) and Europe's In-service Aircraft for a Global Observing System (IAGOS).

The world's space agencies are actively working to coordinate ambitious plans for an expanded space-based remote sensing capability that supports atmospheric CO_2 measurements, high resolution maps of land surface type and biomass and ocean biological productivity. These efforts are being led by the Committee on Earth Observation Satellites (CEOS) and Coordination Group on Meteorological Satellites (CGMS) through their Joint Working Group on Climate

(WGClimate) Greenhouse Gas Task team. The modeling systems needed to ingest and analyze the data collected by these expanding measurement systems are also advancing. However, efforts to coordinate carbon cycle modeling efforts are receiving less attention from the carbon cycle science community and their stakeholders.

7 Conclusions

Fossil fuel use, LUC and other human activities are now adding more than 10 petagrams of carbon to the atmosphere each year. These emissions have increased the atmospheric CO_2 mixing ratio by almost 50% since the beginning of the industrial age and would have produced much larger changes if natural sinks in the land biosphere and ocean had not removed over half of this anthropogenic CO_2. As the world embarks on efforts to monitor and control CO_2 emissions, there is growing evidence that the natural carbon cycle is evolving in response to human activities, severe weather, disturbances and climate change.

Our understanding of the carbon cycle and its response to natural and anthropogenic forcing has grown steadily over the past two decades as more advanced carbon cycle measurement systems have been deployed and their results have been analyzed with more sophisticated top-down atmospheric CO_2 flux inversions as well as bottom-up diagnostic and prognostic carbon cycle models. These measurements and models reveal a strongly coupled, dynamic system that responds on daily, to seasonal, to interannual time scales across spatial scales spanning individual fields, forest plots or coal-fired power plants on land or individual eddies in the ocean to entire continents or ocean basins.

On decadal or longer time scales, measurements of changes in carbon stocks in the ocean and on land provide a reliable integral constraint on fluxes of CO_2 to the atmosphere. These measurements show that while the ocean and terrestrial biosphere now absorb comparable amounts of anthropogenic CO_2, LUC emissions have roughly balanced the terrestrial sink over the industrial era and the ocean has provided the primary cumulative net sink of anthropogenic carbon. Over this period, the CO_2 uptake by the ocean has increased as the atmospheric CO_2 partial pressure (pCO_2) has increased nearly exponentially and the ocean overturning has continually circulated from depth to surface, thus exposing pristine deep waters to the anthropogenically-perturbed atmosphere. However, additional study is needed to reconcile diverging estimates of the decadal trend of the ocean sink. For the land carbon cycle, the emerging picture is regionally dependent. Over the past three decades, the uptake of CO_2 by intact tropical humid forests appears to be declining. These reductions in the tropical land sink are offset by net increases across mid- and high-latitudes associated with CO_2 fertilization, afforestation, the agricultural green revolution, and longer growing seasons associated with climate change.

Direct measurements and model-derived estimates of CO_2 fluxes at the Earth's surface provide additional insight into variability on seasonal to decadal timescales. Surface ocean pCO_2 measurements and ocean models indicate that the global ocean carbon sink did not grow significantly over the 1990s, but then grew steadily since 2000, a pattern that can be explained, to first order, by the changing growth rate of atmospheric pCO_2. This implies that a rapid decline of the ocean sink can be expected when atmospheric levels are reduced through emission reductions. The evolution of the land sink is more difficult to predict given its ongoing declines in strength in tropical regions and enhancements in strength across the extratropics, both strongly driven by human activities and climate change.

While these observations and models are providing new insights into the carbon cycle, they are also revealing measurement gaps and modeling limitations that will have to be addressed to diagnose its current state and predict its evolution. In particular, they reinforce the urgent need for more comprehensive measurements of stocks, fluxes and atmospheric CO_2 concentrations in humid tropical forests and at high latitudes, which appear to be experiencing rapid changes. This requires expanded ground-based and airborne measurement capabilities, because these regions are intrinsically difficult to monitor with emerging remote sensing techniques due to persistent cloud cover and limited sunlight at high latitudes during the winter. Similarly, existing uncertainties in the measurements and the physical and biological processes controlling air-sea CO_2 fluxes on seasonal to decadal time scales support the need for continued ship-based observations combined with expanded deployments of autonomous platforms with next-generation sensors to quantify ocean-atmosphere fluxes with increased accuracy and greater spatial and temporal resolution. These updates, combined with ongoing advances in space-based remote sensing and modeling capabilities are essential elements of a global carbon monitoring system that can diagnose ongoing trends in the emissions and uptake of CO_2 by the land biosphere and oceans and to predict their evolution as the climate evolves.

8 Open Research

This is a review of other published work. No new data has been created or archived specifically for this manuscript. Original data are available through the citations listed here. Figures have been redrawn to avoid copyright conflicts.

9 Acknowledgments

Some of the work presented here was performed at the Jet Propulsion Laboratory, California Institute of Technology under contract to the National Aeronautics and Space Administration (NASA). Government sponsorship acknowledged. Figure 6 was designed by GAM and Natalie Renier, WHOI Creative, with funding from Ocean Carbon & Biogeochemistry (OCB) Project Office that has support from the US National Science Foundation (NSF) and NSF, NASA. We thank Amanda Fay for assistance with Figures 7 and 8. GAM acknowledges support from NSF OCE-1948624 and US National Oceanic and Atmospheric Administration (NA20OAR4310340). HD was supported by the European Commission, Horizon 2020 Framework Programme (VERIFY, grant no. 776810, COCO2 grant no. 958927) and the Netherlands Earth System Science Centre (NESSC), financially supported by the Ministry of Education, Culture and Science (OCW) (grant 024.002.001). JH acknowledges funding from the Initiative and Networking Fund of the Helmholtz Association (Helmholtz Young Investigator Group Marine Carbon and Ecosystem Feedbacks in the Earth System, MarESys), Grant Number: VH- NG-1301. TT acknowledges support from the EU H2020 framework program (EuroSea, grant no. 862626). AB acknowledges funding by the European Space Agency Climate Change Initiative ESA-CCI RECCAP2 project (ESRIN/ 4000123002/18/I-NB). The writing of this paper was initiated at the GCOS joint panel meeting in Marrakech, 18-22 March, 2019. We thank Mike O'Sullivan for the provision of Figure 17 and the TRENDY consortium modelers for use of the multi-model mean ensemble. We also wish to acknowledge the tremendous value of the products produced annually the Global Carbon Project.

10 References

Ahlström, A., Raupach, M. R., Schurgers, G., Smith, B., Arneth, A., Jung, M., Reichstein, M., Canadell, J. G., Friedlingstein, P., Jain, A. K., and Kato, E. (2015). The dominant role of semi-arid ecosystems in the trend and variability of the land CO_2 sink, *Science*, **348**, 895–899. doi: 10.1126/science.aaa1668

Álvarez, M., Fajar, N. M., Carter, B. R., Guallart, E. F., Pérez, F. F., Woosley, R. J. and Murata, A. (2020). Global Ocean Spectrophotometric pH Assessment: Consistent Inconsistencies. *Environmental Science and Technology,* **54**, 10977-10988. doi:10.1021/acs.est.9b06932

Anav, A., Friedlingstein, P., Beer, C., Ciais, P., Harper, A., Jones, C., Murray-Tortarolo, G., Papale, D., Parazoo, N. C., Peylin, P., Piao, S., Sitch, S., Viovy, N., Wiltshire, A. and Zhao, M. (2015). Spatiotemporal patterns of terrestrial gross primary production: A review. *Rev. Geophys.*, **53**, 785–818. doi:10.1002/2015RG000483

Anderegg, W. R. L., Hicke, J. A., Fisher, R. A., Allen, C. D., Aukema, J., Bentz, B., Hood, S., Lichstein, J. W., Macalady, A. K., McDowell, N., Pan, Y., Raffa, K., Sala, A., Shaw, J. D., Stephenson, N. L., Tague, C. and Zeppel, M. (2015). Tree mortality from drought, insects, and their interactions in a changing climate. *New Phytologist*, **208**: 674-683. doi:10.1111/nph.13477

Andrew, R. M. (2019). Global CO_2 emissions from cement production, 1928–2018. *Earth System Science Data*, **11**, 1675–1710. doi: 10.5194/essd-11-1675-2019

Andrew, R. M. (2020). A comparison of estimates of global carbon dioxide emissions from fossil carbon sources. *Earth System Science Data,* **12**, 1437–1465. doi:10.5194/essd-12-1437-2020

Angert, A., Biraud, S., Bonfils, C., Buermann, W. & Fung, I. (2004). CO_2 seasonality indicates origins of post-Pinatubo sink. *Geophys Res Lett*ers, **31**, L11103. doi: 10.1029/2004GL019760

Aragão, L. E. O. C., Anderson, L. O., Fonseca, M. G., Rosan, T. M., Vedovato, L. B., Wagner, F. H., Silva, C. V. J., Silva Junior, C. H. L., Arai, E., Aguiar, A. P. Barlow, J., Berenguer, E., Deeter, M. N., Domingues, L. G., Gatti, L., Gloor, M., Malhi, Y., Marengo, J. A., Miller, J. B., Phillips, O., L., and Saatchi, S. (2018). 21st Century drought-related fires counteract the decline of Amazon deforestation carbon emissions. *Nature Communications*, **9**, 536. doi: 10.1038/s41467-017-02771-y

Argles, A. P. K., Moore, J. R., Huntingford, C., Wiltshire, A. J., Harper, A. B., Jones, C. D., and Cox, P. M. (2020). Robust Ecosystem Demography (RED version 1.0): a parsimonious approach to modelling vegetation dynamics in Earth system models, *Geoscientific Model Development*, **13**, 4067–4089. doi:10.5194/gmd-13-4067-2020.

Arneth, A., Sitch, S., Pongratz, J., Stocker, B. D., Ciais, P., Poulter, B., Bayer, A. D., Bondeau, A., Calle, L., Chini, L. P., Grasser, T., Fader, M, Friedlingstein, P., Kato, E., Li, W., Lindeskog, M., Nabel, J. E. M. S., Pugh, T. A. M., Robertson, E., Viovy, N., Yue, C. and Zaehle, S. (2017). Historical carbon dioxide emissions caused by land-use changes are possibly larger than assumed, *Nature Geoscience*, **10**, 79-84. doi: 10.1038/NGEO2882.

Aumont, O., Orr, J. C., Monfray, P., Ludwig, W., Amiotte-Suchet, P. and Probst, J. -L. (2001). Riverine-driven interhemispheric transport of carbon. *Global Biogeochemical Cycles.* **15**, 393–405. doi:10.1029/1999GB001238

Aumont, O., Ethé, C., Tagliabue, A., Bopp, L. and Gehlen, M. (2015). PISCES-v2: An ocean biogeochemical model for carbon and ecosystem studies. *Geoscientific Model Development*, **8**, 2465–2513. doi:10.5194/gmd-8-2465-2015

Ayers, J.M. and Strutton, P.G. (2013). Nutrient variability in Subantarctic Mode Waters forced by the Southern Annular Mode and ENSO: Subantarctic mode water nutrients. *Geophysical Research Letters,* **40**, 3419–3423. doi:10.1002/grl.50638

Bacastow, R. B., Keeling, C. D., and Whorf, T. P. (1985). Seasonal amplitude increase in atmospheric CO_2 concentration at Mauna Loa, Hawaii, 1959–1982. *Journal of Geophysical Research: Atmospheres*, **90**, 10529– 10540.

Baccini, A., Walker, W., Carvalho, L., Farini, M., Sulla-Menashe, D. and Houghton, R. A. (2017). Tropical forests are a net carbon source based on aboveground measurements of gain and loss. *Science.* **358**, 230–234. doi:10.1126/science.aam5962

Bacour, C., Maignan, F., MacBean, N., Porcar-Castell, A., Flexas, J., Frankenberg, C., Peylin, P., Chevallier, F., Vuichard, N., and Bastrikov, V. (2019). Improving estimates of Gross Primary Productivity by assimilating solar-induced fluorescence satellite retrievals in a terrestrial biosphere model using a process-based SIF model, *Journal of Geophysical. Research-Biogeosciences*, **124**, 3281–3306

Badgley G., Field C. B., Berry J. A. (2017). Canopy near-infrared reflectance and terrestrial photosynthesis. *Science Advances*, **3**, e1602244. doi: 10.1126/sciadv.1602244. PMID: 28345046; PMCID: PMC5362170

Baier, B., Sweeney, C., Wolter, S., Newberger, T. and Higgs, J. (2020). 2017-2018 Full-Column Greenhouse Gas Sampling Field Campaign Report. DOE/SC-ARM-19-014

Baker, D. F., Doney, S. C., and Schimel, D. S. (2006a). Variational data assimilation for atmospheric CO_2, *Tellus, B*, 359–365. doi: 10.1111/j.1600-0889.2006.00218.x

Baker, D. F., Law, R. M., Gurney, K. R., Rayner, P., Peylin, P., Denning, A. S., Bousquet, P., Bruhwiler, L., Chen, Y. H., Ciais, P., Fung, I. Y., Heimann, M. , John, J., Maki, T., Maksyutov, S., Masarie, K., Prather, M., Pak, B., Taguchi, S., and Zhu, Z. (2006b). TransCom 3 inversion intercomparison: Impact of transport model errors on the interannual variability of regional CO_2 fluxes, 1988-2003. *Global Biogeochem. Cycles*, **20**, 01 [GB1002]. doi:10.1029/2004GB002439

Bakker, D. C. E., Pfeil, B., Smith, K., Hankin, S., Olsen, A., Alin, S. R., Cosca, C., Harasawa, S., Kozyr, A., Nojiri, Y., O'Brien, K. M., Schuster, U., Telszewski, M., Tilbrook, B., Wada, C., Akl, J., Barbero, L., Bates, N. R., Boutin, J., Bozec, Y., Cai, W.-J., Castle, R. D., Chavez, F. P., Chen, L., Chierici, M., Currie, K., de Baar, H. J. W., Evans, W., Feely, R. A., Fransson, A., Gao, Z., Hales, B., Hardman-Mountford, N. J., Hoppema, M., Huang, W.-J., Hunt, C. W., Huss, B., Ichikawa, T., Johannessen, T., Jones, E. M., Jones, S. D., Jutterström, S., Kitidis, V., Körtzinger, A., Landschützer, P., Lauvset, S. K., Lefévre, N., Manke, A. B., Mathis, J. T., Merlivat, L., Metzl, N., Murata, A., Newberger, T., Omar, A. M., Ono, T., Park, G.-H., Paterson, K., Pierrot, D., Ríos, A. F., Sabine, C. L., Saito, S., Salisbury, J., Sarma, V. V. S. S., Schlitzer, R., Sieger, R., Skjelvan, I., Steinhoff, T., Sullivan, K. F., Sun, H., Sutton, A. J., Suzuki, T., Sweeney, C., Takahashi, T., Tjiputra, J., Tsurushima, N., van Heuven, S. M. A. C., Vandemark, D., Vlahos, P., Wallace, D. W. R., Wanninkhof, R. and Watson, A. J. (2014). An update to the Surface Ocean CO_2 Atlas (SOCAT version 2). *Earth System Science Data,* **6**, 69-90. doi:10.5194/essd-6-69-2014

2346 Bakker, D. C. E., Pfeil, B., Landa, C. S., Metzl, N., O'Brien, K. M., Olsen, A., Smith, K., Cosca,
2347 C., Harasawa, S., Jones, S. D., Nakaoka, S. I., Nojiri, Y., Schuster, U., Steinhoff, T.,
2348 Sweeney, C., Takahashi, T., Tilbrook, B., Wada, C., Wanninkhof, R., Alin, S. R., Balestrini,
2349 C. F., Barbero, L., Bates, N. R., Bianchi, A. A., Bonou, F., Boutin, J., Bozec, Y., Burger, E.
2350 F., Cai, W. J., Castle, R. D., Chen, L., Chierici, M., Currie, K., Evans, W., Featherstone, C.,
2351 Feely, R. A., Fransson, A., Goyet, C., Greenwood, N., Gregor, L., Hankin, S., Hardman-
2352 Mountford, N. J., Harlay, J., Hauck, J., Hoppema, M., Humphreys, M. P., Hunt, C. W., Huss,
2353 B., Ibanhez, J. S. P., Johannessen, T., Keeling, R., Kitidis, V., Kortzinger, A., Kozyr, A.,
2354 Krasakopoulou, E., Kuwata, A., Landschutzer, P., Lauvset, S. K., Lefevre, N., Lo Monaco,
2355 C., Manke, A., Mathis, J. T., Merlivat, L., Millero, F. J., Monteiro, P. M. S., Munro, D. R.,
2356 Murata, A., Newberger, T., Omar, A. M., Ono, T., Paterson, K., Pearce, D., Pierrot, D.,
2357 Robbins, L. L., Saito, S., Salisbury, J., Schlitzer, R., Schneider, B., Schweitzer, R., Sieger,
2358 R., Skjelvan, I., Sullivan, K. F., Sutherland, S. C., Sutton, A. J., Tadokoro, K., Telszewski,
2359 M., Tuma, M., van Heuven, S. M. A. C., Vandemark, D., Ward, B., Watson, A. J. and Xu, S.
2360 (2016). A multi-decade record of high-quality fCO_2 data in version 3 of the Surface Ocean
2361 CO_2 Atlas (SOCAT). *Earth System Science Data*, **8**, 383-413. doi:10.5194/essd-8-383-2016
2362 Bakker, D. C. E., Alin, S. R., Bates, N., Becker, M., Castaño-Primo, R., Cosca, C. E., Cronin, M.,
2363 Kadono, K., Kozyr, A., Lauvset, S. K., Metzl, N., Munro, D. R., Nakaoka, S., O'Brien, K.
2364 M., Ólafsson, J., Olsen, A., Pfeil, B., Pierrot, D., Smith, K., Sutton, A. J., Takahashi, T.,
2365 Tilbrook, B., Wanninkhof, R., Andersson, A., Atamanchuk, D., Benoit-Cattin, A., Bott, R.,
2366 Burger, E. F., Cai, W.-J., Cantoni, C., Collins, A., Corredor, J. E., Cronin, M. F., Cross, J. N,
2367 Currie, K. I., De Carlo, E. H., DeGrandpre, M. D., Dietrich, C., Emerson, S., Enright, M. P.,
2368 Evans, W., Feely, R. A., García-Ibáñez, M. I., Gkritzalis, T., Glockzin, M., Hales, B.,
2369 Hartman, S. E., Hashida, G., Herndon, J., Howden, S. D., Humphreys, M. P., Hunt, C. W.,
2370 Jones, S. D., Kim, S., Kitidis, V., Landa, C. S, Landschützer, P., Lebon, G. T., Lefèvre, N.,
2371 Lo Monaco, C., Luchetta, A., Maenner Jones, S., Manke, A. B., Manzello, D., Mears, P.,
2372 Mickett, J., Monacci, N. M., Morell, J. M., Musielewicz, S., Newberger, T., Newton, J.,
2373 Noakes, S., Noh, J.-H., Nojiri, Y., Ohman, M., Ólafsdóttir, S., Omar, A. M., Ono, T.,
2374 Osborne, J., Plueddemann, A. J., Rehder, G., Sabine, C. L, Salisbury, J. E., Schlitzer, R.,
2375 Send, U., Skjelvan, I., Sparnocchia, S., Steinhoff, T., Sullivan, K. F., Sutherland, S. C.,
2376 Sweeney, C., Tadokoro, K., Tanhua, T., Telszewski, M., Tomlinson, M., Tribollet, A., Trull,
2377 T., Vandemark, D., Wada, C., Wallace, D. W. R., Weller, R. A., and Woosley, R. J. (2020).
2378 Surface Ocean CO_2 Atlas Database Version 2020 (SOCATv2020) (NCEI Accession
2379 0210711), NOAA National Centers for Environmental Information. doi:10.25921/4xkx-ss49
2380 Baldocchi, D., Falge, E., Gu, L., Olson, R., Hollinger, D., Running, S. W., Anthoni, P.,
2381 Bernhofer, C., Davis, K. J., Evans, R., Fuentes, J., Goldstein, A., Katul, G., Law, B., Lee,
2382 X., Malhi, Y., Meyers, T., Munger, W., Oechel, W., Paw, U. K. T., Pilegaard, K., Schmid, H.
2383 P., Valentini, R., Verma, S., Vesala, T., Wilson, K. and Wofsy, S. (2001). FLUXNET: A new
2384 tool to study the temporal and spatial variability of ecosystem-scale carbon dioxide, water
2385 vapor, and energy flux densities. *Bull. Amer. Meteor. Soc.*, **82**, 2415–2434.
2386 doi:10.1175/1520-0477
2387 Baldocchi D. D. (2003). Assessing the eddy covariance technique for evaluating carbon dioxide
2388 exchange rates of ecosystems: past, present and future. *Global Change Biology*, **9**, 479–492.
2389 doi:10.1046/j.1365-2486.2003.00629.x

2390 Ballantyne, A. P., Alden, C. B., Miller, J. B., Tans, P. P. and White, J. W. C. (2012). Increase in
2391 observed net carbon dioxide uptake by land and oceans during the past 50 years. *Nature*,
2392 **488**, 70–72. doi:10.1038/nature11299
2393 Ballantyne, A. P., Andres, R., Houghton, R., Stocker, B. D., Wanninkhof, R., Anderegg, W.,
2394 Cooper, L. A., DeGrandpre, M., Tans, P. P., Miller, J. B., Alden, C., and White, J. W. C.
2395 (2015). Audit of the global carbon budget: estimate errors and their impact on uptake
2396 uncertainty, *Biogeosciences*, **12**, 2565–2584. doi: 10.5194/bg-12-2565-2015.
2397 Barichivich, J., Briffa, K.R., Myneni, R.B., Osborn T.J., Melvin, T.M., Ciais, P., Piao, S.,
2398 Tucker, C. (2013). Large-scale variations in the vegetation growing season and annual cycle
2399 of atmospheric CO_2 at high northern latitudes from 1950 to 2011. *Global Change. Biology*,
2400 19,3167-3183. doi:10.1111/gcb.12283
2401 Bastos, A., Running, S. W., Gouveia, C., and Trigo, R. M. (2013). The global NPP dependence
2402 on ENSO: La Niña and the extraordinary year of 2011. *Journal of Geophysical Research:*
2403 *Biogeosciences*, 118, 1247-1255. doi: 10.1002/jgrg.20100
2404 Bastos, A., Ciais, P., Park, T., Zscheischler, J., Yue, C., Barichivich, J., Myneni, R. B., Peng, S.,
2405 Piao, S., and Zhu, Z. (2017). Was the extreme Northern Hemisphere greening in 2015
2406 predictable? *Environmental Research Letters*, **12**, 044016. doi: 10.1088/1748-9326/aa67b5
2407 Bastos, A., Friedlingstein, P., Sitch, S., Chen, C., Mialon, A., Wigneron, J.-P., Arora, V. K.,
2408 Briggs, P. R., Canadell, J. G., and Ciais, P. (2018). Impact of the 2015/2016 El Niño on the
2409 terrestrial carbon cycle constrained by bottom-up and top-down approaches, *Philosophical*
2410 *Transactions of the Royal Society London B*., **373**, 1760. doi: 10.1098/rstb.2017.0304
2411 Bastos, A., Ciais, P., Chevallier, F., Rödenbeck, C., Ballantyne, A. P., Maignan, F., Yin, Y.,
2412 Fernández-Martínez, M., Friedlingstein, P., Peñuelas, J., Piao, S. L., Sitch, S., Smith, W. K.,
2413 Wang, X., Zhu, Z., Haverd, V., Kato, E., Jain, A. K., Lienert, S., Lombardozzi, D., Nabel, J.
2414 E. M. S., Peylin, P., Poulter, B., and Zhu, D. (2019). Contrasting effects of CO_2 fertilization,
2415 land-use change and warming on seasonal amplitude of Northern Hemisphere CO_2
2416 exchange, *Atmospheric Chemistry and Physics*, **19**, 12361–12375,
2417 https://doi.org/10.5194/acp-19-12361-2019.
2418 Bastos, A., O'Sullivan, M., Ciais, P., Makowski, D., Sitch, S., Friedlingstein, P., Chevallier, F.,
2419 Rödenbeck, C., Pongratz, J., Luijkx, I. T., Patra, P. K., Peylin, P., Canadell, J. G.,
2420 Lauerwald, R., Li, W., Smith, N. E., Peters, W., Goll, D. S., Jain, A.K., Kato, E., Lienert, S.,
2421 Lombardozzi, D. L., Haverd V., Nabel, J. E. M. S., Poulter, B., Tian, H., Walker, A. P. and
2422 Zaehle, S. (2020). Sources of uncertainty in regional and global terrestrial CO_2 exchange
2423 estimates. *Global Biogeochemical Cycles*, **34**, e2019GB006393. doi:
2424 10.1029/2019GB006393
2425 Bauer, J. E., Cai, W. -J., Raymond, P. A., Bianchi, T. S., Hopkinson, C. S., and Regnier, P. A. G.
2426 (2013). The changing carbon cycle of the coastal ocean. *Nature* **504**, 61-70. doi:
2427 10.1038/nature12857
2428 Beck, S. A. and Goetz, S. J. (2011). Satellite observations of high northern latitude vegetation
2429 productivity changes between 1982 and 2008: ecological variability and regional
2430 differences. *Environmental Research Letters*, **6**, 045501. doi:10.1088/1748-
2431 9326/6/4/045501
2432 Becker, M., Andersen, N., Fiedler, B., Fietzek, P., Körtzinger, A., Steinhoff, T., and Friedrichs, G.
2433 (2012). Using cavity ringdown spectroscopy for continuous monitoring of $\delta^{13}C(CO_2)$ and

2434 fCO_2 in the surface ocean. *Limnology and Oceanography: Methods,* **10**, 752-766.
2435 doi:10.4319/lom.2012.10.752
2436 Beer, C., Reichstein, M., Tomelleri, E., Ciais, P., Jung, M., Carvalhais, N., Rödenbeck, C.,
2437 Arain, M. A., Baldocchi, D., Bonan, G., B., Bondeau, A., Cescatti, A., Lasslop,G., Lindroth,
2438 A., Lomas, M., Luyssaert, S., Margolis, H., Oleson, K. W., Roupsard, O., Veenendaal, E.,
2439 Viovy, N., Williams, C., Woodward, F., I. and Papale, D. (2010). Terrestrial gross carbon
2440 dioxide uptake: global distribution and covariation with climate. *Science,* **329**, 834–838.
2441 doi:10.1126/science.1184984
2442 Bennedsen, M., Hildebrand, E. and Koopman, S. (2019). Trend analysis of the airborne fraction
2443 and sink rate of anthropogenically released CO_2. *Biogeosciences*, **16**, 3651–3663.
2444 doi:10.5194/bg-16-3651-2019
2445 Bloom, A. A., Bowman, K. W., Liu, J., Konings, A. G., Worden, J. R., Parazoo, N. C., Meyer, V.,
2446 Reager, J. T., Worden, H. M., Jiang, Z., Quetin, G. R., Smallman, T. L., Exbrayat, J.-F., Yin,
2447 Y., Saatchi, S. S., Williams, M., and Schimel, D. S. (2020). Lagged effects regulate the
2448 inter-annual variability of the tropical carbon balance, Biogeosciences, 17, 6393–6422,
2449 2020. doi: 10.5194/bg-17-6393-2020
2450 Boden T. A., Marland G. and Andres R. J. (2017). Global, Regional, and National Fossil-Fuel
2451 CO_2 Emissions. Carbon Dioxide Information Analysis Center, Oak Ridge National
2452 Laboratory, U.S. Department of Energy, Oak Ridge, Tenn., U.S.A.
2453 doi:10.3334/CDIAC/00001_V2017
2454 Bolin, B., Björkström, A., Holmén, K. and Moore, B. (1983). The simultaneous use of tracers for
2455 ocean circulation studies. *Tellus B*, **35B**, 206–236. doi:10.1111/j.1600-0889.1983.tb00025.x
2456 Booth, B. B. B., C. D. Jones, M. Collins, I. J. Totterdell, P. M. Cox, S. Sitch, C. Huntingford, R.
2457 Betts, G. R. Harris, and J. Lloyd. (2012). High sensitivity of future global warming to land
2458 carbon cycle processes, *Environmental Research Letters,* **7**, 024002. doi: 10.1088/1748-
2459 9326/7/2/024002
2460 Bousquet, P., Peylin, P., Ciais, P., Le Quéré, C., Friedlingstein, P., and Tans, P. (2000). Regional
2461 Changes in Carbon Dioxide Fluxes of Land and Oceans Since 1980. *Science*, **290**,1342-
2462 1346. doi: 10.1126/science.290.5495.1342
2463 Bowman, D. M. J. S., Williamson, G. J., Abatzoglou, J. T., Kolden, C. A., Cochrane, M. A. and
2464 Smith, A. M. S. (2017). Human exposure and sensitivity to globally extreme wildfire
2465 events. *Nature Ecology and Evolution*, **1**, 0058. doi: 10.1038/s41559-016-0058
2466 Bowman, D. M. J. S., Williamson, G. J., Price, O. F., Ndalila, M. N., and Bradstock, R. A.
2467 (2021). Australian forests, megafires and the risk of dwindling carbon stocks. *Plant Cell &*
2468 *Environment,* **44**, 347–355. doi: 10.1111/pce.13916
2469 BP Statistical Review of World Energy 2020. available at
2470 https://www.bp.com/en/global/corporate/energy-economics/statistical-review-of-world-
2471 energy/co2-emissions.html, last access 30 November 2021.
2472 Brandt, M., Wigneron, J.-P., Chave, J., Tagesson, T., Peñuelas, J., Ciais, P., Rasmussen, K., Tian,
2473 F., Mbow, C., Al-Yaari, A., Rodriguez-Fernandez, N., Schurgers, G., Zhang, W., Chang, J.,
2474 Kerr, Y., Verger, A., Tucker, C., Mialon, A., Rasmussen, L., Fan, L., and Fensholt, R. (2018).
2475 Satellite passive microwaves reveal recent climate-induced carbon losses in African
2476 drylands. *Nature Ecology and Evolution,* **2**, 827–835. doi: 10.1038/s41559-018-0530-6
2477 Brienen, R. J.W., Phillips, O. L., Feldpausch, T. R., Gloor, E., Baker, T. R., Lloyd, J., Lopez-
2478 Gonzalez, G., Monteagudo-Mendoza, A., Malhi, Y., Lewis, S. L., Vásquez Martinez, R.,

2479 Alexiades, M., Álvarez Dávila, E., Alvarez-Loayza, P., Andrade, A., Aragão, L. E. O. C.,
2480 Araujo-Murakami, A., Arets, E. J. M. M., Arroyo, L., Aymard, C. A. G., Bánki, O.S.,
2481 Baraloto, C., Barroso, J., Bonal, D., Boot, R. G. A. , Camargo, J. L. C., Castilho, C. V.,
2482 Chama, V., Chao, K. J., Chave, J., Comiskey, J. A., Cornejo Valverde, F., da Costa, L., de
2483 Oliveira, E. A., Di Fiore, A., Erwin, T. L., Fauset, S., Forsthofer, M., Galbraith, D. R.,
2484 Grahame, E. S., Groot, N., Hérault, B., Higuchi, N., Honorio Coronado, E. N., Keeling, H.,
2485 Killeen, T. J., Laurance, W. F., Laurance, S., Licona, J., Magnussen, W. E., Marimon, B. S.,
2486 Marimon-Junior, B. H., Mendoza, C., Neill, D. A., Nogueira, E. M., Núñez, P., Pallqui
2487 Camacho, N. C., Parada, A., Pardo-Molina, G., Peacock, J., Peña-Claros, M., Pickavance,
2488 G. C., Pitman, N. C. A., Poorter, L., Prieto, A., Quesada C. A., Ramírez, F., Ramírez-
2489 Angulo, H., Restrepo, Z., Roopsind, A., Rudas, A., Salomão, R. P., Schwarz, M., Silva, N.,
2490 Silva-Espejo, J. E., Silveira, M., Stropp, J., Talbot, J., ter Steege, H., Teran-Aguilar, J.,
2491 Terborgh, J., Thomas-Caesar, R., Toledo, M., Torello-Raventos, M., Umetsu, R. K., van der
2492 Heijden, G. M. F., van der Hout, P., Guimarães, Vieira I. C., Vieira, S. A., Vilanova, E., Vos,
2493 V. A. and Zagt, R. J. (2015). Long-term decline of the Amazon carbon sink. *Nature,* **519**,
2494 344-348. doi: 10.1038/nature14283

2495 Bronselaer,B., and Zanna, L. (2020), Heat and carbon coupling reveals ocean warming due to
2496 circulation changes. *Nature,* **584**, 227–233. doi:10.1038/s41586-020-2573-5

2497 Bushinsky, S. M., Landschützer, P., Rödenbeck, C., Gray, A. R., Baker, D., Mazloff, M. R.,
2498 Resplandy, L., Johnson, K. S., and Sarmiento, J. L. (2019). Reassessing Southern Ocean air-
2499 sea CO_2 flux estimates with the addition of biogeochemical float observations. *Global*
2500 *Biogeochemical Cycles*, **33**, 1370-1388, doi:10.1029/2019GB006176

2501 Byrne, B., Wunch, D., Jones, D. B. A., Strong, K., Deng, F., Baker, I., Köhler, P., Frankenberg,
2502 C., Joiner, J., Arora, V. K., Badawy, B., Harper, A. B., Warneke, T., Petri, C., Kivi, R. and
2503 Roehl, C. M. (2018). Evaluating GPP and respiration estimates over northern midlatitude
2504 ecosystems using solar-induced fluorescence and atmospheric CO_2 measurements. *Journal*
2505 *of Geophysical Research: Biogeosciences*, **123**, 2976–2997. doi:10.1029/2018JG004472

2506 Byrne, B., Liu, J., Lee, M., Baker, I., Bowman, K. W., Deutscher, N. M., Feist, D. G., Griffith D.
2507 W. T., Iraci, L. T., Kiel, M., Kimball, J. S., Miller, C. E., Morino, I., Parazoo, N. C., Petri,
2508 C., Roehl, C. M., Sha, M. K., Strong, K., Velazco, V. A., Wennberg, P. O. and Wunch, D.
2509 (2020a). Improved constraints on northern extratropical CO_2 fluxes obtained by combining
2510 surface-based and space-based atmospheric CO_2 measurements. *Journal of Geophysical*
2511 *Research: Atmospheres*, **125**, e2019JD032029. doi:10.1029/2019JD032029

2512 Byrne, B., Jones, D. B. A., Strong, K., Polavarapu, S. M., Harper, A. B., Baker, D. F.,
2513 Maksyutov, S. (2019). On what scales can GOSAT flux inversions constrain anomalies in
2514 terrestrial ecosystems? *Atmospheric Chemistry and Physics,* **19**, 13017–13035. doi:
2515 10.5194/acp-19-13017-2019

2516 Byrne, B., Liu, J., Lee, M., Baker, I., Bowman, K. W., Deutscher, N. M., Feist, D. G., Griffith D.
2517 W. T., Iraci, L. T., Kiel, M., Kimball, J. S., Miller, C. E., Morino, I., Parazoo, N. C., Petri, C.,
2518 Roehl, C. M., Sha, M. K., Strong, K., Velazco, V. A., Wennberg, P. O., and Wunch, D.
2519 (2020b). Improved constraints on northern extratropical CO_2 fluxes obtained by combining
2520 surface-based and space-based atmospheric CO_2 measurements. *Journal of Geophysical*
2521 *Research: Atmospheres*, **125**, e2019JD032029. doi: 10.1029/2019JD032029

2522 Cadule P., Friedlingstein P., Bopp L., Sitch, S., Jones, C. D., Ciais, P., Piao, S. L., and Peylin, P.
2523 (2010). Benchmarking coupled climate-carbon models against long-term atmospheric CO2
2524 measurements. *Global Biogeochemical Cycles*, **24**, GB2016. doi: 10.1029/2009gb003556
2525 Cai, W., Cowan, T., and Raupach, M. (2009), Positive Indian Ocean Dipole events precondition
2526 southeast Australia bushfires, *Geophysical Research Letters*, **36**, L19710, doi:
2527 10.1029/2009GL039902
2528 Campbell, J. E., Berry, J. A., Seibt, U., Smith, S. J., Montzka, S. A., Launois, T., Belviso, S.,
2529 Bopp, L., and Laine, M. (2017). Large historical growth in global terrestrial gross primary
2530 production, Nature, 544, 84–87. doi: 10.1038/nature22030
2531 Canadell, J. G., Le Quéré, C., Raupach, M. R., Field, C. B. , Buitenhuis, E., Ciais, P., Conway, T.
2532 J., Gilett, N. P., Houghton, J. T. and Marland, G. (2007). Contributions to accelerating
2533 atmospheric CO_2 growth from economic activity, carbon intensity, and efficiency of natural
2534 sinks. *Proceedings of the National Academy of Sciences, USA*, **104**, 18,866 – 18,870.
2535 doi:10.1073/ pnas.0702737104
2536 Canadell, J. G., Ciais, P., Gurney, K., Le Quéré, C., Piao, S., Raupach, M. R., and Sabine, C. L.
2537 (2011). An International Effort to Quantify Regional Carbon Fluxes, *Eos Transactions*
2538 *AGU*, **92**, 81–82. doi: 10.1029/2011EO100001
2539 Carroll, D., Menemenlis, D., Adkins, J. F., Bowman, K. W., Brix, H., Dutkiewicz, S., Fenty, I.,
2540 Gierach, M. M., Hill, C., Jahn, O., Landschützer, P., Lauderdale, J. M., Liu, J., Manizza, M.,
2541 Naviaux, J. D., Rödenbeck, C., Schimel, D. S., Van der Stocken, T. and Zhang, H. (2020).
2542 The ECCO-Darwin data-assimilative global ocean biogeochemistry model: Estimates of
2543 seasonal to multi-decadal surface ocean pCO_2 and air-sea CO_2 flux. *Journal of Advances in*
2544 *Modeling Earth Systems*, **12**, e2019MS001888. doi:10.1029/2019MS001888
2545 Carvalhais, N., Forkel, M., Khomik, M., Bellarby, J., Jung, M., Migliavacca, M. Mu, M.,
2546 Saatchi, S., Santoro, M., Thurner, M., Weber, U., Ahrens, B., Beer, C., Cescatti, A.,
2547 Randerson, J. T. and Reichstein, M. (2014). Global covariation of carbon turnover times
2548 with climate in terrestrial ecosystems. *Nature*, **514**, 213-217. doi:10.1038/nature13731
2549 Casperson, J. P., S. W. Pacala, J. C. Jenkins, G. C. Hurtt, P. R. Moorcroft, and R. A. Birdsey
2550 (2000). Contributions of land use history to carbon accumulation in U.S. Forests. *Science*,
2551 **290**, 1148-1151. doi: 10.1126/science.290.5494.1148
2552 Castro, A. O., Chen, J., Zang, C. S., Shekhar, A., Jimenez, J. C., Bhattacharjee, S., Kindu, M.,
2553 Morales, V. H. and Ramming, A. (2020). OCO-2 Solar-Induced Chlorophyll Fluorescence
2554 Variability across Ecoregions of the Amazon Basin and the Extreme Drought Effects of El
2555 Nino (2015-2016), *Remote Sensing*, **12**, 1202. doi:10.3390/rs12071202
2556 Catherman, C. (2021). Ocean scientists confront a critical bottleneck, *Science*, **374** (6563), doi:
2557 10.1126/science.acx9218
2558 Chatterjee, A., Gierach, M. M., Sutton, A. J., Feely, R. A., Crisp, D., Eldering, A., Gunson, M.
2559 R., O'Dell, C. W., Stephens, B. B. and Schimel, D. S. (2017). Influence of El Niño on
2560 atmospheric CO_2 over the tropical Pacific Ocean: Findings from NASA's OCO-2 mission.
2561 *Science,* **358**, eaam5776. doi:10.1126/science.aam5776
2562 Chen, Z., Huntzinger, D. N., Liu, J. Piao, S., Wang, X. Sitch, S., Friedlingstein, P., Anthoni, P.,
2563 Arneth, A., Bastrikov, V., Goll, D. S., Haverd, V., Jain, A. K., Joetzjer, E., Kato, E., Lienert,
2564 S., Lombardozzi, D. L., McGuire, P. C., Melton, J. R., Nabel, J. E. M. S., Pongratz, J.,
2565 Poulter, B., Tian, H., Wiltshire, A., J., and Miller, S. (2021a). Five years of variability in the
2566 global carbon cycle: comparing an estimate from the Orbiting Carbon Observatory-2 and

process-based models. *Environmental Research Letters*, **16**, 054041. doi: 10.1088/1748-9326/abfac1

Chen, Z., Liu, J., Henze, D. K., Huntzinger, D. N., Wells, K. C., Sitch, S., Friedlingstein, P., Joetzjer, E., Bastrikov, V., Goll, D. S., Haverd, V., Jain, A. K., Kato, E., Lienert, S., Lombardozzi, D. L., McGuire, P. C., Melton, J. R., Nabel, J. E. M. S., Poulter, B., Tian, H., Wiltshire, A. J., Zaehle, S., and Miller, S. M. (2021b). Linking global terrestrial CO_2 fluxes and environmental drivers: inferences from the Orbiting Carbon Observatory 2 satellite and terrestrial biospheric models. *Atmospheric Chemistry and Physics*, **21**, 6663–6680. doi:10.5194/acp-21-6663-2021

Cheng, L., Normandeau, C., Bowden, R., Doucett, R., Gallagher, B., Gillikin, D.P., Kumamoto, Y., Mckay, J.L., Middlestead, P., Ninnemann, U., Nothaft, D., Dubinina, E.O., Quay, P., Reverdin, G., Shirai, K., Mørkved, P.T., Theiling, B.P., Van Geldern, R., and Wallace, D.W.R. (2019). An international intercomparison of stable carbon isotope composition measurements of dissolved inorganic carbon in seawater. *Limnology and Oceanography: Methods,* **17**, 200-209. doi: 10.1002/lom3.10300

Cheng, L., Normandeau, C., Cai, W.-J., Wallace D.W.R. (2021). Shipboard measurement of DIC and δ^{13}C-DIC on discrete seawater samples using Cavity Ring-Down Spectroscopy: system testing and performance during three research cruises in the North Atlantic. *Isotopes in Environmental and Health Studies,* In revision, [preprint]

Chevallier, F., Ciais, P., Conway, T. J., Aalto, T., Anderson, B. E., Bousquet, P., Brunke, E. G., Ciattaglia, L., Esaki, Y., Frohlich, M., Gomez, A. J., Gomez-Pelaez, A. J., Haszpra, L., Krummel, P., Langenfelds, R., Leuenberger, M., Machida, T., Maignan, F., Matsueda, H., Morgui, J. A., Mukai, H., Nakazawa, T., Peylin, P., Ramonet, M., Rivier, L., Sawa, Y., Schmidt, M., Steele, P., Vay, S. A., Vermeulen, A. T., Wofsy, S. and Worthy, D. (2010). CO_2 surface fluxes at grid point scale estimated from a global 21-year reanalysis of atmospheric measurements. *Journal of Geophysical Research: Atmospheres*, **115**, D21307. doi:10.1029/2010JD013887

Chevallier, F., Remaud, M. O'Dell, C. W., Baker, D., Peylin, P. and Cozic, A. (2019). Objective evaluation of surface and satellite driven CO_2 atmospheric inversion. *Atmospheric Chemistry and Physics*, **19**, 14233–14251. doi:10.5194/acp-19-14233-2019

Chevallier, F. (2021). Fluxes of carbon dioxide from managed ecosystems estimated by national inventories compared to atmospheric inverse modeling. *Geophysical Research Letters*, **48**, e2021GL093565. doi: 10.1029/2021GL093565

Chini, L., Hurtt, G., Sahajpal, R., Frolking, S., Goldewijk, K. K., Sitch, S., Ganzenmüller, R., Ma, L., Ott, L., Pongratz, J., and Poulter, B. (2021). Land-use harmonization datasets for annual global carbon budgets, *Earth System Science Data*, **13**, 4175–4189. doi: 10.5194/essd-13-4175-2021

Church, J. A., White, N. J., Arblaster, J. M. (2005). Significant decadal-scale impact of volcanic eruptions on sea level and ocean heat content. *Nature*, **438**, 74–77. doi:10.1038/nature04237

Chuvieco, E., Yue, C., Heil, A., Mouillot, F., Alonso-Canas, I., Padilla, M., Pereira, J.M.C., Oom, D., Tansey, K. (2016) A new global burned area product for climate assessment of fire impacts. *Global Ecology and Biogeography*, 25, 619-629. doi:10.1111/geb.12440

Ciais, P., Tans, P. P., Trolier, M., White, J. W. C., and Francey, R. J. (1995). A Large Northern Hemisphere Terrestrial CO_2 Sink Indicated by the $^{13}C/^{12}C$ Ratio of Atmospheric CO_2. *Science*, **269**, 1098-1102. doi: 10.1126/science.269.5227.1098

Ciais, P., Tans, P. P., Denning, A. S., Francey, R. J., Trolier, M., Meijer, A. J., White, J. W. C, Berry, J. A., Randall, D. A., Collatz, G. J., Sellers, P. J., Monfray, P., and Heimann, M. (1997). A three-dimensional synthesis study of $\delta^{18}O$ in atmospheric CO_2 2. Simulations with the TM2 transport model. *Journal of Geophysical Research*, **102**, 5873-5883. doi: 10.1029/96JD02361

Ciais, P., Reichstein, M., Viovy, N., Granier, A., Ogee, J., Allard, V., Aubinet, M., Buchmann, N., Bernhofer, C., Carrara, A., Chevallier, F., De Noblet, N., Friend, A. D., Friedlingstein, P., Grunwald, T., Heinesch, B., Keronen, P., Knohl, A., Drinner, G., Loustau, D., Manca, G., Matteucci, G., Miglietta, F., Ourcival, J. M., Papale, D., Pilegaard, K., Rambal, S., Seufert, G., Soussana, J. F., Sanz, M. J., Schulze, E. D., Vesala, T. and Valentini, R. (2005). Europe-wide reduction in primary productivity caused by the heat and drought in 2003. *Nature,* **437**, 529–533. doi: 10.1038/nature03972

Ciais, P., Sabine, C., Bala, G., Bopp, L., Brovkin, V., Canadell, J., Chhabra, A., DeFries, R., Galloway, J., Heimann, M., Jones, C., Le Quere, C., Myneni, R.B., Piao, S. and Thornton, P. (2013). Carbon and Other Biogeochemical Cycles. In: Climate Change 2013: The Physical Science Basis. Contribution of Working Group I to the Fifth Assessment Report of the Intergovernmental Panel on Climate Change [Stocker, T.F., D. Qin, G.-K. Plattner, M. Tignor, S.K. Allen, J. Boschung, A. Nauels, Y. Xia, V. Bex and P.M. Midgley (eds.)]. Cambridge University Press, Cambridge, United Kingdom and New York, NY, USA.

Ciais, P., Dolman, A. J., Bombelli, A., Duren, R., Peregon, A., Rayner, P. J., Miller, C., Gobron, N., Kinderman, G., Marland, G., Gruber, N., Chevallier, F., Andres, R. J., Balsamo, G., Bopp, L., Bréon, F.-M., Broquet, G., Dargaville, R., Battin, T. J., Borges, A., Bovensmann, H., Buchwitz, M., Butler, J., Canadell, J. G., Cook, R. B., DeFries, R., Engelen, R., Gurney, K. R., Heinze, C., Heimann, M., Held, A., Henry, M., Law, B., Luyssaert, S., Miller, J., Moriyama, T., Moulin, C., Myneni, R. B., Nussli, C., Obersteiner, M., Ojima, D., Pan, Y., Paris, J.-D., Piao, S. L., Poulter, B., Plummer, S., Quegan, S., Raymond, P., Reichstein, M., Rivier, L., Sabine, C., Schimel, D., Tarasova, O., Valentini, R., Wang, R., van der Werf, G., Wickland, D., Williams, M. and Zehner, C. (2014). Current systematic carbon-cycle observations and the need for implementing a policy-relevant carbon observing system, *Biogeosciences*, **11**, 3547–3602. doi:10.5194/bg-11-3547-2014

Ciais, P., Tan, J., Wang, X., Roedenbeck, C., Chevallier, F., Piao, S.-L., Broquet, G., Le Quéré, C., Canadell, J. G., Peng, S., Poulter, B., Liu, Z., and Tans, P. (2019). Five decades of northern land carbon uptake revealed by the interhemispheric CO_2 gradient. *Nature*, **568**, 221-225. doi: 10.1038/s41586-019-1078-6

Ciais, P., Bastos, A., Chevallier, F., Lauerwald, R., Poulter, B., Canadell, P., Hugelius, G., Jackson, R. B., Jain, A., Jones, M., Kondo, M., Luijkx, I. T., Patra, P. K., Peters, W., Pongratz, J., Petrescu, A. M., R., Piao, S., Qiu, C., Von Randow, C., Regnier, P., Saunois, M., Scholes, R., Shvidenko, A., Tian, H., Yang, H., Wang, X., and Zheng, B (2020a). Definitions and methods to estimate regional land carbon fluxes for the second phase of the REgional Carbon Cycle Assessment and Processes Project (RECCAP-2), *Geoscientific Model Development Discussions*, doi: 10.5194/gmd-2020-259 [preprint]

Ciais, P. Wang, Y., Andrew, R. M., Bréon, F. M., Chevallier, F., Broquet, G., Nabuurs, G. J., Peters, G. P., McGrath, M. J., Meng, W., Zheng, B. and Tao, S. (2020b). Biofuel burning and human respiration bias on satellite estimates of fossil fuel CO_2 emissions. *Environmental Research Letters*, **15**, 074036. doi:10.1088/1748-9326/ab7835

2657 Ciais, P., Yao, Y., Gasser, T., Baccini, A., Wang, Y., Lauerwald, R., Peng, S., Bastos, A., Li, W.,
2658 Raymnd, P. A., Canadell, J. G., Peters, G. P., Andres, R. J., Chang, J., Yue, C., Dolman, A.
2659 J., Haverd, V., Hartman, J., Laruelle, G., Konings, A. G., King, A. W., Liu, Y., Luyssaert, S.,
2660 Maignan, F., Patra, P. K., Peregon, A., Regnier, P., Pongratz, J., Poulter, B., Shvidenko, A.,
2661 Valentini, R., Wang, R., Broquet, G., Yin, Y., Zscheischler, J., Guenet, B., Goll, D., S.,
2662 Ballantyne, A.-P., Yang, H., Qiu, C. and Zhu, D. (2020c). Empirical estimates of regional
2663 carbon budgets imply reduced global soil heterotrophic respiration. *National Science*
2664 *Review*, **0**, nwaa145,1-14. doi:10.1093/nsr/nwaa145

2665 Clark, H., Bennouna, Y., Tsivlidou, M., Wolff, P., Sauvage, B., Barret, B., Le Flochmoën, E.,
2666 Blot, R., Boulanger, D., Cousin, J.-M., Nédélec, P., Petzold, A., and Thouret, V. (2021). The
2667 effects of the COVID-19 lockdowns on the composition of the troposphere as seen by In-
2668 service Aircraft for a Global Observing System (IAGOS) at Frankfurt, *Atmospheric*
2669 *Chemistry and Physics*, **21**, 16237–16256. doi: 10.5194/acp-21-16237-2021

2670 Claustre, H., Johnson, K. S., and Takeshita, Y. (2020). Observing the global ocean with
2671 Biogeochemical-Argo, *Annual Review of Marine Science*, **12**, 23-48. doi:10.1146/annurev-
2672 marine-010419-010956

2673 Claustre, H., Legendre, L., Boyde, P.W., and Levy, M. (2021). The Oceans' Biological Carbon
2674 Pumps: Framework for a Research Observational Community Approach. *Frontiers in*
2675 *Marine Science, Ocean Observation*, **8**, 780052. doi: 10.3389/fmars.2021.780052

2676 Clement, D., and Gruber, N. (2018). The eMLR(C*) Method to determine decadal changes in the
2677 global ocean storage of anthropogenic CO_2. *Global Biogeochemical Cycles,* **32**, 654-679.
2678 doi:10.1002/2017gb005819

2679 Cleverly, J., Eamus, D., Luo, Q., Coupe, N. R., Kljun, N., Ma, X., Ewenz, C., Li, L., Yu, Q. and
2680 Huete, A. (2016). The importance of interacting climate modes on Australia's contribution
2681 to global carbon cycle extremes. *Scientific Reports,* **6**, 23113. doi: 10.1038/srep23113

2682 Cortés, J., Mahecha, M. D., Reichstein, M., Myneni, R. B., Chen, C., and Brenning, A. (2021).
2683 Where are global vegetation greening and browning trends significant? *Geophysical*
2684 *Research Letters*, *48*, e2020GL091496. doi:10.1029/2020GL091496

2685 Cox, P. M., Pearson, D., Booth, B. B., Friedlingstein, P., Huntingford, C., Jones, C. D., and Luke,
2686 C. M. (2013). Sensitivity of tropical carbon to climate change constrained by carbon dioxide
2687 variability, *Nature*, **494**, 341–344. doi: 10.1038/nature11882

2688 Crisp, D., Atlas, R. M., Bréon, F.-B., Brown, L. R., Burrows, J. P., Ciais, P., Connor, B.J .,
2689 Doney, S. C., Fung, I. Y., Jacob, D. J., Miller, C. E., O'Brien, D., Pawson, S., Randerson, J.
2690 T., Rayner, P., Salawitch, R. J., Sander, S. P., Sen, B., Stephens, G. L., Tans, P. P., Toon, G.
2691 C., Wennberg, P. O., Wofsy, S. C., Yung, Y. L., Kuang, Z., Chudasama, B., Sprague, G.,
2692 Weiss, B., Pollock, R., Kenyon, D., Schroll, S. (2004). The Orbiting Carbon Observatory
2693 (OCO) mission. *Advances in Space Research*, **34**, 700–709, doi: 10.1016/j.asr.2003.08.062

2694 Crisp, D., Miller, C. E., and DeCola, P. L. (2008). NASA Orbiting Carbon Observatory:
2695 measuring the column averaged carbon dioxide mole fraction from space. *Journal of*
2696 *Applied Remote Sensing*, **2**, 023508; doi: 10.1117/1.2898457

2697 Crowell, S., Baker, D., Schuh, A., Basu, S., Jacobson, A., Chevallier, F., Liu, J., Deng, F., Feng,
2698 L., McKain, K., Chatterjee, A., Miller, J., Stephens, B., Eldering, A., Crisp, D., Schimel, D.,
2699 Nassar, R., O'Dell. C., Oda, T., Sweeney, C., Palmer, P., and Jones, D. (2019). The 2015-
2700 2016 carbon cycle as seen from OCO-2 and the global in situ network. *Atmospheric*
2701 *Chemistry and Physics*, **19**, 7347–7376. doi:10.5194/acp-19-7347-2019

2702 Dannenberg, M. P., Wise, E. K., Janko, M., Hwang, T., and Smith_W. K. (2018). Atmospheric
2703 teleconnection influence on North American land surface phenology. *Environmental*
2704 *Research Letters*, **13**, 034029. doi: 10.1088/1748-9326/aaa85a/meta
2705 Dannenberg, M. P., Smith, W. K., Zhang, Y., Song, C., Huntzinger, D. N., and Moore, D. J. P.
2706 (2021). Large-Scale Reductions in Terrestrial Carbon Uptake Following Central Pacific El
2707 Niño, *Geophysical Research Letters*, **48**, e2020GL092367. doi: 10.1029/2020GL092367
2708 Deng, F., D. B. A. Jones, C. W. O'Dell, R. Nassar, and N. C. Parazoo (2016). Combining GOSAT
2709 XCO_2 observations over land and ocean to improve regional CO_2 flux estimates, Journal of
2710 *Geophysical Research Atmospheres*, **121**, 1896–1913. doi:10.1002/2015JD024157.
2711 Deng, Z., Ciais, P., Tzompa-Sosa, Z. A., Saunois, M., Qiu, C., Tan, C., Sun, T., Ke, P., Cui, Y.,
2712 Tanaka, K., Lin, X., Thompson, R. L., Tian, H., Yao, Y., Huang, Y., Lauerwald, R., Jain, A.
2713 K., Xu, X., Bastos, A., Sitch, S., Palmer, P. I., Lauvaux, T., d'Aspremont, A., Giron, C.,
2714 Benoit, A., Poulter, B., Chang, J., Petrescu, A. M. R., Davis, S. J., Liu, Z., Grassi, G.,
2715 Albergel, C., and Chevallier, F. (2021). Comparing national greenhouse gas budgets
2716 reported in UNFCCC inventories against atmospheric inversions, *Earth System Science*
2717 *Data Discuss.* [preprint]. doi:10.5194/essd-2021-235, in review, 2021.
2718 Denman, K. L., Brasseur, G., Chidthaisong, A., Ciais, P., Cox, P. M., Dickinson, R. E.,
2719 Hauglustaine, D., Heinze, C., Holland, E., Jacob, D., Lohmann, U., Ramachandran, S., Leite
2720 da Silva Dias, P., Wofsy, S. C., and Zhang, X. (2007). Couplings Between Changes in the
2721 Climate System and Biogeochemistry, in: Climate Change 2007: *The Physical Science*
2722 *Basis.* Contribution of Working Group I to the Fourth Assessment Report of the
2723 Intergovernmental Panel on Climate Change, edited by: Solomon, S., Qin, D., Manning, M.,
2724 Marquis, M., Averyt, K., Tignor, M. M. B., Miller, H. L., and Chen, Z. L., Cambridge
2725 University Press, Cambridge, UK and New York, USA, 499–587.
2726 Denvil-Sommer, A., M. Gehlen, M. Vrac, and C. Mejia (2019). LSCE-FFNN-v1: A two-step
2727 neural network model for the reconstruction of surface ocean pCO_2 over the global ocean.
2728 *Geoscientific Model Development*, **12**, 2091–2105. doi:10.5194/gmd-12-2091-2019
2729 DeVries, T. (2014). The oceanic anthropogenic CO_2 sink: Storage, air-sea fluxes, and transports
2730 over the industrial era, *Global Biogeochemical Cycles*, **28**, 631–647.
2731 doi:10.1002/2013GB004739
2732 DeVries, T., Holzer, M. and Primeau, F. (2017). Recent increase in oceanic carbon uptake driven
2733 by weaker upper-ocean overturning. *Nature,* **542**, 215–218. doi:10.1038/nature21068
2734 DeVries, T., Le Quéré, C., Andrews, O., Berthet, S., Hauck, J., Ilyina, T., Landschützer, P.,
2735 Lenton, A., Lima, I. D., Nowicki, M., Schwinger, J., Séférian, R. (2019). Decadal trends in
2736 the ocean carbon sink. *Proceedings of the National Academy of Sciences,* **116**, 11646-11651.
2737 doi:10.1073/pnas.1900371116
2738 Diaz, H. F., Hoerling, M. P. and Eischeid, J. K. (2001). ENSO variability, teleconnections and
2739 climate change, *Int. J. Climatol*., **21**, 1845–1862. doi: 10.1002/joc.631
2740 Dlugokencky, E. J., Hall, B.D., Montzka, S.A., Dutton, G., Muhle, J. and Elkins, J.W. (2018).
2741 Long-lived greenhouse gases [in "State of the Climate in 2017"]. *Bulletin of the American*
2742 *Meteorological Society*, **99**, S46-S48. doi:10.1175/2018BAMSStateoftheClimate.1
2743 Doney S.C., Lindsay, K., Caldeira, K., Campin, J.-M., Drange, H., Dutay, J. C., Follows, M.,
2744 Gao, Y., Gnanadesikan, A., Gruber, N., Ishida, A., Joos, F., Madec, G., Maier-Reimer, E.,
2745 Marshall, J. C., Matear, R. J., Monfray, P., Mouchet, A., Najjar, R., Orr, J. C., Plattner, G.-
2746 K., Sarmiento, J., Schlitzer, R., Slater, R., Totterdell, I. J., Weirig, M. F., Yamanaka, Y.

and Yool, A. (2004). Evaluating global ocean carbon models: The importance of realistic physics. *Global Biogeochemical Cycles,* **18** (3), GB3017. doi:10.1029/2003GB002150

Doughty, C. E. and Goulden, M. L. (2008). Are tropical forests near a high temperature threshold? *Journal of Geophysical Research: Biogeosciences,* **113**, G00B07. doi:10.1029/2007JG000632

Duffy, K., A., Schwalm, C. R., Arcus, V. L., Koch, G. W., Liang, L. L. and Schipper, L. A. (2021). How close are we to the temperature tipping point of the terrestrial biosphere? *Science Advances*, **7**, eaay1052. doi: 10.1126/sciadv.aay1052

Duncanson, L., Armston, J., Disney, M., Avitabile, V., Barbier, N., Calders, K., Carter, S., Chave, J., Herold, M., Crowther, T. W., Falkowski, M., Kellner, J. R., Labrière, N., Lucas, R., MacBean, N., McRoberts, R. E., Meyer, V., Naesset, E., Nickeson, J. E., Paul, K. I., Phillips, O. L., Réjou-Méchain, M., Román, M., Roxburgh, S., Saatchi, S., Schepaschenko, D., Scipal, K., Siqueira, P. R., Whitehurst, A. and Williams, M. (2019). The importance of consistent global forest aboveground biomass product Validation. *Surveys in Geophysics,* **40**, 979–999. doi: 10.1007/s10712-019-09538-8

Eddebbar, Y. A., Rodgers, K. B., Long, M. C., Subramanian, A. C., Xie S.-P. and Keeling, R. F. (2019). El Niño-like physical and biogeochemical ocean response to tropical eruptions. *Journal of Climate*, **32**, JCLI–D–18–0458.1, doi:10.1175/JCLI-D-18-0458.1

Eldering, A.,Wennberg, P. O., Crisp, D., Schimel, D., Gunson, M. R., Chatterjee, A., Liu J., Schwandner, Y. Sun, C.W. O'Dell, C. Frankenberg, T. Taylor, B. Fisher, G.B. Osterman, D. Wunch, F., Hakkarainen, J. and Tamminen, J. **(**2017). The Orbiting Carbon Observatory-2 early science investigations of regional carbon dioxide fluxes. *Science*, **358**, eaam5745. doi:10.1126/science.aam5745

Enting, I.G., Trudinger, C.M. and Francey, R.J. (1995). A synthesis inversion of the concentration and $\delta^{13}C$ atmospheric CO_2. *Tellus*, **47B**, 35-52. doi:10.1034/j.1600-0889.47.issue1.5.x

Enting, I. G. (2002). Inverse Problems in Atmospheric Constituent Transport, Cambridge University Press, Cambridge, doi: 10.1017/CBO9780511535741

Erb, K. H., Kastner, T., Plutzar, C., Bais, A. L. S., Carvalhais, N., Fetzel, T., Gingrich, S., Haberl, H., Lauk, C., Niedertscheider, M., Pongratz, J., Thurner, M. and Luyussaert, S. (2018). Unexpectedly large impact of forest management and grazing on global vegetation biomass. *Nature,* **553**, 73–76. doi: 10.1038/nature25138

Etheridge, D. M., Steele, L. P., Langenfelds, R. L. and Francey (1996). Natural and anthropogenic changes in atmospheric CO_2 over the last 1000 years from air in Antarctic ice and firn. Journal of Geophysical Research, 101, 4115-4128. doi: 10.1029/95JD03410

Fan, S., Gloor, M., Mahlman, J., Pacala, S., Sarmiento, J., Takahashi, T., and Tans, P. (1998). A Large Terrestrial Carbon Sink in North America Implied by Atmospheric and Oceanic Carbon Dioxide Data and Models. *Science*, **282**, 442-446. doi: 10.1126/science.282.5388.442

Fan, L., Wigneron, J.-P., Ciais, P., Chave, J., Brandt, M., Fensholt, R., Saatchi, S. S. Bastos, A., Al-Yaari, A., Hufkens, K., Qin, Y., Xiao, X., Chen, C., Myneni, R. B., Rernandez-Moran, R., Mialon, A., Rodriguez-Fernandez, N. J., Kerr, Y., Tian, F. and Peñuelas, J. (2019). Satellite-observed pantropical carbon dynamics. *Nature Plants,* **5**, 944–951. doi:10.1038/s41477-019-0478-9

Fay, A. R. and McKinley, G. A. (2013). Global trends in surface ocean pCO_2 from in situ data. *Global Biogeochemical Cycles*, **27**, 541–557. doi:10.1002/gbc.20051

Fay, A. R., Lovenduski, N. S., McKinley, G. A., Munro, D. R., Sweeney, C., Gray, A. R., Landschützer, P., Stephens, B. B., Takahashi ,T. and Williams, N. (2018). Utilizing the Drake Passage Time-series to understand variability and change in subpolar Southern Ocean pCO_2. *Biogeosciences*, **15**, 3841–3855. doi:10.5194/bg-15-3841-2018

Fay, A.R., Gregor, L., Landschützer, P. McKinley, G.A., Gruber, N., Gehlen, M., Iida, Y., Laruelle, G. G., Rödenbeck, C. and Zeng J. (2021). Harmonization of global surface ocean pCO_2 mapped products and their flux calculations; an improved estimate of the ocean carbon sink. *Earth System Science Data*, submitted 2021 [preprint].

Fay, A. R., and McKinley, G. A. (2021). Observed regional fluxes to constrain modeled estimates of the ocean carbon sink. *Geophysical Research Letters*, **48**, e2021GL095325. doi: 10.1029/2021GL095325

Feely, R. A., Wanninkhof, R., Takahashi, T., and, Tans P. (1999). Influence of El Niño on the equatorial Pacific contribution of atmospheric CO_2 accumulation, *Nature*, **398**, 597–601. doi: 10.1038/19273

Fernández-Martínez, M., Sardans, J., Chevallier, F., Ciais, P., Obersteiner, M., Vicca, S., Canadell, J. G., Bastos, A., Friedlingstein, P., Sitch, S., Piao, S. L., Janssens_I. A. and Peñuelas, J. (2019). Global trends in carbon sinks and their relationships with CO_2 and temperature. *Nature Climate Change,* **9**, 73–79. doi: 10.1038/s41558-018-0367-7

Fisher, J. B., Huntzinger, D. N., Schwalm, C. R. and Sitch, S. (2014). Modeling the terrestrial biosphere. *Annual Review of Environment and Resources*, **39**, 91–123. doi:10.1146/annurev-environ-012913-093456

Fong, M. B. and Dickson, A. G. (2019). Insights from GO-SHIP hydrography data into the thermodynamic consistency of CO_2 system measurements in seawater. *Marine Chemistry*, **211**, 52-63. doi:10.1016/j.marchem.2019.03.006

Forkel, M., Drüke, M., Thurner, M., Dorigo, W., Schaphoff, S., Thonicke, K., von Bloh, W., and Carvalhais, N. (2019) Constraining modelled global vegetation dynamics and carbon turnover using multiple satellite observations. *Scientific Reports*, **9**, 18757. doi:10.1038/s41598-019-55187-7

Francey, R., Tans, P., Allison, C. E., Enting, I. G., White, J. W., C. and Trolier, M. (1995). Changes in oceanic and terrestrial carbon uptake since 1982. *Nature* **373,** 326–330. doi: 10.1038/373326a0

Frankenberg, C., O'Dell, C., Berry, J., Guanter, L., Joiner, J., Köhler, P., Pollock, R. and Taylor, T. E. (2014). Prospects for chlorophyll fluorescence remote sensing from the orbiting carbon observatory-2. *Remote Sensing of Environment*, **147**, 1–12. doi: 10.1016/j.rse.2014.02.007. ISSN 0034–4257

Frey, M., Sha, M. K., Hase, F., Kiel, M., Blumenstock, T., Harig, R., Surawicz, G., Deutscher, N. M., Shiomi, K., Franklin, J. E., Bösch, H., Chen, J., Grutter, M., Ohyama, H., Sun, Y., Butz, A., Mengistu Tsidu, G., Ene, D., Wunch, D., Cao, Z., Garcia, O., Ramonet, M., Vogel, F. and Orphal, J. (2019). Building the COllaborative Carbon Column Observing Network (COCCON): long-term stability and ensemble performance of the EM27/SUN Fourier transform spectrometer. *Atmospheric Measurement Technologies*, **12**, 1513–1530. doi: 10.5194/amt-12-1513-2019

2835 Friedlingstein, P., Cox, P., Betts, R., Bopp, L., von Bloh, W., Brovkin, V., Cadule, P., Doney, S.,
2836 Eby, M., Fung, I., Bala, G., John, J., Jones, C., Joos, F., Kato, T., Kawamiya, M., Koor, W.,
2837 Lindsay, D., Matthews, H. D., Raddatz, T., Rayner, P., Reick, C., Roekner, E., Schnitzler,
2838 D.-G., Schnur, R., Strassmann, K., Weaver, A., J., Yoshikawa, C., and Zeng, N. (2006).
2839 Climate–Carbon Cycle Feedback Analysis: Results from the C^4MIP Model Intercomparison.
2840 *Journal of Climate*, **19**, 3337-3353. doi: 10.1175/JCLI3800.1
2841 Friedlingstein, P., Jones, M. W., O'Sullivan, M., Andrew, R. M., Hauck, J., Peters, G. P., Peters,
2842 W., Pongratz, J., Sitch, S., Le Quéré, C., Bakker, D. C. E., Canadell, J. G., Ciais, P., Jackson,
2843 R. B., Anthoni, P., Barbero, L., Bastos, A., Bastrikov, V., Becker, M., Bopp, L., Buitenhuis,
2844 E., Chandra, N., Chevallier, F., Chini, L. P., Currie, K. I., Feely, R. A., Gehlen, M., Gilfillan,
2845 D., Gkritzalis, T., Goll, D. S., Gruber, N., Gutekunst, S., Harris, I., Haverd, V., Houghton, R.
2846 A., Hurtt, G., Ilyina, T., Jain, A. K., Joetzjer, E., Kaplan, J. O., Kato, E., Klein Goldewijk,
2847 K., Korsbakken, J. I., Landschützer, P., Lauvset, S. K., Lefèvre, N., Lenton, A., Lienert, S.,
2848 Lombardozzi, D., Marland, G., McGuire, P. C., Melton, J. R., Metzl, N., Munro, D. R.,
2849 Nabel, J. E. M. S., Nakaoka, S.-I., Neill, C., Omar, A. M., Ono, T., Peregon, A., Pierrot, D.,
2850 Poulter, B., Rehder, G., Resplandy, L., Robertson, E., Rödenbeck, C., Séférian, R.,
2851 Schwinger, J., Smith, N., Tans, P. P., Tian, H., Tilbrook, B., Tubiello, F. N., van der Werf, G.
2852 R., Wiltshire, A. J. and Zaehle, S. (2019). Global Carbon Budget 2019. *Earth System*
2853 *Science Data*, **11**, 1783–1838. doi:10.5194/essd-11-1783-2019
2854 Friedlingstein, P., O'Sullivan, M., Jones, M. W., Andrew, R. M., Hauck, J., Olsen, A., Peters, G.
2855 P., Peters, W., Pongratz, J., Sitch, S., Le Quéré, C., Canadell, J. G., Ciais, P., Jackson, R. B.,
2856 Alin, S., Aragão, L. E. O. C., Arneth, A., Arora, V., Bates, N. R., Becker, M., Benoit-Cattin,
2857 A., Bittig, H. C., Bopp, L., Bultan, S., Chandra, N., Chevallier, F., Chini, L. P., Evans, W.,
2858 Florentie, L., Forster, P. M., Gasser, T., Gehlen, M., Gilfillan, D., Gkritzalis, T., Gregor, L.,
2859 Gruber, N., Harris, I., Hartung, K., Haverd, V., Houghton, R. A., Ilyina, T., Jain, A. K.,
2860 Joetzjer, E., Kadono, K., Kato, E., Kitidis, V., Korsbakken, J. I., Landschützer, P., Lefèvre,
2861 N., Lenton, A., Lienert, S., Liu, Z., Lombardozzi, D., Marland, G., Metzl, N., Munro, D. R.,
2862 Nabel, J. E. M. S., Nakaoka, S.-I., Niwa, Y., O'Brien, K., Ono, T., Palmer, P. I., Pierrot, D.,
2863 Poulter, B., Resplandy, L., Robertson, E., Rödenbeck, C., Schwinger, J., Séférian, R.,
2864 Skjelvan, I., Smith, A. J. P., Sutton, A. J., Tanhua, T., Tans, P. P., Tian, H., Tilbrook, B., van
2865 der Werf, G., Vuichard, N., Walker, A. P., Wanninkhof, R., Watson, A. J., Willis, D.,
2866 Wiltshire, A. J., Yuan, W., Yue, X. and Zaehle, S. (2020). Global Carbon Budget 2020.
2867 *Earth System Science Data*, **12**, 3269–3340. doi:10.5194/essd-12-3269-2020
2868 Friedlingstein, P., Jones, M. W., O'Sullivan, M., Andrew, R. M., Bakker, D. C. E., Hauck, J., Le
2869 Quéré, C., Peters, G. P., Peters, W., Pongratz, J., Sitch, S., Canadell, J. G., Ciais, P., Jackson,
2870 R. B., Alin, S. R., Anthoni, P., Bates, N. R., Becker, M., Bellouin, N., Bopp, L., Chau, T. T.
2871 T., Chevallier, F., Chini, L. P., Cronin, M., Currie, K. I., Decharme, B., Djeutchouang, L.,
2872 Dou, X., Evans, W., Feely, R. A., Feng, L., Gasser, T., Gilfillan, D., Gkritzalis, T., Grassi,
2873 G., Gregor, L., Gruber, N., Gürses, Ö., Harris, I., Houghton, R. A., Hurtt, G. C., Iida, Y.,
2874 Ilyina, T., Luijkx, I. T., Jain, A. K., Jones, S. D., Kato, E., Kennedy, D., Klein Goldewijk,
2875 K., Knauer, J., Korsbakken, J. I., Körtzinger, A., Landschützer, P., Lauvset, S. K., Lefèvre,
2876 N., Lienert, S., Liu, J., Marland, G., McGuire, P. C., Melton, J. R., Munro, D. R., Nabel, J.
2877 E. M. S., Nakaoka, S.-I., Niwa, Y., Ono, T., Pierrot, D., Poulter, B., Rehder, G., Resplandy,
2878 L., Robertson, E., Rödenbeck, C., Rosan, T. M., Schwinger, J., Schwingshackl, C., Séférian,
2879 R., Sutton, A. J., Sweeney, C., Tanhua, T., Tans, P. P., Tian, H., Tilbrook, B., Tubiello, F.,
2880 van der Werf, G., Vuichard, N., Wada, C., Wanninkhof, R., Watson, A., Willis, D., Wiltshire,

A. J., Yuan, W., Yue, C., Yue, X., Zaehle, S., and Zeng, J. (2021). Global Carbon Budget 2021, Earth System Science Data Discuss. [preprint], doi: 10.5194/essd-2021-386, in review, 2021.

Friis, K., Körtzinger, A., Pätsch, J. and Wallace, D. W. R. (2005). On the temporal increase of anthropogenic CO_2 in the subpolar North Atlantic. *Deep-Sea Research.* **52**, 681-698. doi:10.1016/j.dsr.2004.11.017

Frölicher, T. L., Joos, F. and Raible, C. C. (2011). Sensitivity of atmospheric CO_2 and climate to explosive volcanic eruptions. *Biogeosciences*, **8**, 2317–2339. doi: 10.5194/bg-8-2317-2011

Frölicher, T. L., Joos, F., Raible, C. C. and Sarmiento, J. L. (2013). Atmospheric CO_2 response to volcanic eruptions: The role of ENSO, season, and variability. *Global Biogeochemical Cycles*, **27**, 239-251. doi:10.1002/gbc.20028

Frölicher, T.L., Rodgers, K. B., Stock, C. A., Cheung, W. W. L. (2016). Sources of uncertainties in 21st century projections of potential ocean ecosystem stressors: Uncertainties in stressor projections. *Global Biogeochemical Cycles,* **30**, 1224–1243. doi:10.1002/2015GB005338

Galbraith, E. D. and Skinner, L. C. (2020). The biological pump during the last glacial maximum. *Annual Reviews of Marine Science* **12**, 559–586. doi:10.1146/annurev-marine-010419-010906

Gampe, D., Zscheischler, J., Reichstein, M., O'Sullivan, M., Smith, W. K., Sitch, S. and Buermann, W. (2021). Increasing impact of warm droughts on northern ecosystem productivity over recent decades. *Nature Climate Change*, **11**, 772–779. doi: 10.1038/s41558-021-01112-8

Gasser, T., Crepin, L., Quilcaille, Y., Houghton, R. A., Ciais, P., and Obersteiner, M. (2020). Historical CO_2 emissions from land use and land cover change and their uncertainty, *Biogeosciences*, **17**, 4075–4101. doi: 10.5194/bg-17-4075-202

Gatti, L.V., Gloor, M., Miller, J. B., Doughty, C. E., Malhi, Y., Domingues, L. G., Basso, L. S., Martinewski, A., Correia, C. S., Borges, V. F., Freitas, S., Braz, R., Anderson, L. O., Rocha, H., Grace, J., Phillips, O. L. and Lloyd, J. (2014). Drought sensitivity of Amazonian carbon balance revealed by atmospheric measurements. *Nature*, **506**, 76-80. doi:10.1038/nature12957

Gatti, L, V., Basso, L., S., Miller, J., B., Gloor, M., Domingues, L. G., Cassol, H. L. G., Tejada, G., Arango, L. E. O. C. Nobre, C., Peters, W., Marani, L., Arai, E., Sanches, A. H., Correa, S. M., Anderson, L., von Randow, C., Correia, C. S. C., Crispim, S., P., and Neves, R. A. L. (2021). Amazonia as a carbon source linked to deforestation and climate change. *Nature*, **595**, 388-393. doi: 10.1038/s41586-021-03629-6

Gaubert, B., Stephens, B. B., Basu, S., Chevallier, F., Deng, F., Kort, E. A., Patra, P. K., Peters, W., Rödenbeck, C., Saeki, T., Schimel, D., Van der Laan-Luijx, I., Wofsy, S., Yin, Y. (2019). Global atmospheric CO_2 inverse models converging on neutral tropical land exchange, but disagreeing on fossil fuel and atmospheric growth rate. *Biogeosciences*, **16**, 117–134. doi: 10.5194/bg-16-117-2019

Gitz, V. and Ciais, P. (2003) Amplifying effects of land-use change on future atmospheric CO_2 levels. Global Biogeochemical Cycles, 17, 1024. doi: 10.1029/2002GB001963

Gloege, L., McKinley, G. A., Landschützer, P., Fay, A., Frölicher, T., Fyfe, J. C., Illyina ,T., Jones, S.D., Lovenduski, N. S., Rödenbeck ,C., Rodgers K. B., Schlunegger, S. and Takano, Y. (2021). Quantifying errors in observationally-based estimates of ocean carbon sink

variability. *Global Biogeochemical Cycles,* **35**, e2020GB006788. doi: 10.1029/2020GB006788

Gloor, M., Sarmiento, J. L. and Gruber, N. (2010). What can be learned about carbon cycle climate feedbacks from the CO_2 airborne fraction? *Atmospheric Chemistry and Physics,* **10**, 7739–7751. doi: 10.5194/acp-10-7739-2010

Gonsamo, A., Chen, J. M., He, L., Sun, Y., Rogers, C. and Liu, J. (2019). Exploring SMAP and OCO-2 observations to monitor soil moisture control on photosynthetic activity of global drylands and croplands, *Remote Sensing of Environment*, **232**, 111314. doi:10.1016/j.rse.2019.111314

Gonsamo, A., Ciais, P., Miralles, D. G., Sitch, S., Dorigo, W., Lombardozzi, D., Friedlingstein, P., Nabel, J. E. M. S., Goll, D. S., O'Sullivan, M., Arneth, A., Anthoni, P., Jain, A. K., Wiltshire, A., Peylin, P. and Cescatti, A. (2021). Greening drylands despite warming consistent with carbon dioxide fertilization effect. *Glob Change Biol*, **27**, 3336-3349. doi: 10.1111/gcb.15658

Goris, N., Tjiputra, J. F., Olsen, A., Schwinger, J., Lauvset S. K. and Jeansson E. (2018). Constraining projection-based estimates of the future North Atlantic carbon uptake. *Journal of Climate*, **31**, 3959–3978, doi:10.1175/JCLI-D-17-0564.1

Grace, J., Mitchard, E., and Gloor, E. (2014). Perturbations in the carbon budget of the tropics. *Global Change Biology*, **20**, 3238–3255. doi: 10.1111/gcb.12600

Grassi, G., House, J., Kurz, W. A., Cescatti, A., Houghton, R. A., Peters, G. P., Sanz, M. J., Viñas, R. A., Alkama, R., Arneth, A., Bondeau, A., Dentener, F., Fader, M., Federici, S., Friedlingstein, P., Jain, A. K., Kato, E., Koven, C. D., Lee, D., Nabel, J. E. M. S., Nassikas, A. A., Perugini, L., Rossi, S., Sitch, S., Viovy, N., Wiltshire, A. and Zaehle, S. (2018). Reconciling global-model estimates and country reporting of anthropogenic forest CO_2 sinks. *Nature Climate Change*, **8**, 914–920. doi: 10.1038/s41558-018-0283-x

Graven, H. D., Keeling, R. F., Piper, S. C., Patra, P. K., Stephens, B. B., Wofsy, S. C., Welp, L. R., Sweeney, C. and Tans, P. P. (2013). Enhanced seasonal exchange of CO_2 by northern ecosystems since 1960, *Science*, **341**, 1085–1089. doi:10.1126/science.1239207

Gregor, L., Lebehot, A. D. Kok, S. and Scheel Monteiro, P. M. (2019). A comparative assessment of the uncertainties of global surface-ocean CO_2 estimates using a machine learning ensemble (CSIR-ML6 version 2019a); have we hit the wall? *Geoscientific Model Development*, **12**, 5113–5136. doi:10.5194/gmd-12-5113-2019

Gruber, N., Clement, D., Carter, B.R., Feely, R.A., Van Heuven, S., Hoppema, M., Ishii, M., Key, R.M., Kozyr, A., Lauvset, S.K., Lo Monaco, C., Mathis, J.T., Murata, A., Olsen, A., Perez, F.F., Sabine, C.L., Tanhua, T., and Wanninkhof, R. (2019a). The oceanic sink for anthropogenic CO_2 from 1994 to 2007. *Science,* **363**, 1193-1199. doi:10.1126/science.aau5153

Gruber, N., Landschützer, P., and Lovendusk, N. S. (2019b). The variable Southern Ocean carbon sink. *Annual Reviews of Marine Sci*ence, **11**, 159–186. doi:10.1146/annurev-marine-121916-063407

Guan, K., Berry, J. A., Zhang, Y., Joiner, J., Guanter, L., Badgley, G. and Lobell, D. B. (2016). Improving the monitoring of crop productivity using spaceborne solar-induced fluorescence. *Global Change Biology*, **22**, 716–726. doi:10.1111/gcb.13136

Guan, K., Wu, J., Kimball, J. S., Anderson, M. C., Frolking, S., Li, B., Hain, C. R. and Lobell, D. B. (2017). The shared and unique values of optical, fluorescence, thermal and microwave

satellite data for estimating large-scale crop yields. *Remote Sensing of Environment*, **199**, 333–349. doi:10.1016/j.rse.2017.06.043

Gurney, K. R., Law, R. M., Denning, A. S., Rayner, P. J., Baker, D., Bousquet, P., Bruhwiler, L., Chen, Y.-H., Ciais, P., Fan, S., Fung, I. Y., Gloor, M., Heimann, M., Higuchi, K., John, J., Maki, T., Maksyutov, S., Masarie, K., Peylin, P., Prather, M., Pak, B. C., Randerson, J., Sarmiento, J., Taguchi, S., Takahashi, T., and Yuen, C.-W. (2002). Towards robust regional estimates of CO_2 sources and sinks using atmospheric transport models, *Nature*, **415**, 626–630. doi: 10.1038/415626a

Gurney, K. R., Law, R. M., Denning, A. S., Rayner, P. J., Baker, D., Bousquet, P., Bruhwiler, L., Chen, Y.-H., Ciais, P., Fan, S., Fung, I. Y., Gloor, M., Heimann, M., Higuchi, K., John, J., Kowalczyk, E., Maki, T., Maksyutov, S., Peylin, P., Prather, M., Pak, B. C., Sarmiento, J., Taguchi, S., Takahashi, T., and Yuen, C.-W. (2003). TransCom 3 CO2 inversion intercomparison: 1. Annual mean control results and sensitivity to transport and prior flux information, *Tellus B,* **55**, 555–579. doi: 10.3402/tellusb.v55i2.16728

Gurney, K. R., Liang, J., O'Keeffe, D., Patarasuk, R., Hutchins, M., Huang, J., Rao, P. and Song, Y. (2019). Comparison of global downscaled versus bottom-up fossil fuel CO_2 emissions at the urban scale in four U.S. urban areas. *Journal of Geophysical Research: Atmospheres*, **124**, 2823--2840. doi:10.1029/2018JD028859

Hakkarainen, J., Ialongo, I. and Tamminen, J. (2016). Direct space-based observations of anthropogenic CO_2 emission areas from OCO-2. *Geophysical Research Letters,* **43**, 11,400–11,406. doi:10.1002/2016GL070885

Hakkarainen, J., Ialongo, I., Maksyutov, S., and Crisp, D. (2019). Analysis of Four Years of Global XCO_2 Anomalies as Seen by Orbiting Carbon Observatory-2, *Remote Sensing*, **11**, 850. doi:10.3390/rs11070850

Hakkarainen, J., Szelag, M. E., Ialongo, I., Retscher, C., Oda, T. and Crisp, D. (2021). Analyzing nitrogen oxides to carbon dioxide emission ratios from space: A case study of Matimba Power Station in South Africa. *Atmospheric Environment*, **10**, 100110. doi: 10.1016/j.aeaoa.2021.100110

Hansen, J., Sato, M., Russell, G. and Kharecha, P., (2013a). Climate sensitivity, sea level and atmospheric carbon dioxide, *Philosophical Transactions of the Royal Society. A*., **371**, 20120294. doi: 10.1098/rsta.2012.0294

Hansen, M. C., Potapov ,P. V., Moore, R., Hancher, M., Turubanova ,S. A., Tyukavina, A., Thau, D., Stehman, S. V., Goetz ,S. J., Loveland, T. R., Kommareddy, A., Egorov, A., Chini, L., Justice, C. O., and Townshend, J. R. G. (2013b). High-Resolution Global Maps of 21st-Century Forest Cover Change. *Science*, **342**, 850–53. doi: 10.1126/science.1244693.

Hansis, E., Davis, S. J. and Pongratz, J. (2015). Relevance of methodological choices for accounting of land use change carbon fluxes. *Global Biogeochemical Cycles*, **29**, 1230–1246. doi:10.1002/2014GB004997

Harris, N. L., Hagen, S. C., Saatchi, S. S., Pearson, T. R. H., Woodall, C. W., Domke, G. M., Braswell, B. H., Walters, B. F., Brown, S., Salas, W., Fore, A., and Yu, Y. (2016). Attribution of net carbon change by disturbance type across forest lands of the conterminous United States. *Carbon Balance and Management*, **11**, 24. doi: 10.1186/s13021-016-0066-5

Harris, N. L., Gibbs, D. A., Baccini, A., Birdsey, R. A., de Bruin, S., Farina, M., Fatoyinbo, L., Hansen, M. C., Herold, M., Houghton, R. A., Potapov, P. V., Suarez, D. R., Roman-Cuesta, R. M., Saatchi,S., S., Slay, C. M., Turubanova, S., A., and Tyukavina, A. (2021). Global

maps of twenty-first century forest carbon fluxes. *Nature Climate Change,* **11**, 234–240. doi:10.1038/s41558-020-00976-6

Hauck, J., Völker, C., Wang, T., Hoppema, M., Losch, M. and Wolf-Gladrow, D.A. (2013). Seasonally different carbon flux changes in the Southern Ocean in response to the southern annular mode. *Global Biogeochemical Cycles,* **27**, 1236–1245. doi:10.1002/2013GB004600

Hauck, J., Völker, C., Wolf-Gladrow, D. A., Laufkötter, C., Vogt, M., Aumont, O., Bopp, L., Buitenhuis, E. T., Doney, S. C., Dunne, J., Gruber, N., Hashioka, T., John, J., Le Quéré, C., Lima, I. D., Nakano, H., Séférian, R. and Totterdell, I. (2015). On the Southern Ocean CO_2 uptake and the role of the biological carbon pump in the 21st century. *Global Biogeochemical Cycles,* **29**, 1451–1470. doi:10.1002/2015GB005140

Hauck, J., Zeising, M., Le Quéré, C., Gruber, N., Bakker, D. C. E., Bopp, L., Chau, T. T. T., Gürses, Ö., Ilyina, T., Landschützer, P., Lenton, A., Resplandy, L., Rödenbeck, C., Schwinger, J. and Séférian, R. (2020). Consistency and challenges in the ocean carbon sink estimate for the Global Carbon Budget. *Frontiers in Marine Science,* **7**, 571720. doi:10.3389/fmars.2020.571720

Hausfather, Z. and Peters, G. P. (2020). Emissions - the "business as usual" story is misleading. *Nature*, **577**, 618–620, doi:10.1038/d41586-020-00177-3

He, L., Magney, T., Dutta, D., Yin, Y., Köhler, P., Grossmann, K., Stutz, J., Dold, C., Hatfield, J., Guan, K., Peng, B. and Frankenberg, C. (2020). From the ground to space: Using solar-induced chlorophyll fluorescence to estimate crop productivity. *Geophysical Research Letters*, **47**, e2020GL087474. doi:10.1029/2020GL087474

Hedelius, J. K., Feng, S., Roehl, C. M., Wunch, D., Hillyard, P. W., Podolske, J. R., Iraci, L. T., Patarasuk, R., Roa, P., O'Keeffe, D., Gurney, K. R., Lauvaux, T., and Wennberg, P. O. (2017). Emissions and topographic effects on column CO_2 (XCO_2) variations, with a focus on the Southern California Megacity. *Journal of Geophysical Research, Atmospheres,* **122**, 7200–7215, doi:10.1002/2017JD026455

Hedelius, J. K., Liu, J., Oda, T., Maksyutov, S., Roehl, C. M., Iraci, L., Podolske, J., Hillyard, P., Liang, J., Gurney, K., Wunch, D. and Wennberg P. (2018). Southern California megacity CO_2, CH_4, and CO flux estimates using ground- and space-based remote sensing and a Lagrangian model, *Atmospheric Chemistry and Physics,* **18**, 16271-16291. doi:10.5194/acp-18-16271-2018

Henson, S. A., Beaulieu, C. and Lampitt, R. (2016). Observing climate change trends in ocean biogeochemistry: when and where. *Global Change Biology,* **22**, 1561–1571. doi:10.1111/gcb.13152

Hersbach, H., Bell. B., Berrisford, P., Hirahara, S., Horányi, A., Muñoz-Sabater, J., Nicolas, J., Peubey, C., Radu, R., Schepers, D., Simmons, A., Soci. C., Abdalla, S., Abellan, X., Balsamo G., Bechtold, P., Biavati ,G., Bidlot, J., Bonavita, M., De Chiara, G., Dahlgren, P., Dee, D., Diamantakis, M., Dragani, R., Flemming, J., Forbes, R., Fuentes, M., Geer A., Haimberger L., Healy, S., Hogan, R. J., Hólm, E., Janisková, M., Keeley, S., Laloyaux, P., Lopez, P., Radnoti, G., de Rosnay, P., Rozum, I., Vamborg, F., Villaume ,S. and Thépaut J.-N. (2020). The ERA5 Global Reanalysis. *Quarterly Journal of the Royal Meteorological Society*, **146**, 1999-2049. doi: https://doi.org/10.1002/qj.3803

Heymann, J., Reuter, M., Buchwitx, M., Schneising, O., Bovensmann, H., Burrows, J. P., Massart, S., Kaiser, J. W., and Crisp, D. (2017). CO_2 emission of Indonesian fires in 2015

3059 estimated from satellite-derived atmospheric CO_2 concentrations. *Geophysical Research*
3060 *Lett*ers, **44**, 1537-1544. doi: 10.1002/2016GL072042
3061 Hlásny, T., Zimová, S., Merganičová, K., Štěpánek, P., Modlinger, R., and Turčáni, M. (2021).
3062 Devastating outbreak of bark beetles in the Czech Republic: Drivers, impacts, and
3063 management implications, *Forest Ecology and Management*, **490**,119075, doi:
3064 10.1016/j.foreco.2021.119075
3065 Hong, C., Burney, J. A., Pongratz, J., Nabel., J. E. M. S., Mueller, N. D., Jackson, R. B., and
3066 Davis, S. J. (2021). Global and regional drivers of land-use emissions in 1961–2017.
3067 *Nature*, **589**, 554-561. doi: 10.1038/s41586-020-03138-y
3068 Hoppema, M., Bakker, K., van Heuven, S. M. A. C., van Ooijen, J. C. and de Baar, H. J. W.
3069 (2015). Distributions, trends and inter-annual variability of nutrients along a repeat section
3070 through the Weddell Sea (1996–2011). *Marine Chemistry,* **177**, 545–553.
3071 doi:10.1016/j.marchem.2015.08.007
3072 Houghton, R. A. (2003). Revised estimates of the annual net flux of carbon to the atmosphere
3073 from changes in land use and land management 1850–2000. *Tellus*, **55B**, 378–390.
3074 doi:10.1034/j.1600-0889.2003.01450.x
3075 Houghton, R. A., House, J. I., Pongratz, J., van der Werf, G. R., DeFries, R. S., Hansen, M. C.,
3076 Le Quéré, C., and Ramankutty, N. (2012). Carbon emissions from land use and land-cover
3077 change, *Biogeosciences*, **9**, 5125–5142, doi: 10.5194/bg-9-5125-2012
3078 Houghton, R. A. and Nassikas, A. A. (2017). Global and regional fluxes of carbon from land use
3079 and land cover change 1850–2015. *Global Biogeochemical Cycles*, **31**, 456–472.
3080 doi:10.1002/2016GB005546
3081 Houweling, S., Baker, D., Basu, S., Boesch, H., Butz, A., Chevallier, F., Deng, F., Dlugokencky,
3082 E. J., Feng, L., Ganshin, A., Hasekamp, O., Jones, D., Maksyutov, S., Marshall, J., Oda, T.,
3083 O'Dell, C. W., Oshchepkov, S., Palmer, P. I., Peylin, P., Poussi, Z., Reum, F., Takagi, H.,
3084 Yoshida, Y., and Zhuravlev, R. (2015). An intercomparison of inverse models for estimating
3085 sources and sinks of CO_2 using GOSAT measurements, *Journal of Geophysical Research*
3086 *Atmospheres*, **120**, 5253–5266. doi: 10.1002/2014JD022962
3087 Hubau, W., Lewis, S. L., Phillips O. L., Affum-Baffoe, Beeckman, K. H., Cuni-Sanchez, A.,
3088 Ewango, C. E. N., Fauset, S., Sheil, D., Sonké, B., Sullivan, M. J. P., Sunderland,T.,
3089 Thomas, S. C., Abernethy, K. A., Adu-Bredu, S., Amani C. A., Baker, T. R., Banin, L. F.,
3090 Baya, F., Begne, S. K., Bennett, A. C., Benedet, F., Bitariho, R., Bocko, Y. E., Boeckx, P.,
3091 Boundja, P., Brienen, R. J. W., Brncic, T., Chezeaux, E., Chuyong, G. B., Clark, C. J.,
3092 Collins, M., Comiskey, J. A., Coomes, D. A., Dargie, G. C., de Haulleville, T., Kamdem, M.
3093 N. D., Doucet, J. L., Esquivel-Muelbert, A., Feldpausch, T. R., Fofanah, A., Foli, E. G.,
3094 Gilpin, M., Gloor, E., Gonmadje, C., Gourlet-Fleury, S., Hall, J. S., Hamilton, A. C., Harris,
3095 D. J., Hart, T. B., Hockemba, M. B. N., Hladik, A., Ifo, S. F., Jeffery, K. J., Jucker, T.,
3096 Yakusu, E. K., Kearsley, E., Kenfack, D., Koch, A., Leal, M. E., Levesley, A., Lindsell, J.
3097 A., Lisingo, J., Lopez-Gonzalez, G., Lovett, J. C., Makana, J. R., Malhi, Y., Marshall, A. R.,
3098 Martin, J., Martin, E. H., Mbayu, F. M., Medjibe ,V. P., Mitchard, E. T. A., Moore, S.,
3099 Munishi, P. K. T., Bengone, N. N., Ojo, L., Ondo, F. E., Peh, K. S., Pickavance, G. C.,
3100 Poulsen, A. D., Poulsen, J. R., Qie, L., Reitsma, J., Rovero, F., Swaine, M. D., Talbot, J.,
3101 Taplin J., Taylor, D. D., Thomas, D. W., Toirambe, B., Mukendi, J. T., Tuagben, D.,
3102 Umunay, P. M., van der Heijden, G. M. F., Verbeeck, H., Vleminckx, J., Willcock, S., Wöll,

H., Woods, J. T. and Zemagho, L. (2020). Asynchronous carbon sink saturation in African and Amazonian tropical forests. *Nature,* **579**, 80–87. doi:10.1038/s41586-020-2035-0

Huber, M. B. and Zanna, L. (2017). Drivers of uncertainty in simulated ocean circulation and heat uptake. *Geophysical Research Letters,* **44**, 1402-1413. doi:10.1002/2016GL071587

Humphrey, V., Zscheischler, J., Ciais, P., Gudmundsson, L., Sitch, S., & Seneviratne, S. I. (2018). Sensitivity of atmospheric CO_2 growth rate to observed changes in terrestrial water storage. *Nature*, **560**, 628. doi: 10.1038/s41586-018-0424-4

Humphrey, V., Berg, A., Ciais, P., Gentine, P., Jung, M., Reichstein, M., Seneviratne, S. I., and Frankenberg, C. (2021). Soil moisture–atmosphere feedback dominates land carbon uptake variability. *Nature*, **592**, 65-69. doi: 10.1038/s41586-021-03325-5

Hurtt, G. C., Chini, L., Sahajpal, R., Frolking, S., Bodirsky, B. L., Calvin, K., Doelman, J. C., Fisk, J., Fujimori, S., Klein Goldewijk, K., Hasegawa, T., Havlik, P., Heinimann, A., Humpenöder, F., Jungclaus, J., Kaplan, J. O., Kennedy, J., Krisztin, T., Lawrence, D., Lawrence, P., Ma, L., Mertz, O., Pongratz, J., Popp, A., Poulter, B., Riahi, K., Shevliakova, E., Stehfest, E., Thornton, P., Tubiello, F. N., van Vuuren, D. P. and Zhang, X. (2020). Harmonization of global land use change and management for the period 850–2100 (LUH2) for CMIP6. *Geoscientific Model Development*, **13**, 5425–5464. doi: 10.5194/gmd-13-5425-2020

Hwang, Y. Schlüter, S. Choudhury, T.; Um, J.-S. (2021). Comparative Evaluation of Top-Down GOSAT XCO_2 vs. Bottom-Up National Reports in the European Countries. *Sustainability*, **13**, 6700. doi: 10.3390/su1312670

Iida, T., Odate, T., Fukuchi, M. (2013). Long-Term Trends of Nutrients and Apparent Oxygen Utilization South of the Polar Front in Southern Ocean Intermediate Water from 1965 to 2008. *PLoS ONE,* **8**, e71766. doi:10.1371/journal.pone.0071766

IEA World Energy Balances, 2020 Edition. Available from https://www.iea.org/subscribe-to-data-services/world-energy-balances-and-statistics, last viewed on 30 November 2021.

IPCC 2006, 2006 IPCC Guidelines for National Greenhouse Gas Inventories, Prepared by the National Greenhouse Gas Inventories Programme, Eggleston H.S., Buendia L., Miwa K., Ngara T. and Tanabe K. (eds). Published: IGES, Japan.

IPCC 2014, Intergovernmental Panel on Climate Change. (2014). Climate change 2013: The physical science basis: Working Group I contribution to the Fifth Assessment Report of the Intergovernmental Panel on Climate Change. In T. F. Stocker, D. Qin, G.-K. Plattner, M. Tignor, S. K. Allen, J. Boschung, et al. (Eds.), Cambridge University Press. doi: 10.1017/CBO9781107415324

IPCC 2019, 2019 Refinement to the 2006 IPCC Guidelines for National Greenhouse Gas Inventories, Calvo Buendia, E., Tanabe, K., Kranjc, A., Baasansuren, J., Fukuda, M., Ngarize S., Osako, A., Pyrozhenko, Y., Shermanau, P. and Federici, S. (eds). Published: IPCC, Switzerland.

IPCC, 2021: Summary for Policymakers. In: Climate Change 2021: The Physical Science Basis. Contribution of Working Group I to the Sixth Assessment Report of the Intergovernmental Panel on Climate Change [Masson-Delmotte, V., P. Zhai, A. Pirani, S.L. Connors, C. Péan, S. Berger, N. Caud, Y. Chen, L. Goldfarb, M.I. Gomis, M. Huang, K. Leitzell, E. Lonnoy, J.B.R. Matthews, T.K. Maycock, T. Waterfield, O. Yelekçi, R. Yu, and B. Zhou (eds.)]. Cambridge University Press. In Press.

Ito, A. (2020). Constraining size-dependence of vegetation respiration rates, *Scientific Reports*, **10**, 4304. doi:10.1038/s41598-020-61239-0

Iudicone, D., Rodgers, K. B., Plancherel, Y., Aumont, O., Ito, T., Key, R. M., Madec, G. and Ishii, M. (2016). The formation of the ocean's anthropogenic carbon reservoir. *Scientific Reports*, **6**, 35473. doi:10.1038/srep35473

Jacobson, A. R., Mikaloff Fletcher, S. E., Gruber, N., Sarmiento, J. L. and Gloor, M. (2007). A joint atmosphere-ocean inversion for surface fluxes of carbon dioxide: 1. Methods and global-scale fluxes. *Global Biogeochemical Cycles*, **21**, 273. doi:10.1029/1999GL900363

Janssens-Maenhout, G., Crippa, M., Guizzardi, D., Muntean, M., Schaaf, E., Dentener, F., Bergamaschi, P., Pagliari, V., Olivier, J. G. J., Peters, J. A. H. W., van Aardenne, J. A., Monni, S., Doering, U., Petrescu, A. M. R., Solazzo, E. and Oreggioni, G. D. (2019). EDGAR v4.3.2 Global Atlas of the three major greenhouse gas emissions for the period 1970–2012. *Earth System Science Data*, **11**, 959-1002. doi:10.5194/essd-11-959-2019

Janssens-Maenhout, G., Pinty, B., Dowell, M., Zunker, H., Andersson, E., Balsamo, G., Bézy, J. L., Brunhes, T., Bösch, H., Bojkov, B., Brunner, D., Buchwitz, M., Crisp, D., Ciais, P., Counet, P., Dee, D., Denier van der Gon, H., Dolman, H., Drinkwater, M., Dubovnik O., Engelen, R., Fehr, T., Fernandez, V., Heimann, M., Holmlund, K., Houweling, S., Husband, R., Juvyns, O., Kentarchos, A., Landgraf, J., Lang, R., Löscher, A., Marshall, J., Meijer, Y., Nakajima, M., Palmer, P. I., Peylin, P., Rayner, P., Scholze, M., Sierk, B., Tamminen, J., Veefkind, P. (2020). Toward an operational anthropogenic CO_2 emissions monitoring and verification support capacity. *Bulletin of the American Meteorological Society*, **101**, E1439-E1451. doi:10.1175/BAMS-D-19-0017.1

Jeong, S.-J., Bloom, A. A., Schimel, D., Sweeney, C., Parazoo, N. C., Medvigy, D., Schaepman-Strub, G., Zheng, C., Schwalm, C. R., Huntzinger, D. N., Michalak, A. M., and Miller, C. E. (2018). Accelerating rates of Arctic carbon cycling revealed by long-term atmospheric CO_2 measurements. *Science Advances*, **4**. Eaao1167. doi: 10.1126/sciadv.aao1167

Jian, J., Vargas, R., Anderson-Teixeira, K., Stell, E., Herrmann, V., Horn, M., Kholod, N., Manzon, J., Marchesi, R., Paredes, D. and Bond-Lamberty, B. (2021). A restructured and updated global soil respiration database (SRDB-V5). *Earth System Science Data*, **13**, 255-267, doi: 10.5194/essd-13-255-2021

Jiang, C., and Ryu, Y. (2016). Multi-scale evaluation of global gross primary productivity and evapotranspiration products derived from Breathing Earth System Simulator (BESS). *Remote Sensing of Environment*, **186**, 528-547. doi: 10.1016/j.rse.2016.08.030

Johnson, K. S., Jannasch, H. W., Coletti, L. J., Elrod, V. A., Martz, T. R., Takeshita, Y., Carlson, R. J. and Connery, J. G. (2016). Deep-Sea DuraFET: A pressure tolerant pH sensor designed for global sensor networks. *Analytical Chemistry*, **88**, 3249-3256. doi:10.1021/acs.analchem.5b04653

Joiner, J., Yoshida, Y., Zhang, Y., Duveiller, G., Jung, M., Lyapustin, A., Wang, Y., and Tucker C. J. (2018). Estimation of Terrestrial Global Gross Primary Production (GPP) with Satellite Data-Driven Models and Eddy Covariance Flux Data. Remote Sensing, 10, 1346, doi: 10.3390/rs10091346

Jones, C. D. Ciais, P., Davis, S. J., Friedlingstein, P., Gasser, T., Peters, G. P., Rogelj, J., van Vuuren, D. P., Canadell, J. G., Cowie, A., Jackson, R. B., Jonas, M., Kriegler, E., Littleton, E., Lowe, J. A., Milne, J., Shrestha, G., Smith, P., Torvanger, A., and Wiltshire, A. (2016).

3191 Simulating the Earth system response to negative emissions. *Environmental Research*
3192 *Letters,* **11**, 095012. doi: 10.1088/1748-9326/11/9/095012
3193 Joos, F., Bruno, M., Fink, R., Siegenthaler, U., Stocker, T. F., Le Quéré, C. and Sarmiento, J. L.
3194 (1996). An efficient and accurate representation of complex oceanic and biospheric models
3195 of anthropogenic carbon uptake. *Tellus B*, **48**, 397. doi:10.1034/j.1600-0889.1996.t01-2-
3196 00006.x
3197 Joos, F. and Spahni, R. (2008). Rates of change in natural and anthropogenic radiative forcing
3198 over the past 20,000 years, *Proceedings of the National Academy of Sciences, USA*, **105**,
3199 1425–1430. doi: 10.1073/pnas.0707386105
3200 Jung, M., Reichstein, M. and Bondeau, A. (2009). Towards global empirical upscaling of
3201 FLUXNET eddy covariance observations: validation of a model tree ensemble approach
3202 using a biosphere model. *Biogeosciences*, **6**, 2001–2013. doi:10.5194/bg-6-2001-2009
3203 Jung, M., Reichstein, M., Schwalm, C. R., Huntingford, C., Sitch, S., Ahlström, A., Arneth, A.,
3204 Camps-Valls, G., Ciais, P., Friedlingstein, P., Gans, F., Ichii, K., Jain, A. K., Kato, E.,
3205 Papale, D., Poulter, B., Raduly, B., Rödenbeck, C., Tramontana, G., Viovy, N., Wang, Y.-P.,
3206 Weber, U., Zaehle, S., and Zeng, N. (2017). Compensatory water effects link yearly global
3207 land CO_2 sink changes to temperature, *Nature*, **541**, 516–520. doi: 10.1038/nature20780
3208 Jung, M., Schwalm, C. Migliavacca, M., Walther, S., Camps-Valls, G., Koirala, S., Anthoni, P.,
3209 Besnard, S., Bodesheim, P., Carvalhais, N., Chevallier, F., Gans, F., Goll, D. S., Haverd, V.,
3210 Koehler, P., Ichii, K., Jain, A. K., Liu, J., Lombardozzi, D., Nabel, J. E. M. S., Nelson, J. A.,
3211 O'Sullivan, M., Pallandt, M., Papale, D., Peters, W., Pongratz, J., Roedenbeck, C., Sitch, S.,
3212 Tramontana, G., Walker, A., Weber, U. and Reichstein, M. (2020). Scaling carbon fluxes
3213 from eddy covariance sites to globe: synthesis and evaluation of the FLUXCOM approach.
3214 *Biogeosciences*, **17**, 1343–1365. doi: 10.5194/bg-17-1343-2020
3215 Kao, H.-Y. and Yu, J.-Y. (2009). Contrasting Eastern-Pacific and Central-Pacific Types of ENSO,
3216 *J. Clim*., 22, 615–632. doi: 10.1175/2008JCLI2309.1
3217 Kaminski, T., and Heimann, M. (2001). Inverse Modeling of Atmospheric Carbon Dioxide
3218 Fluxes. *Science*, **294**, 259a. doi: 10.1126/science.294.5541.259a
3219 Kaminski, T., Scholze, M., Vossbeck, M., Knorr, W., Buchwitz, M., & Reuter, M. (2017).
3220 Constraining a terrestrial biosphere model with remotely sensed atmospheric carbon
3221 dioxide. Remote Sensing of Environment, 203, 109–124. doi: 10.1016/j.rse.2017.08.017
3222 Karion, A., Sweeney, C., Tans, P. P. and Newberger, T. (2010). AirCore: An innovative
3223 atmospheric sampling system. *Journal of Atmospheric and Oceanic Technology*, **27**, 1839–
3224 1853. doi:10.1175/2010JTECHA1448.1
3225 Keeling, C. D. (1960). The concentration and isotopic abundances of carbon dioxide in the
3226 atmosphere. Tellus, 12, 200-203. doi: 10.1111/j.2153-3490.1960.tb01300.x
3227 Keeling, C. D. (1973) *The Carbon Dioxide Cycle: Reservoir Models to Depict the Exchange of*
3228 *Atmospheric Carbon Dioxide with the Oceans and Land Plants*. In Chemistry of the Lower
3229 Atmosphere. Springer. doi: 10.1007/978-1-4684-1986-3_6
3230 Keeling, C. D., Bacastow, R. B., Carter, A. F., Piper, S. C., Whorf, T. P., Heimann, M., Mook, W.
3231 G., and Roeloffzen, H. (1989). A Three-Dimensional Model of Atmospheric CO_2 Transport
3232 Based on Observed Winds: 1. Analysis of Observational Data. *Geophysical Monograph,*
3233 **55**, 165-236. doi: 10.1029/GM055p0165

3234 Keeling, C., Whorf, T., Wahlen, M., and van der Plichtt, J. (1995). Interannual extremes in the
3235 rate of rise of atmospheric carbon dioxide since 1980. *Nature,* **375,** 666–670 (1995). doi:
3236 10.1038/375666a0
3237 Keeling, C. D., Chin, J. F. S., and Whorf, T. P. (1996). Increased activity of northern vegetation
3238 inferred from atmospheric CO_2 measurements. *Nature*, **382**, 146-149. doi:
3239 10.1038/382146a0
3240 Keeling, C. D., Piper, S. C., Bacastow, R. B., Wahlen, M., Whorf, T. P., Heimann, M., and
3241 Meijer, H. A. (2001). Exchanges of Atmospheric CO_2 and $^{13}CO_2$ with the Terrestrial
3242 Biosphere and Oceans from 1978 to 2000.I. Global Aspects, UC San Diego: Library –
3243 Scripps Digital Collection. Retrieved from https://escholarship.org/uc/item/09v319r9
3244 Keeling, C. D., Piper, S. C., Bacastow, R. B., Wahlen, M., Wahlen, M., Whorf, T. P., Heinmann,
3245 M. and Meijer, H. A. (2005) 'Atmospheric CO_2 and $^{13}CO_2$ exchange with the terrestrial
3246 biosphere and oceans from 1978 to 2000: Observations and carbon cycle implications', in *A*
3247 *history of atmospheric CO_2 and its effects on plants, animals, and ecosystems*. Springer, pp.
3248 83–113.
3249 Keenan, T. F., and Riley, W. J. (2018). Greening of the land surface in the world's cold regions
3250 consistent with recent warming. *Nature Climate Change*, **8**, 825-828. doi: 10.1038/s41558-
3251 018-0258-y
3252 Keenan, T. F., and Williams, C. A. (2018). The terrestrial carbon sink. *Annual Review of*
3253 *Environment and Resources*. **43**, 219-243. doi:10.1146/annurev-environ- 102017-030204
3254 Keppler, L., Landschützer, P. (2019). Regional wind variability modulates the Southern Ocean
3255 carbon sink. *Scientific Reports,* **9**, 7384. doi:10.1038/s41598-019-43826-y
3256 Key, R. M., Kozyr, A., Sabine, C. L., Lee, K., Wanninkhof, R., Bullister, J. L., Feely, R. A.,
3257 Millero, F. J., Mordy, C. and Peng, T. H. (2004). A global ocean carbon climatology: Results
3258 from Global Data Analysis Project (GLODAP). *Global Biogeochemical Cycles*, **18**(4),
3259 GB4031. doi:10.1029/2004GB002247
3260 Khatiwala, S., Primeau, F. and Hall, T. (2009). Reconstruction of the history of anthropogenic
3261 CO_2 concentrations in the ocean. *Nature,* **462,** 346–349. doi:10.1038/nature08526
3262 Khatiwala, S., Tanhua, T., Mikaloff Fletcher, S., Gerber, M., Doney, C. S., Graven, H. D.,
3263 Gruber, N., Mckinley, G. A., Murata, A. and Sabine, C. (2013). Global storage of
3264 anthropogenic carbon. *Biogeosciences,* **10**, 2169-2191, 2013. doi: 10.519/bg-10-2169-2013
3265 Kiel, M., O'Dell, C. W., Fisher, B., Eldering, A., Nassar, R., MacDonald, C. G. and Wennberg, P.
3266 O. (2019). How bias correction goes wrong: measurement of XCO_2 affected by erroneous
3267 surface pressure estimates. *Atmospheric Measurement Techniques*, **12**, 2241-2259. doi:
3268 10.5194/amt-12-2241-2019
3269 King, A. W., Andres, R. J., Davis, K. J., Hafer, M., Hayes, D. J., Huntzinger, D. N., de Jong, B.,
3270 Kurz, W. A., McGuire, A. D., Vargas, R., Wei, Y., West, T. O., and Woodall, C. W. (2015).
3271 North America's net terrestrial CO2 exchange with the atmosphere 1990–2009.
3272 *Biogeosciences*, **12**, 399–414. doi: 10.5194/bg-12-399-2015
3273 Knorr, W. (2009). Is the airborne fraction of anthropogenic CO_2 emissions increasing?
3274 *Geophysical Research Letters*, 36, L21710. doi:10.1029/2009GL040613
3275 Kondo, M., Ichii, K., Takagi, H., & Sasakawa, M. (2015). Comparison of the data-driven top-
3276 down and bottom-up global terrestrial CO_2 exchanges: GOSAT CO_2 inversion and empirical
3277 eddy flux upscaling. Journal of Geophysical Research: Biogeosciences, 120(7), 1226–1245.
3278 doi: 10.1002/2014J G002866

Kondo, M., Patra, P. K., Sitch, S., Friedlingstein, P., Poulter, B., Chevallier, F., Ciais, P., Canadell, J. G., Bastos, A., Lauerwald, R., Calle, L., Ichii, K., Anthoni, P., Arneth, A., Haverd, V., Jain, A. K., Kato, E., Kautz, M., Law, R. M., Lienert, S., Lombardozzi, D., Maki, T., Nakamura, T., Peylin, P., Rödenbeck, C., Zhuravlev, R., Saeki, T., Tian, H., Zhu, D and Ziehn, T. (2020). State of the science in reconciling top-down and bottom-up approaches for terrestrial CO_2 budget. *Global Change Biology*, **26**, 1068–1084. doi: 10.1111/gcb.14917

Konings, A. G., Piles, M., Das, N., and Entekhabi, D.(2017). L-band vegetation optical depth and effective scattering albedo estimation from SMAP, *Remote Sensing of Environment*, **198**, 460-470. doi:10.1016/j.rse

Koren, G., van Schaik, E., Araujo, A. C., Boersma, K. F., Gartner, A., Killaars, L., Kooreman, M. L., Kruijt, B., van der Laan-Luijkx, I. T., von Randow, C., Smith, N. E., and Peters, W. (2018). Widespread reduction in sun-induced fluorescence from the Amazon during the 2015/2016 El Nino. *Philosophical Transactions of the Royal Society of London. Series B: Biological Sciences*, **373**, 20170408. doi:10.1098/rstb.2017.0408

Kuze, A., Suto, H., Nakajima, M., and Hamazaki, T. (2009). Thermal and near infrared sensor for carbon observation Fourier-transform spectrometer on the Greenhouse Gases Observing Satellite for greenhouse gases monitoring, *Applied Opt*ics, **48**, 6716–6733, doi:10.1364/AO.48.006716

Kuze, A., Suto, H., Shiomi, K., Kawakami, S., Tanaka, M., Ueda, Y., Deguchi, A., Yoshida, J., Yamamoto, Y., Kataoka, F., Taylor, T. E., and Buijs, H. L. (2016). Update on GOSAT TANSOFTS performance, operations, and data products after more than 6 years in space, *Atmospheric Measurment Technology*, **9**, 2445–2461. doi: 10.5194/amt-9-2445-2016

Kwon, E.Y., Devries, T., Galbraith, E.D., Hwang, J., Kim, G., and Timmermann, A. (2021). Stable carbon isotopes suggest large terrestrial carbon inputs to the global ocean. *Global Biogeochemical Cycles*, **35**, e2020GB006684. doi: 10.1029/2020GB006684

Lacroix, F., T. Ilyina, and J. Hartmann (2020). Oceanic CO_2 outgassing and biological production hotspots induced by pre-industrial river loads of nutrients and carbon in a global modeling approach. *Biogeosciences*, **17**(1), 55–88. doi:10.5194/bg-17-55-2020

Lamarche, C., Santoro, M., Bontemps, S., d'Andrimont, R., Radoux, J., Giustarini, L., Brockmann, C., Wevers, J., Defourny, P. and Arino, O. (2017). Compilation and validation of SAR and optical data products for a complete and global map of inland/ocean water tailored to the climate modeling community. *Remote Sensing*, **9**, 36. doi:10.3390/rs9010036

Landschützer, P., Gruber, N., Bakker, D. C. E., Schuster, U., Nakaoka, S., Payne, M. R., Sasse, T. P. and Zeng, J. (2013). A neural network-based estimate of the seasonal to inter-annual variability of the Atlantic Ocean carbon sink. *Biogeosciences,* **10**, 7793–7815. doi:10.5194/bg-10-7793-2013

Landschützer, P., Gruber, N., Bakker, D. C. E. and Schuster, U. (2014). Recent variability of the global ocean carbon sink. *Global Biogeochemical Cycles*, **28**, 927–949. doi:10.1002/2014GB004853

Landschützer, P., Gruber, N., Haumann, F. A., Rödenbeck, C., Bakker, D. C. E., van Heuven, S., Hoppema, M., Metzl, N., Sweeney, C., Takahashi, T., Tilbrook, B. and Wanninkhof, R. (2015). The reinvigoration of the Southern Ocean carbon sink. *Science,* **349**, 1221–1224. doi:10.1126/science.aab2620

3323 Landschützer, P., Gruber, N., and Bakker, D. C. E. (2017). An updated observation-based global
3324 monthly gridded sea surface pCO_2 and air-sea CO_2 flux product from 1982 through 2015
3325 and its monthly climatology (NCEI Accession 0160558), Version 2.2, NOAA National
3326 Centers for Environmental Information, Dataset [2017-07-11].
3327 Landschützer, P., Laruelle, G. G. , Roobaert, A. and Regnier, P. (2020). A uniform pCO_2
3328 climatology combining open and coastal oceans. *Earth System Science Data*, **12**, 2537–
3329 2553. doi:10.5194/essd-2020-90
3330 Langlais, C. E., Lenton, A., Matear, R., Monselesan, D., Legresy, B., Cougnon, E. and Rintoul,
3331 S. (2017). Stationary Rossby waves dominate subduction of anthropogenic carbon in the
3332 Southern Ocean. *Scientific Reports,* **7**, 17076. doi:10.1038/s41598-017-17292-3
3333 Laufkötter, C., Vogt, M., Gruber, N., Aita-Noguchi, M., Aumont, O., Bopp, L., Buitenhuis, E.,
3334 Doney, S. C., Dunne, J., Hashioka, T., Hauck, J., Hirata, T., John, J., Le Quéré, C., Lima,
3335 I.D., Nakano, H., Seferian, R., Totterdell, I., Vichi, M. and Völker, C. (2015). Drivers and
3336 uncertainties of future global marine primary production in marine ecosystem models.
3337 *Biogeosciences,* **12**, 6955–6984. doi:10.5194/bg-12-6955-2015
3338 Laufkötter, C., Vogt, M., Gruber, N., Aumont, O., Bopp, L., Doney, S.C., Dunne, J.P., Hauck, J.,
3339 John, J.G., Lima, I.D., Seferian, R. and Völker, C. (2016). Projected decreases in future
3340 marine export production: the role of the carbon flux through the upper ocean ecosystem.
3341 *Biogeosciences,* **13**, 4023–4047. doi:10.5194/bg-13-4023-2016
3342 Lauvset, S. K., Lange, N., Tanhua, T., Bittig, H. C., Olsen, A., Kozyr, A., Álvarez, M., Becker,
3343 S., Brown, P. J., Carter, B. R., Cotrim Da Cunha, L., Feely, R. A., van Heuven, S.,
3344 Hoppema, M., Ishii, M., Jeansson, E., Jutterström, S., Jones, S. D., Karlsen, M. K., Lo
3345 Monaco, C., Michaelis, P., Murata, A., Pérez, F. F., Pfeil, B., Schirnick, C., Steinfeldt, R.,
3346 Suzuki, T., Tilbrook, B., Velo, A., Wanninkhof, R., Woosley, R. J., and Key, R. M. (2021).
3347 An updated version of the global interior ocean biogeochemical data product,
3348 GLODAPv2.2021. *Earth System Science Data.* 13, 5565–5589. doi: 10.5194/essd-13-5565-
3349 2021
3350 Lei, R., Feng, S., Danjou, A., Broquet, G., Wu, D., Lin, J. C., O'Dell, C. W., and Lauvaux, T.
3351 (2021). Fossil fuel CO_2 emissions over metropolitan areas from space: A multi-model
3352 analysis of OCO-2 data over Lahore, Pakistan. *Remote Sensing of Environment*, **264**,
3353 112625. doi: 10.1016/j.rse.2021.112625
3354 Lenton, A. and Matear, R. J. (2007). Role of the Southern Annular Mode (SAM) in Southern
3355 Ocean CO_2 uptake. *Global Biogeochemical Cycles,* **21**, GB2016.
3356 doi:10.1029/2006GB002714
3357 Le Quéré, C., Rödenbeck, C., Buitenhuis, E. T., Conway, T. J., Langenfelds, R., Gomez, A.,
3358 Labuschagne, C., Ramonet, M., Nakazawa, T., Metzl, N., Gillett, N. and Heimann, M.
3359 (2007). Saturation of the Southern Ocean CO_2 Sink Due to Recent Climate Change.
3360 *Science,* **316**, 1735–1738. doi:10.1126/science.1136188
3361 Le Quéré, C., Raupach, M. R., Canadell, J. G., Marland, G., Bopp, L., Ciais, P., Conway, T. J.,
3362 Doney, S. C., Feely, R. A., Foster, P., Friedlingstein, P., Gurney, K., Houghton, R. A., House,
3363 J. I., Huntingford, C., Levy, P. E., Lomas, M. R., Majkut, J., Metzl, N., Ometto, J. P., Peters,
3364 G. P., Prentice, I. C., Randerson, J. T., Running, S. W., Sarmiento, J. L., Schuster, U., Sitch,
3365 S., Takahashi, T., Viovy, N., van der Werf, G. R. and Woodward, F. I. (2009). Trends in the
3366 sources and sinks of carbon dioxide. *Nature Geosciences,* **2**, 831–836. doi:10.1038/ngeo689

Le Quéré, C., Takahashi, T., Buitenhuis, E. T., Rödenbeck, C. and Sutherland, S. C. (2010). Impact of climate change and variability on the global oceanic sink of CO_2. *Global Biogeochemical Cycles,* **24**, GB4007. doi:10.1029/2009GB003599

Le Quéré, C., Andres, R. J., Boden, T., Conway, T., Houghton, R. A., House, J. I., Marland, G., Peters, G. P., van der Werf, G. R., Ahlström, A., Andrew, R. M., Bopp, L., Canadell, J. G., Ciais, P., Doney, S. C., Enright, C., Friedlingstein, P., Huntingford, C., Jain, A. K., Jourdain, C., Kato, E., Keeling, R. F., Klein Goldewijk, K., Levis, S., Levy, P., Lomas, M., Poulter, B., Raupach, M. R., Schwinger, J., Sitch, S., Stocker, B. D., Viovy, N., Zaehle and S. and Zeng, N. (2013). The global carbon budget 1959–2011. *Earth System Science Data,* **5**, 165–185. doi:10.5194/essd-5-165-2013

Le Quéré, C., Peters, G. P., Andres, R. J., Andrew, R. M., Boden, T. A., Ciais, P., Friedlingstein, P., Houghton, R. A., Marland, G., Moriarty, R., Sitch, S., Tans, P., Arneth, A., Arvanitis, A., Bakker, D. C. E., Bopp, L., Canadell, J. G., Chini, L. P., Doney, S. C., Harper, A., Harris, I., House, J. I., Jain, A. K., Jones, S. D., Kato, E., Keeling, R. F., Klein Goldewijk, K., Körtzinger, A., Koven, C., Lefèvre, N., Maignan, F., Omar, A., Ono, T., Park, G.-H., Pfeil, B., Poulter, B., Raupach, M.R., Regnier, P., Rödenbeck, C., Saito, S., Schwinger, J., Segschneider, J., Stocker, B.D., Takahashi, T., Tilbrook, B., van Heuven, S., Viovy, N., Wanninkhof, R., Wiltshire, A. and Zaehle, S. (2014). Global carbon budget 2013. *Earth System Science Data,* **6**, 235–263. doi:10.5194/essd-6-235-2014

Le Quéré, C., Moriarty, R., Andrew, R. M., Peters, G. P., Ciais, P., Friedlingstein, P., Jones, S. D., Sitch, S., Tans, P., Arneth, A., Boden, T. A., Bopp, L., Bozec, Y., Canadell, J. G., Chini, L. P., Chevallier, F., Cosca, C. E., Harris, I., Hoppema, M., Houghton, R. A., House, J. I., Jain, A. K., Johannessen, T., Kato, E., Keeling, R. F., Kitidis, V., Klein Goldewijk, K., Koven, C., Landa, C. S., Landschützer, P., Lenton, A., Lima, I. D., Marland, G., Mathis, J. T., Metzl, N., Nojiri, Y., Olsen, A., Ono, T., Peng, S., Peters, W., Pfeil, B., Poulter, B., Raupach, M. R., Regnier, P., Rödenbeck, C., Saito, S., Salisbury, J. E., Schuster, U., Schwinger, J., Séférian, R., Segschneider, J., Steinhoff, T., Stocker, B. D., Sutton, A. J., Takahashi, T., Tilbrook, B., van der Werf, G. R., Viovy, N., Wang, Y.-P., Wanninkhof, R., Wiltshire, A. and Zeng, N. (2015a). Global carbon budget 2014. *Earth System Science Data,* **7**, 47–85. doi:10.5194/essd-7-47-2015

Le Quéré, C., Moriarty, R., Andrew, R. M., Canadell, J. G., Sitch, S., Korsbakken, J. I., Friedlingstein, P., Peters, G. P., Andres, R.J., Boden, T. A., Houghton, R. A., House, J. I., Keeling, R. F., Tans, P., Arneth, A., Bakker, D. C .E., Barbero, L., Bopp, L., Chang, J., Chevallier, F., Chini, L. P., Ciais, P., Fader, M., Feely, R. A., Gkritzalis, T., Harris, I., Hauck, J., Ilyina, T., Jain, A. K., Kato, E., Kitidis, V., Klein Goldewijk, K., Koven, C., Landschützer, P., Lauvset, S. K., Lefèvre, N., Lenton, A., Lima, I. D., Metzl, N., Millero, F., Munro, D. R., Murata, A., Nabel, J. E. M. S., Nakaoka, S., Nojiri, Y., O'Brien, K., Olsen, A., Ono, T., Pérez, F. F., Pfeil, B., Pierrot, D., Poulter, B., Rehder, G., Rödenbeck, C., Saito, S., Schuster, U., Schwinger, J., Séférian, R., Steinhoff, T., Stocker, B. D., Sutton, A. J., Takahashi, T., Tilbrook, B., van der Laan-Luijkx, I. T., van der Werf, G. R., van Heuven, S., Vandemark, D., Viovy, N., Wiltshire, A., Zaehle, S. and Zeng, N. (2015b). Global Carbon Budget 2015. *Earth System Science Data,* **7**, 349–396. doi:10.5194/essd-7-349-2015

Le Quéré, C., Andrew, R. M., Canadell, J. G., Sitch, S., Korsbakken, J. I., Peters, G. P., Manning, A. C., Boden, T. A., Tans, P. P., Houghton, R. A., Keeling, R. F., Alin, S., Andrews, O. D., Anthoni, P., Barbero, L., Bopp, L., Chevallier, F., Chini, L. P., Ciais, P., Currie, K., Delire, C., Doney, S. C., Friedlingstein, P., Gkritzalis, T., Harris, I., Hauck, J., Haverd, V.,

3413 Hoppema, M., Klein Goldewijk, K., Jain, A. K., Kato, E., Körtzinger, A., Landschützer, P.,
3414 Lefèvre, N., Lenton, A., Lienert, S., Lombardozzi, D., Melton, J. R., Metzl, N., Millero, F.,
3415 Monteiro, P. M. S., Munro, D. R., Nabel, J. E. M. S., Nakaoka, S., O'Brien, K., Olsen, A.,
3416 Omar, A. M., Ono, T., Pierrot, D., Poulter, B., Rödenbeck, C., Salisbury, J., Schuster, U.,
3417 Schwinger, J., Séférian, R., Skjelvan, I., Stocker, B. D., Sutton, A. J., Takahashi, T., Tian,
3418 H., Tilbrook, B., van der Laan-Luijkx, I. T., van der Werf, G. R., Viovy, N., Walker, A. P.,
3419 Wiltshire, A. J. and Zaehle, S. (2016). Global Carbon Budget 2016. *Earth System Science*
3420 *Data,* **8**, 605–649. doi:10.5194/essd-8-605-2016

3421 Le Quéré, C., Andrew, R. M., Friedlingstein, P., Sitch, S., Pongratz, J., Manning, A. C.,
3422 Korsbakken, J. I., Peters, G. P., Canadell, J. G., Jackson, R. B., Boden, T. A., Tans, P. P.,
3423 Andrews, O. D., Arora, V. K., Bakker, D. C. E., Barbero, L., Becker, M., Betts, R. A., Bopp,
3424 L., Chevallier, F., Chini, L. P., Ciais, P., Cosca, C .E., Cross, J., Currie, K., Gasser, T.,
3425 Harris, I., Hauck, J., Haverd, V., Houghton, R. A., Hunt, C. W., Hurtt, G., Ilyina, T., Jain, A.
3426 K., Kato, E., Kautz, M., Keeling, R. F., Klein Goldewijk, K., Körtzinger, A., Landschützer,
3427 P., Lefèvre, N., Lenton, A., Lienert, S., Lima, I., Lombardozzi, D., Metzl, N., Millero, F.,
3428 Monteiro, P. M. S., Munro, D. R., Nabel, J. E. M. S., Nakaoka, S., Nojiri, Y., Padin, X. A.,
3429 Peregon, A., Pfeil, B., Pierrot, D., Poulter, B., Rehder, G., Reimer, J., Rödenbeck, C.,
3430 Schwinger, J., Séférian, R., Skjelvan, I., Stocker, B. D., Tian, H., Tilbrook, B., Tubiello, F.
3431 N., van der Laan-Luijkx, I. T., van der Werf, G. R., van Heuven, S., Viovy, N., Vuichard, N.,
3432 Walker, A. P., Watson, A. J., Wiltshire, A. J., Zaehle, S. and Zhu, D. (2018a). Global Carbon
3433 Budget 2017. *Earth System Science Data,* **10**, 405–448. doi:10.5194/essd-10-405-2018

3434 Le Quéré, C., Andrew, R. M., Friedlingstein, P., Sitch, S., Hauck, J., Pongratz, J., Pickers, P. A.,
3435 Korsbakken, J .I., Peters, G. P., Canadell, J. G., Arneth, A., Arora, V. K., Barbero, L.,
3436 Bastos, A., Bopp, L., Chevallier, F., Chini, L.P., Ciais, P., Doney, S. C., Gkritzalis, T., Goll,
3437 D. S., Harris, I., Haverd, V., Hoffman, F. M., Hoppema, M., Houghton, R. A., Hurtt, G.,
3438 Ilyina, T., Jain, A.K., Johannessen, T., Jones, C. D., Kato, E., Keeling, R. F., Goldewijk, K.
3439 K., Landschützer, P., Lefèvre, N., Lienert, S., Liu, Z., Lombardozzi, D., Metzl, N., Munro,
3440 D. R., Nabel, J. E. M. S., Nakaoka, S., Neill, C., Olsen, A., Ono, T., Patra, P., Peregon, A.,
3441 Peters, W., Peylin, P., Pfeil, B., Pierrot, D., Poulter, B., Rehder, G., Resplandy, L.,
3442 Robertson, E., Rocher, M., Rödenbeck, C., Schuster, U., Schwinger, J., Séférian, R.,
3443 Skjelvan, I., Steinhoff, T., Sutton, A., Tans, P. P., Tian, H., Tilbrook, B., Tubiello, F. N., van
3444 der Laan-Luijkx, I. T., van der Werf, G. R., Viovy, N., Walker, A. P., Wiltshire, A. J., Wright,
3445 R., Zaehle, S. and Zheng, B. (2018b). Global Carbon Budget 2018. *Earth System Science*
3446 *Data,* **10**, 2141–2194. doi:10.5194/essd-10-2141-2018

3447 Le Quéré, C., Jackson, R. B., Jones, M. W., Smith, A. J. P., Abernethy, S., Andrew, R. M., De-
3448 Gol, A. J., Willis, D. R., Shan, Y., Canadell, J. G., Friedlingstein, P., Creutzig, F. and Peters,
3449 G. P. (2020). Temporary reduction in daily global CO_2 emissions during the COVID-19
3450 forced confinement. *Nature Climate Change* **10,** 647–653. doi: 10.1038/s41558-020-0797-x

3451 Liang, M. C., Mahata, S., Laskar, A. H., Thiemens, M. H., and Newman, S. (2017). Oxygen
3452 isotope anomaly in tropospheric CO_2 and implications for CO_2 residence time in the
3453 atmosphere and gross primary productivity. *Scientific Reports,* **7**, 13180. doi:
3454 10.1038/s41598-017-12774-w

3455 Liao, E., Resplandy, L., Liu, J. and Bowman, K. W. (2020). Amplification of the Ocean Carbon
3456 Sink During El Niños: Role of Poleward Ekman Transport and Influence on Atmospheric
3457 CO_2. *Global Biogeochemical Cycles* **34**, e2020GB006574. doi: 10.1029/2020GB006574

3458 Liu, J., Bowman, K., Schimel, D., Parazoo, N., Jiang, Z., Lee, M., Bloom, A., Wunch, D.,
3459 Gurney, K., Menemenlis, D., Girerach, M., Crisp, D. and Eldering A. (2017). Contrasting
3460 carbon cycle responses of the tropical continents to the 2015–2016 El Niño. *Science,* **358**,
3461 eaam5690. doi: 10.1126/science.aam5690
3462 Liu, J., Wennberg, P. O., Parazoo, N. C., Yin, Y. and Frankenberg, C. (2020a). Observational
3463 constraints on the response of high-latitude northern forests to warming. *AGU Advances*, **2**,
3464 e2020AV000228. doi:10.1029/2020AV000228
3465 Liu, Y. Y., de Jeu, R. A. M., McCabe, M. F., Evans, J. P., and van Dijk, A. I. J. M. (2011), Global
3466 long-term passive microwave satellite-based retrievals of vegetation optical depth,
3467 *Geophysical Research Letters*, **38**, L18402, doi:10.1029/2011GL048684.
3468 Liu, Y. Y., Van Dijk, A. I., De Jeu, R. A., Canadell, J. G., McCabe, M. F., Evans, J. P., and Wang,
3469 G. (2015). Recent reversal in loss of global terrestrial biomass, *Nature Climate Change*, **5**,
3470 470–474. doi: 10.1038/nclimate2581
3471 Liu, Z., Dreybrodt, W. and Wang, H. (2010). A new direction in effective accounting for the
3472 atmospheric CO_2 budget: Considering the combined action of carbonate dissolution, the
3473 global water cycle and photosynthetic uptake of DIC by aquatic organisms. *Earth Science*
3474 *Reviews,* **99**, 169-172. doi:10.1016/j.earscirev.2010.03.001
3475 Liu, Z., Ciais, P., Deng, Z., Lei, R., Davis, S. J., Feng, S., Zheng, B., Cui, D., Dou, X., Zhu, B.,
3476 Guo, R., Ke, P., Sun, T., Lu, C., He, P., Wang, Y., Yue, X., Wang, Y., Lei, Y., Zhou, H., Cai,
3477 Z., Wu, Y., Guo, R., Han, T., Xue, J., Boucher, O., Boucher, E., Chevallier, F., Tanaka, K.,
3478 Wei, Y., Zhong, H., Kang, C., Zhang, N., Chen, B., Xi, F., Liu, M., Bréon, F. M., Lu, Y.,
3479 Zhang, Q., Guan, D., Gong, P., Kammen, D. M., He, K., and Schellnhuber, H. J. (2020b).
3480 Near-real-time monitoring of global CO_2 emissions reveals the effects of the COVID-19
3481 pandemic, *Nature Communications*, **11**, 1–12. doi: 10.1038/s41467-020-18922-7
3482 Long, M. C., Lindsay, K., Peacock, S., Moore, J. K., and Doney, S. C. (2013). Twentieth-century
3483 oceanic carbon uptake and storage in CESM1(BGC). *Journal of Climate*, **26**, 6775–6800.
3484 doi:10.1175/JCLI-D-12-00184.1
3485 Lovenduski, N. S., Gruber, N., Doney, S. C. and Lima, I. D. (2007). Enhanced CO_2 outgassing in
3486 the Southern Ocean from a positive phase of the Southern Annular Mode. *Global*
3487 *Biogeochemical Cycles,* **21**, GB2026. doi:10.1029/2006GB002900
3488 Lovenduski, N. S., Gruber, N. and Doney, S.C. (2008). Toward a mechanistic understanding of
3489 the decadal trends in the Southern Ocean carbon sink: Southern Ocean CO_2 flux trends.
3490 *Global Biogeochemical Cycles,* **22**(3), GB3016. doi:10.1029/2007GB003139
3491 Lucht, W., Prentice, C., Myneni, R. B., Sitch, S., Friedlingstein, P., Cramer, W., Bousquet, P.,
3492 Buermann, W. and Smith, B. (2002). Climatic control of the high-latitude vegetation
3493 greening trend and Pinatubo effect. *Science*, **296**, 1687–1689. doi:10.1126/science.1071828
3494 Ma, X., Huete, A., Cleverly, J., Eamus, D., Chevallier, F., Joiner, J., Poulter, B., Zhang, Y.,
3495 Guanter, L., Meyer, W., Xie, Z. and Ponce-Campos, G. (2016). Drought rapidly diminishes
3496 the large net CO_2 uptake in 2011 over semi-arid Australia. *Scientific Reports,* ***6***, 37747
3497 (2016). doi: 10.1038/srep37747
3498 Macbean, N., Maignan, F., Bacour, C., Lewis, P., Peylin, P., Guanter, L., Köhler, P., Gomez-
3499 Dans, J., and Disney, M. (2018). Strong constraint on modelled global carbon uptake using
3500 solar-induced chlorophyll fluorescence data. *Scientific Reports*, **8**, 1973. doi:
3501 10.1038/s41598-018-20024-w

MacDougall, A. H., Frölicher, T. L., Jones, C. D., Rogelj, J., Matthews, H. D., Zickfeld, K., Arora, V. K., Barrett, N. J., Brovkin, V., Burger, F. A., Eby, M., Eliseev, A. V., Hajima, T., Holden, P. B., Jeltsch-Thömmes, A., Koven, C., Mengis, N., Menviel, L., Michou, M., Mokhov, I. I., Oka, A., Schwinger, J., Séférian, R., Shaffer, G., Sokolov, A., Tachiiri, K., Tjiputra , J., Wiltshire, A. and Ziehn, T. (2020). Is there warming in the pipeline? A multi-model analysis of the zero emissions commitment from CO_2. *Biogeosciences,* **17**, 2987–3016. doi:10.5194/bg-17-2987-2020

Maier-Reimer, E. (1993). Geochemical cycles in an ocean general circulation model. Preindustrial tracer distributions. *Global Biogeochemical Cycles,* **7**, 645–677, 1993. doi:10.1029/93GB01355

Maier-Reimer, E., Mikolajewicz, U. and Winguth, A. (1996). Future ocean uptake of CO_2: interaction between ocean circulation and biology. *Climate Dynamics*, 12, 711-721. doi: 10.1007/s003820050138

Maksyutov, S., Takagi, H., Valsala, V. K., Saito, M., Oda, T., Saeki, T., Belikov, D. A., Saito, R., Ito, A., Yoshida, Y., Morino, I., Uchino, O., Andres, R. J. and Yokota, T. (2013). Regional CO_2 flux estimates for 2009–2010 based on GOSAT and ground-based CO_2 observations. *Atmospheric Chemistry and Physics*, **13**, 2351-9373. doi: 1 0.5194/acp-13-9351-2013

Marsay, C.M., Sanders, R. J., Henson, S. A., Pabortsava, K., Achterberg, E. P. and Lampitt, R. S. (2015). Attenuation of sinking particulate organic carbon flux through the mesopelagic ocean. *Proceedings of the National Academy of Sciences,* **112**, 1089. doi:10.1073/pnas.1415311112

Marchant, R., Mumbi, C., Behera, S., and Yamagata, T. (2006). The Indian Ocean dipole – the unsung driver of climatic variability in East Africa. *African Journal_of Ecology*, **45**, 4-16. doi: 10.1111/j.1365-2028.2006.00707.x

Marrs, J. K., Reblin, J. S., Logan, B. A., Allen, D. W., Reinmann, A. B., Bombard, D. M., Tabachnik, D. and Hutyra, L. R. (2020). Solar-induced fluorescence does not track photosynthetic carbon assimilation following induced stomatal closure. *Geophysical Research Letters*, **47**, e2020GL087956. doi: 10.1029/2020GL087956

Marshall, G. J., Trends in the Southern Annular Mode from Observations and Reanalyses. *Journal of Climate*, **16**, 4134-4143. doi: 10.1175/1520-0442(2003)016<4134:TITSAM>2.0.CO;2

Mau, A. C., Reed, S. C., Wood, T. E. and Cavaleri, M. A. (2018). Temperate and tropical forest canopies are already functioning beyond their thermal thresholds for photosynthesis. *Forests*, **9**, 47. doi:10.3390/f9010047

McGuire, A. D. , S. Sitch, J. S. Clein, R. Dargaville, G. Esser, J. Foley, M. Heimann, F. Joos, J. Kaplan, D. W. Kicklighter, R. A. Meier, J. M. Melillo, B. Moore, I. C. Prentice, N. Ramankutty, T. Reichenau, A. Schloss, H. Tian, L. J. Williams, and U. Wittenberg. (2001). Carbon balance of the terrestrial biosphere in the twentieth century: analyses of CO_2, climate and land use effects with four process-based ecosystem models. *Global Biogeochemical Cycles* **15**, 183-206. doi: 10.1029/2000GB001298

McKinley, G., Follows, M. & Marshall, J. (2004). Mechanisms of air-sea CO_2 flux variability in the equatorial Pacific and the North Atlantic. *Global Biogeochemical Cycles*, **18**, GB2011. doi:10.1029/2003GB002179

McKinley, G., Follows, M., and Marshall, J. (2004). Mechanisms of air-sea CO_2 flux variability in the equatorial Pacific and the North Atlantic. *Global Biogeochemical Cycles*, **18**, GB2011. doi:10.1029/2003GB002179

McKinley, G. A., Fay, A. R., Takahashi, T. and Metzl, N. (2011). Convergence of atmospheric and North Atlantic carbon dioxide trends on multidecadal timescales. *Nature Geosci,* **4**, 606–610. doi:10.1038/ngeo1193

McKinley, G. A., Pilcher, D. J., Fay, A. R., Lindsay, K., Long, M. C. and Lovenduski, N. S. (2016). Timescales for detection of trends in the ocean carbon sink. *Nature*, **530**, 469–472. doi:10.1038/nature16958

McKinley, G. A., Fay, A. R., Lovenduski ,N. S. and Pilcher, D. J. (2017). Natural variability and anthropogenic trends in the ocean carbon sink. *Annual Review of Marine Science*, **9**, 125–150, doi:10.1146/annurev-marine-010816-060529

McKinley, G. A., Fay, A. R., Eddebbar, Y. A., Gloege L. and Lovenduski, N. S. (2020). External forcing explains recent decadal variability of the ocean carbon sink. *AGU Advances*, **1**, 1, e2019AV000149. doi:10.1029/2019AV000149

McPhaden, M. J., Zebiak, S. E., and Glantz, M. H. (2006). ENSO as an Integrating Concept in Earth Science, *Science*, **314**, 1740–1745. doi: 10.1126/science.1132588

Medlyn, B., Zaehle, S., De Kauwe, M., Walker, A. P., Dietze, M. C., Hanson, P. J., Hickler, T., Jain, A. K., Luo, Y., Parton, W., Prentice, I., C., Thornton, P. E., Wang, S., Wang, Y.-P., Weng, E., Iversen, C. M., McCarthy, H. R., Warren, J. M., Oren, R., and Norby, R. J. (2015). Using ecosystem experiments to improve vegetation models. *Nature Climate Change,* **5**, 528–534. doi: 10.1038/nclimate2621

Mercado, L.M., Medlyn, B. E., Huntingford, C., Oliver, R. J., Clark, D. B., Sitch, S., Zelazowski, P., Kattge, J., Harper, A. B. and Cox, P. M. (2018). Large sensitivity in land carbon storage due to geographical and temporal variation in the thermal response of photosynthetic capacity, *New Phytologist*, **218**, 1462-1477, doi: 10.1111/nph.15100.

Meroni, M., Rossini, M., Guanter, L., Alonso L. , Rascher, U., Colombo, R. , and Moreno, J. (2009). Remote sensing of solar-induced chlorophyll fluorescence: Review of methods and applications, *Remote Sensing of Environment*, **113**,2037-2051, ISSN 0034-4257, doi: 10.1016/j.rse.2009.05.003

Mikaloff Fletcher, S. E., Gruber, N., Jabobson, A. R., Doney, S., C., Sutkiewicz, S., Gerber, M., Follows, M., Joos, F., Lindsay, K., Menemenlis, D., Mouchet, A., Müller, S., A. and Sarmiento, J. L. (2006). Inverse estimates of anthropogenic CO_2 uptake, transport, and storage by the ocean, *Global Biogeochemical Cycles*, **20**, GB2002. doi:10.1029/2005GB002530

Miller, J. B., Lehman, S. J., Montzka, S. A., Sweeney, C., Miller, B. R., Karion, A., Wolak, C., Dlugokencky, E. J., Southon, J., Turnbull, J. C. and Tans, P. P. (2012). Linking emissions of fossil fuel CO_2 and other anthropogenic trace gases using atmospheric $^{14}CO_2$. *Journal of Geophysical Research: Atmospheres,* **117**, D08302. doi:10.1029/2011JD017048

Miller, J. B., Lehman, S. J., Verhulst, K. R., Miler, C., E., Duren, R. M., Yadav, V., Newman, S. and Sloop, C. D. (2020). Large and seasonally varying biospheric CO_2 fluxes in the Los Angeles megacity revealed by atmospheric radiocarbon. *Proceedings of the National Academy of Sciences*, **117**, 26681-26687. doi:10.1073/pnas.2005253117

Mohammed, G. H., Colombo, R., Middleton, E. M., Rascherd, U., van der Tol, C., Nedbal, L., Goulasf, Y., Pérez-Priego, O., Damm, A., Meroni, M., Joiner, J., Cogliati, S., Verhoef, W.,

3590 Malenovský, Z., Gastellu-Etchegorry, J.-P., Miller, J. R., Guanter, L., Morenoo, J., Moya,
3591 I., Berry, J. A., Frankenberg, C., Zarco-Tejadaj, P. J. (2019). Remote sensing of solar-
3592 induced chlorophyll fluorescence (SIF) in vegetation: 50 years of progress, *Remote Sensing*
3593 *of Environment*, **31** 111177. doi:10.1016/j.rse.2019.04.030
3594 Molod, A., Takacs, L., Suarez, M., & Bacmeister, J. (2015). Development of the GEOS-5
3595 atmospheric general circulation model: Evolution from MERRA to MERRA2. *Geoscientific*
3596 *Model Development*, **8**, 1339–1356. doi: 10.5194/gmd-8-1339-015.
3597 Mongwe, N. P., Vichi, M. and Monteiro, P. M. S. (2018). The seasonal cycle of pCO_2 and CO_2
3598 fluxes in the Southern Ocean: diagnosing anomalies in CMIP5 Earth system models.
3599 *Biogeosciences*, **15**, 2851–2872. doi:10.5194/bg-15-2851-2018
3600 Monteil, G., Broquet, G., Scholze, M., Lang, M., Karstens, U., Gerbig, C., Koch, F.-T., Smith, N.
3601 E., Thompson, R. L., Luijkx, I. T., White, E., Meesters, A., Ciais, P., Ganesan, A. L.,
3602 Manning, A., Mischurow, M., Peters, W., Peylin, P., Tarniewicz, J., Rigby, M., Rödenbeck,
3603 C., Vermeulen, A., and Walton, E. M. (2020). The regional European atmospheric transport
3604 inversion comparison, EUROCOM: first results on European-wide terrestrial carbon fluxes
3605 for the period 2006–2015, *Atmospheric Chemistry and Physics*, **20**, 12063–12091. doi:
3606 10.5194/acp-20-12063-2020
3607 Moore, J. K., Fu, W., Primeau, F., Britten, G. L., Lindsay, K., Long, M., Doney, S. C.,
3608 Mahowald, N., Hoffman, F. and Randerson, J. T. (2018). Sustained climate warming drives
3609 declining marine biological productivity. *Science,* **359**, 1139–1143.
3610 doi:10.1126/science.aao6379
3611 Müller, A., Tanimoto, H., Sugita, T., Machida, T., Nakaoka, S., Patra, P. K., Laughner, J., and
3612 Crisp, D. (2021).New approach to evaluate satellite-derived XCO_2 over oceans by
3613 integrating ship and aircraft observations, *Atmospheric Chemistry and Physics*, **21**, 8255–
3614 8271. doi: 10.5194/acp-21-8255-2021.
3615 Myneni, R., Knyazikhin, Y., Park, T. (2015). MOD15A2H MODIS Leaf Area Index/FPAR 8-Day
3616 L4 Global 500m SIN Grid V006. NASA EOSDIS Land Processes DAAC.
3617 http://doi.org/10.5067/MODIS/MOD15A2H.006 (Last referenced 5 Dec 2021)
3618 Nabuurs, G. J., Lindner, M., Verkerk, P., Gunia, K., Deda, Paola, Michalak,, R. and Grassi, G.
3619 (2013). First signs of carbon sink saturation in European forest biomass. *Nature Climate*
3620 *Change,* **3**, 792–796. doi: 10.1038/nclimate1853
3621 Nassar, R., Hill, T. G., McLinden, C. A., Wunch, D., Jones, D. B.A. and Crisp D. (2017).
3622 Quantifying CO_2 emissions from individual power plants from space. *Geophysical Research*
3623 *Letters*, **44**, 10045-10053. doi:10.1002/2017GL074702
3624 Nassar, R., Mastrogiacomo, J.-P., Bateman-Hemphill, W., McCracken, C., MacDonald, C. G.,
3625 Hill, T., O'Dell, C. W., Kiel, M., Crisp, D. (2021): Advances in quantifying power plant
3626 CO_2 emissions with OCO-2. *Remote Sensing of Environment,* **264**, 112579. doi:
3627 10.1016/j.rse.2021.112579
3628 Nemani, R. R., Keeling, C. D., Hashimoto, H., Jolly, W. M., Piper, S. C., Tucker, C. J., Myneni,
3629 R. B., and Running, S. W. (2003). Climate-Driven Increases in Global Terrestrial Net
3630 Primary Production from 1982 to 1999. *Science*, **300**, 1560-1563. doi:
3631 10.1126/science.1082750
3632 Obermeier, W. A., Nabel, J. E. M. S., Loughran, T., Hartung, K., Bastos, A., Havermann, F.,
3633 Anthoni, P., Arneth, A., Goll, D. S., Lienert, S., Lombardozzi, D., Luyssaert, S., McGuire, P.
3634 C., Melton, J. R., Poulter, B., Sitch, S., Sullivan, M. O., Tian, H., Walker, A. P., Wiltshire, A.

J., Zaehle, S., and Pongratz, J. (2021). Modelled land use and land cover change emissions – a spatio-temporal comparison of different approaches, *Earth System Dynamics*, **12**, 635–670, doi: 10.5194/esd-12-635-2021

Oda, T., Maksyutov, S. and Andres, S. J. (2018). The Open-source Data Inventory for Anthropogenic Carbon dioxide (CO_2), version 2016 (ODIAC2016): A global, monthly fossil-fuel CO_2 gridded emission data product for tracer transport simulations and surface flux inversions. *Earth System Science Data,* **10**, 87-107. doi:10.5194/essd-10-87-2018

O'Dell, C. W., Eldering, A., Wennberg, P. O., Crisp, D., Gunson, M. R., Fisher, B., Frankenberg, C., Kiel, M., Lindqvist, H., Mandrake, L., Merrelli, A., Natraj, V., Nelson, R. R., Osterman, G. B., Payne, V. H., Taylor, T. E., Wunch, D., Drouin, B. J., Oyafuso, F., Chang, A., McDuffie, J., Smyth, M., Baker, D. F., Basu, S., Chevallier, F., Crowell, S. M. R., Feng, L., Palmer, P. I., Dubey, M., García, O. E., Griffith, D. W. T., Hase, F., Iraci, L. T., Kivi, R., Morino, I., Notholt, J., Ohyama, H., Petri, C., Roehl, C. M., Sha, M. K., Strong, K., Sussmann, R., Te, Y., Uchino, O. and Velazco, V. A. (2018). Improved retrievals of carbon dioxide from Orbiting Carbon Observatory-2 with the version 8 ACOS algorithm, *Atmospheric Measurement Techniques,* **11**: 6539–6576. doi:10.5194/amt-11-6539-2018

Olsen, A., Key, R. M., van Heuven, S., Lauvset, S. K., Velo, A., Lin, X. H., Schirnick, C., Kozyr, A., Tanhua, T.,Hoppema, M., Jutterstrom, S., Steinfeldt, R., Jeansson, E., Ishii, M., Perez, F. F., and Suzuki, T. (2016). The Global Ocean Data Analysis Project version 2 (GLODAPv2) - an internally consistent data product for the world ocean, *Earth System Science Data*, **8**, 297-323. doi: 10.5194/essd-8-297-2016

Olsen, A. , Lange, N. , Key, R. M. , Tanhua, T. , Bittig, H. C. , Kozyr, A. , Álvarez, M. , Azetsu-Scott, K. , Becker, S. , Brown, P. J. , Carter, B. R. , Cotrim da Cunha, L. , Feely, R. A. , van Heuven, S. , Hoppema, M. , Ishii, M. , Jeansson, E. , Jutterström, S. , Landa, C. S. , Lauvset, S. K. , Michaelis, P. , Murata, A. , Pérez, F. F. , Pfeil, B. , Schirnick, C. , Steinfeldt, R. , Suzuki, T. , Tilbrook, B. , Velo, A. , Wanninkhof, R. and Woosley, R. J. (2020): An updated version of the global interior ocean biogeochemical data product, GLODAPv2.2020 , *Earth System Science Data*, **12**, 3653-3678 . doi: 10.5194/essd-12-3653-2020

Pacala, S. W., Hurtt, G. C., Baker, D., Peylin, P., Houghton, R. A., Birdsey, R. A., Heath, L., Sundquist, E. T., Stallard, R. F., Ciais, P., Moorcroft, P., Caspersen, J. P., Shevliakova, E., Moore, B., Kohlmaier, G., Holland, E., Gloor, M., Harmon, M. E., Fan, S.-M., Sarmiento, J. L., Goodale, C. L., Schimel, D. and Field, C. B. (2001), Consistent land- and atmosphere-based U.S. carbon sink estimates, *Science*, **292**, 2316– 2320, doi: 10.1126/science.1057320

Page. S. E., Siegert, F., Rieley, L. O., Boehm, H.-D. V., Jaya, A., and Limin, S. (2002). The amount of carbon released from peat and forest fires in Indonesia during 1997. *Nature,* **420**, 61–65. doi: 10.1038/nature01131

Palmer, P. I., Feng, L., Baker, D., Chevallier, F., Bösch, H. and Somkuti, P. (2019). Net carbon emissions from African biosphere dominate pan-tropical atmospheric CO_2 signal, *Nature Communications*, **10**, 3344. doi:10.1038/s41467-019-11097-w

Pan, Y., Birdsey, R. A., Fang, J., Houghton, R., Kauppi, P. E., Kurz, W. A., Phillips, O. L., Shvidenko, A., Lewis, S. L., Canadell, J. G., Ciais, P., Jackson, R. B., Pacala, S. W., McGuire, A. S., Piao, S., Rautiainen, A., Sitch, S. and Hayes, D. (2011). A large and persistent carbon sink in the world's forests. *Science*, **333**, 988-993. doi:10.1126/science.1201609

Panassa, E., Santana-Casiano, J. M., González-Dávila, M., Hoppema, M., van Heuven, S. M. A. C., Völker, C., Wolf-Gladrow, D. and Hauck, J. (2018). Variability of nutrients and carbon dioxide in the Antarctic Intermediate Water between 1990 and 2014. *Ocean Dynamics,* **68**, 295–308. doi:10.1007/s10236-018-1131-2

Parazoo, N. C., Magney, T., Norton, A., Raczka, B., Bacour, C., Maignan, F., Baker, I., Zhang, Y., Qiu, B., Shi, M., MacBean, N., Bowling, D. R., Burns, S., Blanken, P. D., Stutz, J., Grossmann, K. and Frankenberg, C. (2020). Wide discrepancies in the magnitude and direction of modeled solar-induced chlorophyll fluorescence in response to light conditions. *Biogeosciences*, **17**, 3733–3755. doi:10.5194/bg-17-3733-2020

Pardo, P. C., Tilbrook, B., Langlais, C., Trull, T.W. and Rintoul, S. R. (2017). Carbon uptake and biogeochemical change in the Southern Ocean, south of Tasmania. *Biogeosciences,* **14**, 5217–5237. doi:10.5194/bg-14-5217-2017

Pearson, T. R. H., Brown, S., Murray, L. and Sidman, G. (2017). Greenhouse gas emissions from tropical forest degradation: an underestimated source. *Carbon Balance and Management*, **12**, 3. doi:10.1186/s13021-017-0072-2

Peiro, H., Crowell, S., Schuh, A., Baker, D. F., O'Dell, C., Jacobson, A. R., Chevallier, F., Liu, J., Eldering, A., Crisp, D., Deng, F., Weir, B., Basu, S., Johnson, M. S., Philip, S., and Baker, I.: Four years of global carbon cycle observed from OCO-2 version 9 and in situ data, and comparison to OCO-2 v7, *Atmospheric Chemistry and Physics Discussions* [preprint], doi: 10.5194/acp-2021-373, accepted, 2021 12 04.

Peng, B., Guan, K. Y., Zhou, W. , Jiang, C. Y., Frankenberg, C., Sun, Y., He, L. Y. and Kohler, P. (2020). Assessing the benefit of satellite-based Solar-Induced Chlorophyll Fluorescence in crop yield prediction. *International Journal of Applied Earth Observation and Geoinformation*, **90**, 102126. doi:10.1016/j.jag.2020.102126

Peñuelas, J., Ciais, P., Canadell, J. G., Janssens, I. A., Fernández-Martínez, M., Carnicer, J., Obersteiner, M., Piao, S., Vautard, R, Sardans, J. (2017). Shifting from a fertilization-dominated to a warming-dominated period. *Nat Ecol Evol.* **1**, 1438-1445. doi: 10.1038/s41559-017-0274-8.

Peters, W., Miller, J. B., Whitaker, J., Denning, A. S., Hirsch, A., Krol, M. C., Zupanski, D., Bruhwiler, L., and Tan, P. P. (2005). An ensemble data assimilation system to estimate CO_2 surface fluxes from atmospheric trace gas observations, *Journal of Geophysical Research*, **110**, D24304, doi:10.1029/2005JD006157

Peters, W., Bastos, A., Ciais, P., and Vermeulen, A.(2020). A historical, geographical and ecological perspective on the 2018 European summer drought. *Philosophical Transactions of the Royal Society B: Biological Sciences*, **375**, 20190505, doi: 10.1098/rstb.2019.0505

Petrescu, A. M. R., Peters, G. P., Janssens-Maenhout, G., Ciais, P., Tubiello, F. N., Grassi, G., Nabuurs, G.-J., Leip, A., Carmona-Garcia, G., Winiwarter, W., Höglund-Isaksson, L., Günther, D., Solazzo, E., Kiesow, A., Bastos, A., Pongratz, J., Nabel, J. E. M. S., Conchedda, G., Pilli, R., Andrew, R. M., Schelhaas, M.-J. and Dolman, A. J. (2020). European anthropogenic AFOLU greenhouse gas emissions: a review and benchmark data. *Earth System Science Data*, **12**, 961–1001, doi:10.5194/essd-12-961-2020

Petrescu, A. M. R., McGrath, M. J., Andrew, R. M., Peylin, P., Peters, G. P., Ciais, P., Broquet, G., Tubiello, F. N., Gerbig, C., Pongratz, J., Janssens-Maenhout, G., Grassi, G., Nabuurs, G.-J., Regnier, P., Lauerwald, R., Kuhnert, M., Balkovič, J., Schelhaas, M.-J., Denier van der Gon, H. A. C., Solazzo, E., Qiu, C., Pilli, R., Konovalov, I. B., Houghton, R. A.,

Günther, D., Perugini, L., Crippa, M., Ganzenmüller, R., Luijkx, I. T., Smith, P., Munassar, S., Thompson, R. L., Conchedda, G., Monteil, G., Scholze, M., Karstens, U., Brockmann, P., and Dolman, A. J. (2021). The consolidated European synthesis of CO_2 emissions and removals for the European Union and United Kingdom: 1990–2018, *Earth System Science Data*, **13**, 2363–2406, https://doi.org/10.5194/essd-13-2363-2021

Peylin, P., Bousquet, P., Le Quéré, C., Sitch, S., Friedlingstein, P., McKinley, G., Gruber, N., Rayner, P., and Ciais, P. (2005). Multiple constraints on regional CO_2 flux variations over land and oceans, *Global Biogeochemical Cycles*, **19**, GB1011. doi: 10.1029/2003GB002214

Peylin, P., Law, R. M., Gurney, K. R., Chevallier, F. Jacobson, A. R., Maki, T., Niwa, Y., Patra, P. K., Peters, W., Rayner, P. J., Rödenbeck, C., van der Laan-Luijkx, I. T., and Zhang, X. (2013). Global atmospheric carbon budget: results from an ensemble of atmospheric CO_2 inversions. *Biogeosciences*, **10**, 6699-6720. doi: 10.5194/bg-10-6699-2013

Pfeil, B., Olsen, A., Bakker, D. C. E., Hankin, S., Koyuk, H., Kozyr, A., Malczyk, J., Manke, A., Metzl, N., Sabine, C. L., Akl, J., Alin, S. R., Bates, N., Bellerby, R. G. J., Borges, A., Boutin, J., Brown, P. J., Cai, W.-J., Chavez, F. P., Chen, A., Cosca, C., Fassbender, A. J., Feely, R. A., González-Dávila, M., Goyet, C., Hales, B., Hardman-Mountford, N., Heinze, C., Hood, M., Hoppema, M., Hunt, C. W., Hydes, D., Ishii, M., Johannessen, T., Jones, S. D., Key, R. M., Körtzinger, A., Landschützer, P., Lauvset, S. K., Lefèvre, N., Lenton, A., Lourantou, A., Merlivat, L., Midorikawa, T., Mintrop, L., Miyazaki, C., Murata, A., Nakadate, A., Nakano, Y., Nakaoka, S., Nojiri, Y., Omar, A. M., Padin, X. A., Park, G.-H., Paterson, K., Perez, F. F., Pierrot, D., Poisson, A., Ríos, A. F., Santana-Casiano, J. M., Salisbury, J., Sarma, V. V. S. S., Schlitzer, R., Schneider, B., Schuster, U., Sieger, R., Skjelvan, I., Steinhoff, T., Suzuki, T., Takahashi, T., Tedesco, K., Telszewski, M., Thomas, H., Tilbrook, B., Tjiputra, J., Vandemark, D., Veness, T., Wanninkhof, R., Watson, A. J., Weiss, R., Wong, C. S. and Yoshikawa-Inoue, H. (2013). A uniform, quality controlled Surface Ocean CO_2 Atlas (SOCAT). *Earth System Science Data,* **5**, 125–143. doi:10.5194/essd-5-125-2013

Piao, S., Fang, J., Ciais, P., Peylin, P., Huang, Y., Sitch, S. and Wang T. (2009). The carbon balance of terrestrial ecosystems in China. *Nature,* **458**, 1009–1013. doi: 10.1038/nature07944

Piao, S., Sitch, S., Ciais, P., Friedlingstein, P., Peylin, P., Wang, X., Ahlström, A., Anav, A., Canadell, J. G., Cong, N., Huntingford, C., Jung, M., Levis, S., Levy, P. E., Li, J., Lomas, M. R., Lu, M., Luo, Y., Ma, Y., Myneni, R. B., Poulter, B., Sun, Z., Wang, T., Viovy, N., Zaehle, S. and Zeng, N. (2013). Evaluation of terrestrial carbon cycle models for their response to climate variability and to CO_2 trends. *Global Change Biology*, **19**, 2117–2132. doi: 10.1111/gcb.12187

Piao, S., Liu, Z., Wang, Y., Ciais, P., Yao, Y., Peng, S., Chevallier, F., Friedlingstein, P., Janssens, I. A., Peñuelas, J., and Sitch, S. (2017). On the causes of trends in the seasonal amplitude of atmospheric CO_2. *Global Change Biology*, **24**, 608–616. doi: 10.1111/gcb.13909

Piao, S., Wang, X., Wang, K., Li, X., Bastos, A., Canadell, J. G., Ciais, P., Friedlingstein, P., and Sitch, S. (2020a). Interannual Variation of Terrestrial Carbon Cycle: Issues and Perspectives, *Global Change Biology*, **26**, 300–318. doi: 10.1111/gcb.14884

Piao, S., Wang, X., Park, T., Chen, C., Lian, X., He, Y. Bjerke, J. W., Chen, A., Ciais, P., Tommervik, H., Nemani, R. R. and Myneni, R. B. (2020b). Characteristics, drivers and

feedbacks of global greening. *Nature Reviews Earth & Environment.,* **1**, 14–27. doi:10.1038/s43017-019-0001-x

Pongratz, J., Reick, C. H., Houghton, R. A. and House, J. I. (2014). Terminology as a key uncertainty in net land use and land cover change carbon flux estimates. *Earth System Dynamics*, **5**, 177–195, 2014. doi: 10.5194/esd-5-177-2014

Poulter, B., Frank, D., Ciais, P., Myneni, R. B., Andela, N., Bi, J., Broquet, G., Canadell, J. G., Chevallier, F., Liu, Y. Y., Running, S. W., Sitch, S. and van der Werf, G. R. (2014). Contribution of semi-arid ecosystems to interannual variability of the global carbon cycle. Nature, 509, 600-603. doi:10.1038/nature13376

Qin, Y. W. Xiao, X., Wigneron, J.-P., Ciais, P., Brandt, M., Fan, L., Li, X., Crowell, S., Wu, X., Doughty, R., Zhang, Y., Liu, F., Sitch, S., and Moore III, B. (2021). Carbon loss from forest degradation exceeds that from deforestation in the Brazilian Amazon, *Nature Climate Change*, **11**, 442-448. doi: 10.1038/s41558-021-01026-5, 2021.

Qiu, B., Ge, J., Guo, W. D., Pittman, A. J. and Mu, M. Y. (2020). Responses of Australian dryland vegetation to the 2019 heat wave at a sub daily scale. *Geophysical Research Letters,* **47**, e2019GL086569. doi:10.1029/2019GL086569

Quegan, S., Toan, L. T., Chave, J., Dall, J., Exbrayat, J. F., Minh, D. H. T., Lomas, M., D'Alessandro, M. M., Paillou, P., Papathanassiou, K., Rocca, F., Saatchi, S., Scipal, K., Shugart, H., Smallman, T. L., Soja, M. J., Tebaldini, S., Ulander, L., Villard, L. and Williams, M. (2019). The European Space Agency BIOMASS mission: measuring forest above-ground biomass from space. *Remote Sensing of the Environment,* **227**, 44–60. doi:10.1016/j.rse.2019.03.032

Quilcaille, Y., Gasser, T., Ciais, P., Lecocq, F., Janssens-Maenhout, G., and Mohr, S. (2018). Uncertainty in projected climate change arising from uncertain fossil-fuel emission factors. *Environmental Research Letters*, **13**, 044017. doi: 10.1088/1748-9326/aab304#references

Rabin, S. S., Melton, J. R., Lasslop, G., Bachelet, D., Forrest, M., Hantson, S., Kaplan, J. O., Li, F., Mangeon, S., Ward, D. S., Yue, C., Arora, V. K., Hickler, T., Kloster, S., Knorr, W., Nieradzik, L., Spessa, A., Folberth, G. A., Sheehan, T., Voulgarakis, A., Kelley, D. I., Prentice, I. C., Sitch, S., Harrison, S., and Arneth, A. (2017). The Fire Modeling Intercomparison Project (FireMIP), phase 1: experimental and analytical protocols with detailed model descriptions, *Geoscientific Model Development*, **10**, 1175–1197. doi: 10.5194/gmd-10-1175-2017.

Ramankutty N., Gibbs, H. K., Achard, F., Defries, R., Foley, J. A. and Houghton, R. A. (2007). Challenges to estimating carbon emissions from tropical deforestation. *Global Change Biology,* **13**, 51–66. doi: 10.1111/j.1365-2486.2006.01272.x

Randerson, J. T., Hoffman, F. M., Thornton, P. E., Mahowald, N. M., Lindsay, K., Lee, Y. H., Nevison, C. D. Doney, S. C., Bonan, G., Stöckli, R., Covey, C., Running, S. W. and Fung, I. Y. (2009). Systematic assessment of terrestrial biogeochemistry in coupled climate–carbon models. *Global Change Biology*, **15**, 2462-2484. doi: 10.1111/j.1365-2486.2009.01912.x

Randerson, J. T., Lindsay, K., Munoz, E., Fu, W., Moore, J. K., Hoffman, F. M., Mahowald, N. M. and Doney, S. C. (2015). Multi-century changes in ocean and land contributions to the climate-carbon feedback. *Global Biogeochemical Cycles*, **29**, 744-759. doi:10.1002/2014GB005079

3811 Raupach, M. R., Canadell, J. G. and Le Quéré, C. (2008). Anthropogenic and biophysical
3812 contributions to increasing atmospheric CO_2 growth rate and airborne fraction.
3813 *Biogeosciences*, **5**, 1601–1613. doi:10.5194/bg-5-1601-2008
3814 Raupach, M. R., Gloor, M., Sarmiento, J. L., Canadell, J. G., Frölicher, T. L., Gasser, T.,
3815 Houghton, R. A., Le Quéré, C. and Trudinger, C. M. (2014). The declining uptake rate of
3816 atmospheric CO_2 by land and ocean sinks. *Biogeosciences*, **11**, 3453–3475.
3817 doi:10.1007/s10584-009-9596-0
3818 Regnier, P., Friedlingstein, P., Ciais, P., Mackenzie, F. T., Gruber, N., Janssens, I. A., Laruelle, G.
3819 G., Lauerwald, R., Luyssaert, S., Andersson, A. J., Arndt, S., Arnosti, C., Borges, A. V.,
3820 Dale, A. W., Gallego-Sala, A., Goddéris, Y., Goossens, N., Hartmann, J., Heinze, C., Ilyina,
3821 T., Joos, F., LaRowe, D. E., Leifeld, J., Meysman, F. J. R., Munhoven, G., Raymond, P. A.,
3822 Spahni, R., Suntharalingam, P. and Thullner, M. (2013). Anthropogenic perturbation of the
3823 carbon fluxes from land to ocean. *Nature Geosciences,* **6**, 597–607. doi:10.1038/ngeo1830
3824 Reichstein, M., Bahn, M., Ciais, P., Frank, D., Mahecha, M. D., Seneviratne, S. I., Zscheischler,
3825 J., Beer, C., Buchmann, N., Frank, D. C., Papale, D., Rammig, A., Smith, P., Thonicke, K.,
3826 van der Velde, M., Vicca, S., Walz, A., and Wattenbach, M. (2013). Climate extremes and
3827 the carbon cycle, *Nature*, **500**, 287–295. doi: 10.1038/Nature12350, 2013
3828 Remaud, M., Chevallier, F., Maignan, F., Belviso, S., Berchet, A., Parouffe, A., Abadie, C.,
3829 Bacour, C., Lennartz, S., and Peylin, P. (2021). Plant gross primary production, plant
3830 respiration and carbonyl sulfide emissions over the globe inferred by atmospheric inverse
3831 modelling, Atmos. Chem. Phys. Discuss. [preprint]. doi: 10.5194/acp-2021-326, in review,
3832 2021.
3833 Resplandy, L., Keeling, R. F., Rödenbeck, C.,. Stephens, B. B, Khatiwala, S., Rodgers, K. B.,
3834 Long, M. C., Bopp, L. and. Tans, P. P. (2018). Revision of global carbon fluxes based on a
3835 reassessment of oceanic and riverine carbon transport. *Nature Geoscience*, **11**, 504–509.
3836 doi:10.1038/s41561-018-0151-3
3837 Reuter, M., Buchwitz, M., Hilker, M., Heymann, J., Schneising, O., Pillai, D., Bovensmann, H.,
3838 Burrows, J. P., Bösch, H., Parker, R., Butz, A., Hasekamp, O., O'Dell, C. W., Yoshida, Y.,
3839 Gerbig, C., Nehrkorn, T., Deutscher, N. M., Warneke, T., Notholt, J., Hase, F., Kivi, R.,
3840 Sussmann, R., Machida, T., Matsueda, H. and Sawa, Y. (2014). Satellite-inferred European
3841 carbon sink larger than expected. *Atmospheric Chemistry and Physics*, **14**, 13739-13753.
3842 doi: 10.5194/acp-14-13739-2014
3843 Reuter, M., Buchwitz., M., Schneising, O., Krautwurst, S., O'Dell, C. W., Richter, A.,
3844 Bovensmann, H. and Burrows, J. P. (2019). Towards monitoring localized CO_2 emissions
3845 from space: Co-located regional CO_2 and NO_2 enhancements observed by the OCO-2 and
3846 S5P satellites. *Atmospheric Chemistry and Physics*, **19**, 9371–9383. doi:10.5194/acp-19-
3847 9371-2019
3848 Ridge, S. M. and McKinley, G. A. (2020). Advective controls on the North Atlantic
3849 anthropogenic carbon sink. *Global Biogeochemical Cycles*, **34**, 1138.
3850 doi:10.1029/2019GB006457
3851 Ridge, S. M. and McKinley, G. A. (2021). Ocean carbon uptake under aggressive emission
3852 mitigation. *Biogeosciences* **18**, 2711–2725. doi: 10.5194/bg-18-2711-2021
3853 Rödenbeck, C., Houweling, S., Gloor, M., and Heimann, M. (2003). CO_2 flux history 1982–2001
3854 inferred from atmospheric data using a global inversion of atmospheric transport,
3855 *Atmospheric Chemistry and Physics*, **3**, 1919-1964. doi: 10.5194/acp-3-1919-2003, 2003.

3856 Rödenbeck, C., Bakker, D. C. E., Metzl, N., Olsen, A., Sabine, C., Cassar N., Reum, F., Keeling,
3857 R. F and Heimann, M. (2014). Interannual sea-air CO_2 flux variability from an observation-
3858 driven ocean mixed-layer scheme. *Biogeosciences*, **11**, 4599–4613. doi:10.5194/bg-11-
3859 4599-2014
3860 Rödenbeck, C., Bakker, D. C. E., Gruber, N., Iida, Y., Jacobson, A. R., Jones, S., Landschützer,
3861 P., Metzl, N., Nakaoka, S., Olsen, A., Park, G.-H., Peylin, P., Rodgers, K. B., Sasse, T. P.,
3862 Schuster, U., Shutler, J. D., Valsala, V., Wanninkhof, R. and Zeng, J. (2015). Data-based
3863 estimates of the ocean carbon sink variability – first results of the Surface Ocean pCO_2
3864 Mapping intercomparison (SOCOM). *Biogeosciences*, **12**, 7251–7278. doi:10.5194/bg-12-
3865 7251-2015
3866 Rodgers, K. B., Schlunegger, S., Slater, R. D., Ishii, M., Frolicher, T. L., Toyama, K., Plancherel,
3867 Y., Aumont, O. and Fassbender, A. J. (2020). Reemergence of anthropogenic carbon into the
3868 ocean's mixed layer strongly amplifies transient climate sensitivity. *Geophysics Research*
3869 *Letters*, **47**, 130. doi:10.1002/2017GL073758
3870 Rosan, T. M., Goldewijk, K. K., Ganzenmüller, R., O'Sullivan, M., Pongratz, J., Mercado, L. M.,
3871 Aragao, L. E. O. C., Heinrich, V., von Randow, C., Wiltshire, A., Tubiello, F. N., Bastos, A.,
3872 Friedlingstein, P, and Sitch, S. (2021). A multi-data assessment of land use and land cover
3873 emissions from Brazil during 2000–2019. Environmental Research Letters, 16, 074004. doi:
3874 10.1088/1748-9326/ac08c3
3875 Rosen, P., Hensley, S., Shaffer, S., Edelstein, W., Kim, Y., Kumar, R., Misra, T., Bhan, R., Satish,
3876 R. and Sagi, R. (2016). An update on the NASA-ISRO dual-frequency dbf SAR (NISAR)
3877 mission. *2016 IEEE International Geoscience and Remote Sensing Symposium*. IEEE, New
3878 York, pp. 2106–2108. doi:10.1109/IGARSS.2016.7729543
3879 Rowland, L., da Costa, A. C., L., Galbraith, D. R., Oliveira, R. S., Binks, O. J., Oliveira, A. A.
3880 R., Pullen, A. M., Doughty, C. E., Metcalfe, D. B., Vsconcelos, S., S., Ferreia, L. V., Malhi,
3881 Y., Grace, J., Mencuccini, M., and Meir, P. (2015). Death from drought in tropical forests is
3882 triggered by hydraulics not carbon starvation. *Nature*, **528**, 119-122. doi:
3883 10.1038/nature15539
3884 Rubino, M., Etheridge, D. M., Thornton, D. P., Howden, R., Allison, C. E., Francey, R. J.,
3885 Langenfelds, R. L., Steele, L. P., Trudinger, C. M., Spencer, D. A., Curran, M. A. J., van
3886 Ommen, T. D., and Smith, A. M.(2019). Revised records of atmospheric trace gases CO_2,
3887 CH4, N2O, and δ13C-CO2 over the last 2000 years from Law Dome, Antarctica, *Earth*
3888 *System Science Data*, **11**, 473–492. doi:10.5194/essd-11-473-2019
3889 Rudnick, D. L. (2016). Ocean Research Enabled by Underwater Gliders. *Annual Review of*
3890 *Marine Science*, **8**, 519-541. doi:10.1146/annurev-marine-122414-033913
3891 Saatchi, S. S., Harris, N. L., Brown, S., Lefsky, M., Mitchard, E. T. A., Salas, W., Zutta, B. R.,
3892 Buermann, W., Lewis, S. L., Hagen, S., Petrova, S., White, L., Silman, M. and Morel, A.
3893 (2011). Benchmark map of forest carbon stocks in tropical regions across three continents.
3894 *Proceedings of the National Academy of Sciences*, **108**, 9899-9904. doi:
3895 10.1073/pnas.1019576108
3896 Sabine, C. L., Feely, R. A., Gruber, N., Key, R. M., Lee, K., Bullister, K. L., Wanninkhof, R.
3897 Wong, C. S., Wallace, D. W. R. Wallace, Tilbrook, B., Millero, F. J., Peng, T.-H., Kozyr, A.,
3898 Ono, T. and Rois, A. F. (2004). The oceanic sink for anthropogenic CO_2. *Science,* **305**, 367–
3899 371. doi:10.1126/science.1097403

3900 Sabine, C. L. and Tanhua, T. (2010). Estimation of anthropogenic CO_2 inventories in the ocean.
3901 *Annual Reviews of Marine Sciences,* **2**, 175-198. doi:10.1146/annurev-marine-120308-
3902 080947
3903 Sabine, C., Sutton, A., McCabe, K., Lawrence-Slavas, N., Alin, S., Feely, R., Jenkins, R.,
3904 Maenner, S., Meinig, C., Thomas, J., van Ooijen, E., Passmore, A. and Tilbrook, B. (2020).
3905 Evaluation of a new carbon dioxide system for autonomous surface vehicles. *J. Atmos.*
3906 *Ocean. Technol.*, **37**, 1305-1317. doi:10.1175/JTECH-D-20-0010.1
3907 Sarmiento, J. L., and Sundquist E. T. (1992). Revised budget for the oceanic uptake of
3908 anthropogenic carbon dioxide, *Nature*, **356**, 589–593. doi:10.1038/356589a0
3909 Sarmiento, J. L. and Gruber, N. (2006). Ocean Biogeochemical Dynamics. Princeton University
3910 Press. ISBN: 0-691-01707-7. doi:10.1017/S0016756807003755
3911 Sarmiento, J. L., Gloor, M., Gruber, N., Beaulieu, C., Jacobson, A. R., Mikaloff Fletcher, S. E.,
3912 Pacala, S., and Rodgers, K. (2010). Trends and regional distributions of land and ocean
3913 carbon sinks. *Biogeosciences*, **7**, 2351-2367. doi: 10.5194/bg-7-2351-2010
3914 Scharlemann, J. P. W., Tanner, E. V. J., Hiederer, R. and Kapos, V. (2014). Global soil carbon:
3915 understanding and managing the largest terrestrial carbon pool. *Carbon Management*, **5**, 81-
3916 91. doi:10.4155/cmt.13.77
3917 Schepaschenko, D., Moltchanova, E., Shvidenko, A., Blyshchyk, V., Dmitriev, E., Martynenko,
3918 O., See, L. and Kraxner F. (2018). Improved estimates of biomass expansion factors for
3919 Russian forests. *Forests*, **9**, 312. doi:10.3390/f9060312
3920 Schimel, D., Stephens, B. B., and Fisher, J. B. (2015). Effect of increasing CO_2 on the terrestrial
3921 carbon cycle, *Proceeding of the National Academy of Sciences*, **112**, 436-441. doi:
3922 10.1073/pnas.1407302112
3923 Scholze, M., Kaminski, T., Knorr, W., Voßbeck, M., Wu, M., Ferrazzoli, P., Kerr, Y., Mialon, A.,
3924 Richaume, P., Rodríguez-Fernández, N., Vittucci, C., Wigneron, J. P., Mechlenburg, S. and
3925 Drusch, M. (2019). Mean European carbon sink over 2010–2015 estimated by simultaneous
3926 assimilation of atmospheric CO2, soil moisture, and vegetation optical depth. *Geophysical*
3927 *Research Letters*, **46**. doi:10. 1029/2019GL085725
3928 Schourup-Kristensen, V., Sidorenko, D., Wolf-Gladrow, D. A. and Völker, C. (2014). A skill
3929 assessment of the biogeochemical model REcoM2 coupled to the Finite Element Sea Ice–
3930 Ocean Model (FESOM 1.3). *Geoscientific Model Development*, **7**, 2769–2802.
3931 doi:10.5194/gmd-7-2769-2014
3932 Schuh, A., Jacobson, A. R., Basu, S., Weir, B., Baker, D., Bowman, K., Chevallier, F., Crowell,
3933 S., Davis, K., Deng, F., Denning, S., Feng, L., Jones, D., Liu, J., and Palmer, P. (2019).
3934 Quantifying the Impact of Atmospheric Transport Uncertainty on CO_2 Surface Flux
3935 Estimates, *Global Biogeochemical Cycles*, **33**, 484–500. doi: 10.1029/2018GB0060
3936 Schwinger, J., Tjiputra, J. F., Heinze, C., Bopp, L., Christian, J. R., Gehlen, M., Ilyina, T., Jones,
3937 C. D., Salas-Mélia, D., Segschneider, J., Séférian, R. and Totterdell, I. (2014). Nonlinearity
3938 of ocean carbon cycle feedbacks in CMIP5 Earth system models. *Journal of Climate,* **27**,
3939 3869–3888. doi:10.1175/JCLI-D-13-00452.1
3940 Schwinger, J., Goris, N., Tjiputra, J. F., Kriest, I., Bentsen, M., Bethke, I., Ilicak, M., Assmann,
3941 K. M. and Heinze, C. (2016). Evaluation of NorESM-OC (versions 1 and 1.2), the ocean
3942 carbon-cycle stand-alone configuration of the Norwegian Earth System Model (NorESM1).
3943 *Geoscientific Model Development*, **9**, 2589–2622. doi:10.5194/gmd-9-2589-2016

3944 Schwinger, J. and Tjiputra, J. (2018). Ocean carbon cycle feedbacks under negative emissions.
3945 *Geophysical Research Letters*, **26**, 5289. doi:10.1088/1748-9326/11/5/055006
3946 Seelmann, K., Aßmann, S. and Körtzinger, A. (2019). Characterization of a novel autonomous
3947 analyzer for seawater total alkalinity: Results from laboratory and field tests. *Limnology and*
3948 *Oceanography: Methods*, **17**, 515-532. doi:10.1002/lom3.10329
3949 Séférian, R., Berthet, S., Yool, A., Palmieri, J., Bopp, L., Tagliabue, A., Kwaitkowski, L.,
3950 Aumont, O., Christian, J., Dunne, J., Gehlen, M., Ilyina, T., John, J. G., Li, H., Long, M. C.,
3951 Luo, J. Y., Nakano, H., Romanou, A., Schwinger, J., Stock, C., Santana-Falcon, Y., Takano,
3952 Y., Tjiputra, J., Tsujino, H., Wantanabe, M., Wu, T., Wu, F. and Yamamoto, A. (2020).
3953 Tracking Improvement in Simulated Marine Biogeochemistry Between CMIP5 and CMIP6.
3954 *Curr. Clim. Change Rep.,* **6,** 95–119. doi: 10.1007/s40641-020-00160-0
3955 Sellers, P. J., Schimel, D. S., Moore III, B., Liu, J. and Eldering, A. (2018). Observing Carbon
3956 Cycle-Climate Feedbacks from Space, *Proceedings of the National Academy of Sciences*,
3957 **115**, 7860-7868. doi:10.1073/pnas.1716613115
3958 Sigman, D. M., Hain, M. P. and Haug, G. H. (2010). The polar ocean and glacial cycles in
3959 atmospheric CO_2 concentration. *Nature,* **466**, 47–55. doi:10.1038/nature09149
3960 Sitch, S., Brovkin, V., von Bloh, W., van Vuuren, D., Eickhout, B. and Ganopolski, A. (2005).
3961 Impacts of future land cover changes on atmospheric CO_2 and climate. *Global*
3962 *Biogeochemical Cycles*, **19**, GB2013. doi: 10.1029/2004GB002311
3963 Sitch, S., Friedlingstein, P., Gruber, N., Jones, S. D., Murray-Tortarolo, G., Ahlström, A., Doney,
3964 S. C., Graven, H., Heinze, C., Huntingford, C., Levis, S., Levy, P. E., Lomas, M., Poulter,
3965 B., Viovy, N., Zaehle, S., Zeng, N., Arneth, A., Bonan, G., Bopp, L., Canadell, J. G.,
3966 Chevallier, F., Ciais, P., Ellis, R., Gloor, M., Peylin, P., Piao, S. L., Le Quéré, C., Smith, B.,
3967 Zhu, Z. and Myneni, R. (2015). Recent trends and drivers of regional sources and sinks of
3968 carbon dioxide. *Biogeosciences*, **12**, 653–679. doi:10.5194/bg-12-653-2015
3969 Sloyan, B. M., Wanninkhof, R., Kramp, M., Johnson, G. C., Talley, L. D., Tanhua, T.,
3970 McDonagh, E., Cusack, C., O'Rourke, E., McGovern, E., Katsumata, K., Diggs, S.,
3971 Hummon, J., Ishii, M., Azetsu-Scott, K., Boss, E., Ansorge, I., Perez, F. F., Mercier, H.,
3972 Williams, M. J. M., Anderson, L., Lee, J. H., Murata, A., Kouketsu, S., Jeansson, E.,
3973 Hoppema, M. & Campos, E. (2019). The Global Ocean Ship-Based Hydrographic
3974 Investigations Program (GO-SHIP): A Platform for Integrated Multidisciplinary Ocean
3975 Science. *Frontiers in Marine Science*, **6**, 445. doi: 10.3389/fmars.2019.00445
3976 Smith, B., Prentice, I. C., and Sykes, M. T. (2001). Representation of vegetation dynamics in the
3977 modelling of terrestrial ecosystems comparing two contrasting approaches within European
3978 climate space, *Global Ecol. Biogeogr.*, **10**, 621–637. doi: 10.1046/j.1466-822X.2001.t01-1-
3979 00256.x
3980 Smith P., Bustamante, M., Ahammad, H., Clark, H., Dong, H., Elsiddig, E. A., Haberl, H.,
3981 Harper, R., House, J., Jafari M., Masera, O., Mbow, C., Ravindranath N. H., Rice C. W.,
3982 Robledo Abad, C., Romanovskaya, A., Sperling, F. and Tubiello F. (2014). Agriculture,
3983 Forestry and Other Land Use (AFOLU). In: Climate Change 2014: Mitigation of Climate
3984 Change. Contribution of Working Group III to the Fifth Assessment Report of the
3985 Intergovernmental Panel on Climate Change [Edenhofer, O., R. Pichs-Madruga, Y. Sokona,
3986 E. Farahani, S. Kadner, K. Seyboth, A. Adler, I. Baum, S. Brunner, P. Eickemeier, B.
3987 Kriemann, J. Savolainen, S. Schlömer, C. von Stechow, T. Zwickel and J.C. Minx (eds.)].
3988 Cambridge University Press, Cambridge, United Kingdom and New York, NY, USA.

3989 Smith, W. K., Reed, S. C., Cleveland, C. C. Ballantyne, A. P., Anderegg, W. R. L., Wieder, W. R.
3990 Liu, Y. Y. and Running, S. (2015). Large divergence of satellite and Earth system model
3991 estimates of global terrestrial CO2 fertilization. *Nature Climate Change*, **6**, 306-310. doi:
3992 Song, X.-P., Hansen, M. C., Stehman, S. V., Potapov, P. V., Tyukavina, A., Vermote, E. F. and
3993 Townshend, J. R. (2018). Global land change from 1982 to 2016. *Nature*, **560**, 639-343.
3994 doi:10.1038/s41586-018-0411-9
3995 Soong, J. L., Fuchslueger, L., Marañon-Jimenez, S., Torn, M. S., Janssens, I. A., Penuelas, J., and
3996 Richter, A. (2019). Microbial carbon limitation: The need for integrating microorganisms
3997 into our understanding of ecosystem carbon cycling. *Global Change Biology,* **26**, 1953–
3998 1961. doi:10.1111/gcb.14962
3999 Spawn, S. A., Sullivan, C. C., Lark, T. J. and Gibbs, H. K. (2020). Harmonized global maps of
4000 above and belowground biomass carbon density in the year 2010. *Scientific Data,* **7,** 112.
4001 doi:10.1038/s41597-020-0444-4
4002 Stamell, J., Rustagi, R. R., Gloege, L. and McKinley, G. A. (2021). Strengths and weaknesses of
4003 three Machine Learning methods for pCO_2 interpolation. *Geoscientific Model Development*
4004 *Discuss.* [preprint], doi:10.5194/gmd-2020-311, in review, 2020.
4005 Stock, C. A., Dunne, J. P., Fan, S., Ginoux, P., John, J., Krasting, J. P., Laufkötter, C., Paulot, F.
4006 and Zadeh, N. (2020). Ocean biogeochemistry in GFDL's Earth System Model 4.1 and its
4007 response to increasing atmospheric CO_2. *J. Adv. Model. Earth Syst.*, **12**, e2019MS002043.
4008 doi:10.1029/2019MS002043
4009 Sun, Y., Frankenberg, C., Jung, J., Joiner, J., Guanter, L., Köhler, P. and Magney, T. (2018).
4010 Overview of solar-Induced chlorophyll fluorescence (SIF) from the Orbiting Carbon
4011 Observatory-2: Retrieval, cross-mission comparison, and global monitoring for GPP.
4012 *Remote Sensing of Environment*, **209**, 808-823. doi:10.1016/j.rse.2018.02.016
4013 Sundquist, E.T., (1993). The global carbon dioxide budget. *Science,* **259**, 934–941.
4014 doi:10.1126/science.259.5097.934
4015 Sutton, A. J., Sabine, C. L., Maenner-Jones, S., Lawrence-Slavas, N., Meinig, C., Feely, R. A.,
4016 Mathis, J. T., Musielewicz, S., Bott, R., McLain, P. D., Fought, H. J. and Kozyr, A. (2014).
4017 A high-frequency atmospheric and seawater pCO_2 data set from 14 open-ocean sites using a
4018 moored autonomous system. *Earth System Science Data,* **6**, 353-366. doi:10.5194/essd-6-
4019 353-2014
4020 Sutton, A. J., Williams, N. L., & Tilbrook, B. (2021). Constraining Southern Ocean CO_2 Flux
4021 Uncertainty Using Uncrewed Surface Vehicle Observations. *Geophysical Research Letters*,
4022 **48**, e2020GL091748. doi:10.1029/2020gl091748
4023 Takahashi, T., Sutherland, S. C., Sweeney, C., Poisson, A., Metzl, N., Tilbrook, B., Bates, N.,
4024 Wanninkhof, R., Feely, R. A., Sabine, C., Olafsson, J., Nojiri, Y. (2002). Global sea–air CO_2
4025 flux based on climatological surface ocean pCO_2, and seasonal biological and temperature
4026 effects. *Deep Sea Research Part II: Topical Studies in Oceanography*, **49**, 9–10, 1601-1622.
4027 doi:10.1016/S0967-0645(02)00003-6
4028 Takahashi, T., Sutherland, S. C., Wanninkhof, R., Sweeney, C., Feely, R. A., Chipman, D. W.,
4029 Hales, B., Friederich, G., Chavez, F., Sabine, C., Watson, A., Bakker, D. C. E., Schuster, U.,
4030 Metzl, N., Yoshikawa-Inoue, H., Ishii, M., Midorikawa, T., Nojiri, Y., Körtzinger, A.,
4031 Steinhoff, T., Hoppema, M., Olafsson, J., Arnarson, T.S., Tilbrook, B., Johannessen, T.,
4032 Olsen, A., Bellerby, R., Wong, C. S., Delille, B., Bates, N. R. and de Baar, H. J. W. (2009).
4033 Climatological mean and decadal change in surface ocean pCO_2, and net sea–air CO_2 flux

4034 over the global oceans. *Deep Sea Research Part II: Topical Studies in Oceanography,* **56**,
4035 554–577. doi:10.1016/j.dsr2.2008.12.009
4036 Takeshita, Y., Johnson, K. S., Martz, T. R., Plant, J. N. and Sarmiento, J. L. (2018). Assessment
4037 of autonomous pH measurements for determining surface seawater partial pressure of CO_2.
4038 *Journal of Geophysical Research: Oceans,* **123**, 4003-4013. doi:10.1029/2017jc013387
4039 Takeshita, Y., Johnson, K. S., Coletti, L., J., Jannasch, H. W., Walz, P. M. and Warren, J. W.
4040 (2020). Assessment of pH dependent errors in spectrophotometric pH measurements of
4041 seawater. *Marine Chemistry*, **223**, 103801. doi: 10.1016/j.marchem.2020.103801
4042 Tanhua, T., van Heuven, S., Key, R. M., Velo, A., Olsen, A. and Schirnick, C. (2010). Quality
4043 control procedures and methods of the CARINA database. *Earth System Science Data* **2**,
4044 35–49. doi:10.5194/essd-2-35-2010
4045 Tanhua, T. and Keeling, R. F. (2012). Changes in column inventories of carbon and oxygen in the
4046 Atlantic Ocean. *Biogeosciences,* **9**, 4819-4833. doi:10.5194/bg-9-4819-2012
4047 Tans, P. P., Fung, I. Y., and Takahashi, T. (1990). Observational constraints on the global
4048 atmospheric CO_2 budget, *Science*, **247**, 1431– 1438. doi: 10.1126/science.247.4949.1431
4049 Teubner, I. E., Forkel, M., Jung, M., Liu, Y. Y., Miralles, D. G., Parinussa, R., van der Schalie,
4050 R., Vreugdenhil, M., Schwalm, C. R., Tramontana, G., Camps-Valls, G., and Dorigo, W. A.
4051 (2018). Assessing the relationship between microwave vegetation optical depth and gross
4052 primary production, *International Journal of Applied Earth Observation and*
4053 *Geoinformation*, **65**, 79–91. doi: 10.1016/j.jag.2017.10.006
4054 Thomas, R. T., Prentice, I. C., Graven, H., Ciais, P., Fisher, J. B., Hayes, D. J., Huang, M.,
4055 Huntzinger, D. N., Ito, A., Jain, A., and Mao, J. (2016). Increased light-use efficiency in
4056 northern terrestrial ecosystems indicated by CO_2 and greening observations, *Geophysical*
4057 *Research Letters*, **43**, 11339–11349. doi: 10.1002/2016GL070710
4058 Tohjima, Y., Mukai, H., Machida, T., Hoshina, Y., and Nakaoka, S.-I. (2019). Global carbon
4059 budgets estimated from atmospheric O_2/N_2 and CO_2 observations in the western Pacific
4060 region over a 15-year period, *Atmospheric Chemistry and Physics*, **19**, 9269–9285, doi:
4061 10.5194/acp-19-9269-2019
4062 Torres, A. D., Keppel-Aleks, G., Doney, S. C., Fendrock, M., Luis, K., De Mazière, M., Hase, F.,
4063 Petri, C., Pollard, D. F., Roehl, C. M., Sussmann, R., Velazco, V. A., Warneke, T. and Wunch
4064 D. (2019). A geostatistical framework for quantifying the imprint of mesoscale atmospheric
4065 transport on satellite trace gas retrievals. *Journal of Geophysical Research: Atmospheres*,
4066 **124**. doi: 10.1029/2018JD029933
4067 Trenberth, K. E., and Smith, L. (2005). The mass of the atmosphere: A constraint on global
4068 analysis. *Journal of Climate*, **18**, 864-875. doi: 10.1175/JCLI-3299.1
4069 Umezawa, T., Matsueda, H., Sawa, Y., Niwa, Y., Machida, T., and Zhou, L. (2018). Seasonal
4070 evaluation of tropospheric CO_2 over the Asia-Pacific region observed by the CONTRAIL
4071 commercial airliner measurements. *Atmospheric Chemistry and Physics*, **18**, 14851–14866,
4072 doi: 10.5194/acp-18-14851-2018
4073 van der Laan-Luijkx, I. T., van der Velde, I. R., Krol, M. C., Gatti, L. V., Domingues, L. G.,
4074 Correia, C. S. C., Miller, J. B., Gloor, M., van Leeuwen, T. T., Kaiser, J. W., Wiedinmyer,
4075 C., Basu, S., Clerbaux, C. and Peters, W. (2015). Response of the Amazon carbon balance to
4076 the 2010 drought derived with CarbonTracker South America, Global *Biogeochem. Cycles*,
4077 **29**, 1092– 1108. doi: 10.1002/2014GB005082

van der Velde, I. R., van der Werf, G. R., Houweling, S., Maasakkers, J. D., Borsdorff, T., Landgraf, J., Tol, P., van Kempen, T. A., van Hees, R., Hoogeveen, R., Veefkind, P. J., and Aben, A. (2021). Vast CO_2 release from Australian fires in 2019–2020 constrained by satellite. *Nature*, **597**, 366-369. doi: 10.1038/s41586-021-03712-y

van der Werf, G. R., Randerson, J. T., Giglio, L., van Leeuwen, T. T., Chen, Y., Rogers, B. M., Mu, M., van Marle, M. J. E., Morton, D. C., Collatz, G. J., Yokelson, R. J. and Kasibhatla, P. S. (2017). Global fire emissions estimates during 1997–2016. *Earth System Science Data*, **9**, 697–720. doi:10.5194/essd-9-697-2017

Varon, D. J., Jacob, D. J., McKeever, J., Jervis, D., Durak, B. O. A., Xia, y., and Huang, Y. (2018). Quantifying methane point sources from fine-scale satellite observations of atmospheric methane plumes. *Atmospheric Measurement Technology*, **11**, 5673-5686. doi: 10.5194/amt-11-5673-2018

Verdy, A. Mazloff, M. R. (2017). A data assimilating model for estimating Southern Ocean biogeochemistry. *Journal of Geophysical Research: Oceans,* **122**, 6968–6988. doi:10.1002/2016JC012650

Walker, A. P., De Kauwe, M. G., Bastos, A., Belmecheri, S., Georgiou, K., Keeling, R. F., McMahon, S. M., Medlyn, B. E., Moore, D. J. P., Norby, R. J., Zaehle, S., Anderson-Teixeira, K. J., Battipaglia, G., Brienen, R. J. W., Cabugao, K. G., Cailleret, M., Campbell, E., Canadell, J. G., Ciais, P., Craig, M. E., Ellsworth, D. S., Farquhar, G. D., Fatichi, S., Fisher, J. B., Frank, D. C., Graven, H., Gu, L., Haverd, V., Heilman, K., Heimann, M., Hungate, B. A., Iversen, C. M., Joos, F., Jiang, M., Keenan, T. F., Knauer, J., Körner, C., Leshyk, V. O., Leuzinger, S., Liu, Y., MacBean, N., Malhi, Y., McVicar, T. R., Penuelas, J., Pongratz, J., Powell, A.S., Riutta, T., Sabot, M. E. B., Schleucher, J., Sitch, S., Smith, W. K., Sulman, B., Taylor, B., Terrer, C., Torn, M. S., Treseder, K. K., Trugman, A. T., Trumbore, S. E., van Mantgem, P. J., Voelker, S. L., Whelan, M. E. and Zuidema, P. A. (2021). Integrating the evidence for a terrestrial carbon sink caused by increasing atmospheric CO_2. *New Phytol.*, **229**, 2413-2445. doi: 10.1111/nph.16866

Wang, J., Wang, M., Kim, J.-S., Joiner, J., Zeng, N., Jiang, F., Wang, H., He, W., Wu, M., Chen, T., Ju, W. and Chen, J. M. (2021). Modulation of land photosynthesis by the Indian Ocean Dipole: Satellite-based observations and CMIP6 future projections. *Earth's Future*, **9**, e2020EF001942. doi: 10.1029/2020EF001942

Wang, S., Zhang, Y., Hakkarainen, J., Ju, W., Liu, Y., Jiang, F. and He, W. (2018). Distinguishing anthropogenic CO_2 emissions from different energy intensive industrial sources using OCO-2 observations: A case study in northern China. *Journal of Geophysical Research: Atmospheres*, **123**, 9462–9473. doi:10.1029/2018JD029005

Watson, A. J., Schuster, U., Shutler, J. D., Holding, T., Ashton, I. G. C.,Landschützer, P. , Woolf, D. K. and Goddijn-Murphy, L. (2020). Revised estimates of ocean-atmosphere CO_2 flux are consistent with ocean carbon inventory. *Nature Communications*, **11**, 4422. doi:10.1038/s41467-020-18203-3

Waugh, D. W., Hall, T. M., McNeil, B. I., Key, R. and Matear, R. J. (2006). Anthropogenic CO_2 in the oceans estimated using transit-time distributions. *Tellus,* **58B**, 376-389. doi:10.1111/j.1600-0889.2006.00222.x

Weir, B., Crisp, D., O'Dell, C. W., Basu, S., Chatterjee, A., Kolassa, J., Oda, T., Pawson, S., Poulter, B., Zhang, Z., Ciais, P., Davis, S. J., Liu, Z., and Ott, L. E. (2021). Regional

4122 impacts of COVID-19 on carbon dioxide detected worldwide from space. *Science*
4123 *Advances*, **7**, eabf9415. Doi: 10.1126/sciadv.abf9415
4124 Welp, L., Keeling, R. and Meijer, H. A. J. (2011). Interannual variability in the oxygen isotopes
4125 of atmospheric CO_2 driven by El Niño. *Nature*, **477**, 579–582. doi:10.1038/nature10421
4126 Wigneron, J.-P., Fan, L., Ciais, P., Bastos, A., Brandt, M., Chave, J., Saatchi, S., Baccini, A. and
4127 Fensholt, R. (2020). Tropical forests did not recover from the strong 2015–2016 El Niño
4128 event. *Science Advances*, **6**, eaay4603. doi:10.1126/sciadv.aay4603
4129 Williams, N. L., Juranek, L. W., Feely, R. A., Johnson, K. S., Sarmiento, J. L., Talley, L. D.,
4130 Dickson, A. G., Gray, A. R., Wanninkhof, R., Russell, J. L., Riser, S. C. and Takeshita, Y.
4131 (2017). Calculating surface ocean pCO_2 from biogeochemical Argo floats equipped with
4132 pH: An uncertainty analysis. *Global Biogeochemical Cycles*, **31**, 591-604.
4133 doi:10.1002/2016GB005541
4134 Wohlfahrt, G., Gerdel, K., Migliavacca, M., Rotenberg, E., Tatarinov, F., M., Müller, J.,
4135 Hammerle, A., Julitta, T., Spielmann, F. M., and Yakir, D. (2018). Sun-induced fluorescence
4136 and gross primary productivity during a heat wave. *Scientific Reports*, **8**, 14169. doi:
4137 10.1038/s41598-018-32602-z
4138 Wolf, S., Keenan, T. F., Fisher, J. B., Baldocchi, D. D., Desai, A. R., Richardson, A. D., Scott, R.
4139 L., Law, B. E., Litvak, M. E., Brunsell, N. A., Peters, W., and van der Laan-Luijkx, I. T.
4140 (2016). Warm spring reduced carbon cycle impact of the 2012 US summer drought, *Proc*
4141 *Natl Acad Sci USA*, **113**, 5880. doi: 10.1073/pnas.1519620113
4142 Woolf, D. K., Shutler, J. D., Goddijn-Murphy, L., Watson, A. J., Chapron, B., Nightingale, P. D.,
4143 Donlon, C. J., Piskozub, J., Yelland, M. J., Ashton, I., Holding, T., Schuster, U., Girard-
4144 Ardhuin, F., Grouazel, A., Piolle, J.-F., Warren, M., Wrobel-Niedzwiecka, I., Land, P. E.,
4145 Torres, R., Prytherch, J., Moat, B., Hanafin, J., Ardhuin, F. and Paul, F. (2019). Key
4146 uncertainties in the recent air-sea flux of CO_2. *Global Biogeochemical Cycles*, **33**, 1548-
4147 1563. doi:10.1029/2018GB006041
4148 Wu, D., Lin, J. C., Fasoli, B., Oda, T., Ye, X., Lauvaux, T., Yang, E. G. and Kort, E. A. (2018). A
4149 Lagrangian approach towards extracting signals of urban CO_2 emissions from satellite
4150 observations of atmospheric column CO_2 (XCO_2): X-Stochastic Time-Inverted Lagrangian
4151 Transport model ("X-STILT v1"). *Geoscientific Model Development*, **11**: 4843–4871.
4152 doi:10.5194/gmd-11-4843-2018
4153 Wu, D. E., Lin, J. C., Oda, T. and Kort, E. A. (2020). Space-based quantification of per capita
4154 CO_2 emissions from cities, *Environmental Research Letters*, **15**, 035004. doi:10.1088/1748-
4155 9326/ab68eb
4156 Wunch, D., Toon, G. C., Blavier, J.-F. L., Washenfelder, R. A., Notholt, J., Connor, B. J.,
4157 Griffith, D. W., Sherlock, V., and Wennberg, P. O. (2011). The total carbon column
4158 observing network, *Philosophical Transactions of the Royal. Society A*, **369**, 2087–2112,
4159 doi:10.1098/rsta.2010.0240.
4160 Wunch, D., Wennberg, P. O., Osterman, G., Fisher, B., Naylor, B., Roehl, C. M., O'Dell, C.,
4161 Mandrake, L., Viatte, C., Griffith, D. W., Deutscher, N. M., Velazco, V. A., Notholt, J.,
4162 Warneke, T., Petri, C., De Maziere, M., Sha, M. K., Sussmann, R., Rettinger, M., Pollard,
4163 D., Robinson, J., Morino, I., Uchino, O., Hase, F., Blumenstock, T., Kiel, M., Feist, D. G.,
4164 Arnold, S. G., Strong, K., Mendonca, J., Kivi, R., Heikkinen, P., Iraci, L., Podolske, J.,
4165 Hillyard, P. W., Kawakami, S., Dubey, M. K., Parker, H. A., Sepulveda, E., Rodriguez, O. E.
4166 G., Te, Y., Jeseck, P., Gunson, M. R., Crisp, D. and Eldering, A. (2017). Comparisons of the

4167 Orbiting Carbon Observatory-2 (OCO-2) XCO_2 measurements with TCCON, *Atmospheric*
4168 *Measurement Tech*niques, **10**, 2209–2238. doi: 10.5194/amt-10-2209-2017
4169 Xiao, J., J. Chen, Davis, K. J. and Reichstein, M. (2012). Advances in upscaling of eddy
4170 covariance measurements of carbon and water fluxes. *Journal Geophysical Research:*
4171 *Biogeosciences*, **117**, G00J01. doi:10.1029/2011JG001889
4172 Xiao, J., Chevallier, F., Gomez, C., Guanter, L., Hicke, J. A., Huete, A. R., Ichii, K., Ni, W.,
4173 Pang, Y., Rahman, A. F. Sun, G., Yuan, W., Zhang, L. and Zhang, X. (2019). Remote
4174 sensing of the terrestrial carbon cycle: A review of advances over 50 years. *Remote Sensing*
4175 *of Environment*, **233**, 111383. doi:10.1016/j.rse.2019.111383
4176 Xu, L., Saatchi, S. S., Yang, Y., Yu. Y., Pongratz, J., Bloom, A. A., Bowman, K., Worden, J., Liu,
4177 J., Yin, Y., Domke, G., McRoberts, R. E., Woodall, C., Nabuurs, G.-J., de-Miguel, S., Keller,
4178 M., Harris, N., Maxwell, S., and Schimel, D. (2021). Changes in global terrestrial live
4179 biomass over the 21st century. *Science Advances*, **7**, eabe9829. doi: 10.1126/sciadv.abe9829
4180 Xue, L., Cai, W.-J., Takahashi, T., Gao, L., Wanninkhof, R., Wei, M., Li, K., Feng, L., and Yu, W.
4181 (2018). Climatic modulation of surface acidification rates through summertime wind forcing
4182 in the Southern Ocean. *Nature Communications*, **9**, 3240. doi: 10.1038/s41467-018-05443-7
4183 Ye, X., Lauvaux, T., Kort, E.A., Oda, T., Feng, S., Lin, J. C., Yang, E. G., and Wu, D. (2020).
4184 Constraining fossil fuel CO_2 emissions from urban area using OCO-2 observations of total
4185 column CO_2. *Journal of Geophysical Research, Atmospheres*, **125**, e2019JD030528. doi:
4186 10.1029/2019JD030528.
4187 Yin, Y., Byrne, B., Liu, J., Wennberg, P., Davis, K. J., Magney, T., Koehler, P., He, L., Jeyaram,
4188 R., Humphrey, V., Gerken, T., Feng, S., Digangi, J. P. and Frankenberg, C. (2020). Cropland
4189 carbon uptake delayed and reduced by 2019 Midwest floods. *AGU Advances*, **1**,
4190 e2019AV000140. doi:10.1029/2019AV000140
4191 Yoshida, Y., Ota, Y., Eguchi, N., Kikuchi, N., Nobuta, K., Tran, H., Morino, I., and Yokota, T.
4192 (2011). Retrieval algorithm for CO_2 and CH_4 column abundances from short-wavelength
4193 infrared spectral observations by the Greenhouse Gases Observing Satellite, *Atmospheric*
4194 *Measurment Technology*, **4**, 717–734. doi:10.5194/amt-4-717-2011
4195 Yuan, W., Zheng, Y., Ciais, P., Lombardozzi, D., Wang, Y., Ryu, Y., Chen, G., Dong, W., Hu, Z.,
4196 Jian, A. K., Jiang, C., Kato, E., Li, S., Lienert, S., Liu, S., Nabel, J. E. M. S., Qin, Z., Quine,
4197 T., Sitch, S., Smith, W. K., Wang, F., Wu, C., Xiao, Z, and Yang, S. (2019). Increased
4198 atmospheric vapor pressure deficit reduces global vegetation growth, *Science Advances*, **5**,
4199 eaax1396. doi: 10.1126/sciadv.aax1396
4200 Zavarsky, A. and Marandino, C. A. (2019). The influence of transformed Reynolds number
4201 suppression on gas transfer parameterizations and global DMS and CO_2 fluxes. *Atmospheric*
4202 *Chemistry and Physics*, **19**, 1819-1834. doi:10.5194/acp-19-1819-2019
4203 Zeebe, R. and Wolf-Gladrow, D. (2001). CO_2 in seawater: Equilibrium, kinetics, isotopes.
4204 *Elsevier Oceanogr. Ser.*, **65**, Elsevier, Amsterdam.
4205 Zeng, N., Zhao, F., Collatz, G. J., Kalnay, E., Salawitch, R., West, T. O. and Guanter, L. (2014).
4206 Agricultural Green Revolution as a driver of increasing atmospheric CO_2 seasonal
4207 amplitude. *Nature,* **515**, 394–397. doi: 10.1038/nature13893
4208 Zhang, Q., Li, M., Wang, M., Mizzi, A.P., Huang, Y., Wei, C., Jin, J., Gu, Q. (2021). CO_2 Flux
4209 over the Contiguous United States in 2016 Inverted by WRF-Chem/DART from OCO-2
4210 XCO_2 Retrievals. *Remote Sens*., **13**, 2996. doi: 10.3390/rs13152996

4211 Zhu, Z., Bi, J., Pan, Y., Ganguly, S., Anav, A., Xu, L., Samanta, A., Piao, S., Nemani, R. R., and
4212 Myneni, R. B.. (2013). Global data sets of vegetation leaf area index (LAI)3g and fraction
4213 of Photosynthetically active radiation (FPAR)3g derived from global inventory modeling
4214 and mapping studies (GIMMS) normalized difference vegetation index (NDVI3g) for the
4215 period 1981 to 2011. *Remote Sensing*, **5**, 927‑948. doi: 10.3390/rs5020927

4216 Zhu, Z., Piao, S., Myneni, R. B., Huang, M., Zeng, Z., Canadell, J. G., Ciais, P., Sitch, S.,
4217 Friedlingstein, P., Arneth, A., Cao, C., Cheng, L., Kato, E., Koven, C., Li, Y., Sian, X., Liu,
4218 Y., Liu, R., Mao, J., Pan, Y., Peng, S., Peñuelas , J., Poulter, B., Pugh, T. A. M., Stocker, B.
4219 D., Vlovy, N., Wang, X., Wang, Y., Xiao, Z., Yang, H., Zaehle, S., and Zeng, N. (2016).
4220 Greening of the Earth and its drivers. *Nature Climate Change*, **6**, 791–795. doi:
4221 10.1038/NCLIMATE3004

4222 Zhu, Z., Piao, S., Xu, Y., Bastos, A., Ciais, P., Peng, S. (2017). The effects of teleconnections on
4223 carbon fluxes of global terrestrial ecosystems. *Geophysical Research Letters*, **44**, 3209-
4224 3218. doi: 10.1002/2016GL071743

4225 Zickfeld, K., MacDougall, A. H., and Matthews, H. D. (2016). On the proportionality between
4226 global temperature change and cumulative CO_2 emissions during periods of net negative
4227 CO_2 emissions. *Environmental Research Letters*, **11**, 055006, doi:10.1088/1748-
4228 9326/11/5/055006

4229 Zscheischler, J., Michalak, A. M., Schwalm, C., Mahecha, M. D., Huntzinger, D. N., Reichstein,
4230 M., Berthier, G., Ciais, P., Cook, R. B. El-Masri, B., Huang, M., Ito, A., Jain, A., King, A.,
4231 Lei, H., Lu, C., Mao, J., Peng, S., Poulter, B., Ricciuto, D., Shi, X., Tao, B., Tian, H., Viovy,
4232 N., Wang, W., Wei, X., Yang, J., and Zeng, N. (2014). Impact of large-scale climate
4233 extremes on biospheric carbon fluxes: An inter-comparison based on MsTMIP data, *Global*
4234 *Biogeochem. Cycles*, **28**, 585–600, doi: 10.1002/2014GB004826